E-ISSN 2667-5846

EXPERIMED

Volume **13** Issue **3 December** 2023

experimed.istanbul.edu.tr

ISTANBUL UNIVERSITY PRESS

EXPERIMED

INDEXING AND ABSTRACTING

Scopus
ULAKBIM TR Index
Chemical Abstracts Service (CAS)
EBSCO - Central & Eastern European Academic Source
SOBIAD

EXPERIMED

OWNER

Prof. Dr. Gunnur DENIZ

Department of Immunology, Istanbul University, Aziz Sancar Institute of Experimental Medicine, Istanbul, Turkiye

RESPONSIBLE MANAGER

Prof. Dr. Bedia CAKMAKOGLU

Department of Molecular Medicine, Istanbul University, Aziz Sancar Institute of Experimental Medicine, Istanbul, Turkiye

CORRESPONDENCE ADDRESS

Istanbul University, Aziz Sancar Institute of Experimental Medicine,
Vakıf Gureba Avenue, 34093, Capa, Fatih, Istanbul, Turkiye
Phone: +90 (212) 414 22 29
E-mail: experimed@istanbul.edu.tr

PUBLISHER

Istanbul Üniversitesi Yayınevi / Istanbul University Press
Istanbul University Central Campus,
34452 Beyazit, Fatih / Istanbul, Turkiye
Phone: +90 (212) 440 00 00

The publication language of the journal is English.

This is a scholarly, international, peer-reviewed and open-access journal published triannually in April, August and December.

Publication Type: Periodical

EXPERIMED

EDITORIAL MANAGEMENT BOARD

EXPERIMED

EDITORIAL BOARD

EXPERIMED

CONTENTS

ORIGINAL ARTICLES

163 **Alteration in Gene Expression of *STAT4* and *PIAS2* in Individuals with Type 2 Diabetes Mellitus Treated with the Dipeptidyl Peptidase 4 Inhibitor**
Sina Nabiyi, Firozeh Sajedi, Alireza Zamani, Mahdi Behzad

170 **Age and Regional Features of Quantitative Indicators of Lymphoid Nodules of the Human Intrahepatic Bile Ducts**
Naile Aliyeva, Sabina Shadlinskaya

174 **Efficacy of Speleotherapy on Atopic Bronchial Asthma in Children**
Lala Allahverdiyeva, Naila Efendiyeva, Afag Khalilova

180 **Assessment of Cardiac Myosin-binding Protein C Levels in Coronavirus Disease 2019**
Dilay Karabulut, Cennet Yildiz, Umut Karabulut, Ersan Oflar, Fatma Nihan Turhan Caglar, Kadriye Kart Yasar, Gulcin Sahingoz Erdal, Osman Pirhan, Pınar Kasapoglu, Nilgun Isiksacan

187 **Effects of Neurocognitive Rehabilitation on the Levels of Neurotransmitters and Memory Proteins in Patients with Multiple Sclerosis**
Ozlem Totuk, Erdil Arsoy, Recai Turkoglu

194 **Propolis: Intrinsic Pathway-Induced Apoptosis, G1 Cell Cycle Arrest, Reduced Chemotherapeutic Resistance in Adenocarcinoma, and Healthy Cell Preservation**
Nursel Isci, Sibel Dogan, Sahika Yardim, Seyhun Solakoglu, Ilhan Tahrali, Gunnur Deniz, Gulnaz Nural Bekiroglu, Elif Kervancioglu Demirci

205 **Exploring PI3K Pathway Inhibitors for Acute Myeloid Leukemia: A Drug-Repurposing Approach**
Cansu Ergun, Buse Zeren Kiremitci, Gizem Arslantas, Busenur Bozkurt, Gizem Ayna Duran, Yagmur Kiraz

213 **Indomethacin Affects the Inflammatory Response via Interaction with the RhoA-Actin Cytoskeleton in THP-1 Cells**
Ebru Haciosmanoglu Aldogan, Fulya Dal Yontem, Seyma Bulut, Hande Yapislar, Basak Guncer, Muhammet Bektas

218 **Epigenetic Regulation and Therapeutic Potential of Gasdermin Genes in Colorectal Adenocarcinoma**
Feyzanur Caldiran, Rumeysa Senol, Ercan Cacan

257 **Quantitative Measurement of HER2/neu Oncogene Amplification and p53 Tumor Suppressor Gene Deletion by RT-PCR in Breast Cancer**
Gozde Ulfer

263 **Copy Number Variations in a Turkish Cohort of Children with Intellectual Disability**
Deniz Sunnetci-Akkoyunlu, Bulent Kara, Naci Cine, Seda Eren-Keskin, Buket Dogruoglu, Zeynep Ilkay, Tolgahan Ozer, Hakan Savli

276 **Effect of MCP-1 and CCR2 Serum Levels on COVID-19 Severity**
Selen Zeliha Mart Komurcu, Seydanur Dogan, Ebru Kaya, Sevim Yavas, Serkan Dogan, Utku Murat Kalafat, Hayriye Senturk Ciftci, Selcuk Dasdemir

281 **Peroxisome Proliferator-activated Receptor-alpha (*PPARA*) and – Gamma (*PPARG*) Polymorphisms as Risk Factors for Dyslipidemia and MetS in Turkish Adults**
Filiz Guclu-Geyik, Evrim Komurcu-Bayrak, Gunay Can, Nihan Erginel-Unaltuna

290 **Stem Cell Mobilization Efficiency and Engraftment Kinetics in Patients with Hematologic Malignancies Undergoing Autologous Stem Cell Transplantation: A Retrospective Cohort Study**
Nuri Baris Hasbal, Mutlu Arat

Experimed 2023; 13(3): 163-169

ORIGINAL ARTICLE

DOI: 10.26650/experimed.1377167

Alteration in Gene Expression of *STAT4* and *PIAS2* in Individuals with Type 2 Diabetes Mellitus Treated with the Dipeptidyl Peptidase 4 Inhibitor

Sina Nabiyi[1], Firozeh Sajedi[2], Alireza Zamani[1], Mahdi Behzad[1]

[1]Department of Immunology, School of Medicine, Hamadan University of Medical Sciences, Hamadan, Iran
[2]Department of Internal Medicine, School of Medicine, Hamadan University of Medical Sciences, Hamadan, Iran

ORCID ID: S.N. 0000-0002-7531-3998; F.S. 0000-0002-1232-6003; A.Z. 0000-0001-6146-6013; M.B. 0000-0002-8940-3847

Cite this article as: Nabiyi S, Sajedi F, Zamani A, Behzad M. Alteration in gene expression of STAT4 and PIAS2 in individuals with type 2 diabetes mellitus treated with the dipeptidyl peptidase 4 inhibitor. Experimed 2023; 13(3): 163-169.

ABSTRACT

Objective: Impairment of immune cell signaling molecules is involved in diseases pathogenesis. The evaluation of signal transducer and activator of transcription (*STAT*) 4 and protein inhibitor of activated STAT (PIAS) 2 as well as immunoregulatory role of the dipeptidyl peptidase-4 inhibitor, sitagliptin were investigated in type 2 diabetes mellitus (T2DM).

Materials and Methods: Peripheral blood mononuclear cells (PBMC) were purified from three study groups including healthy controls, T2DM patients with 6 months of sitagliptin treatment, and T2DM patients without sitagliptin. Expressions of *STAT4* and *PIAS2* were assessed with real-time polymerase chain reaction (qPCR).

Results: The expression of *STAT4* in patients without sitagliptin was higher than the healthy controls (p=0.001). Its expression was down-regulated in the sitagliptin treated patient group compared to those without sitagliptin (p=0.005). *PIAS2* expression in patients without sitagliptin was lower than the healthy controls (p=0.009). *PIAS2* was elevated in the sitagliptin treated group versus patients without sitagliptin (p=0.003). A negative correlation between *STAT4* and *PIAS2* was found in individuals without sitagliptin (p=0.01). In patients without sitagliptin, fasting plasma glucose was positively and negatively correlated with *STAT4* and *PIAS2*, respectively (p=0.004 and p=0.001).

Conclusion: Aberrant expression of *STAT4* and reduced expression of *PIAS2* were found in the T2DM patients. Sitagliptin may regulate the cell signaling pathways by elevating *PIAS2* and reducing *STAT4*.

Keywords: Type 2 diabetes mellitus, STAT, PIAS, dipeptidyl peptidase 4 inhibitor

INTRODUCTION

Type 2 diabetes mellitus (T2DM), as a prevalent and intricate metabolic disorder, is primarily defined by hyperglycemia and inflammation (1). Disruption in cytokine secretion and signal transducer and activator of transcription (STAT), and protein inhibitor of activated STAT (PIAS) signaling components play a fundamental role in the inflammation (2, 3).

Several pro-inflammatory cytokines exert their functions through janus kinase (JAK)-STAT (consist of STAT 1-6) signaling molecules (4). STAT4, the most specific member of this family, has a pro-inflammatory impact on the immune system. STAT4 is activated by various inflammatory mediators such as Interleukin (IL)-12, IL-2, and IL-23 in the peripheral blood mononuclear cells (PBMCs) (2). STAT4 can influence a wide range of intracellular processes including T helper (Th) 1 cell differentiation and Interferon (IFN)-γ secretion (5). PIAS family (composed of PIAS 1-4) negatively regulate the intracellular cytokine pathways by acting on STATs molecules. PIAS2 binds to activated STAT4 and suppresses the pro-inflammatory process and signal transduction (3). Previous studies have reported that both STAT4 and PIAS2 take part in various diseases progression. For example, a recent study demonstrated that

Corresponding Author: Mahdi Behzad **E-mail:** mhd.behzad@yahoo.com & m.behzad@umsha.ac.ir
Submitted: 17.10.2023 **Revision Requested:** 04.11.2023 **Last Revision Received:** 05.11.2023 **Accepted:** 23.11.2023 **Published Online:** 29.11.2023

the expression of *PIAS2* was diminished in Parkinson patients, and its levels were involved in disease severity (6). Moreover, *PIAS2* expression was down-regulated in rheumatoid arthritis (RA) fibroblast-like synovial cells (7). Alteration in *STAT4* expression was reported in systemic lupus erythematosus (SLE) and rheumatoid arthritis (RA) patients accompanied by association with disease activity (8, 9).

Dipeptidyl peptidase 4 inhibitor, sitagliptin is an anti-diabetic agent prescribed for diabetes patients (10). Previously, we and others have reported diverse anti-inflammatory effects of sitagliptin. For example, this medication has inhibitory effects on the cell proliferation and differentiation (11). Sitagliptin can diminish the protein levels of JAK2 and STAT3 in diabetic rats (12). A reduction in IL-17 and Th17 transcription factor, RORγt, was reported in diabetes patients (13).

Altogether, the changes in STAT4 and PIAS2 levels were implicated in the pathogenesis of several diseases. However, no scientific reports are available in T2DM. In the current study, mRNA levels of *STAT4* and *PIAS2* were investigated in T2DM patients treated with/without sitagliptin in comparison to healthy subjects. The possible regulatory role of sitagliptin on *STAT4* and *PIAS2* was also explored. The relationship between the genes and diabetes parameters was analyzed.

MATERIALS AND METHODS

Subjects

This investigation was confirmed by the local ethics committee (IR. UMSHA. REC. 1402. 364) and written permission was given by all subjects. Three groups were included in this study: 1. T2DM patients without sitagliptin therapy (n=35, 19 females and 16 males, mean age: 50.97 ± 6.44), 2. T2DM patients with sitagliptin (n=35, 20 females and 15 males, mean age: 52.71 ± 5.8), and 3. healthy subjects without any noticeable illness (n=35, 19 females and 16 males, mean age: 50.54 ± 7.58). Patients received sitagliptin by using a fixed dose of 1000 mg/24h in the last 6 months. All patients had received background metformin medication (50 mg/day) one year before blood sampling. More information of the participants is indicated in supplementary Table 1.

Inclusion criterias: 1. T2DM patients were identified according to the American Diabetes Association 2022 principle, 2. fasting plasma glucose (FPG) for each person was > 125 mg/dL, and 3. hemoglobin A1c (HbA1c) was > 6.5%. Exclusion criterias: 1. people with autoimmune and chronic diseases, 2. people with neoplasia and allergic illness, 3. patients who had been taking insulin, immunosuppressants, and antibiotics, and 4. people with diabetes-related problems such as hyperketonemia, retinopathy, and nephropathy.

Cell Purification

PBMCs were isolated from 5 mL of fresh whole blood sample (in EDTA tube) using ficoll gradient centrifugation method (Sigma, MO, USA) (14). Concisely, each sample was diluted 1:2 with phosphate buffered saline (PBS) and was drawn into a tube containing the ficoll solution. PBMC layer was separated by centrifugation at 2200 rpm for 15 min at 4℃. Cells were washed 3 times prior to RNA isolation.

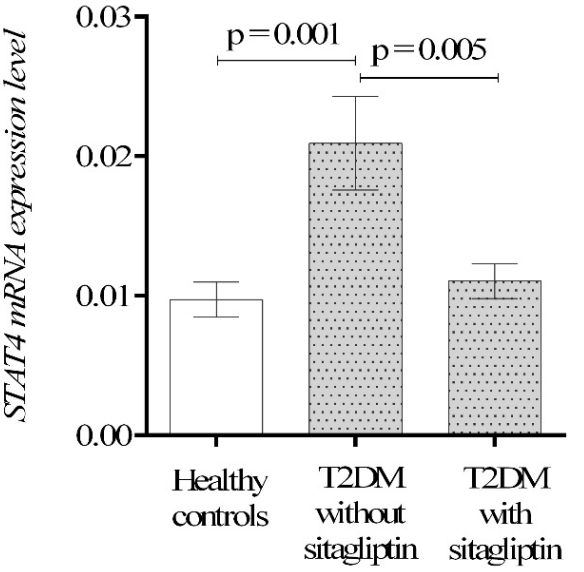

Figure 1. mRNA expression level of *STAT4* in patients and healthy controls. Gene expression level of *STAT4* in PBMCs of T2DM patients with and without sitagliptin, and healthy controls were determined using qPCR. Number of participants for each group is 35.

RNA Preparation and cDNA Generation

Total RNA was prepared from PBMCs. The RNA sensitive kit (Qiagen, USA) with relevant protocol was considered for RNA extraction. A 260/280 nm ratio of ~ 1.8 was accepted for cDNA synthesis. RNA was converted to cDNA using a human kit (Takara, Japan) with recommended protocol.

Real-time polymerase chain reaction (qPCR) (Roche 96 system, Germany) was used to measure gene expression. SYBR green fluorescent reporters (Ampliqon A/S, Denmark) was used to detect the products based on the instructions provided by the manufacturer. Time and temperature for the reactions were along these steps: 1. initial stage (95℃ for 15 min), 2. denaturation (95℃ for 15 s), 3. annealing (60℃ for 30 s), and 4. extension stage (72℃ for 30 s). Housekeeping glyceraldehyde 3-phosphate dehydrogenase (*GAPDH)* as an internal control was used for gene normalization. The relative mRNA expression levels of *STAT4* and *PIAS2* were calculated using the $2^{-\Delta Cq}$ method (15).

Specific primers were used as follows: 1) human *STAT4* (NM_003151.4), sense sequence is 5′-*CAGTGAAAGCCATCTCGGAGGA*-3′, and antisense sequence is 5′-*TGTAGTCTCGCAGGATGTCAGC*-3′, 2) human *PIAS2* (NM_173206.4),

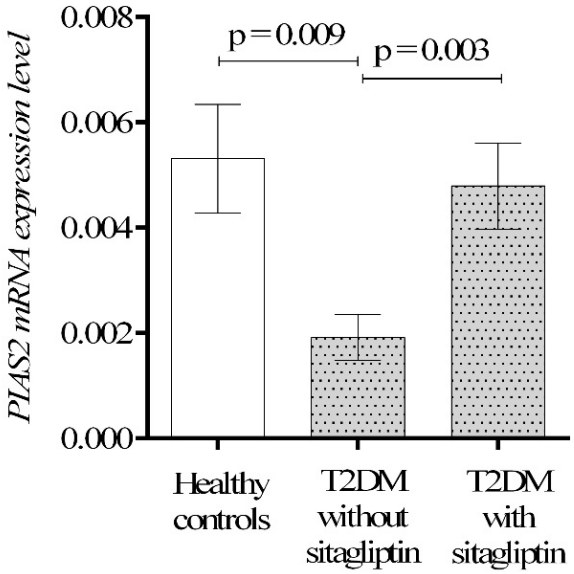

Figure 2. mRNA expression level of *PIAS2* in patients and healthy controls. *PIAS2* expression in PBMCs of patients with and without sitagliptin, and healthy controls were assessed using qPCR. Number of participants for each group is 35.

sense is 5′- *ATCCACGAACTCTTGAAGGACT* -3′, and antisense is 5′- *TGTGGGCTTAGTATCTTGAAGCA* -3′, and 3) human *GAPDH* (NM_002046.7), sense is 5′- *GGAG CGAGATCCCTCCAAAAT* -3′, and antisense primer is 5′- *GGCTGTTGTCATACTTCTCATGG* -3′.

Statistical Analyses

SPSS 21.0 and GraphPad Prism 9.0 were employed for statistical evaluation and graph creation. Analysis of variance (ANOVA) followed by Tukey's test as post hoc (to compare three groups), independent t-test (to compare two groups), and Pearson coefficient for correlations, were applied. Data was expressed as mean ± SD or mean ± SEM (for graphs). A $p<0.05$ was considered statistically significant.

RESULTS

The participants were consisted of T2DM patients without sitagliptin, T2DM patients with 6 months of sitagliptin, and healthy controls. The levels of *STAT4* and *PIAS2* genes were compared between the groups. The expression of *STAT4* was appreciably up-regulated in T2DM patients without sitagliptin when compared to healthy controls (p=0.001, Figure 1). *STAT4* expression was diminished in the T2DM patients treated with sitagliptin compared to the sitagliptin negative group (p=0.005, Figure 1). In contrast, *PIAS2* expression was markedly down-regulated in T2DM patients without sitagliptin in comparison with healthy subjects (p=0.009, Figure 2), and its expression was increased in the sitagliptin treated group compared to the sitagliptin negative group (p=0.003, Figure 2). No significant changes in *STAT4* and *PIAS2* levels were observed among the T2DM patients using sitagliptin and the healthy controls (Figure 1 and 2).

Table 1. Correlation between the *STAT4* and *PIAS2* in study groups.

T2DM patients without sitagliptin		
		PIAS2 expression
STAT4 expression	r value	-0.42
	p value	**0.01**
T2DM patients with sitagliptin		
STAT4 expression	r value	0.26
	p value	0.12
Healthy controls		
STAT4 expression	r value	-0.065
	p value	0.71

Results of Pearson correlation test are shown with r and p values.

In T2DM patients without sitagliptin, a significant negative correlation between the *STAT4* and *PIAS2* was found (p=0.01, Table 1). As indicated in Table 2, FPG was positively and negatively related to the *STAT4* and *PIAS2* expression in patients without sitagliptin, (p=0.004 and p=0.001, respectively). No obvious correlations between the HbA1c and *STAT4 / PIAS2* expression were observed in study groups (Table 2). No correlations in *STAT4* and *PIAS2* were observed in the control and the sitagliptin positive groups. The expression of *STAT4* and *PIAS2* was approximately similar between females and males in the different study groups (Table 3).

DISCUSSION

Chronic inflammation besides an excessive immune activation has received increased focus in T2DM pathogenesis (1). In this study, the gene expression of *STAT4* and its regulator, *PIAS2*, was investigated in T2DM with and without sitagliptin compared to healthy controls. The role of *STATs* as a trigger of inflammation has been suggested by immunological studies (2). *STAT4* participates in the pro-inflammatory immune process including Th1 differentiation and cytokine production (5). The inhibitory effect of *PIAS2* is performed by regulating multiple functional genes including *STAT4* (3). We first observed that the expression of *STAT4* in patients without sitagliptin was much higher than in the healthy controls, whereas the *PIAS2* expression was lower in the patients. *STAT4* expression was reversely related to *PIAS2*. In keeping with this finding, the alterations in *STATs/ PIASs* have previously been published in a diverse range of diseases. A higher mRNA level of *STAT4* in the synovial tissue of RA patients accompanied

Table 2. Correlation between the *STAT4/ PIAS2* expression and diabetes criteria in study groups.

		STAT4 expression	*PIAS2 expression*
T2DM patients without sitagliptin			
Fasting plasma glucose	r	0.56	-0.52
	p	**0.004**	**0.001**
HbA1c	r	0.29	-0.21
	p	0.08	0.20
T2DM patients with sitagliptin			
Fasting plasma glucose	r	-0.008	0.23
	p	0.96	0.18
HbA1c	r	0.13	0.21
	p	0.44	0.22
Healthy controls			
Fasting plasma glucose	r	-0.08	0.023
	p	0.64	0.87
HbA1c	r	-0.80	0.02
	p	0.64	0.87

Results of Pearson correlation test are shown with r and p values.

by correlation with RA progression and rheumatoid factor has been published (16). Activation of *STAT4* by IL-23 stimulation has been reported in multiple sclerosis patients (17). Consistent with our results, the enhanced phosphorylation of JAK2 and STAT3 were noticed in diabetes patients with macrovascular complication *in vitro* (18). Moreover, down-regulated *PIAS2* in RA fibroblast-like synovial cells has been reported (7). It seems that enhanced expression of *STAT4* and impaired expression of *PIAS2* might potentially lead to the amplification of inflammation in T2DM, and it may have an effect on the T2DM pathogenesis.

We next found out that sitagliptin has a regulatory effect on the aberrant expression of *STAT4* and *PIAS2*. The expression of *STAT4* was considerably reduced after 6 months of sitagliptin therapy while *PIAS2* expression was reduced. A few regulatory mechanisms of sitagliptin have been previously reported. For example, sitagliptin treatment reduces Th1 and Th17 cytokines including IFN-γ and IL-17, and increases Treg transcription factor, *FOXP3,* in the patients (13). Sitagliptin can reduce the excessive proliferation of T cells in T2DM (11). Moreover, the modulatory action of sitagliptin on *JAK2*, *STAT3* and suppressors of cytokine signaling (*SOCSs*) were recently demonstrated by our team (19). In a study on diabetic rats focusing on the JAK-STAT pathway, it has been reported that pJAK2/pSTAT3 were significantly diminished following sitagliptin therapy (12). It should be considered that some potential drugs targeting inhibitory genes such as SOCSs were already discussed in diabetes for the protection of pancreatic β-cell function and insulin secretion (20). Our results demonstrate that sitagliptin has a regulatory activity on *PIAS2* and *STAT4*. Further *in vivo* works are needed to evaluate the direct effect of sitagliptin on pancreatic β-cells. Also, the *STAT4* and *PIAS2* targets could be the potential aim for medical intervention.

We realized that increased levels of FPG in T2DM patients without sitagliptin were directly related to *STAT4* and negatively related to *PIAS2*. In line with this finding, a reverse connection among the IL-17 and HbA1c levels was reported in patients with retinopathy by Chen et al (21). Moreover, up-regulation of the *JAK* gene in diabetic mice leads to a deterioration in disease severity and it is linked to an albuminuria complication (22). This finding suggests that *STAT4* and *PIAS2* might have a role in the glucose metabolism by reducing inflammation. However, further works are needed to know the mechanism of action of STAT4 and PIAS2 on diabetes-related clinical parameters.

This work has some limitations. We considered only the mRNA levels of *STAT4* and *PIAS2* genes in PBMCs. Flow cytometric or blotting experiments could be applied to confirm the alteration of these molecules in protein levels. Several cytokines such as IL-12, IL-2, IFNs, and IL-23 could activate or regulate *STAT4* and *PIAS2* signaling molecules, and the contribution of the unique cytokines in relation to *STAT4* and *PIAS2* might require further exploration.

Table 3. Comparison of *STAT4* and *PIAS2* expression in different genders of study groups.

T2DM patients without sitagliptin			
	Female	Male	p value
STAT4 expression	0.018 ± 0.017	0.20 ± 0.02	0.35
PIAS2 expression	0.0019 ± 0.001	0.002 ± 0.003	0.19
T2DM patients with sitagliptin			
STAT4 expression	0.010 ± 0.006	0.012 ± 0.008	0.34
PIAS2 expression	0.0047 ± 0.004	0.0054 ± 0.005	0.87
Healthy controls			
STAT4 expression	0.008 ± 0.006	0.011 ± 0.007	0.29
PIAS2 expression	0.0051 ± 0.0049	0.0056 ± 0.0043	0.79

Mean ± SD values are shown

Following studies could confirm these observations in isolated T cells by using recombinant cytokines to clarify the specific signaling pathways. Moreover, it could be beneficial to investigate the follow-up effects of sitagliptin in the T2DM patients.

CONCLUSION

Impaired gene expression levels of *PIAS2* and elevated mRNA levels of *STAT4* in T2DM patients who did not receive sitagliptin were demonstrated by this study. The beneficial effects of sitagliptin were illustrated by the up-regulation of *PIAS2* and down-regulation of *STAT4* in the T2DM patients. Therefore, sitagliptin might have an immunomodulatory role in the reduction of T2DM-related inflammation through *STAT4* and *PIAS2* molecules. This finding illustrated probable mechanisms underlying the anti-inflammatory action of dipeptidyl peptidase 4 inhibitor, sitagliptin.

Ethics Committee Approval: The study was approved by the ethics committee of Hamadan University of Medical Sciences, Iran (Approval number: IR.UMSHA.REC.1402.364).

Informed Consent: Signed consent was obtained from the participants.

Peer-review: Externally peer-reviewed.

Authors' Contributions: Conception/ design of Study- M.B.; Data acquisition: S.N., F.S., M.B.; Data Analysis/Interpretation: M.B., A.Z.; Drafting Manuscript: S.N., M.B.; Critical Revision of Manuscript: S.N., F.S., A.Z., M.B.; Final Approval and Accountability: S.N., F.S., A.Z., M.B.

Conflict of Interest Statement: All authors declare that they have no conflicts of interest.

Financial Disclosure: This study has been adapted from an MSc thesis at Hamadan University of Medical Sciences. The study was funded by the Vice-chancellor for Research and Technology, Hamadan University of Medical Sciences, Hamadan, Iran (Number: 140205244164).

REFERENCES

1. Donath MY, Shoelson SE. Type 2 diabetes as an inflammatory disease. Nat Rev Immunol 2011; 11(2): 98-107.
2. Liang Y, Pan HF, Ye DQ. Therapeutic potential of STAT4 in autoimmunity. Expert Opin Ther Targets 2014; 18(8): 945-60.
3. Shuai K, Liu B. Regulation of gene-activation pathways by PIAS proteins in the immune system. Nat Rev Immunol 2005; 5(8): 593-605.
4. O'Shea JJ, Lahesmaa R, Vahedi G, Laurence A, Kanno Y. Genomic views of STAT function in CD4+ T helper cell differentiation. Nat Rev Immunol 2011; 11(4): 239-50.
5. Yang C, Mai H, Peng J, Zhou B, Hou J, Jiang D. STAT4: an immunoregulator contributing to diverse human diseases. Int J Biol Sci 2020; 16(9): 1575-85.
6. Magalhaes J, Tresse E, Ejlerskov P, Hu E, Liu Y, Marin A, et al. PIAS2-mediated blockade of IFN-beta signaling: a basis for sporadic Parkinson disease dementia. Mol Psychiatry 2021; 26(10): 6083-99.
7. Xiao J, Cai X, Zhou W, Wang R, Ye Z. Curcumin relieved the rheumatoid arthritis progression via modulating the linc00052/miR-126-5p/PIAS2 axis. Bioengineered 2022; 13(4): 10973-83.
8. Ueno H. The IL-12-STAT4 axis in the pathogenesis of human systemic lupus erythematosus. Eur J Immunol 2020; 50(1): 10-6.
9. Remmers EF, Plenge RM, Lee AT, Graham RR, Hom G, Behrens TW, et al. STAT4 and the risk of rheumatoid arthritis and systemic lupus erythematosus. N Engl J Med 2007; 357(10): 977-86.
10. Lee M, Rhee MK. Sitagliptin for Type 2 diabetes: a 2015 update. Expert Rev Cardiovasc Ther 2015; 13(6): 597-610.
11. Mahabadi-Ashtiyani E, Sheikh V, Borzouei S, Salehi I, Alahgholi-Hajibehzad M. The increased T helper cells proliferation and inflammatory responses in patients with type 2 diabetes mellitus is suppressed by sitagliptin and vitamin D3 in vitro. Inflamm Res 2019; 68(10): 857-66.
12. Al-Rasheed NM, Al-Rasheed NM, Hasan IH, Al-Amin MA, Al-Ajmi HN, Mahmoud AM. Sitagliptin attenuates cardiomyopathy by modulating the JAK/STAT signaling pathway in experimental diabetic rats. Drug Des Devel Ther 2016; 10: 2095-107.

13. Telikani Z, Sheikh V, Zamani A, Borzouei S, Salehi I, Amirzargar MA, et al. Effects of sitagliptin and vitamin D3 on T helper cell transcription factors and cytokine production in clinical subgroups of type 2 diabetes mellitus: highlights upregulation of FOXP3 and IL-37. Immunopharmacol Immunotoxicol 2019; 41(2): 299-311.
14. Alahgholi-Hajibehzad M, Durmus H, Aysal F, Gulsen-Parman Y, Oflazer P, Deymeer F, et al. The effect of interleukin (IL)-21 and CD4(+) CD25(++) T cells on cytokine production of CD4(+) responder T cells in patients with myasthenia gravis. Clin Exp Immunol 2017; 190(2): 201-7.
15. Borzouei S, Gholamian-Hamadan M, Behzad M. Impact of interleukin-32alpha on T helper cell-related cytokines, transcription factors, and proliferation in patients with type 2 diabetes mellitus. Immunopharmacol Immunotoxicol 2023; 45(3): 268-76.
16. Walker JG, Ahern MJ, Coleman M, Weedon H, Papangelis V, Beroukas D, et al. Characterisation of a dendritic cell subset in synovial tissue which strongly expresses Jak/STAT transcription factors from patients with rheumatoid arthritis. Ann Rheum Dis 2007; 66(8): 992-9.
17. Lee PW, Smith AJ, Yang Y, Selhorst AJ, Liu Y, Racke MK, et al. IL-23R-activated STAT3/STAT4 is essential for Th1/Th17-mediated CNS autoimmunity. JCI Insight 2017; 2(17): e91663.
18. Yang M, Tian M, Zhang X, Xu J, Yang B, Yu J, et al. Role of the JAK2/STAT3 signaling pathway in the pathogenesis of type 2 diabetes mellitus with macrovascular complications. Oncotarget 2017; 8(57): 96958-69.
19. Rezaeepoor M, Hoseini-Aghdam M, Sheikh V, Eftekharian MM, Behzad M. Evaluation of Interleukin-23 and JAKs/STATs/SOCSs/ROR-gammat expression in type 2 diabetes mellitus patients treated with or without sitagliptin. J Interferon Cytokine Res 2020; 40(11): 515-23.
20. Feng X, Tang H, Leng J, Jiang Q. Suppressors of cytokine signaling (SOCS) and type 2 diabetes. Mol Biol Rep 2014; 41(4): 2265-74.
21. Chen H, Ren X, Liao N, Wen F. Th17 cell frequency and IL-17A concentrations in peripheral blood mononuclear cells and vitreous fluid from patients with diabetic retinopathy. J Int Med Res 2016; 44(6): 1403-13.
22. Zhang H, Nair V, Saha J, Atkins KB, Hodgin JB, Saunders TL, et al. Podocyte-specific JAK2 overexpression worsens diabetic kidney disease in mice. Kidney Int 2017; 92(4): 909-21.

Experimed 2023; 13(3): 163-169

Supplementary Table 1. Information of the study groups.

	T2DM patients without sitagliptin	T2DM patients with sitagliptin	Healthy controls
FPG level (mg/dL)*	139.69 ± 39.81	129.37 ± 27.01	89.25 ± 11.32
HbA1c level (%)*	7.35 ± 0.76	7.21 ± 1.13	4.69 ± 0.54
Duration of diabetes (year)	1.85 ± 0.74	1.95 ± 1.10	-
Body mass index (kg/m^2)	25.39 ± 4.17	24.86 ± 2.04	24.42 ± 2.77

FPG: Fasting plasma glucose, Mean ± SD values are shown and $p<0.05$ was considered significant using ANOVA.

*$p<0.001$; control group compared to each patient group.

Experimed 2023; 13(3): 170-173

ORIGINAL ARTICLE

DOI: 10.26650/experimed.1297722

Age and Regional Features of Quantitative Indicators of Lymphoid Nodules of the Human Intrahepatic Bile Ducts

Naile Aliyeva[1], **Sabina Shadlinskaya**[1]

[1]Department of Human Anatomy and Medical Terminology, Azerbaijan Medical University, Baku, Azerbaijan

ORCID ID: N.A. 0000-0001-8447-8092; S.S. 0000-0002-6672-3725

Cite this article as: Aliyeva N, Shadlinskaya S. Age and regional features of quantitative ındicators of lymphoid nodules of the human intrahepatic bile ducts. Experimed. Experimed 2023; 13(3): 170-173.

ABSTRACT

Objective: This study aimed to elucidate the age and regional characteristics of the quantitative indicators of lymphoid nodules the intrahepatic bile ducts in humans.

Materials and Methods: In our study, the lymphoid structures of the intrahepatic bile duct walls taken from the corpses of 48 people, including newborns, early childhood, puberty, adolescence, adulthood and, elderly were examined. Lymphoid formations were stained using Hellman's method, a macro microscopic method. The digital data obtained during the study were subjected to statistical processing. At the same time, the general recommendations for medical and biological research were observed.

Results: A macro microscopic study of lymphoid formations in the human intrahepatic bile ducts showed that lymphoid formations in the walls of these organs were represented by lymphoid nodules and diffuse lymphoid tissue. Lymphoid formations were determined in the neonatal period and throughout subsequent life. Lymphoid nodules on total preparations were detected as dark (mostly dark blue) structures located against a lighter background of the surrounding organ wall. The peripheral contours of the lymphoid nodules were clearly defined, and the germinal centers were constantly absent. The number of lymphoid nodules was maximal in the lobular ducts and minimal in the common bile duct. This indicator was increased from the neonatal period to early childhood and then gradually decreased.

Conclusion: The results of this study have revealed that lymphoid nodules of the intrahepatic bile ducts acquire maximum development in early childhood. Further, the morphometric parameters of the lymphoid structures gradually decrease, and involutive transformations were noted.

Keywords: Intrahepatic bile ducts, lymphoid nodules, diffuse lymphoid tissue, regional characteristics

INTRODUCTION

In modern times, chronic liver diseases, including cirrhosis, annually cause the deaths of more than 1 million people (1, 2). Every tenth inhabitant of the globe suffers from diseases of the liver and biliary tract, which indicates the importance of early and adequate diagnosis (3, 4). Therefore, the liver remains the focus of attention not only for surgeons and therapists but also for morphologists (5, 6).

There are many studies in the literature about lymphoid formations being the source of many diseases (7-11). The study aimed to elucidate the age and regional characteristics of the quantitative indicators of lymphoid nodules of the human intrahepatic bile ducts.

MATERIALS AND METHODS

The material of the study consisted of the lymphoid structures of the intrahepatic bile duct walls obtained from the corpses of 48 people who died at different ages, from the neonatal period to old age, as newborns, early childhood, puberty, adolescence, adulthood, and elderly.

In our study, when creating the groups, it was taken into account that the people were healthy throughout their lives

Corresponding Author: Naile Aliyeva **E-mail:** medun91@mail.ru
Submitted: 17.05.2023 **Revision Requested:** 29.07.2023 **Last Revision Received:** 28.08.2023 **Accepted:** 28.09.2023 **Published Online:** 01.12.2023

and that they lost their lives due to various injuries, asphyxia, and acute poisoning. Cases with concomitant diseases of the immune system, and large glands of the body (liver, pancreas) were excluded from the general sample group.

The study used a macro microscopic method for the study of total preparations. After the removal of the liver, the bile ducts were separated from the surrounding tissues. The isolated preparations were washed with a light stream of running water. The lymphoid formations thus obtained on total preparations were stained according to the method of Hellman T. (12). Total preparations were initially placed for 2-3 days in a 3% solution of acetic acid (until the walls of these organs became transparent), then washed in running water. Harris hematoxylin was used to stain lymphoid nodules. Staining was carried out within 36–48 hours.

Statistical Analyses

The digital data obtained during the study were carried out for statistical evaluations using the programs of the Statistical Packages MS Excel 2016 and SPSS 22 (13, 14).

For a preliminary assessment of the difference between the variation series, the parametric criterion Student-t test was used. Further, to compare and determine the reliability of quantitative differences in groups and subgroups, a non-parametric rank, Mann-Whitney U test was used. The mean values of the obtained samples, standard errors, minimum (min), and maximum (max) values of the series were calculated. $p<0.05$ was accepted as the significance limit.

RESULTS

A macro microscopic study of lymphoid formations in the human intrahepatic bile ducts showed that lymphoid formations in the walls of these organs were represented by lymphoid nodules and diffuse lymphoid tissue. Lymphoid formations were determined in the neonatal period and throughout subsequent life.

Lymphoid nodules on total preparations were detected as dark (mostly dark blue) structures located against a lighter background of the surrounding organ wall. The peripheral contours of the lymphoid nodules were clearly defined, but the germinal centers were constantly absent (Figure 1).

On total preparations, we counted the number of lymphoid nodules in the walls of these organs (Table 1).

The number of lymphoid nodules in the wall of the common hepatic duct compared with newborn children in early childhood was increased by 1.72 times ($p<0.001$), and was then gradually decreased. In comparison with early childhood, this indicator decreased in puberty by 1.39 times ($p<0.01$), in people in the 1st period of adulthood by 1.76 times ($p<0.001$), and in senile age by 2.93 times ($p<0.001$).

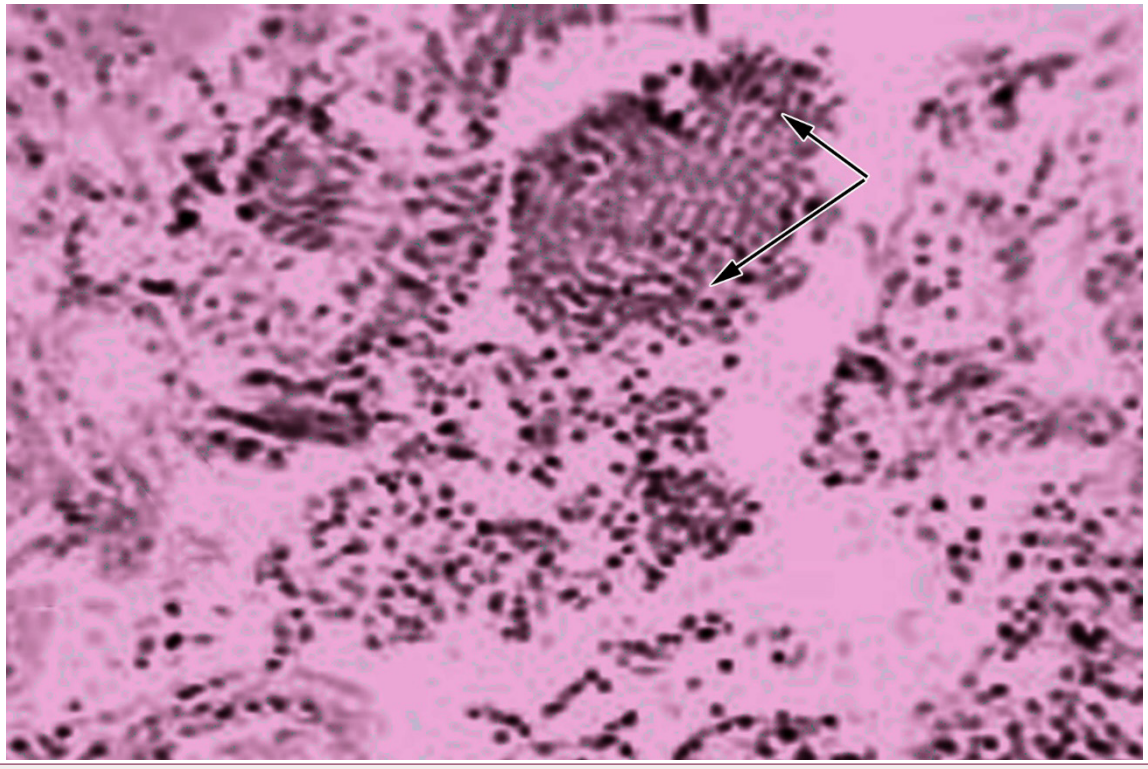

Figure 1. Lymphoid nodule in the wall of the common hepatic duct (indicated by arrows). Cross section. Hematoxylin-eosin staining. Magnification 96X

Table 1. The number of lymphoid nodules per area of 1 cm^2 walls of the intrahepatic bile ducts of humans of different periods.

		Number of lymphoid nodules, bile ducts		
Life Periods	**n**	**Common bile duct [a]**	**Interlobar ducts [a]**	**Lobular ducts[a]**
Newborns	6	35.2 ± 1.1 (28-40)	30.0 ± 1.2 (24-38)	20.4 ± 1.5 (16-32)
Early childhood	5	85.6 ± 4.4 (50-98)[1, 2]	64.2 ± 3.6 (33-72)[1, 2]	35.2 ± 3.5 (26-64)[2, 3]
Puberty	8	63.4 ± 4.7 (44-80)	45.2 ± 3.9 (30-60)	25.3 ± 4.2 (20-52)
Adolescence	8	60.0 ± 4.7 (40-76)	40.0 ± 3.3 (29-54)	22.8 ± 3.7 (18-46)
Adulthood	10	54.2 ± 3.2 (32-64)	32.2 ± 2.4 (26-50)	20.0 ± 3.0 (12-42)
Elderly	11	30.2 ± 4.1 (15-56)	24.5 ± 2.9 (13-42)	16.2 ± 3.0 (10-40)

[1]: p<0.01, versus Puberty

[2]: p<0.001, versus Newborns, Adulthood, and Elderly

[3]: p<0.01, versus Adolescence

[a]: Values are shown as mean ± standard errors (min-max).

n: Number of observations

The number of lymphoid nodules in the wall of the interlobar ducts, compared with neonates in early childhood, increased by 2.14 times (p<0.001), reaching maximum numbers during postnatal ontogenesis. In comparison with early childhood, this indicator was decreased in puberty by 1.42 times (p<0.01), in the first period of adulthood by 1.99 times (p<0.001), and in senile age by 3.21 times (p<0.001).

The number of lymphoid nodules in the wall of the lobular ducts were maximal in early childhood, when the value of this indicator was 2.43 times (p<0.001) higher than in newborns. Compared with this indicator in the period of early childhood, the value decreased in adolescents by 1.35 times (p<0.01), in the first period of adulthood by 1.58 times (p<0.001), and in senile age by 3.03 times (p<0.001).

Thus, the number of lymphoid wall nodules from the lobular ducts to the common bile duct was found to be increased. This indicator has been increasing from the neonatal period to early childhood and was then gradually decreasing during postnatal ontogenesis.

DISCUSSION

According to our data, lymphoid formations in the intrahepatic bile ducts of a human are constantly determined in the walls of these organs, being detected in the neonatal period and throughout subsequent life. In this regard, our results were supported by Yunusov R. who believes that lymphoid structures (lymph follicles in the author's terminology) were present only occasionally (15).

Analysis of morphometric studies showed that lymphoid formations of the intrahepatic bile ducts acquired the maximum development in early childhood, which is typical for many other immune organs (1, 7, 8, 15).

According to Shadlinskaya S. (11) the number and size of lymphoid formations of the vaginal vestibule was individually variable. The level of variability (amplitude of the variation series of indicators) was mainly increased during postnatal ontogenesis. The amplitude of the variational series of dimensional indicators of the lymphoid structures in newborns and early childhood was more than that of women of adulthood periods, elderly and senile ages (11).

Further, as these indicators gradually decrease, involutive transformations are noted. The involution of the lymphoid tissue is manifested by a decrease in the number of lymphoid nodules, which progressively increases with age.

According to Huseynov B. (9), maximal development in lymphoid formations of the trachea and main bronchi were acquired in early childhood. Further, the morphometric parameters of the lymphoid structures were gradually decreased, and involutive transformations were noted. The involution of lymphoid tissue is manifested by a decrease in the number and size of lymphoid nodules, a decrease in the density of the arrangement of cells of the lymphoid series in their composition and in diffuse lymphoid tissue, which progressively increases towards the elderly and senile ages (9).

Ethics Committee Approval: Approval was received from the Ethics Committee of Azerbaijan Medical University (dated 05.07.2023 and numbered 28).

Informed Consent: Consent was obtained from the relatives of 48 people.

Peer-review: Externally peer-reviewed.

Authors' Contributions: Conception/ design of Study- N.A., S.S.; Data acquisition: N.A.; Data Analysis/Interpretation: S.S.; Drafting Manuscript: N.A.; Critical Revision of Manuscript: S.S.; Final Approval and Accountability: N.A., S.S.

Conflict of Interest: All authors declare that they have no conflicts of interest.

Financial Disclosure: The authors declare that this study has received no financial support.

REFERENCES

1. Baumann U, Ure B. Biliary atresia. Clin Res Hepatol Gastroenterol 2012; 36(3): 257-59
2. IOM (Institute of Medicine). Hepatitis and liver cancer: a national strategy for privet control of hepatitis B and C. Washington: National Academies Press. 2010.
3. Dietrich P, Hellerbrand C. Non-alcoholic fatty liver disease, obesity and the metabolic syndrome. Best Pract Res Clin Gastroenterol 2014; 28(4): 637-53.
4. Alswat K, Fallatah H, Al-Judaibi B, Elsiesy H, Al-Hamoudi W Adel N. et al. Qutub Position statement on the diagnosis and management of non-alcoholic fatty liver disease. Saudi Med 2019; 40(6): 531-40.
5. Garg S, Kumar KH, Sahni D, Yadav T, Aggarwal A, Gupta T. Anatomy of the hepatic arteries and their extrahepatic branches in the human liver: A cadaveric study. Ann Anat 2020; 227: 151409.
6. Kruepunga N, Hakvoort T, Hikspoors J, Köhler S, Lamers W. Anatomy of rodent and human livers: What are the differences? Biochim Biophys Acta Mol Basis Dis 2019; 1865(5): 869-78.
7. Lee S, Nodit L. Phyllodes tumor of vulva: a brief diagnostic review. Arch Pathol Lab Med 2014; 138(11): 1546-50.
8. Allahverdiev M. Structural - functional characteristics and patterns of morphogenesis of the glandular and lymphoid apparatuses of the human extrahepatic biliary tract in postnatal ontogenesis. Abstract of diss. doctor of medical sciences. Baku, 2007.
9. Huseynov B. Morphological features of the glands and lymphoid structures of the trachea and main bronchi in humans in postnatal ontogenesis and in the experiment in rats exposed to water procedures with different salt composition. Abstract of diss. doctor of medical sciences. Baku, 2011.
10. Huseynova G. Structural and functional characteristics and features of the morphogenesis of the glands and lymphoid formations of the bladder in postnatal ontogenesis in the norm and in the experiment. Abstract of diss. doctor of medical sciences. Baku, 2013.
11. Shadlinskaya S. Macro microscopic anatomy, regularities of morphogenesis of small glands and lymphoid formations of the vaginal vestibule in human's postnatal ontogenesis and in experiment. Abstract of diss. doctor of medical sciences. Baku, 2021.
12. Hellman T. Studien uber das lymphoid Gewebe. Beit Path Anat All Pathol 1921; 68: 333-63
13. Glantz S. Medico-biological statistics. Moscow. Practice .1999. 200p.
14. Borovikov VP. A popular introduction to modern data analysis in the STATISTICA system. Moscow. Telecom. 2015. 288p.
15. Yunusov R. Lymphoid accumulations of the walls of the human trachea and bronchi in postnatal ontogenesis: Abstract of diss. candidate of medical sciences. Andijan. 1988

Experimed 2023; 13(3): 174-179

ORIGINAL ARTICLE

DOI: 10.26650/experimed.1326693

Efficacy of Speleotherapy on Atopic Bronchial Asthma in Children

Lala Allahverdiyeva[1], Naila Efendiyeva[1], Afag Khalilova[2]

[1]Department of Allergy and Clinical Immunology, Azerbaijan Medical University, Baku, Azerbaijan
[2]Department of Immunology, Scientific Research Center, Azerbaijan Medical University, Baku, Azerbaijan

ORCID ID: L.A. 0009-0001-6838-5088; N.E. 0009-0004-6708-3792; A.K. 0000-0002-4452-1516

Cite this article as: Allahverdiyeva L, Efendiyeva N, Khalilova A. Efficacy of speleotherapy on atopic bronchial asthma in children. Experimed. Experimed 2023; 13(3): 174-179.

ABSTRACT

Objective: Despite stunning advances in drug treatment, the present modern drugs that are used in the treatment of bronchial asthma don't always achieve complete control over the disease. It may be useful to get support from complementary and alternative medicine (CAM) in such cases. CAM is understood as a non-traditional treatment, one of the varieties of which is speleotherapy. With the purpose of studying the therapeutic effect of speleotherapy in children, a treatment of speleotherapy was conducted for 50 children and adolescents suffering from atopic bronchial asthma.

Materials and Methods: To evaluate the effectiveness of speleotherapy, the following research methods were used: Spirometry method was used to assess the ventilation function of the lungs, nitric oxide in exhaled air was measured for the assessment of airway inflammation, and laboratory examination of patients were evaluated including Interleukin (IL)-5, IL-13 and Interferon-gamma (IFN-γ) in serum by using enzyme-linked immunosorbent assay (ELISA).

Results: As a result of the speleotherapy, patients improved their external respiratory function. The study also showed a positive impact with speleotherapy on exhaled nitric oxide and cytokine parameters in children with mild and moderate atopic bronchial asthma.

Conclusion: Speleotherapy, as a method of medical rehabilitation for patients with bronchial asthma, leads to a decrease in the number of attacks, reduces the use of bronchodilators, and improves the indicators of the function of external respiration.

Keywords: Allergy, asthma, children, nitric oxide, speleotherapy, spirometry

INTRODUCTION

Asthma is a chronic inflammatory disorder that affects the airways and causes coughing, chest tightness, shortness of breath, and wheezing. Atopic (allergic) asthma is the most common type of asthma in children and characterized by airway hyper-responsiveness to an allergen (1, 2). This form of asthma develops due to Immunoglobulin E (Ig E)-type hypersensitivity reactions, generally in response to inhaled allergens. The airways of individuals with allergic asthma are infiltrated by activated T lymphocytes, mast cells, eosinophils, and other cells that are involved in type 2 inflammation (3, 4). Exposure to a variety of trigger factors results in the contraction of smooth muscle of airways and subsequently asthma attacks.

There are many international recommendations and guidelines for effective asthma treatment and management. Currently, there are multiple advanced medications that are used in the treatment of bronchial asthma. Despite this, full control of the disease is not always achieved. In such cases, non-pharmacological treatment and medical rehabilitation must be applied. Complementary and alternative medicine (CAM) is the term used to refer to unconventional treatment (5, 6). Speleotherapy is one of the CAM options for an allergic form of bronchial asthma. Speleotherapy is an adjuvant therapy for asthma in caves and salt mines that is only available in certain areas of the world (7, 8).

These caves are characterized by a specific microclimate (speleoclimate), that is associated with stable temperature, absence of irritants, pollutants, and allergens, high

Corresponding Author: Afag Khalilova **E-mail:** afakhalilova@gmail.com
Submitted: 12.07.2023 **Revision Requested:** 29.07.2023 **Last Revision Received:** 08.09.2023 **Accepted:** 01.11.2023 **Published Online:** 04.12.2023

humidity, and specific ratio of microelements such as Na^{+}, Cl^{-}, Mg^{+2} and Ca^{+2} ions (9, 10). Studies revealed that microclimate has a beneficial effect on the functioning of the respiratory system of asthmatic patients and provides bronchodilation and mucolytic effects, hyposensitivity, immunoprotective, and restorative effects. All this makes it possible to widely use speleotherapy in pediatrics (11).

MATERIALS AND METHODS

Study Group

The study was approved by the Ethics Committee (Protocol No: 28) of Azerbaijan Medical University. Parents signed a consent form for their children to participate in this study.

To investigate the therapeutic effects of speleotherapy in bronchial asthma, new research was conducted on children in Azerbaijan Nakhcivan "Duzdag" Physiotherapy Center. This study included a test group that comprised 50 children and adolescents (37 boys, 13 girls) aged between 5-18 years suffering from atopic bronchial asthma. The mean age of 50 children was 11.2 ± 0.4 years. The test group completed a course of speleotherapy in the Nakhchivan Physiotherapy Center "Duzdag Magara". The study also included a comparison group consisting of 30 children with asthma who received only drug treatment (basis therapy) and the control group, which included 10 healthy children without allergic diseases and with a negative history of allergy.

The selection criteria for the test group were the presence of an established diagnosis of atopic bronchial asthma and the absence of its exacerbation for the period of treatment. The study included children diagnosed with mild and moderate persistent asthma. The age of disease onset was 5.0 ± 0.2; the method of the treatment was 15 procedures per day.

Speleotherapy Regimen

Speleotherapy was carried out in the post-attack period under the following scheme: adaptation - main regimen - re-adaptation. The adaptation regimen was conducted during the first 2 days during daylight hours and the underground section stayed according to the following scheme: 4 hours - for children over 10 years and 1.5-2 hours – for children from 5 to 10 years.

The main regimen included a day stay in the speleo section. Children between 5 and 10 years of age were given a 4-hour day sleep in a salt cave. Children over the age of 10 were allowed to sleep in a salt cave for 8-9 hours at night. The re-adaptation regimen included 2 hours for children between 5-10 years, a 4-hour day stay for over the age of 10 years in caves in the last 2 days of treatment and that allowed us to avoid the risk of withdrawal syndrome.

Lung Function Studies

Lung function was evaluated by determining the spirometric indices, such as forced vital capacity (FVC), forced expiratory

Table 1. Subgroup analyses of the effect of speleotherapy on pulmonary function.

Parameters (%)	pre-treatment and post-treatment values	Patients Groups			
		Group I (n=23)	p value	Group II (n=27)	p value
FVC	pre-treatment values	83.3 ± 1.6	p<0 .01	80.5 ± 1.5	p<0 .01
	post-treatment values	100.5 ± 2.6		97.0 ± 1.9	
FEV1	pre-treatment values	70.9 ± 1.6	p<0 .01	67.6 ± 1.2	p<0 .01
	post-treatment values	96.7 ± 2.1		88.4 ± 2.2	
FEV1/FVC	pre-treatment values	92.9 ± 1.8	p<0 .05	76.0 ± 1.2	p<0 .01
	post-treatment values	77.2 ± 6.1		90.7 ± 1.3	
FEF	pre-treatment values	61.0 ± 4.0	p<0 .01	51.0 ± 1.6	p<0 .01
	post-treatment values	79.7 ± 3.6		77.4 ± 2.5	
PEF	pre-treatment values	70.0 ± 2.0	p<0 .01	65.1 ± 1.2	p<0 .01
	post-treatment values	83.1 ± 2.6		80. 9± 2.9	

Abbreviations: FVC: forced vital capacity; FEV1: forced expiratory volume in the first second; FEV1/FVC: forced expiratory volume in 1 sec as a percentage of FVC; FEF: forced expired flow at 25–75%; PEF: Peak expiratory flow.

Values are shown as mean ± standard deviation. Group I - children with mild asthma; Group II - children with moderate persistent asthma

volume in the first second (FEV1), forced expiratory volume in the first second as a percentage of FVC (FEV1/ FVC %), forced expired flow at 25–75% of FVC (FEF 25-75%), peak expiratory flow (PEF). Spirometric values were evaluated with the standard values and the results were expressed in percentages.

Measurement of Fractional Exhaled Nitric Oxide (FeNO)

FeNO is an endogenous gas that can be measured in a human breath test in the presence of airway inflammation. The determination of the marker of airway inflammation, FeNO was carried out by using the non-invasive and portable analyzer; NIOX MINO (Aerocrine AB, Solna, Sweden).

Analysis of Serum Cytokine

The laboratory examination of patients included the study of Interleukin (IL)-5, IL-13, and Interferon-gamma (IFN-γ) in the serum by enzyme-linked immunosorbent assay (ELISA).

Statistical Analyses

Statistical processing of the obtained results was carried out using the non-parametric pairing criterion W-Wilcoxon-a in the Statistical Package SPSS-26. Intergroup comparisons were carried out using the Mann-Whitney U test, and intra-group comparisons were carried out in MS Excel-2000 and SPSS-26 with Wilcoxon criteria. $p<0.05$ was accepted as significant.

RESULTS

The effect of speleotherapy on the amount (volume) and speed (flow) of air that was inhaled or exhaled from the lungs was carried out by dynamic control before and after speleo treatment. At the end of the speleotherapy, patients showed positive changes in the values of lung function.

In asthmatic children with a mild form of bronchial asthma, after a treatment of speleotherapy, FVC was improved significantly from 81.3 ± 1.6% to 100.5 ± 2.6% ($p<0.01$), FEV1 was improved and reached from 70.9 ± 1.6% to 96.7 ± 2.1 ($p<0.01$), FEV1/FVC was increased from 78.9 ± 1.5% to 92.9 ± 1.8% ($p<0.05$), FEF 25-75% was changed from 61.0 ± 4.0% to 79.7 ± 3.6% ($p<0.01$), and finally PEF was increased from 70.0 ± 2.0% to 83.1 ± 2.6% ($p<0.01$) (Table 1). Changes were found only in patients with mild asthma receiving only basic treatment: FVC from 82.4 ± 1.6% to 89.7 ± 2.2% ($p=0.005$), FEV1 from 67.9 ± 1.7% to 79.7 ± 1.7% ($p=0.003$), FEV1/FVC from 77.0 ± 2.1% to 85.0 ± 2.0% ($p=0.003$), FEF from 25-75% 55.5 ± 2.5% to 67.5 ± 3.6% ($p=0.005$), PEF from 70.0 ± 2.0% to 83.1 ± 2.6% ($p<0.001$).

In children with moderate persistent bronchial asthma, positive changes were also observed in lung function after the treatment of speleotherapy. These patients had increased their VC on average by 20.5% (pretreatment value: 80.5 ± 1.5%, posttreatment value: 97.0 ± 1.9%, $p<0.001$), FEV1 by 30.8% (pretreatment value: 67.6 ± 5.2%, posttreatment value: 88.4 ± 7.5%, $p<0.01$), FEV1/VC by 19.8% (pretreatment value: 76.0 ± 1.2%, posttreatment value: 90.7 ± 1.3%, $p<0.01$), FEF 25-75% by 51.7% (pretreatment value: 51.0 ± 1.6%, posttreatment value: 77.4 ± 2.5%, $p<0.01$), PEF by 24.3% (pretreatment value: 65.1 ± 1.2%, posttreatment value: 80.9 ± 2.9%, $p<0.01$). The results show an improvement in bronchial passage at the small, medium, and large bronchi. The indicators of the main treatment group changed as follows: FVC (pretreatment value: 80.9 ± 1.1%, posttreatment value: 89.1 ± 1.9%, $p<0.001$), FEV1 (pretreatment value: 64.0 ± 1.5%, posttreatment value: 77.9 ± 1.5%, $p<0.001$), FEV1/VC by (pretreatment value: 76.1 ± 1.2%, posttreatment value: 82.1 ± 4.4%, $p=0.012$), FEF 25-75% (pretreatment value: 52.5 ± 2.3%, posttreatment value: 64.7 ± 2.5%, $p<0.001$), PEF (pretreatment value: 65.8 ± 1.2%, posttreatment value: 76.3 ± 2.0%, $p<0.001$). In both groups, a positive dynamic change in spirometric indicators was observed. In the group where speleotherapy was performed, the increase in indicators was more significant than the other group.

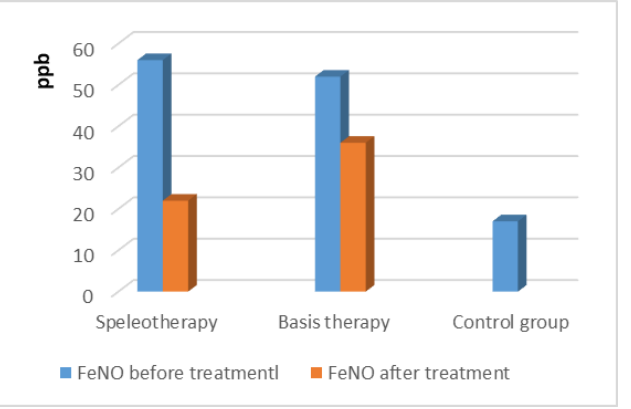

Figure 1. Nitric oxide levels in the exhaled air in children with mild persistent atopic bronchial asthma

Abbreviations: FeNO: Fractional exhaled nitric oxide

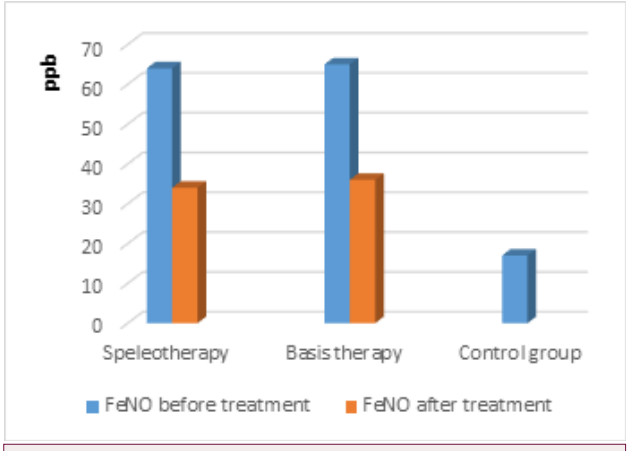

Figure 2. Nitric oxide levels in the exhaled air in children with persistent atopic bronchial asthma of moderate severity

Abbreviations: FeNO: Fractional exhaled nitric oxide

The effectiveness of speleotherapy was evaluated by measurement of FeNO. Prior to treatment, the level of FeNO in all patients, even with a mild form of the disease, was significantly increased compared to the healthy group (17.9 ± 2.4 ppb; p=0.001). Thus, the level of nitric oxide in the exhaled air of patients with a mild course receiving basic therapy was 52.8 ± 4 ppb (p<0.001), in the moderate course of the disease was 65.8 ± 4.6 ppb (p<0.001). In patients with mild disease that undergo complex treatment, the level of FeNO in the exhaled air was 56.9 ± 5.6 ppb (p<0.001) and was 64.0 ± 3.1 ppb (p<0.001) in case of moderate asthma (Figure 1). An increase in the amount of nitric oxide in the exhaled air confirmed the presence of persistent allergic inflammation in the respiratory tract (Figure 2).

The level of FeNO in the exhaled air of patients receiving only basic treatment after treatment was 36.5 ± 2.5 ppb (p=0.003) in a mild form of the disease and 44.0 ± 4.5 ppb (p<0.001) in a moderate form of the disease.

After 4 weeks of treatment, the patients showed a significant positive change in the level of FeNO, which was 22.2 ± 2.2 ppb (p<0.001) and 34.3 ± 33.2 ppb (p<0.001), respectively, reflecting the improvement of the clinical performance against the background of speleotherapy. After 4 weeks, in patients who received speleotherapy, the level of FeNO was decreased by 2.6 times in mild form and 1.9 times in moderate form, against the background of basic treatment, these indicators were decreased by 1.4 and 1.5 times, respectively.

The level of nitric oxide in exhaled air was significantly reduced in patients with speleotherapy compared to the group receiving only basic treatment.

Thus, the obtained results suggest that the level of FeNO varies depending on the severity of the disease and the method of treatment. The level of nitric oxide in respiration, which is the main biomarker of eosinophilic allergic inflammation, decreased more significantly in patients with speleotherapy compared to the group receiving only basic treatment. This, in turn, gives a reason to consider a greater decrease in persistent allergic inflammation in the respiratory tract after speleotherapy.

In the remission period of the disease, in the absence of clinical symptoms, the effectiveness of speleotherapy was evaluated based on the dynamics of cytokine status indicators in our study. Analysis of the results of the cytokine study revealed a regular increase in Th2-like cytokines in patients receiving speleotherapy, depending on the severity of bronchial asthma.

In the group that received only basic treatment for the mild forms of the disease, IL-5 was 7.50 ± 1.12 pg/mL, (p=0.002), IL-13 was 7.38 ± 1.29 pg/mL (p=0.001), and IFN-γ was 3.30 ± 0.97 pg/mL (p=0.019). In the serum of children with mild disease, the level of IL-5 before speleotherapy treatment was 6.52 ± 0.59 pg/mL (p=0.008), with moderate asthma 8.24 ± 1.25 pg/mL (p=0.063). A similar positive improvement was observed for IL-13, whose average serum level before treatment was 5.82 ± 2.54 pg/mL (p=0.063) for mild asthma and 10.41 ± 3.44 pg/mL (p<0.001) for moderate asthma (p=0.094). As the severity of the disease worsened, the level of IFN-γ in the serum of patients decreased and was 2.44 ± 0.52 pg/mL (p=0.002) with mild asthma, with moderate asthma 1.81 ± 0.28 pg/mL (p<0.001).

After a course of speleotherapy treatment in children with mild atopic bronchial asthma, the level of IL-5 in the blood serum decreased to 4.37 ± 0.12 pg/mL (p=0.008). The IL-13 level after treatment also decreased to 1.44 ± 0.26 pg/mL (p=0.038). The IFN-γ level after treatment increased to 6.87 ± 0.93 pg/mL (p=0.008) (Figure 3). In the group where basic treatment was carried out for a mild form of the disease, IL-5 was 5.64 ± 0.49 pg/mL (p=0.225) IL-13 was 2.89±0.61 pg/mL (p=0.043), and IFN-γ was 4.80 ± 15 pg/mL (p=0.138).

In patients who received only basic treatment, with a moderate form, IL-5 decreased from 8.50 ± 2.02 pg/mL to 5.60 pg/mL (p=0.225), (decreased 1.4 times), IL-13 was 6.79 ± 2.12 pg/mL to 3.59 ± 0.98 pg/mL (p=0.063), (decreased by 1.8 times), IFN-γ decreased to 1.73; it increased from 0.24 pg/mL to 4.17 ± 0.97 pg/mL (p=0.128).

In the group of children with moderate asthma, the dynamics of the cytokines after the treatment of speleotherapy were the following. IL-5 level in blood serum decreased to 5.05 ± 0.2 pg/mL (p=0.001). The level of IL-13 after treatment decreased by

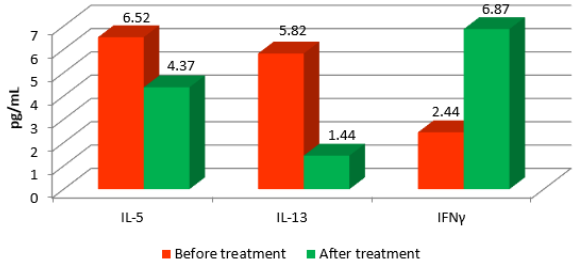

Figure 3. Cytokine indices in the mild course of bronchial asthma in the dynamics of speleotherapy.

Abbreviations: IL-5: Interleukin 5, IL-13: Interleukin 13, IFN-γ: Interferon-gamma

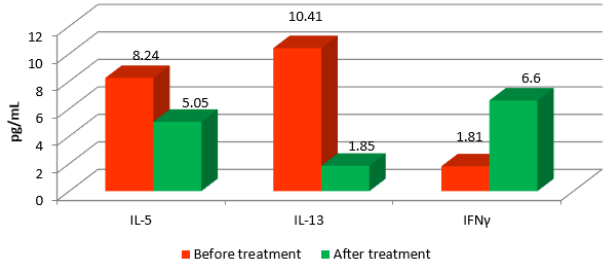

Figure 4. Indicators of cytokines in the medium-heavy bronchial asthma current in the cave therapy dynamics.

Abbreviations: IL-5: Interleukin 5, IL-13: Interleukin 13, IFN-γ: Interferon-gamma

5.6 times and was 1.85 ± 0.65 pg/mL (p=0.001). IFN-γ level after treatment increased by 3.6 times and became 6.60 ± 1.00 pg/mL (p<0.001) (Figure 4).

Thus, during the study of the cytokine profile of patients with atopic bronchial asthma in various variants of treatment, significant changes in the level of Th1 and Th2 cytokines were observed. In patients receiving speleotherapy, these changes have become more significant.

DISCUSSION

As a result of the study, the following was revealed. Before treatment, in all patients, even those with a mild form of the disease, the level of FeNO increased significantly compared to the healthy control group. In patients receiving basic treatment, the levels of FeNO in the exhaled air, hence an eosinophilic allergic inflammation, decreased after treatment compared to the state before treatment (p <0.001). The levels of FeNO in the exhaled air of patients with a mild and moderate form of the disease who received complex treatment with speleotherapy were decreased. After a 4-week course of treatment in patients who received speleotherapy, the level of FeNO in mild and moderate forms of asthma was decreased by 2.6 times and by 1.9 times respectively; against the background of basic treatment, these indicators decreased by 1.4 and 1.5 times, respectively (12).

Studies have shown a naturally positive effect of speleotherapy on cytokine parameters in children with mild and moderate atopic bronchial asthma after complex treatment compared to patients who received only basic treatment (13, 14). Assessment of pulmonary functions also showed improvements in patients after speleotherapy compared to the control group (15).

The "Duzdag Therapeutic Center" is a physiotherapeutic center with salt caves located in Nakhchivan Azerbaijan at an altitude of 1173 meters above sea level. The recreation center is an underground cavern hospital, providing conditions for optimal treatment and health measures. It is a center where atopic asthma and other chronic respiratory diseases are treated. The unique chemical composition of Duzdag salt that doesn't have analogs is: NaCl: 98.4% (highly dispersed aerosol), $MgCl_2$: 0.06%, $CaCl_2$: 0.04% (8).

Our study results revealed that remission of the disease depends on the severity which was observed in 70-80% of our patients and ranged from 6 months to 1-1.5 years due to the speleotherapy. As a method of medical rehabilitation for patients with bronchial asthma, speleotherapy leads to a decrease in the number of attacks, reduces the use of bronchodilators, and improves the indicators of the function of external respiration. The appointment of a course of speleotherapy for children with bronchial asthma according to an adapted scheme is of great practical importance since it may be useful in the treatment of the disease.

Ethics Committee Approval: The study was approved by the Ethics Committee (Protocol No: 28) of Azerbaijan Medical University.

Informed Consent: Parents signed a consent form for their children to participate in this study.

Peer-review: Externally peer-reviewed.

Authors' Contributions: Conception/ design of Study- L.A.; Data acquisition: N.E.; Data Analysis/Interpretation: A.K.; Drafting Manuscript: L.A., A.K.; Critical Revision of Manuscript: N.E.; Final Approval and Accountability: L.A., N.E., A.K.

Conflict of Interest: All authors declare that they have no conflicts of interest.

Financial Disclosure: The authors declare that this study has received no financial support.

REFERENCES

1. Campo P, Eguiluz Gracia I, Plaza Serón MC, Salas M, Rodríguez MJ, Pérez Sánchez N, et al. Bronchial asthma triggered by house dust mites in patients with local allergic rhinitis. Allergy 2019; 74(8): 1502-10.
2. Akar-Ghibril N, Casale T, Custovic A, Phipatanakul W. Allergic endotypes and phenotypes of asthma [published correction appears in J Allergy Clin Immunol Pract. 2020; 8(5): 1779]. J Allergy Clin Immunol Pract 2020; 8(2): 429-40.
3. Gong F, Zhu HY, Zhu J, Dong QJ, Huang X, Jiang DJ. Circulating CXCR5+CD4+ T cells participate in the IgE accumulation in allergic asthma. Immunol Lett 2018; 197: 9-14.
4. Tran TN, Zeiger RS, Peters SP, Colice G, Newbold P, Goldman M, et al. Overlap of atopic, eosinophilic, and TH2-high asthma phenotypes in a general population with current asthma. Ann Allergy Asthma Immunol 2016; 116(1): 37-42.
5. Fjær EL, Landet ER, McNamara CL, Eikemo TA. The use of complementary and alternative medicine (CAM) in Europe. BMC Complement Med Ther 2020; 20(1): 108.
6. Yildiz Y, Yavuz AY. Complementary and alternative medicine use in children with asthma. Complement Ther Clin Pract 2021; 43: 101353.
7. Bjermer L. Complementary and alternative treatment of asthma. Breathe 2005; 1(4): 288–95.
8. Beamon S, Falkenbach A, Fainburg G, Linde K. Speleotherapy for asthma. Cochrane Database Syst Rev 2001; (2): CD001741.
9. Horowitz S. Salt cave therapy: Rediscovering the benefits of an old preservative. Alt Comp Ther 2010; 16(3): 158–62.
10. Freidl J, Huber D, Braunschmid H, Romodow C, Pichler C, Weisböck-Erdheim R. et al Winter exercise and speleotherapy for allergy and asthma: a randomized controlled clinical trial. J Clin Med 2020; 9(10): 3311.
11. Mętel S, Kostrzon M, Adamiak J. Dynamic balance and chest mobility of older adults after speleotherapy combined with pulmonary rehabilitation, endurance and strength training-a prospective study in chronic respiratory diseases. Int J Environ Res Public Health 2022; 19(18): 11760.
12. Escamilla-Gil JM, Fernandez-Nieto M, Acevedo N. Understanding the cellular sources of the fractional exhaled nitric oxide (FeNO) and its role as a biomarker of type 2 inflammation in asthma. Biomed Res Int 2022; 2022: 5753524.

13. Akdis, C A, Arkwright PD, Brüggen MC, Busse W, Gadina M, Guttman-Yassky E., et al. Type 2 immunity in the skin and lungs. Allergy 2020; 75(7): 1582-605.
14. ten Hacken NH, Oosterhoff Y, Kauffman HF, Guevarra L, Satoh T, Tollerud DJ, et al.Elevated serum interferon-γ in atopic asthma correlates with increased airways responsiveness and circadian peak expiratory flow variation. Eur Respir J 1998; 11(2): 312-6.
15. Gallucci M, Carbonara P, Pacilli AMG, di Palmo E, Ricci G, Nava S. Use of symptoms scores, spirometry, and other pulmonary function testing for asthma monitoring. Front Pediatr 2019; 7: 54.

Experimed 2023; 13(3): 180-186

RESEARCH ARTICLE

DOI: 10.26650/experimed.1299445

Assessment of Cardiac Myosin-binding Protein C Levels in Coronavirus Disease 2019

Dilay Karabulut[1], Cennet Yildiz[1], Umut Karabulut[2], Ersan Oflar[1], Fatma Nihan Turhan Caglar[1], Kadriye Kart Yasar[3], Gulcin Sahingoz Erdal[4], Osman Pirhan[1], Pınar Kasapoglu[5], Nilgun Isiksacan[5]

[1]Department of Cardiology, Bakirkoy Dr. Sadi Konuk Education and Research Hospital, Istanbul, Turkiye.
[2]Department of Cardiology, Acibadem International Hospital, Istanbul, Turkiye.
[3]Department of Infectious Diseases, Bakirkoy Dr. Sadi Konuk Education and Research Hospital, Istanbul, Turkiye.
[4]Department of Medical Oncology, Bakirkoy Dr. Sadi Konuk Education and Research Hospital, Istanbul, Turkiye.
[5]Department of Biochemistry, Bakirkoy Dr. Sadi Konuk Education and Research Hospital, Istanbul, Turkiye.

ORCID ID: D.K. 0000-0003-1896-0096; C.Y. 0000-0003-2456-3206; U.K. 0000-0002-3947-9173; E.O. 0000-0002-0757-2496; F.N.T.C. 0000-0001-7925-2398; K.K.T. 0000-0003-2963-4894; G.S.E. 0000-0001-5815-5847; O.P. 0000-0002-4977-3958; P.K. 0000-0003-1703-2204; N.I. 0000-0002-0230-6500

Cite this article as: Karabulut D, Yildiz C, Karabulut U, Oflar E, Turhan Caglar FN, Kart Yasar K, et al. Assessment of cardiac myosin-binding protein C levels in coronavirus disease 2019. Experimed. Experimed 2023; 13(3): 180-186.

ABSTRACT

Objective: This study aimed to evaluate cardiac myosin-binding protein C (cMyBP-C) levels in patients with COVID-19.

Materials and Methods: Overall, 187 patients were enrolled in the study. Patients with mild–moderate and severe–critical illness constituted groups 0 and 1, respectively.

Results: Admission to the intensive care unit and hospitalization period were significantly higher in group 1. Hemoglobin levels, lymphocyte count, and albumin levels were significantly lower, and lactate dehydrogenase, C-reactive protein (CRP), D-dimer, cardiac troponin I (cTnI), and procalcitonin levels, prothrombin time (PT), and CRP/lymphocyte ratio were higher in group 1 patients compared to group 0 patients. cTnI and CRP/lymphocyte ratio were higher, and ferritin/procalcitonin and albumin/CRP ratios were lower in deceased patients than in surviving patients, while MyBP-C levels were similar in the two groups. Multivariate regression analysis revealed that lymphocyte count and urea levels were independent predictors of mortality. Receiver Operating Characteristic (ROC) curve analysis showed that cTnI level and ferritin/procalcitonin, CRP/lymphocyte, and albumin/CRP ratios were valuable biochemical parameters for predicting mortality in patients with COVID-19.

Conclusion: cMyBP-C level may not be a valuable tool for predicting the severity or prognosis of COVID-19.

Keywords: Cardiac myosin-binding protein C, Coronavirus disease 2019, infection

INTRODUCTION

Severe acute respiratory syndrome coronavirus 2 (SARS-CoV-2) is a subgroup of coronavirus initially identified in Wuhan, China, in December 2019. After the diagnosis of coronavirus disease 2019 (COVID-19), the infection rapidly spread into various countries, and it was declared a pandemic on March 11, 2020. The infection is highly contagious, and its mortality is higher than that of seasonal influenza (1). The severity of COVID-19 varies widely in the population, ranging from an asymptomatic state to multi-organ failure and death. Hyper-activation of the immune system, inflammatory response, and cytokine storm are responsible for the pathogenesis and clinical symptoms of the disease (2). Cardiac involvement is relatively common among patients who are hospitalized during the course

Corresponding Author: Cennet Yıldız **E-mail:** cennet_yildiz@live.com
Submitted: 19.05.2023 **Revision Requested:** 17.07.2023 **Last Revision Received:** 29.09.2023 **Accepted:** 16.10.2023

of the infection. Multiple mechanisms have been proposed to clarify the mechanism of cardiac injury in patients with COVID-19. Direct invasion of the myocardial tissue through angiotensin-converting enzyme-2 (ACE-2) receptor binding and release of inflammatory cytokines, coronary plaque destabilization, and hypoxia may contribute to cardiac dysfunction (3, 4). It is now well demonstrated that cardiac involvement is associated with high mortality (5). Myocardial injury in the acute phase of the infection has been reported in up to 15.8% of patients with COVID-19 who are more likely to be older, require intensive care unit (ICU) admission, and have preexisting heart disease (6). Furthermore, cardiovascular morbidities, including hypertension, atrial fibrillation, and coronary artery disease, are linked with the severity of the illness (7). Cardiovascular manifestations of COVID-19 include myocardial injury, myocarditis, arrhythmia, congestive heart failure, and cardiac arrest (8). Several biomarkers have been studied to diagnose cardiac involvement and assess prognosis.

The contraction and relaxation of heart muscles depend on cross-bridge formation between actin and myosin filaments. Cardiac myosin-binding protein C (cMyBP-C) regulates cardiac contraction by controlling the actin–myosin interaction (9). In its dephosphorylated form, cMyBP-C inhibits the interaction between actin and myosin (10). Notably, the phosphorylated form of cMyBP-C decreases in patients with congestive heart failure, ischemic heart disease, and atrial fibrillation (11-14). Furthermore, cMyBP-C mutations are among the most common causes of hypertrophic cardiomyopathy. cMyBP-C is a novel biomarker that may be more useful than cardiac troponin I (cTnI) in clinical practice (15). Thus, this study aimed to evaluate cMyBP-C levels and their prognostic value with respect to in-hospital mortality in patients with COVID-19.

MATERIALS AND METHODS

This study was conducted between April and June 2020 with the inclusion of 187 patients with COVID-19 who were admitted to an infectious disease clinic and ICU in a tertiary hospital in Turkiye. The local ethics committee approved the study, and informed consent from patients or their legal representatives was obtained. The study was conducted in accordance with the Declaration of Helsinki. Demographic and clinical characteristics of the patients were recorded during hospitalization. COVID-19 infection was identified by obtaining viral RNA in nasopharyngeal swabs using real-time polymerase chain reaction. The patients' clinical status was categorized as mild, moderate, severe, and critical according to the China Diagnosis and Treatment of COVID-19 (16). Patients with the absence and presence of pneumonia were described as mild and moderate cases, respectively. Patients who had a respiratory rate of >30 breaths/min, resting oxygen saturation level < 93%, and partial oxygen saturation to fraction of inspired oxygen ratio < 300 mmHg were classified as severe cases. Patients with respiratory failure, shock, or other organ failure that required ICU admission were categorized as critical cases. Patients were classified into two groups according to their clinical situation: patients with mild–moderate disease and severe–critical disease constituted groups 0 and 1, respectively.

Blood samples of the patients were drawn by venipuncture in either a sitting or supine position. Blood parameters, including haemogram; liver and kidney function tests; albumin, ferritin, triglyceride, fibrinogen, and coagulation tests; and D-dimer, cTnI ,and procalcitonin tests, were assessed. Serum cMyBP-C levels were determined using enzyme-linked immunosorbent assay (ELISA) (Allsheng APW-200 microplate washer, Hangzhou Allsheng Instruments Co., China).

Statistical Analyses

All analyses were performed using Number Cruncher Statistical System (NCSS) Statistical Software (Utah, USA). Data with Gaussian and non-Gaussian distributions were expressed as mean ± SD and median (minimum–maximum), respectively. Categorical data were expressed as numbers and percentages. For the comparison of groups, Mann–Whitney U and independent sample t tests were used. Receiver Operating Characteristic (ROC) curve analysis was performed to predict mortality, ICU admission, and severity of the disease. The binomial exact test was used for binary comparison of the variables. For the current study with an alpha level of 0.05 and effect size of 0.38, the estimated power was 80%. p -value < 0.05 was considered significant.

RESULTS

The mean age of the study population was 60.89 ± 16.90 years. A total of 64 patients (34.2%) had severe disease, 54 (28.9%) had diabetes, 97 (51.9%) had hypertension, and 9 (7.0%) were admitted to the ICU, and the in-hospital mortality was 5.3%.

No differences were noted between the two groups with regard to age, sex, prevalence of diabetes mellitus, chronic renal failure, coronary artery disease, hypertension, and chronic obstructive pulmonary disease. As expected, admission to the ICU and hospitalization period were significantly higher in group 1. Hemoglobin (Hgb) level, lymphocyte count, and albumin level were significantly lower, and lactate dehydrogenase (LDH), C-reactive protein (CRP), D-dimer, cTnI, and procalcitonin levels; prothrombin time (PT); and CRP/lymphocyte ratio were higher in group 1 than those in group 0. A comparison of the clinical and biochemical parameters of the two groups is presented in Table 1.

cTnI levels and CRP/lymphocyte ratio were substantially higher, and ferritin/procalcitonin and albumin/CRP ratios were substantially lower in deceased patients than in surviving patients. However, cMYBP-C levels did not differ between the two groups (Table 2).

Logistic regression was used to assess the prognosticators of mortality. According to univariate analysis, Hgb, aspartate aminotransferase (AST), urea, creatinine, albumin, and CRP levels; PT; activated partial thromboplastin time (aPTT); D-dimer

Table 1. Comparison of clinical and biochemical parameters of two groups.

	Patients with mild-moderate disease (Group 0)	Patients with severe-critical disease (Group 1)	p
Age (years)	59.49±16.89	63.58±16.72	0.117
Gender n (%)			0.578
Female	61 (49.6)	29 (45.3)	
Male	62 (50.4)	35 (54.7)	
Diabetes mellitus n (%)	33 (26.8)	31 (32.8)	0.392
Hypertension (n, %)	65 (52.8)	32 (50.0)	0.712
Coronary artery disease n (%)	37 (30.1)	17 (26.6)	0.614
COPD n (%)	19 (15.4)	9 (14.1)	0.800
Chronic renal failure	5 (4.1)	4 (6.3)	0.495
Intensive care unit	0 (0)	13 (20.3)	0.000
Mortality	1 (0.8)	9 (14.1)	<0.001
Hospitalization period (days)	8.00 (3.0-31.0)	13.00 (4.0-49.0)	<0.001
Hemoglobin (g/dL)	12.5 (5.3-16.1)	11.45(7.1-1.5)	0.042
Hematocrit (%)	38.00 (14.8-47.7)	34.75 (22.6-51.6)	0.093
White blood cell (10^9/L)	7.37 (2.47-26.48)	7.6 (1.78-26.81)	0.775
Lymphocyte count (10^9/L)	1.51 (0.45-17.70)	1.20 (0.35-2.75)	0.002
Neutrophil count (10^9/L)	5.00 (1.29-73.10)	5.45 (0.71-22.64)	0.609
Platelet count (10^9/L)	223.00 (113.0-830.0)	229 (29.0-567.0)	0.559
Aspartate aminotransferase (IU/L)	26.00 (10.0-133.0)	29.0 (9.0-227.0)	0.251
Alanine aminotransferase (IU/L)	21.00 (3.0-191.0)	24.00 (5.0-170.0)	0.501
Urea (mg/dL)	32.20(5.0-147.0)	37.00(10.0-249.0)	0.017
Creatinine (mg/dL)	0.78 (0.37-6.71)	0.91 (0.37-8.48)	0.057
Lactate dehydrogenase (IU/L)	264.00 (118.0-968.0)	299.50 (160.0-620.0)	0.005
Albumin (g/dL)	36.71±5.30	33.21±5.16	<0.001
Ferritin (mg/L)	151.00 (5.7-4816.0)	154.40 (11.4-3428.0)	0.340
Triglyceride (mg/dL)	116.00 (31.0-582.0)	108.0 (36.0-401.0)	0.621
Creatine kinase (U/L)	74.00 (14.0-1383.0)	90.0 (10.0-1677.0)	0.445
Procalcitonin (ng/mL)	0.07 (0.01-31.51)	0.13 (0.03-77.26)	0.000
CRP (mg/dL)	21.00 (0.58-358.00)	85.50(4.00-328.97)	<0.001
Fibrinogen (mg/dL)	468.924±120.28	505.37±118.41	0.067
Prothrombin time (s)	12.80(0.0-62.4)	14.00 (0.0-29.2)	0.001
aPTT (s)	34.90 (21.7-65.0)	36.3(24.6-73.1)	0.272
D-dimer (mg/L)	0.42 (0.04-7.8)	0.55 (0.00-7.24)	0.041
cTnI (ng/mL)	5.00 (1.0-836.0)	9.00 (1.0-576.0)	<0.001
cMYBPC (ng/L)	1.64 (0.07-10.48)	1.27 (0.16-10.48)	0.717
Ferritin/Procalcitonin ratio	1682.00 (1.89-96320.00)	892.50 (1.08-26743.33)	0.163
CRP/lymphocyte ratio	16.39 (0.49-344.23)	78.94 (2.47-939)	<0.001
Albumin/CRP ratio	1.55 (0.11-67.24)	0.40 (0.10-9.90)	<0.001

aPTT: Activated partial thromboplastin time, COPD: Chronic obstructive pulmonary disease, cTnI: Cardiac troponin I; cMYBPC: Cardiac myosin-binding protein C; CRP: C-reactive protein. Data were expressed as n(%), mean ± SD or median (minimum–maximum).

Table 2. Comparison of parameters between deceased and survived patients.

	Deceased	Survived	p
cTnI (ng/mL)	16.5 (5-31)	6 (1-836)	0.002
cMyBPC (ng/L)	0.7 (0.3-8.7)	1.5 (0.1-10.5)	0.534
Ferritin/Procalcitonin	255 (14.8-4555)	1680 (1.1-96320)	0.019
CRP/Lymphocyte	113.5 (14-558.7)	35.4 (0.5-939.9)	0.004
Albumin/CRP	0.3 (0.1-2.6)	0.8 (0.1-67.2)	0.011

cTnI: Cardiac troponin I; cMYBPC: Cardiac myosin-binding protein C; CRP: C-reactive protein. Data were expressed as median (minimum–maximum).

Table 3. Univariate and multivariate logistic regression for predictors of mortality.

	UNIVARIATE ANALYSIS			MULTIVARIATE ANALYSIS		
	OR	p	95% CI	OR	p	95% CI
Hgb	0.725	0.021	0.551 – 0.954			
AST	1.013	0.028	1.001 -1.024			
Urea	1.028	0.001	1.012 – 1.043	1.020	0.035	1.001-1.038
Creatinine	1.473	0.016	1.073 -2.020			
Albumin	0.811	0.001	0.714 – 0.921			
CRP	1.007	0.070	0.999 -1.014			
PT	1.070	0.028	1.007 – 1.137			
aPTT	1.080	0.030	1.007-1.157			
D-dimer	1.386	0.047	1.004-1.911			
Lymphocyte	0.145	0.002	0.023-0.876	0.174	0.039	0.033-0.919
CRP/lymphocyte	1.004	0.043	1.000-1.008			

Hgb: Hemoglobin, AST: Aspartate aminotransferase, CRP: C-reactive protein, PT: Prothrombin time, aPTT: activated partial thromboplastin time, OR: odds ratio, 95% CI : 95% confidence interval.

Table 4. ROC curve analysis results for predicting mortality.

				95% CI	
	AUC	Standard Error	p	Lower	Upper
cTnI	0.795	0.062	0.008	0.673	0.918
MYBPC3	0.429	0.116	0.523	0.201	0.656
Ferritin/Procalcitonin	0.831	0.073	0.003	0.764	0.886
CRP/lymphocyte	0.852	0.051	0.002	0.751	0.952
Albumin/CRP	0.823	0.076	0.004	0.755	0.878

cTnI: Cardiac troponin I; cMYBPC: Cardiac myosin-binding protein C; CRP: C-reactive protein.

level; and CRP/lymphocyte count were independent predictors of mortality. Multivariate regression analysis revealed that lymphocyte count and urea level were independent predictors of mortality (Table 3).

ROC curve analysis showed that cTnI level and ferritin/procalcitonin, CRP/lymphocyte, and albumin/CRP ratios were valuable biochemical parameters for predicting mortality in patients with COVID-19 (Table 4).

DISCUSSION

This study showed that patients with severe COVID-19 had longer hospital stays and higher mortality rate; higher urea, LDH, procalcitonin, CRP, D-dimer, and cTnI levels; and higher prothrombin times but had lower Hgb and albumin levels and lymphocyte counts. No significant difference was observed in cMyBP-C levels between patients who had mild–moderate and severe disease. Lymphocyte count and urea concentration were the two parameters that independently predicted mortality.

Cardiac involvement during the course of infection may be mediated through the interaction of the virus with ACE-2 receptor, found in lung and cardiac tissue. Virus can initiate cardiac myocyte damage by entering the cell using the ACE-2 receptor and initiating an inflammatory response (17). Conversely, a dysfunctional immune response with an associated cytokine storm may result in acute respiratory distress syndrome and multiorgan failure, including heart, liver, and kidney failure. A study has shown that myocarditis and virus-induced myocardial injury are among the major causes of death (18).

Identification of myocardial injury during COVID-19 infection is of paramount importance as its prognostic significance has already been demonstrated (18). An ideal biomarker should have high sensitivity and specificity for detecting the extent of myocardial damage. Several biomarkers have been used in clinical practice; however, each of them has certain drawbacks. For example, creatine kinase-MB fraction and myoglobin are present in cardiac and skeletal muscles, which limit their usefulness in diagnosis and management. The most specific and sensitive biomarkers used thus far have been cardiac troponins. cTnI and C are only expressed in cardiac muscles and have both cytosolic and structurally bound molecule release kinetics that result in their continuous release to the circulation (19). Elevation of cardiac troponin levels has been reported in 5%–25% of hospitalized patients with COVID-19 (20, 21). Usually, increased troponin levels have been considered a myocardial infarction equivalent. However, inflammatory response, sepsis, and thromboembolic events are other pathophysiological mechanisms underlying high troponin levels in patients with COVID-19. Moreover, troponin levels elevate together with other acute phase reactants, including procalcitonin, ferritin, CRP, and interleukin-6, suggesting common causation (22). As such, the American College of Cardiology stated that, for the diagnosis of myocardial infarction, troponin can only be used with clinical evaluation (22). Several studies and meta-analyses have shown that increased troponin concentrations have prognostic value in patients with COVID-19 (23-25). Based on this information, the measurement of troponin levels in hospitalized patients has been recommended for prognostic purposes (26). In addition to cardiac troponins, elevation of creatine kinase-MB and N-terminal pro-brain natriuretic peptide levels have been found as indicators of cardiac damage (27).

cMyBP-C, a novel biomarker for several cardiac conditions, has gained interest over the past few years. It plays an important role in sarcomere organization and the regulation of cardiac contraction and relaxation. It has a better diagnostic power than high-sensitivity cardiac troponin T (hs-cTnT) Troponin T for the diagnosis of acute myocardial infarction (28). Values < 10 ng/L had 100% sensitivity for ruling out myocardial infarction in patients with chest pain for 2 h (28). Studies have shown that serum cMyBP-C levels begin to increase within 30 min and significantly decline after 12 h of coronary obstruction (29). Hence, it could be used for the early diagnosis of myocardial infarction (30). While there is no doubt that troponins are reliable indicators of myocardial damage, slow release of the troponin complex may obscure repetitive episodes of injury. Accordingly, this study aimed to analyze cMyBP-C molecule levels, which are cardiac specific and have a short half-life, in COVID-19 victims.

Higher cMyBP-C levels were expected in severe disease, but any significant differences were not found between patients who had severe and mild–moderate disease. Moreover, according to regression analysis, cMyBP-C was not a predictor of mortality in COVID-19. In the present study, serum cMyBP-C levels were measured within 24 h of hospital admission. Since our hospital was a tertiary referral hospital, patients from different hospitals were transferred to our COVID-19 ward. This might cause discrepancies in the timing of blood specimen collection among patients. The hospitalization period of the patients who had been transferred from other institutions was unknown. Hence, blood samples might be collected from these patients during the fall phase. When we looked closely at the data, creatine kinase levels also did not differ between the two groups, which also show rapid rise and fall kinetics. Most studies conducted on cMyBP-C has mainly focused on its diagnostic power to detect myocardial infarction and its role in the pathogenesis of hypertrophic and dilated cardiomyopathies. To the best of our knowledge, no study has been conducted to determine cMyBP-C levels in infectious diseases, including COVID-19. According to our results, cMyBP-C has limited use in the prognostification of COVID-19.

The present study did not assess the function of the left and right ventricules in patients with COVID-19. Previous studies have shown that either left or right ventricular dysfunction predicted mortality in this group of subjects (31). Moreover, there are some datas suggesting that COVID-19 predominantly affect the right ventricle (32). D'alto et al. showed that COVID-19-induced acute respiratory distress syndrome was associated with uncoupling of right ventricular function from pulmonary

function (33). Moody et al. demonstrated that patients with severe COVID-19 pneumonia had reduced right ventricular systolic function without abnormalities of left ventricular function (34). In that study, reduced right ventricular function was found to be an independent predictor of all-cause mortality.

Our study findings were in line with those of previous studies. Further research has already been conducted to determine the best diagnostic/prognostic parameter in patients with COVID-19. Several circulatory biomarkers have been found to be valuable during the course of infection, including procalcitonin, CRP, and Interleukin-6 (35-38). Considering that the early recognition of severe cases is of utmost importance, finding a reliable marker for the management of the disease to improve outcomes is essential. The present study showed that renal function, CRP, procalcitonin, cTnI, and D-dimer tests can be used for the clinical classification of COVID-19. Moreover, lymphocyte count and urea levels should be closely monitored until full recovery, as these levels were associated with increased mortality.

This study has several limitations: (1) It was a single-center and observational study. (2) The sample size was relatively small. (3) Levels of cMyBP-C were measured only once; thus, individual variation in cMyBP-C during the hospital stay stay remain unknown. (4) As the number of deaths in the study population was small, accurate estimation of mortality could not be performed. (5) Echocardiographic examinations of the patients were not performed.

In conclusion, cMyBP-C has limited use in determining the severity and predicting the prognosis of COVID-19. Multicenter and large-scale studies are required to evaluate the role of cMyBP-C in patients with COVID-19.

Ethics Committee Approval: The Bakirkoy Dr. Sadi Konuk Training and Research Hospital Ethics Committee agreed to the study protocol (Date: October 16, 2020/No:20208181).

Informed Consent: Informed consent from patients or their legal representatives was obtained.

Peer-review: Externally peer-reviewed.

Author Contributions: Conception/Design of Study- D.K., U.K., K.K.Y., G.S.E., O.P., P.K., N.I.; Data Acquisition- D.K., K.K.Y., G.S.E., O.P., P.K., N.I.; Data Analysis/Interpretation- D.K., C.Y., U.K., E.O., F.N.T.C.; Drafting Manuscript- D.K., C.Y., U.K., E.O., F.N.T.C, K.K.Y., G.S.E., O.P.; Critical Revision of Manuscript- U.K., E.O., F.N.T.C., K.K.Y., G.S.E., O.P., P.K.; Final Approval and Accountability- D.K., C.Y., U.K., E.O., F.N.T.C., K.K.Y., G.S.E., O.P., P.K., N.I.

Conflicts of Interests: The authors declare that they have no competing interests.

Financial Disclosure: The authors declare that this study has received no financial support.

REFERENCES

1. Piroth L, Cottenet J, Mariet AS, Bonniaud P, Blot M, Bitter PT, et al. Comparison of the characteristics, morbidity, and mortality of COVID-19 and seasonal influenza: a nationwide, population-based retrospective cohort study. Lancet Respir Med 2021; 9(3): 251-9.
2. Shah VK, Firmal P, Alam A, Ganguly D, Chattopadhyay S. Overview of immune response during SARS-CoV-2 infection: lessons from the past. Front. Immunol 2020; 11: 1949.
3. Hoffmann M, Kleine-Weber H, Schroeder S, Krüger N, Herrler T, Erichsen S, et al. SARS-CoV-2 cell entry depends on ACE2 and TMPRSS2 and is blocked by a clinically proven protease inhibitor. Cell 2020; 181: 271-80.
4. Xu Z, Shi L, Wang Y, Zhang J, Huang L, Zhang C, et al. Pathological findings of COVID-19 associated with acute respiratory distress syndrome. The Lancet Respiratory Medicine 2020; 8: 420-2.
5. Cappannoli L, Scacciavillani R, Iannaccone G, Anastasia G, Di Giusto F, Loria V, et al. 2019 novel-coronavirus: cardiovascular insights about risk factors, myocardial injury, therapy and clinical implications. Chronic Dis Transl Med 2020; 6(4): 246-50.
6. Wei JF, Huang FY, Xiong TY, Liu Q, Chen H, Wang H. Acute myocardial injury is common in patients with COVID-19 and impairs their prognosis. Heart 2020; 106(15): 1154-9.
7. Yang J, Zheng Y, Gou X, Pu K, Chen Z, Guo Q, et al. Prevalence of comorbidities and its effects in patients infected with SARS-CoV-2: a systematic review and meta-analysis. Int J Infect Dis 2020; 94: 91-5.
8. Tajbakhsh A, Hayat SMG, Taghizadeh H, Akbari A, Inabadi M, Savardashtaki A, et al. COVID-19 and cardiac injury: clinical manifestations, biomarkers, mechanisms, diagnosis, treatment, and follow up. Expert Rev Anti Infect Ther 2021; 19(3): 345-7.
9. Previs MJ, Beck Previs S, Gulick J, Robbins J, Warshaw DM. Molecular mechanics of cardiac myosin-binding protein C in native thick filaments. Science 2012; 337(6099): 1215–8.
10. Bhuiyan MS, Gulick J, Osinska H, Gupta M, Robbins J. Determination of the critical residues responsible for cardiac myosin binding protein C's interactions. J Mol Cell Cardiol 2012; 53(6): 838–47.
11. El-Armouche A, Pohlmann L, Schlossarek S, Starbatty J, Yeh YH, Nattel S, et al. Decreased phosphorylation levels of cardiac myosin-binding protein-C in human and experimental heart failure. J Mol Cell Cardiol 2007; 43(2): 223-9.
12. Decker RS, Nakamura S, Winegrad S. The dynamic role of cardiac myosin binding protein-C during ischemia. J Mol Cell Cardiol 2012; 52: 1145–54.
13. El-Armouche A, Boknik P, Dobrev D. Molecular determinants of altered Ca^{2+} handling in human chronic atrial fibrillation. Circulation 2006; 114: 670–80.
14. Govindan S, McElligott A, Muthusamy S, Nair N, Barefield D, Martin JL, et al. Cardiac myosin binding protein-C is a potential diagnostic biomarker for myocardial infarction. J Mol Cell Cardiol 2012; 52(1): 154-64.
15. Baker JO, Tyther R, Liebetrau C, Clark J, Howarth R, Patterson T, et al. Cardiac myosin-binding protein C: a potential early biomarker of myocardial injury. Basic Res Cardiol 2015; 110(3): 23.
16. China's National Health Commission Guidelines for COVID-19 Treatment (7th edition). Available from: https://www.elotus.org/promo-files/COVID 19_resources/Guidance%20for%20Corona%20Virus%20Disease%202019%20(English%207th%20Edition%20Draft).pdf.

17. Khan IH, Zahra SA, Zaim S, Harky AE. At the heart of COVID-19. J Card Surg 2020; 35(6): 1287–94.
18. Deng Q, Hu B, Zhang Y, Wang H, Zhou X, Hu W et al. Suspected myocardial injury in patients with COVID- 19: evidence from front-line clinical observation in Wuhan, China. Int J Cardiol 2020; 311: 116-21.
19. Katus HA, Remppis A, Scheffold T, Diederich KW. Intracellular compartmentation of cardiac troponin T and its release kinetics in patients with reperfused and nonreperfused myocardial infarction. Am J Cardiol 1991; 67: 1360-7.
20. Huang C, Wang Y, Li X, Ren L, Zhao J, Hu Y, et al. Clinical features of patients infected with 2019 novel coronavirus in Wuhan, China. Lancet 2020; 395(10223): 497–506.
21. Wang D, Hu B, Hu C, Zhu F, Liu X, Zhang J, et al. Clinical characteristics of 138 hospitalized patients with 2019 novel coronavirus–infected pneumonia in Wuhan, China. Jama 2020; 323(11): 1061–9.
22. Babapoor-Farrokhran S, Gill D, Walker J, Rasekhi RT, Bozorgnia B, Amanullah A. Myocardial injury and COVID-19: possible mechanisms. Life Sci 2020: 253; 117723.
23. Januzzi JL. Troponin and BNP use in COVID-19. American College of Cardiology. Available from: https://www.acc.org/latest-in-cardiology/articles/2020/03/18/15/25/troponin-and-bnp-use-in-covid19. Accessed 21 Oct 2020.
24. Li JW, Han TW, Woodward M, Anderson CS, Zhou H, Chen YD, et al. The impact of 2019 novel coronavirus on heart injury: a systematic review and meta-analysis. Prog Cardiovasc Dis 2020; 63(4):5 18–24.
25. Parohan M, Yaghoubi S, Seraji A. Cardiac injury is associated with severe outcome and death in patients with Coronavirus disease 2019 (COVID-19) infection: a systematic review and meta-analysis of observational studies. Eur Heart J Acute Cardiovasc Care 2020; 9(6): 665–77.
26. Chapman AR, Bularga A, Mills NL. High-sensitivity cardiac troponin can be an ally in the fight against COVID-19. Circulation 2020; 141(22): 1733–5.
27. Li L, Zhou Q, Xu J. changes of laboratory cardiac markers and mechanisms of cardiac injury in coronavirus disease 2019. Biomed Res Int 2020; 2020: 7413673.
28. Kaier TE, Stengaard C, Marjot J, Serensen JT, Alaour B, Stavropoulou-Tatla S, et al. Cardiac myosin-binding protein C to diagnose acute myocardial infarction in the pre-hospital setting. J Am Heart Assoc 2019; 8(15): e013152.
29. Kuster DWD, Cardenas-Ospina A, Miller L, Liebetrau C, Troidl C, Nef HM, et al. Release kinetics of circulating cardiac myosin binding protein-C following cardiac injury. Am J Physiol Heart Circ Physiol 2014; 306: 547-56.
30. Govindan S, Kuster DWD, Lin B, Kahn DJ, Jeske WP, Walenga JM, et al. Increase in cardiac myosin binding protein-C plasma levels is a sensitive and cardiac-specific biomarker of myocardial infarction. Am J Cardiovasc Dis 2013; 3(2): 60–70.
31. Biebrer S, Kraechan A, Hellmuth JC, Muenchhoff M, Scherer C, Schroeder I, et al. Left and right ventricular dysfunction in patients with COVID-19-associated myocardial injury. Infection 2021; 49(3): 491–500.
32. Szekely Y, Lichter Y, Taieb P, Banai A, Hochstadt A, Merdler I, et al. Spectrum of cardiac manifestations in COVID-19: a systematic echocardiographic study. Circulation 2020; 142: 342–53.
33. D'alto M, Marra AM, Severino S, Salzano A, Romeo E, De Rosa R, et al. Right ventricular-arterial uncoupling independently predicts survival in COVID-19 ARDS. Crit Care 2020; 24(1): 670.
34. Moody WE, Mahmoud-Elsayed HM, Senior J, Gul U, Khan-Kheil AM, Horne Si, et al. Impact of right ventricular dysfunction on mortality in patients hospitalized with COVID-19, according to race . CJC Open 2021; 3(1): 91-100.
35. Hu R, Han C, Pei S, Yin M, Chen X. Procalcitonin levels in COVID-19 patients. Int J Antimicrob Agents 2020; 56(2): 106051.
36. Wang L. C-reactive protein levels in the early stage of COVID-19 Med Mal Infect 2020; 50(4): 332-4.
37. Grifoni E, Valoriani A, Cei F, Lamanna R, Gelli AMG, Ciambotti B, et al. Interleukin-6 as prognosticator in patients with COVID-19. J Infect 2020; 81(3): 452–82.
38. Erdal GS, Polat O, Erdem GU, Korkusuz R, Hindilerden F, Yilmaz M, et al. The mortality rate of COVID-19 was high in cancer patients: a retrospective single-center study. Int J Clin Oncol 2021; 24: 1–9.

Experimed 2023; 13(3): 187-193

ORIGINAL ARTICLE

DOI: 10.26650/experimed.1318122

Effects of Neurocognitive Rehabilitation on the Levels of Neurotransmitters and Memory Proteins in Patients with Multiple Sclerosis*

Ozlem Totuk[1], Erdil Arsoy[2], Recai Turkoglu[2]

[1]Department of Neurology, Sehit Prof. Dr. Ilhan Varank Training and Research Hospital, Sancaktepe, Istanbul, Turkiye
[2]Department of Neurology, Haydarpasa Numune Training and Research Hospital, Istanbul, Turkiye

ORCID ID: O.T. 0000-0001-7274-025X; E.A. 0000-0002-9290-9478; R.T. 0000-0001-9724-851X

Cite this article as: Totuk O, Arsoy E, Turkoglu R. Effects of neurocognitive rehabilitation on the levels of neurotransmitters and memory proteins in patients with multiple sclerosis. Experimed. Experimed 2023; 13(3): 187-193.

ABSTRACT

Objective: This study aimed to investigate the role of neurotrophic factors and neurotransmitters in the neurocognitive impairments observed in Multiple Sclerosis (MS) patients, explore potential biomarkers, and evaluate the impact of computer-assisted cognitive rehabilitation (CCR) on these biomarkers.

Materials and Methods: The study included 20 healthy volunteers and 23 relapsing-remitting MS patients with a beck depression inventory score below 17, who could use computers and had no attack in the last 6 months. Serum levels of brain-derived neurotrophic factor (BDNF), cAMP response element-binding protein (CREB), melatonin, and orexin-A were measured using enzyme-linked immunosorbent assay (ELISA) and compared between patients and controls. MS patients underwent assessment using the brief repeatable battery of neuropsychological tests (BRB-N) before (baseline) and after (sixth month) CCR their biomarker levels were measured again, along with administering neuropsychological tests.

Results: Results showed lower levels of BDNF, CREB, melatonin, and orexin-A in MS patients compared to healthy controls before neurorehabilitation. Among the measured cognition-related proteins in the MS group, only BDNF was insignificantly decreased after neurorehabilitation. No significant differences were found in orexin-A, melatonin, and CREB levels before and after neurorehabilitation. Although, correlation analysis revealed no significant correlation between biomarkers and clinical parameters, paced auditory serial addition test and stroop tests which pointed to sustaining attention, information processing speed, verbal fluency, and categorical reasoning were found meaningful after CCR.

Conclusions: CCR may have beneficial effects on cognitive functions, particularly executive functions. However, the four examined molecules did not reflect cognitive changes in MS and cannot be used as biomarkers. Further investigation of other molecules related to CREB and BDNF pathways may shed light on cognitive impairment in MS.

Keywords: Multiple Sclerosis, CCR, BDNF, CREB, melatonin, orexin-A

INTRODUCTION

Multiple Sclerosis (MS) is a chronic, inflammatory, and degenerative disease of the central nervous system, characterized by recurrent or progressive demyelination and axon damage in the white matter (1). The signs and symptoms of MS can be divided into three groups: primary symptoms related to demyelination are paresis, spasticity, sensory disorders, neuropathic pain, problems with balance, bladder-intestinal problems, fatigue, sexual dysfunctions, motor disorders, and cognitive dysfunctions; secondary symptoms are the complications of primary manifestations and include contractures, urinary tract infections, megacolon, pressure sores, and muscle atrophies; and tertiary symptoms are psychological, occupational, and social problems accompanying the remaining findings.

*This article is extracted from Ozlem (Kurklu) Totuk thesis of specialization in neurology supervised by Prof. Dr. Recai Turkoglu with the Council of Higher Education Thesis Center number 497702.

Corresponding Author: Ozlem Totuk **E-mail:** totukozlem@gmail.com
Submitted: 21.06.2023 **Revision Requested:** 20.10.2023 **Last Revision Received:** 09.11.2023 **Accepted:** 10.11.2023

Cognitive impairment, which is common in patients with MS, is an important symptom that affects the quality of life and social and working lives of patients. The prevalence of cognitive impairment in adults with MS reaches 70% in evaluations performed with neuropsychological tests (2). The accurate definition and diagnosis of cognitive dysfunction early in MS is of paramount importance since it can be a useful predictor of the efficacy of preventive measures or a predictor of disease progression. In MS, the most affected areas are attention, information processing speed, memory, executive functions, and visuospatial functions (3). First, information processing speed and executive functions deteriorate, and this is followed by memory and attention deficits. The cortical areas (gnosis and praxis) are usually intact until the later stages of the disease.

Two test batteries are widely used in international studies evaluating patients with MS: the Brief Repeatable Battery of Neuropsychological Tests (BRB-N) and the Minimal Assessment of Cognitive Function in MS (MACFIMS) (4). One of the coactivators accompanying transcription factors in the learning process is the cAMP response element-binding protein (CREB) and the protein that binds it, the cytoplasmic polyadenylation element binding protein. CREB, also a histone acetylase, results in the remodeling of chromatin. It is now well known that CREB controls neuronal plasticity (5, 6). It has been shown that the brain-derived neurotrophic factor (BDNF) molecule shares the same pathways as CREB, is activated together, has a low level in neurodegenerative diseases, and its level increases with treatment methods that stop its destruction. It is known that melatonin and orexin-A, which are associated with the regulation of sleep functions, activate CREB and BDNF molecules and regulate cognitive functions, synaptic plasticity, and neuroprotective functions (7, 8). Melatonin also suppresses inflammation and inhibits myelin breakdown. BDNF, orexin-A, and melatonin have known effects on cognitive functions through the activation of CREB and decrease during MS (9).

Neurocognitive rehabilitation applied with special software has been shown to lead to an improvement in memory functions, parallel to which the levels of memory proteins, neurotrophic factors, and neurotransmitters in the peripheral blood change (10, 11). However, in the literature, there are very few studies on the preventive effect of neurocognitive rehabilitation on cognitive deterioration and changes in the expression of molecules in patients with MS.

In this study, we aimed to reveal the role of neurotrophic factors and neurotransmitters in neurocognitive involvement observed in MS disease, identify possible new biomarkers, and determine whether these biomarker candidates were affected by computer-assisted cognitive rehabilitation (CCR).

MATERIALS AND METHODS

The study included 23 patients with MS followed up at the Neurology Clinic of the University of Health Sciences Haydarpasa Numune Training and Research Hospital. All the patients met the McDonald criteria for classical MS in terms of their clinical and radiological findings. In the selection of patients, attention was paid to ensure that they were able to use computers and that their beck depression inventory (BDI) scores were below 17 because of ruling out the negative impact of depression on neuropsychological tests. Patients who have experienced attacks in the last 6 months and received corticosteroid treatment were not included in the study due to the potential of altering the levels of the proteins under investigation. No criterion was applied concerning the disease duration and the expanded disability status scale (EDSS) scores of the patients.

The study was approved by the Haydarpasa Numune Training and Research Hospital clinical research local ethics committee (dated 28.11.2016 and approved by HNEAH-KAEK2016/KK/114), and eligible patients signed voluntary informed consent forms.

For all patients with MS, data on age, gender, age at disease onset, disease duration, EDSS scores, education year, and progression index (EDSS/duration of disease) were recorded (Table 1). Healthy individuals were selected from the patients who were presented to the outpatient clinic with a headache but were found to have normal neurological and systemic examination results and unremarkable cranial magnetic resonance imaging, complete blood count, and extensive biochemistry examination findings.

Human BDNF (Abbkine), human CREB (Abbkine), human orexin-A (Shanghai Yehuda Biological Technology), and human melatonin (Abbkine) levels were measured from the serum samples of the patients according to the manufacturer's instructions. The serum samples were stored at -80 °C until analysis.

Neuropsychological Evaluation

The participants underwent assessment using the BRB-N before (baseline) and after (sixth month) CCR. The BRB-N,

Table 1. Clinical and demographic features of MS and healthy controls.

	MS	Healthy Controls
Sex (F/M)	17/6	9/11
Age, years, mean±SD	39.3 ± 11	36.0 ± 9.0
Duration of MS, years, mean±SD	13.0 ± 5.0	-
Academic year, mean±SD	11.5 ± 4.2	11.0 ± 3.4
EDSS, mean±SD	3.2 ± 1.3	-
BDI scores, mean±SD	9.0 ± 5.0	7.0 ± 4.0

Abbreviations: F, female; M, male; EDSS, expanded disability status scale; BDI, beck depression inventory.

developed by Rao et al., consists of a series of tests designed to evaluate MS-specific disorders (12). These tests include measures of verbal memory acquisition [selective reminding test - total learning (SRT-TL)], delayed verbal learning (SRT-DL), visual memory acquisition (SPART-TL), delayed visual learning (SPART-DL), sustained attention and processing speed

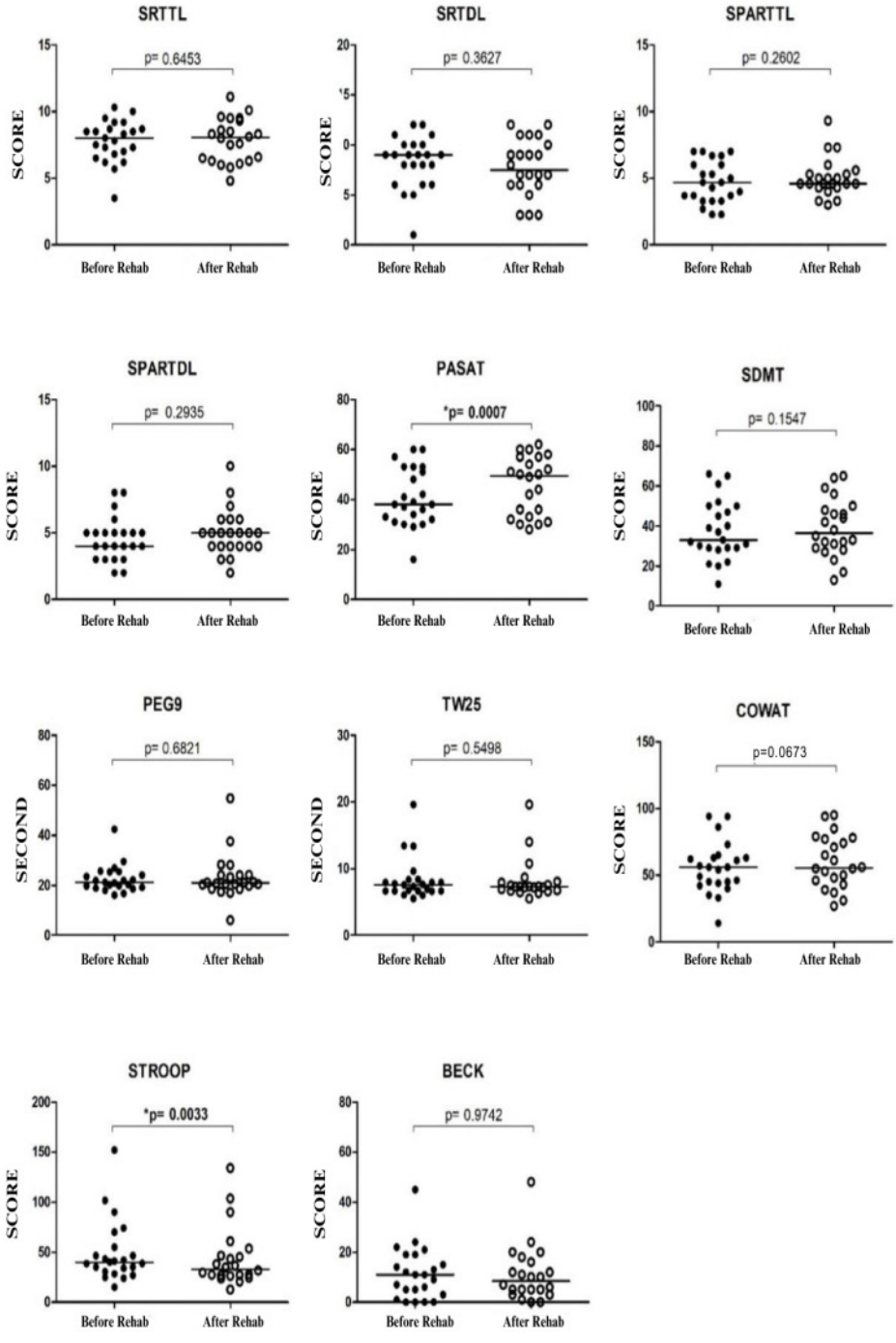

Figure 1. Comparison of the neuropsychological assessment scores before and after rehabilitation. Rehab, rehabilitation.

[paced auditory serial addition test-3 (PASAT-3)], symbol digit modalities test and verbal fluency and categorical reasoning (controlled oral word association test: COWAT). Additionally, executive functions were evaluated using the stroop color and word test, motor functions were assessed using the nine-hole peg and 25-foot walking tests, and mood changes were evaluated using the BDI scores.

Cognitive Rehabilitation

In this study, the CCR utilized the NoroSOFT mental exercise program, which consisted of five modules: attention, memory, reasoning, visual tasks, and verbal tasks. The patients were instructed to engage in 50 minutes of exercise, five days a week. Each session included a 20-minute daily exercise where patients performed tasks from each module, along with a 30-minute personalized training session tailored to their individual BRB-N scores. The patients received weekly follow-up and supervision through the program's institutional interface. Monthly evaluations were conducted for each patient to track their progress.

Statistical Analyses

The serum levels of BDNF, CREB, melatonin, and orexin-A of the patients with MS and healthy controls were compared using the analysis of variance test and Tukey's post hoc test. The pre- and post-rehabilitation values of these parameters and those of neuropsychological tests were compared using paired t-test. Possible correlations between age, disease duration, age at disease onset, EDSS scores, progression index, total number of attacks, and number of attacks per year, and neuropsychological and cognitive test results or serum BDNF, CREB, melatonin, and orexin-A levels were investigated with

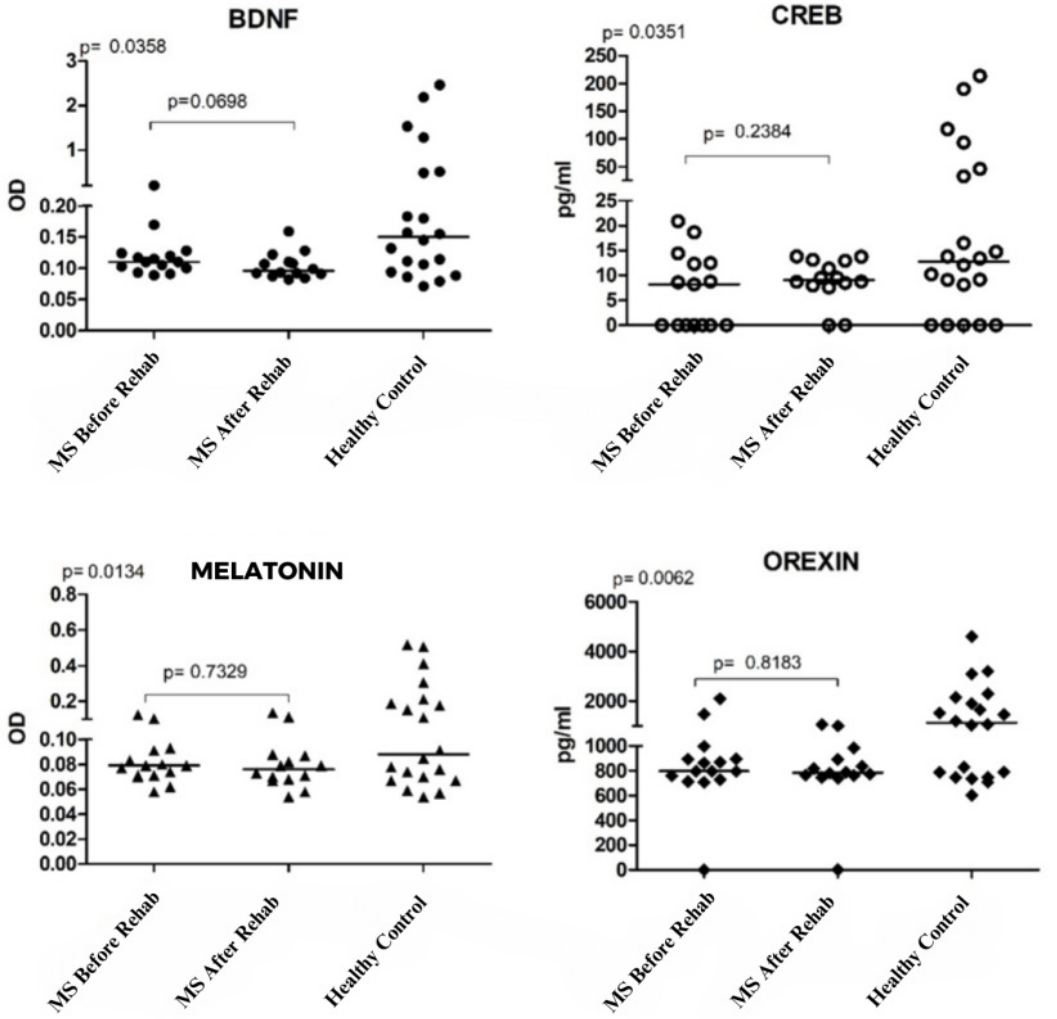

Figure 2. Serum BDNF, CREB, melatonin, and orexin-A levels in the multiple sclerosis (MS) and healthy control groups. The p values presented on the upper left corners of the panels show the results of the analysis of variance, and the p values above the horizontal lines show the results of the test scores before and after rehabilitation, as obtained from the t-test. Rehab, rehabilitation.

the Pearson test. A p-value of <0.05 was considered statistically significant.

RESULTS

Effect of Cognitive Rehabilitation on Neuropsychological Evaluation Results

There was no statistically significant difference between the pre- and post-rehabilitation scores of the SRT-TL, SRT-DL, SPART-TL, SPART-DL, SDMT, and COWAT tests, which primarily evaluate memory functions. Similarly, there was no significant change in the scores of the nine-hole peg and 25-foot walking tests, which measure motor functions, and the BDI, which assesses mood. A significant improvement was found in the scores of the PASAT and Stroop tests after rehabilitation (Figure 1).

ELISA and Correlation Results

The BDNF, CREB, melatonin, and orexin-A levels of the patients with MS (before and after neurorehabilitation) and those of the healthy controls were evaluated. The BDNF, CREB, melatonin, and orexin-A levels were found to be lower than those of the healthy controls (p=0.0358, p=0.0351, p=0.0134, and p=0.0062, respectively) (Figure 1). Among these proteins, which are associated with cognitive functions that are not affected by neurorehabilitation, only BDNF levels have shown trends towards decreasing, albeit at an insignificant level, following rehabilitation (p= 0.0698). There was no significant difference between the pre- and post-neurorehabilitation values of orexin-A, melatonin, and CREB (Figure 2). Lastly, the correlation analysis with the Pearson test revealed no significant correlation between the BDNF, CREB, orexin-A, and melatonin levels and the clinical parameters or neuropsychological evaluation scores of the patients with MS.

DISCUSSION

During MS, it is widely recognized that patients experience impairments in memory, attention, and frontal lobe cognitive functions (13). Cognitive impairment frequency and severity do not significantly differ between individuals with a good or poor prognosis (14). Structural damage to the brain regions connecting the cortical and subcortical areas has been associated with deficits in executive functions, processing speed, and attention (15). In line with previous studies, our study found that patients with MS exhibited deficits in various cognitive functions, including verbal and visual memory, attention, and executive functions. Our results indicate that the brain regions involved in cognitive functions are impacted in MS.

CCR has been widely used to rehabilitate cognitive dysfunction in patients with MS, as it has shown improvements in neuropsychological test scores across a broad range (10, 11). In our study, the most significant improvements were observed in the scores of the PASAT-3, and stroop tests, compared to the verbal and visual memory test scores. Notably, the stroop and PASAT test scores exhibited significant improvements after CCR, reversing the cognitive decline trend in patients with MS. Previous studies have also reported similar tendencies of CCR to enhance PASAT and stroop test performance (11, 16).

The PASAT-3, COWAT, and stroop tests are used to assess sustained attention, information processing speed, verbal fluency, and categorical reasoning, which are known to be closely linked to executive functions (17). The recovery pattern observed in CCR may be attributed to enhanced adaptive recovery activity in the brain's executive functioning regions (15), or these regions may benefit from rehabilitation more rapidly due to higher cognitive reserves. Therefore, neurocognitive rehabilitation shows promise in addressing the severe cognitive deficits experienced by patients with MS. Long-term effects of CCR and optimal cognitive rehabilitation approaches for patients with MS should be further investigated in studies with extended follow-up periods.

In the second phase of our study, we aimed to understand the mechanisms through which CCR improves cognitive processes and identify potential biomarkers that could predict patient response to CCR. To achieve this, we examined four important mediator molecules (CREB, BDNF, orexin-A, and melatonin) that have been associated not only with cognitive functions, neuroprotective effects, and synaptic plasticity but also with the pathophysiology of MS and treatment response in various neurorehabilitation studies. A noteworthy finding from previous research is that CREB and BDNF molecules share common pathways and can be activated together. Furthermore, melatonin and orexin-A, known for their involvement in sleep functions, have been found to activate CREB and BDNF molecules (7, 9).

It has been shown that there is a relationship between low levels of BDNF and cognitive decline in neurodegenerative diseases and that BDNF levels increase in parallel with the improvement in neuropsychological tests following treatments that stop the deterioration in cognitive functions (8). It is also known that repetitive transcranial magnetic stimulation, which is a frequently used neurorehabilitation method, activates neurogenesis by activating the BDNF/TrkB pathway in neuronal damage caused by ischemic cerebrovascular events (8, 18).

The hippocampal expression levels of the phosphorylated and non-phosphorylated CREB molecule have been reported to decrease in ischemic events presenting with neuronal damage, and this decrease has been associated with impairment in cognitive functions (19). It has been determined that CREB levels increase during neurorehabilitation procedures, parallel to which there is improvement in cognitive functions. There are studies supporting the idea that this improvement is due to the neuroprotective effects of apoptosis and oxidative stress inhibitory mechanisms induced by CREB (19, 20).

Melatonin and orexin-A, which are closely related to the regulation of sleep functions, are also known to regulate various cognitive functions, especially memory, synaptic plasticity, and neuroprotective functions. Most importantly, melatonin affects

cognitive functions by activating BDNF expression, and this molecule is also involved in the suppression of inflammation and the prevention of myelin degradation (21-25). Studies are showing that BDNF, melatonin, and orexin-A, which are molecules we identified as biomarker candidates in MS cases, have reduced levels during the disease (26-28). However, we found no study in the literature investigating the serum levels of the CREB molecule. It has been shown that cognitive dysfunction and a decrease in BDNF levels are associated with the early stages of MS. In an experimental animal model study of MS, orexin-A administration was reported to improve the clinical and immunological parameters of the disease through its anti-inflammatory effects (29).

In this study, we determined that the levels of all four molecules we determined as biomarker candidates were significantly lower in the MS group compared to the healthy controls. This finding supports previous studies suggesting that BDNF, CREB, melatonin, and orexin-A are associated with the pathogenesis of MS. In addition, the decreased levels of these molecules in patients with MS whose cognitive functions, especially memory and executive functions, are affected to a certain extent, emphasizes the role of these mediator molecules in normal cognition. The relationship between sleep disorder and the pathogenesis of MS is a well-debated issue. The detection of low levels of melatonin and orexin-A, which facilitate normal sleep functions, in patients with MS once again demonstrates the association between MS and sleep disturbances. Low levels of melatonin and orexin-A, which have immunosuppressive and neuroprotective properties, may cause the development of MS.

It is known that the CREB molecule has characteristics that suppress myelin production and increase Th17-type immune responses, which are known to be involved in the pathogenesis of MS (30). Therefore, low CREB levels detected in patients with MS can be considered as a contradictory finding. However, this change can create a compensatory corrective mechanism by preventing the destruction of myelin and the immune system's attack against myelin.

Another important finding of our study is that there was no significant difference between the pre-and post-neurorehabilitation levels of CREB, BDNF, melatonin, and orexin-A, and no correlation was observed between these molecules and the clinical parameters and neuropsychological test results of the patients with MS. These results suggest that serum levels of the four mediator molecules selected due to their association with MS and cognitive functions do not reflect the cognitive changes that occur in patients with MS, and therefore cannot be used as biomarkers for this purpose. Therefore, a more appropriate approach may be the identification of new biomarker candidates with different methodologies (e.g., the comparison of mRNA expression levels with a microarray analysis before and after rehabilitation).

The limitations of the study include the measurement of possible biomarker levels in serum rather than cerebrospinal fluid, the short follow-up period after rehabilitation, and the evaluation period not being sufficient to observe changes in expression levels. Expanding the study with a greater number of patients, incorporating neuroimaging, comparing with relapsing-remitting MS patients who have not undergone neurorehabilitation, and considering the treatments administered, can provide more information in this regard. In addition, we consider that sleep studies in patients with MS who have low melatonin and orexin-A levels can provide beneficial results by exploring possible correlations between sleep disturbances and the CREB, BDNF, orexin-A, and melatonin levels.

In conclusion, our findings showed that CCR could have beneficial effects on cognitive functions, especially executive functions. The suppression of the four evaluated cognition-related molecules in patients with MS suggests that the pathways responsible for neuroprotection and synaptic plasticity functions may play a role in the development and course of MS. The examination of the other molecules in the pathways to which CREB and BDNF belong can shed further light on cognitive impairment in MS.

Ethics Committee Approval: The study was approved by the Haydarpasa Numune Training and Research Hospital clinical research local ethics committee (dated 28.11.2016 and approved by HNEAH-KAEK2016/KK/114).

Informed Consent: Eligible patients signed voluntary informed consent forms.

Peer-review: Externally peer-reviewed.

Author Contributions: Conception/Design of Study- O.T., E.A., R.T.; Data Acquisition- O.T., E.A., R.T.; Data Analysis/Interpretation- O.T., E.A., R.T.; Drafting Manuscript- O.T., E.A., R.T.; Critical Revision of Manuscript- O.T., E.A., R.T.; Final Approval and Accountability- O.T., E.A., R.T.;

Conflict of Interest: All authors declare that they have no conflicts of interest.

Financial Disclosure: The authors declare that this study has received no financial support.

REFERENCES

1. Bar-Or A, Oliveira EM, Anderson DE, Hafler DA. Molecular pathogenesis of multiple sclerosis. J Neuroimmunol 1999; 100(1-2): 252-9.
2. Chiaravalloti ND, DeLuca J. Cognitive impairment in multiple sclerosis. Lancet Neurol 2008; 7(12): 1139-51.
3. Deloire MS, Salort E, Bonnet M, Arimone Y, Boudineau M, Amieva H, et al. Cognitive impairment as marker of diffuse brain abnormalities in early relapsing remitting multiple sclerosis. J Neurol Neurosurg Psychiatry 2005; 76(4): 519-26.
4. Benedict RH, Weinstock-Guttman B, Fishman I, Sharma J, Tjoa CW, Bakshi R. Prediction of neuropsychological impairment in multiple sclerosis: comparison of conventional magnetic resonance imaging measures of atrophy and lesion burden. Arch Neurol 2004; 61(2): 226-30.

5. Castellucci VF, Kandel ER, Schwartz JH, Wilson FD, Nairn AC, Greengard P. Intracellular injection of the catalytic subunit of cyclic AMP-dependent protein kinase simulates facilitation of transmitter release underlying behavioral sensitization in aplysia. Proc Natl Acad Sci USA 1980; 77(12): 7492-6.
6. Sharma SK, Bagnall MW, Sutton MA, Carew TJ. Inhibition of calcineurin facilitates the induction of memory for sensitization in aplysia: requirement of mitogen-activated protein kinase. Proc Natl Acad Sci USA 2003; 100(8): 4861-6.
7. Zhang G, Zhang T, Li N, Wu L, Gu J, Li C, et al. Tetramethylpyrazine nitrone activates the BDNF/Akt/CREB pathway to promote post-ischaemicneuroregeneration and recovery of neurological functions in rats. Br J Pharmacol 2018; 175(3): 517-31.
8. Alvarez XA, Alvarez I, Iglesias O, Crespo I, Figueroa J, Aleixandre M, et al. Synergistic increase of serum BDNF in Alzheimer patients treated with cerebrolysin and donepezil: Association with cognitive improvement in ApoE4 cases. Int J Neuropsychopharmacol 2016; 19(6): pyw024.
9. Peng C, Hong X, Chen W, Zhang H, Tan L, Wang X, et al. Melatonin ameliorates amygdala-dependent emotional memory deficits in Tg2576 mice by up-regulating the CREB/c-Fos pathway. Neurosci Lett 2017; 638: 76-82.
10. Bonzano L, Pedullà L, Pardini M, Tacchino A, Zaratin P, Battaglia MA, et al. Brain activity pattern changes after adaptive working memory training in multiple sclerosis. Brain Imaging Behav 2020; 14(1): 142-54.
11. Covey TJ, Shucard JL, Benedict RH, Weinstock-Guttman B, Shucard DW. Improved cognitive performance and event-related potential changes following working memory training in patients with multiple sclerosis. MultScler J Exp Transl Clin 2018; 4(1): 2055217317747626.
12. Boringa JB, Lazeron RH, Reuling IE, Adèr HJ, Pfennings L, Lindeboom J, et al. The brief repeatable battery of neuropsychological tests: normative values allow application in multiple sclerosis clinical practice. Mult Scler 2001; 7: 263-7.
13. Mesaros S, Rovaris M, Pagani E, Pulizzi A, Caputo D, Ghezzi A, et al. A magnetic resonance imaging voxel-based morphometry study of regional gray matter atrophy in patients with benign multiple sclerosis. Arch Neurol 2008; 65(9): 1223-30.
14. Gajofatto A, Turatti M, Bianchi MR, Forlivesi S, Gobbin F, Azzarà A, et al. Benign multiple sclerosis: physical and cognitive impairment follow distinct evolutions. Acta Neurol Scand 2016; 133(3): 183-91.
15. Rocca MA, Valsasina P, Ceccarelli A, Absinta M, Ghezzi A, Riccitelli G, et al. Structural and functional MRI correlates of stroop control in benign MS. Hum Brain Mapp 2009; 30(1): 276-90.
16. Cerasa A, Gioia MC, Valentino P, Nisticò R, Chiriaco C, Pirritano D, et al. Computer-assisted cognitive rehabilitation of attentiondeficits for multiple sclerosis: a randomized trial with fMRIcorrelates. Neurorehabil Neural Repair 2013; 27(4): 284-95.
17. Hansen S, Muenssinger J, Kronhofmann S, Lautenbacher S, Oschmann P, Keune PM. Cognitive screening in Multiple Sclerosis: the Five-Point Test as a substitute for the PASAT in measuring executive function. Clin Neuropsychol 2017; 31(1): 179-92.
18. Hansen PE, Videbech P, Clemmensen K, Sturlason R, Jensen HM, Vestergaard P. Repetitive transcranial magnetic stimulation as add-on antidepressant treatment. The applicability of the method in a clinical setting. Nord J Psychiatry 2004; 58(6): 455-7.
19. Lin R, Lin Y, Tao J, Chen B, Yu K, Chen J, et al. Electroacupuncture ameliorates learning and memory in rats with cerebral ischemia-reperfusion injury by inhibiting oxidative stress and promoting p-CREB expression in the hippocampus. Mol Med Rep 2015; 12(5): 6807-14.
20. Wang X, Chen A, Wu H, Ye M, Cheng H, Jiang X, et al. Enriched environment improves post-stroke cognitive impairment in mice by potential regulation of acetylation homeostasis in cholinergic circuits. Brain Res 2016;1650: 232-42.
21. Chen BH, Park JH, Lee TK, Song M, Kim H, Lee JC, et al. Melatonin attenuates scopolamine-induced cognitive impairment via protecting against demyelination through BDNF-TrkB signaling in the mouse dentate gyrus. Chem Biol Interact 2018; 285: 8-13.
22. Alzoubi KH, Mayyas FA, Mahafzah R, Khabour OF. Melatonin prevents memory impairment induced by high-fat diet: Role of oxidative stress. Behav Brain Res 2018; 336: 93-8.
23. Zhang S, Wang P, Ren L, Hu C, Bi J. Protective effect of melatonin on soluble Aβ1-42-induced memory impairment, astrogliosis, and synaptic dysfunction via the Musashi1/Notch1/Hes1 signaling pathway in the rat hippocampus. Alzheimers Res Ther 2016; 8(1): 40.
24. Mavanji V, Butterick TA, Duffy CM, Nixon JP, Billington CJ, Kotz CM. Orexin-A/hypocretin treatment restores hippocampal-dependent memory in orexin-A-deficient mice. Neurobiol Learn Mem 2017; 146: 21-30.
25. Ardeshiri MR, Hosseinmardi N, Akbari E. The effect of orexin-A 1 and orexin-A 2 receptors antagonisms in the basolateral amygdala on memory processing in a passive avoidance task. Physiol Behav 2017; 174: 42-8.
26. Prokopova B, Hlavacova N, Vlcek M, Penesova A, Grunnerova L, Garafova A, et al. Early cognitive impairment along with decreased stress-induced BDNF in male and female patients with newly diagnosed multiple sclerosis. J Neuroimmunol 2017; 302: 34-40.
27. Oka Y, Kanbayashi T, Mezaki T, Iseki K, Matsubayashi J, Murakami G, et al. Low CSF hypocretin-1/orexin-A-A associated with hypersomnia secondary to hypothalamic lesion in a case of multiple sclerosis. J Neurol 2004; 251(7): 885-6.
28. Dokoohaki S, Ghareghani M, Ghanbari A, Farhadi N, Zibara K, Sadeghi H. Corticosteroid therapy exacerbates the reduction of melatonin in multiple sclerosis. Steroids 2017; 128: 32-6.
29. Fatemi I, Shamsizadeh A, Ayoobi F, Taghipour Z, Sanati MH, Roohbakhsh A, et al. Role of orexin-A-A in experimental autoimmune encephalomyelitis. J Neuroimmunol 2016; 291: 101-9.
30. Jana M, Ghosh S, Pahan K. Upregulation of myelin gene expression by a physically-modified saline via phosphatidylinositol 3-kinase-mediated activation of CREB: Implications for multiple sclerosis. Neurochem Res 2018; 43(2): 407-19.

Experimed 2023; 13(3): 194-204

ORIGINAL ARTICLE

DOI: 10.26650/experimed.1343683

Propolis: Intrinsic Pathway-Induced Apoptosis, G1 Cell Cycle Arrest, Reduced Chemotherapeutic Resistance in Adenocarcinoma, and Healthy Cell Preservation

Nursel Isci[1], Sibel Dogan[1], Sahika Yardim[1], Seyhun Solakoglu[1], Ilhan Tahrali[2], Gunnur Deniz[2], Gulnaz Nural Bekiroglu[3], Elif Kervancioglu Demirci[1]

[1]Department of Histology and Embryology, Istanbul Faculty of Medicine, Istanbul University, Istanbul, Turkiye
[2]Department of Immunology, Aziz Sancar Institute of Experimental Medicine, Istanbul University, Istanbul, Turkiye
[3]Department of Biostatistics, Faculty of Medicine, Marmara University, Istanbul, Turkiye

ORCID ID: N.I. 0000-0001-5134-3386; S.D. 0000-0002-3448-8070; S.Y. 0000-0002-5483-6896; S.S. 0000-0002-1389-9639; I.T. 0000-0001-9647-796X; G.D. 0000-0002-0721-6213; G.N.B. 0000-0001-6471-6612; E.K.D. 0000-0002-3158-9300

Cite this article as: Isci N , Dogan S, Yardim S, Solakoglu S, Tahrali I, Deniz G, Bekiroglu GN, Kervancioglu Demirci E. Propolis: Intrinsic pathway-induced apoptosis, G1 cell cycle arrest, reduced chemotherapeutic resistance in adenocarcinoma, and healthy cell preservation. Experimed. Experimed 2023; 13(3): 194-204.

ABSTRACT

Objective: This study investigated the potential synergistic effects of propolis, an antitumor and antioxidant natural product, and carboplatin, a frequently used chemotherapeutic agent for endometrial adenocarcinoma, one of the most common gynaecological cancers treatment.

Materials and Methods: Ishikawa endometrial adenocarcinoma and healthy fibroblast (3T3) cell lines were treated with 0.5 µL of carboplatin and 5 µL of propolis. Cell count, viability, migration, ultrastructure, apoptosis, and cell cycle changes were assessed using cytological and immunocytochemical methods, flow cytometry, and transmission electron microscopy (TEM).

Results: Propolis and carboplatin exhibited cytotoxic effects on Ishikawa cells. The combination of the two agents further reduced cell viability and migration. Propolis induced apoptosis through the intrinsic pathway and arrested the cell cycle in the G1 phase. TEM analysis revealed apoptosis in Ishikawa cells treated with propolis or carboplatin, while the carboplatin+propolis combination resulted in severe cell budding, apoptosis, and vacuolization. Migrasome-like structures were only observed in the Ishikawa carboplatin group. Minimal effects were observed on 3T3 cells.

Conclusion: Propolis demonstrated cytotoxic, anti-proliferative, and proapoptotic effects on tumor cells without harming healthy cells. Its ability to prevent migrasome formation suggests it may reduce chemotherapeutic resistance. Therefore, propolis shows promise as a potential enhancer of anticancer treatments.

Keywords: 3T3, apoptosis, electron microscopy, endometrium, Ishikawa, migrasome

INTRODUCTION

Endometrial cancer is the most common cancer affecting women in both developed and developing countries worldwide, with the potential to cause infertility and even death in affected individuals (1-4). The Ishikawa endometrial epithelium continuous cell line, which expresses both estrogen and progesterone receptors, is a widely used model to study endometrial adenocarcinoma, while the 3T3 fibroblast cell line was often employed as a control group in various *in vitro* studies (4, 5). The platinum group chemotherapeutic agent, carboplatin, is the preferred treatment option for endometrial cancer, with the aim of controlling the disease and increasing patient survival rates (6, 7).

Corresponding Author: Elif Kervancioglu Demirci **E-mail:** elifkervanciogludemirci@istanbul.edu.tr
Submitted: 17.08.2023 **Revision Requested:** 09.10.2023 **Last Revision Received:** 18.10.2023 **Accepted:** 03.11.2023 **Published Online:** 04.12.2023

There is promising evidence to suggest that combining carboplatin with herbal agents can improve cytotoxicity and increase survival rates in patients with endometrial cancer (8, 9). One such herbal supplement is propolis, a resinous substance collected by honeybees from plants, which has been shown to have anticarcinogenic, antioxidant, antifungal, and antibacterial effects, and have cytotoxic effect on various cancer cell lines (10-14). However, there is gap of research investigating the effects of propolis on endometrial cancer at a structural and ultrastructural level, and its mechanism of action remains poorly understood.

In this study, we aimed to investigate the potential of propolis extract to enhance the cytotoxic, apoptotic, and antitumor effects of carboplatin on the Ishikawa endometrial adenocarcinoma cell line, and to assess its effect on healthy 3T3 fibroblast cells. By elucidating the mechanism of action of propolis and carboplatin on both cancerous and healthy cells, we hope to improve the efficacy of cancer chemotherapy and contribute to the development of new treatment options for endometrial adenocarcinoma.

MATERIALS AND METHODS

Cell Culture

Ishikawa endometrial adenocarcinoma cell line derived from human endometrium (99040201, European Collection of Authenticated Cell Culture ECACC, Merck, Darmstadt, Germany), and 3T3 cell lines from mouse embryo fibroblast cells (86052701, European Collection of Authenticated Cell Culture ECACC, Merck, Darmstadt, Germany). Cell lines were cultured in 10% fetal bovine serum (FBS-11A, Capricorn, Germany), 100 µg/mL streptomycin, 100 IU/mL penicillin and 0.2 µM glutamine were filtered into sterile DMEM/F-12 (12500062, Thermo, Massachusetts, USA) medium. Cells were allowed to proliferate for 72 hours in a humidified incubator at 37°C containing 95% air and 5% CO_2.

After conducting preliminary studies to determine the optimal propolis and carboplatin dosages at various time intervals according to the literature, a total of 8 experimental groups were established (15, 16). In these groups, propolis (5 µL) (Eğriçayır, Istanbul, Turkiye) and carboplatin (0.5 µL) (150 mg/15 mL) (Koçak Farma, Tekirdag, Turkiye) were administered individually and in combination (Table 1). All experiments were conducted in triplicate on Ishikawa cells and 3T3 cells, and each experiment was repeated three times.

Table 1. Experimental groups.

Group 1	Ishikawa Control
Group 2	Ishikawa+Propolis
Group 3	Ishikawa+Carboplatin
Group 4	Ishikawa+Propolis+Carboplatin
Group 5	3T3 Control
Group 6	3T3+Propolis
Group 7	3T3+Carboplatin
Group 8	3T3+Propolis+Carboplatin

Cell Viability Assay

$1x10^5$ numbers of Ishikawa and 3T3 cells were cultured in 12-well cell culture plates. The trypan blue test was performed to determine viability at 24 hours. Cell counts were conducted by using a Neubauer slide under the microscope (Olympus CKX41, Tokyo, Japan).

The viability ratio was calculated as follows: Viable cell ratio (%) = Count of unstained cells/Total number of cells x 100

Measurement of Apoptosis in Cells by Flow Cytometry

The Annexin V-FITC Apoptosis Staining/Detection kit (Abcam-14085, Cambridge, Massachusetts, USA) was used to $1x10^5$ Ishikawa and 3T3 cells following the manufacturer's recommended protocol. 5 µL of Annexin V-FITC and 5 µL of propidium iodide (PI) were added to 500 µL of Annexin V binding buffer, followed by a 5-minute incubation in the dark at room temperature. At the 24th hour, the apoptotic effect in the experimental groups were assessed using a flow cytometry device (NovoCyte, ACEA, BD Biosciences, New Jersey, USA).

Cell Migration Assay

The migration of cells was monitored using the wound healing assay. A suspension of $2x10^5$ cells/mL was prepared. Ishikawa and 3T3 cells were seeded in 6-well cell culture plates and allowed for 48 hours to adhere to the ground until they reached confluence. Subsequently, scratches were created with a pipette tip in the wells where the cells were seeded. The wells were then washed with medium to remove cell

Table 2. Effects of drugs on viability at 24th hour in Ishikawa and 3T3 cell lines.

Viability %	Control	Propolis	Carboplatin	Propolis+Carboplatin	p-value
Ishikawa	96.23 ± 1.6	82.24 ± 6.5*	83 ± 3.9*	81.53 ± 3.8*	p<0.01
3T3	95.15 ± 0.7	95.30 ± 2.1	96.30 ± 1.6	95.79 ± 2.0	p>0.05

Cell lines are compared with the control group; values were given as mean ± standard deviation; *p<0.05.

debris, and fresh medium was added and dosed accordingly. The distance of the cells at specified points determined at 0 hours (initial), 24 hours and 48 hours were followed under the inverted microscope at 10x magnification and photographed. Results were measured with the Image J program.

Rate of cell migration was measured as follows:

% of change = - (Initial wound width – Wound width at 24 hours) / Initial wound width x 100

% of change = - (Initial wound width – Wound width at 48 hours) / Initial wound width x 100

Immunocytochemistry

Cytochrome-c was examined to determine the effects of propolis and carboplatin on the intrinsic pathway of apoptosis. P27 showed the effects of propolis and carboplatin on the G1 phase of the cell cycle.

$3x10^4$ Ishikawa and 3T3 cells were seeded and kept in the incubator for 1 hour to adhere to the ground. 5 µL propolis and 0.5 µL carboplatin doses were applied to the cells and incubated for cytochrome-c staining for 24 hours and for p27 staining for 48 hours at 37 °C with 5% CO_2. Cells were fixed with 4% paraformaldehyde. They were then incubated in hydrogen peroxide (H_2O_2) and block serum (TA-125-UB, Thermo Scientific, Massachusetts, USA).

For immunocytochemistry procedures, primary antibodies cytochrome-c (1:100, mouse anti-human, SC-13560, Santa Cruz, California, USA) and p27 (1:100, rabbit anti-human, SC-528, Santa Cruz, California, USA) were applied and incubated at +4°C overnight. A secondary antibody (Biotinylated Goat Anti-Polyvalent, Thermo Scientific, Massachusetts, USA) was applied for 1 hour and washed with PBS. After Streptavidin (TS-125-HR, Thermo Scientific, Massachusetts, USA) application, the cells were stained with AEC chromogen (TA-007-HAC, Thermo Scientific, Massachusetts, USA). Mayer's hematoxylin was used in cytochrome-c-stained preparations for counterstaining. Nuclear counterstaining was not done for p27 due to the staining localization of the primary antibody. At the end of the procedures, cells were sealed with an aqueous mounting medium (TA-125-AM, Thermo Scientific, Massachusetts, USA) and examined under a light microscope (Leica, DMLB, Wetzlar, Germany) and photographed. Two histologists unaware of the experimental groups counted ~400 cells, double-blind, and the mean of stained and unstained cell counts were noted in each preparation.

Staining was calculated as follows: Ratio of Stained Cells (%) = Stained cell count / Total counted cells x 100.

Table 3. Apoptosis rates of Ishikawa and 3T3 cell lines at 24th hour.

Apoptotic Cell %	Control	Propolis	Carboplatin	Propolis+Carboplatin	p-value
Ishikawa	5.68 ± 0.2	12.26 ± 0.4***	6.47 ± 0.2*	12.04 ± 0.3***	p<0.001
3T3	4.15 ± 0.4	3.61 ± 0.02	4.16 ± 0.05	3.69 ± 0.1	p>0.05

Cell lines are compared with the control group; values were given as mean ± standard deviation; *p<0.05, ***p<0.001.

Table 4. Migration rates of Ishikawa and 3T3 cell line at 24th and 48th hour.

Cell Migration %	Control n=30	Propolis n=30	Carboplatin n=30	Propolis+Carboplatin n=30	p-value
Ishikawa 24th hour	75.27 (86.99, 33.34)	54.95** (77.04, 33.42)	44.96** (74.63, 10.16)	38.06** (56.76, 13.20)	p<0.01
Ishikawa 48th hour	98.47 (99.68, 94.95)	77.18** (90.38, 50.80)	80.51** (95.52, 59.06)	76.35** (88.40, 60.65)	p<0.01
3T3 24th hour	62.67 (82.39, 22.37)	76.70* (94.62, 33.03)	79.26* (92.90, 53.52)	86.01*** (95.52, 35.39)	p<0.001
3T3 48th hour	86.11 (96.50, 64.11)	95.48** (98.40, 65.25)	91.99 (96.19, 75.26)	96.63** (98.77, 83.83)	p<0.01

Cell lines are compared with the control group; values were given as median (max, min); *p<0.05 **p<0.01 ***p<0.001.

Table 5. Cytochrome-c ratios of Ishikawa and 3T3 cell lines at 24th hour.

Cytochrome-c %	Control	Propolis	Carboplatin	Propolis+Carboplatin	p-value
Ishikawa	5.67 ± 0.7	11.63 ± 0.8***	7.01 ± 0.3	13.34 ± 0.9***	p<0.001
3T3	4.73 ± 0.1	3.91 ± 1.3	4.74 ± 1.2	4.00 ± 0.3	p>0.05

Cell lines are compared with the control group; values were given as mean ± standard deviation; ***p<0.001.

Table 6. p27 ratios of Ishikawa and 3T3 cell lines at 48th hour.

p27 %	Control	Propolis	Carboplatin	Propolis+Carboplatin	p-value
Ishikawa	9.96 ± 3.5	16.30 ± 2.7	15.33 ± 3.7	22.15 ± 3.4**	p<0.05
3T3	15.68 ± 4.0	15.15 ± 4.2	16.35 ± 1.6	16.80 ± 0.7	p>0.05

Cell lines are compared with the control group; values were given as mean ± standard deviation; **p<0.01.

Investigation of Ultrastructural Changes in Cells by Transmission Electron Microscopy (TEM)

$5x10^5$ live cells from each group were used for the TEM examination. The samples collected at the 24th hour from the experimental groups were prepared for investigation. Cells were fixed in 2.5% glutaraldehyde (104239, Merck, Darmstadt, Germany) solution for primary fixation and 1% osmic acid (124505.0100, Merck, Darmstadt, Germany) in PBS for secondary fixation. Cells were washed with PBS in between the steps. A graded series of alcohol were used for dehydration. After the propylene oxide/epon mixtures, cells were embedded in epon (45359-1EA-F, Epon 812, Sigma, Missouri, USA) and polymerized for 18 hours at 60°C. Thin sections of 60 nm were taken with an ultramicrotome (EM UC7, Leica, Wetzlar, Germany) to pyeloform-coated copper grids. Contrast was performed with uranyl acetate and lead citrate. Three histologists evaluated the specimens using TEM (JEM 1011, JEOL, Tokyo, Japan).

Statistical Analyses

The statistical analyses of the study were conducted using GraphPad Prism 9.2.0 (GraphPad Software, San Diego, California, USA) program and MS-Excel 2013. Normal distribution was assessed using the Kolmogorov-Smirnov and Shapiro-Wilk tests for all data. For normally distributed groups, one-way ANOVA test and post-hoc Tukey tests were employed, while Kruskal-Wallis and post-hoc Dunn's tests were used for groups that did not exhibit normal distribution. Evaluations between Ishikawa and 3T3 groups were performed using Student's t-test and Mann-Whitney U test. A significance level of p<0.05 was considered statistically significant. The results presented in the tables included mean ± standard deviation for normally distributed groups and median, R (max, min) for non-normally distributed groups. The average of three replicates was taken for the study. Changes in wound width during migration experiments were calculated using the percentage change

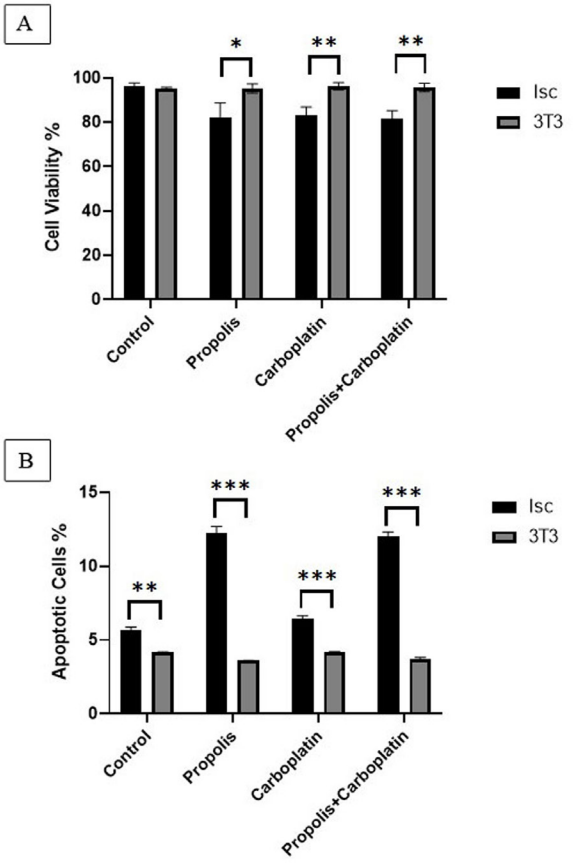

Figure 1. Comparison of Ishikawa (Isc) and 3T3 cell line A) viability and B) apoptosis at 24 hours between groups. Data was expressed as mean and standard deviation, ***p<0.001, **p<0.01, *p<0.05.

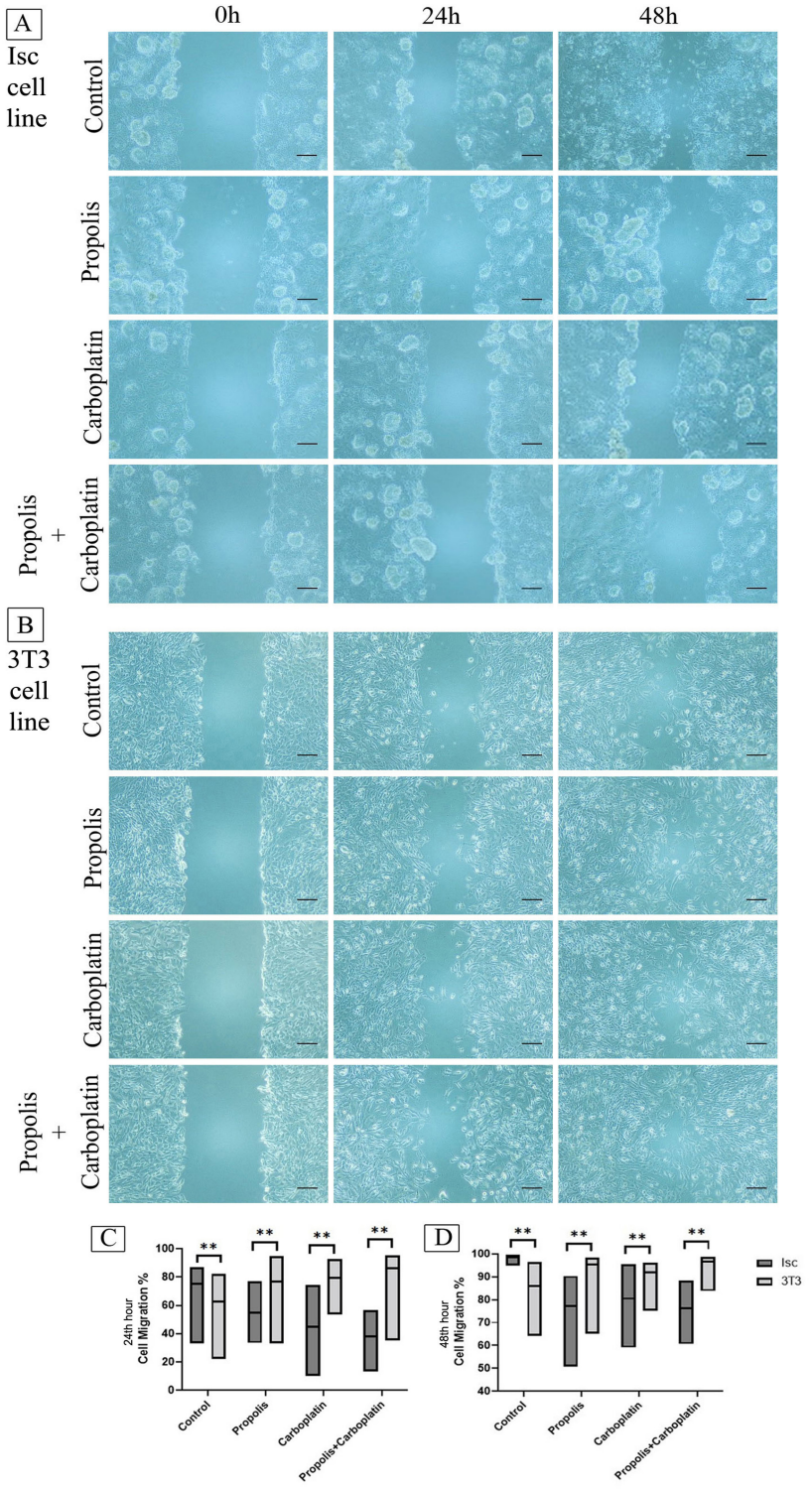

Figure 2. Phase contrast micrographs of cell migration assays at 0, 24 and 48 hours A) Ishikawa (Isc) cell line. Single treatments of propolis or carboplatin reduce migration and most significant migration deteriorating effect was observed in the propolis+carboplatin group. B) 3T3 cell line. There were no difference in cell migration in the 3T3 cell line experimental groups compared to the control group. C) 24 and D) 48-hour migration rates. 10x magnification. Bar: 100 µm; **p<0.01

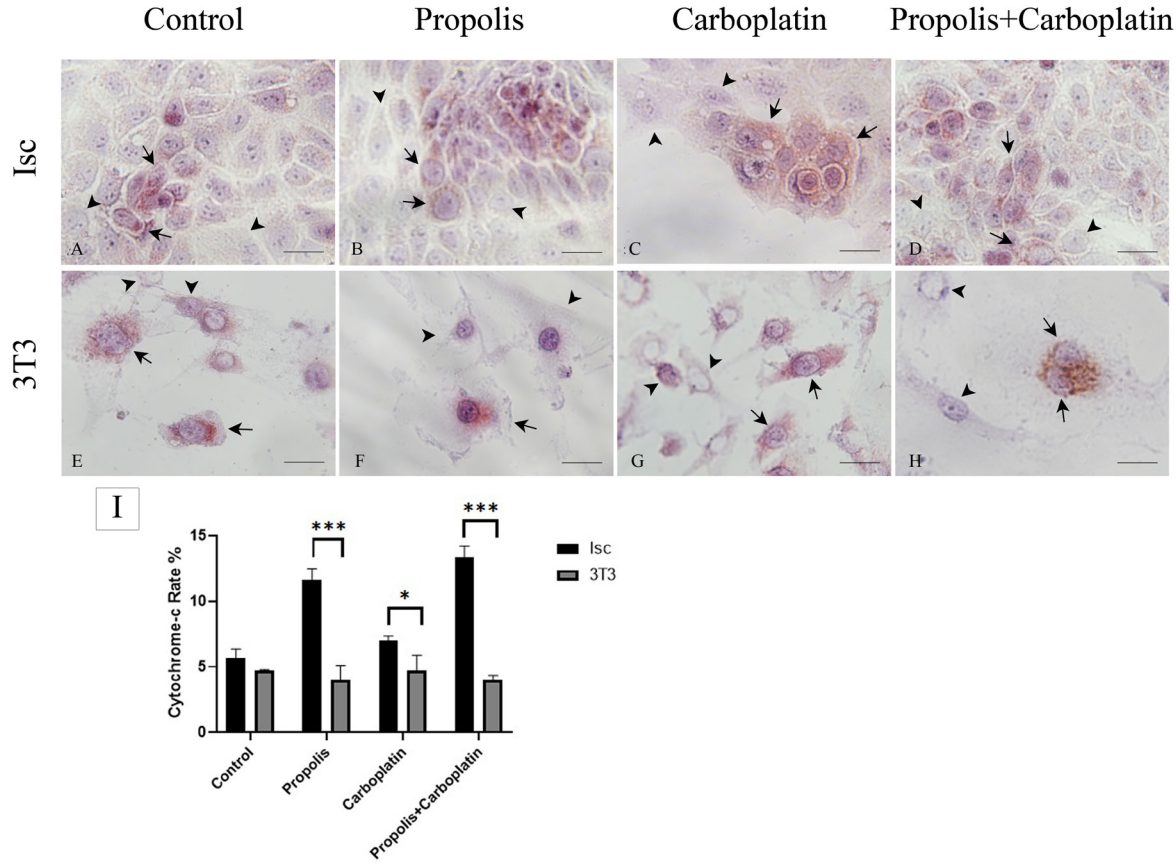

Figure 3. Cytochrome-c immunohistochemistry of A, B, C, D Ishikawa cells and E, F, G, H 3T3 cells at 24 hours. Cytoplasmic cytochrome-c positive cells with red cytoplasm (arrow) and cytochrome-c negative (arrowhead) cells are seen in all groups in different counts. Nuclei was counterstained with hematoxylin (blue) in all cells. I. Cytochrome-c ratios show the comparison of stained cell counts. While cytochrome-c staining was observed in all groups of Ishikawa cells, it was noted that the stained cell count was more in the propolis+carboplatin group. There was no difference in 3T3 cells cytochrome-c staining in experimental groups. The difference between Ishikawa and 3T3 is most profound in propolis+carboplatin groups. 40x magnification. Bar: 100 µm; ***p<0.001, *p<0.05.

formula. Apoptosis data were analyzed using NovoExpress software.

RESULTS

The Exposure of Propolis for 24h Decreased Cell Viability of Ishikawa Cells

The viability of the Ishikawa experimental groups were statistically different from each other (p=0.0086). A pairwise comparison of experimental groups with the control group showed a significant decrease in propolis (p=0.0169), carboplatin (p=0.0226) and propolis+carboplatin (p=0.0129). There was no difference in viability between 3T3 cell groups (Table 2).

The 24th hour viability test results for Ishikawa and 3T3 line experimental groups were significantly different in propolis groups (p=0.0292), carboplatin groups (p=0.0054), and propolis+carboplatin groups (p=0.0044). Carboplatin and/or propolis decreased the viability of Ishikawa cells (Figure 1A).

The Exposure of Propolis for 24h Increased Apoptosis of Ishikawa Cells

Propolis (p=0.0002), carboplatin (p=0.0385), and propolis+carboplatin groups (p=0.0003) had increased apoptosis in Ishikawa cells compared to the control group. There was no difference in the apoptosis rates in experimental groups of 3T3 cells (Table 3).

When apoptosis values of the two cell lines were compared with each other, the difference was significant between control groups (p=0.0044), propolis groups (p=0.0002), carboplatin groups (p=0.0005), and propolis+carboplatin groups (p=0.0003), and apoptosis was increased in the Ishikawa cell line (Figure 1B).

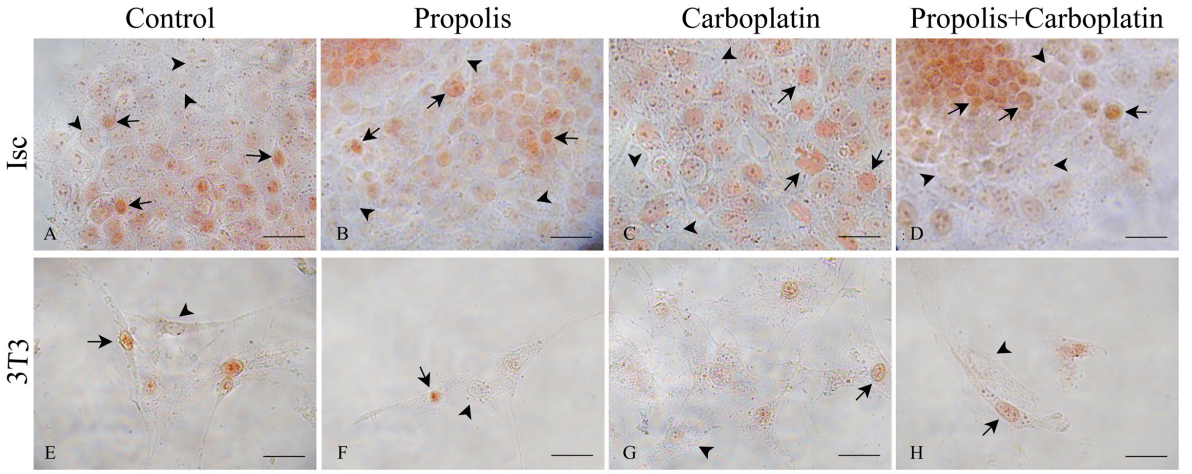

Figure 4. P27 Immunohistochemisry of A, B, C, D Ishikawa cells and E, F, G, H 3T3 cells at 48 hours. The p27 staining (red) intensity of Ishikawa cells was higher in treatment groups than in the control group with the most intense staining in the propolis+carboplatin group. P27 staining of 3T3 cells does not differ between groups. Nuclei of p27 positive (arrow) and p27 negative (arrowhead) cells are seen. 40x magnification. Scale bar: 100 µm.

Propolis Increased Migration in 3T3 Cells and Decreased Migration in Ishikawa Cells

Cell migration assay showed a statistically significant difference between groups of Ishikawa cells at 24 hours ($p<0.01$) and 48 hours ($p<0.01$). Carboplatin and/or propolis decreased the rate of migration of Ishikawa cells. The migration of Ishikawa cells at the 24th hour in propolis ($p=0.0035$), carboplatin ($p=0.0023$), and propolis+carboplatin ($p=0.0015$) experimental groups were lower when compared with the control group. The migration of Ishikawa cells at the 48th hour in propolis ($p=0.0029$), carboplatin ($p=0.0019$) and, propolis+carboplatin ($p=0.0011$) experimental groups were also lower than the control group.

The differences in migration between groups of 3T3 cells were significant at 24 hours ($p<0.001$) and 48 hours ($p<0.01$). However, propolis increased the rate of migration in 3T3 cells. The migration of 3T3 cells at 24th hours was increased in propolis ($p=0.0243$), carboplatin ($p=0.0188$) and propolis+carboplatin ($p=0.0002$) experimental groups than in the control group. The migration rate of 3T3 cells was increased in the propolis ($p=0.0031$), and propolis+carboplatin ($p=0.0018$) experimental groups at 48 hours (Table 4).

The difference between the same groups of Ishikawa and 3T3 cell lines was significant at 24 hours, and the migration in the Ishikawa cell line was lower in the propolis groups ($p=0.0062$), carboplatin groups ($p=0.0032$) and propolis+carboplatin groups ($p=0.0015$). The migration of the control groups at 24 hours was different, and it was lower in the 3T3 cell line ($p=0.0073$). At the 48th hour, migration was less in the Ishikawa cell line and the difference was significant between propolis groups ($p=0.0023$), carboplatin groups ($p=0.0015$) and propolis+carboplatin groups ($p=0.0011$). The difference was significant between the control groups at 48 hours, and the migration was lower in the 3T3 cell line ($p=0.0031$, Figure 2).

Propolis Increased Cytochrome C in Ishikawa Cells

The cytochrome c ratio of Ishikawa cells was statistically different ($p<0.001$). The propolis ($p=0.0006$) and propolis+carboplatin ($p=0.0002$) experimental groups exhibited a higher cytochrome c ratio compared to the control group. However, there was no significant difference in the cytochrome c ratio among the experimental groups of 3T3 cells (Table 5, Figures 3A-H).

Significant differences were observed between the Ishikawa and 3T3 cell lines in the same experimental groups. The cytochrome c levels in the propolis groups ($p=0.0006$), carboplatin groups ($p=0.0323$), and propolis+carboplatin ($p=0.0002$) were higher in the Ishikawa cell line. No significant difference was found between the control groups (Figure 3I).

Propolis+carboplatin Exposure Increased p27 in Ishikawa Cells

Comparing all groups, the p27 ratio of Ishikawa cells showed statistical differences ($p=0.0146$). Pairwise comparison indicated a significant difference only between the control and propolis+carboplatin experimental groups ($p=0.0093$). However, there was no significant difference in the p27 ratio of 3T3 cells (Table 6, Figures 4A-H).

The p27 ratio between the groups of Ishikawa and 3T3 cell lines groups displayed relative, but not statistically significant differences in the propolis groups ($p=0.7079$) and propolis+carboplatin ($p=0.0563$).

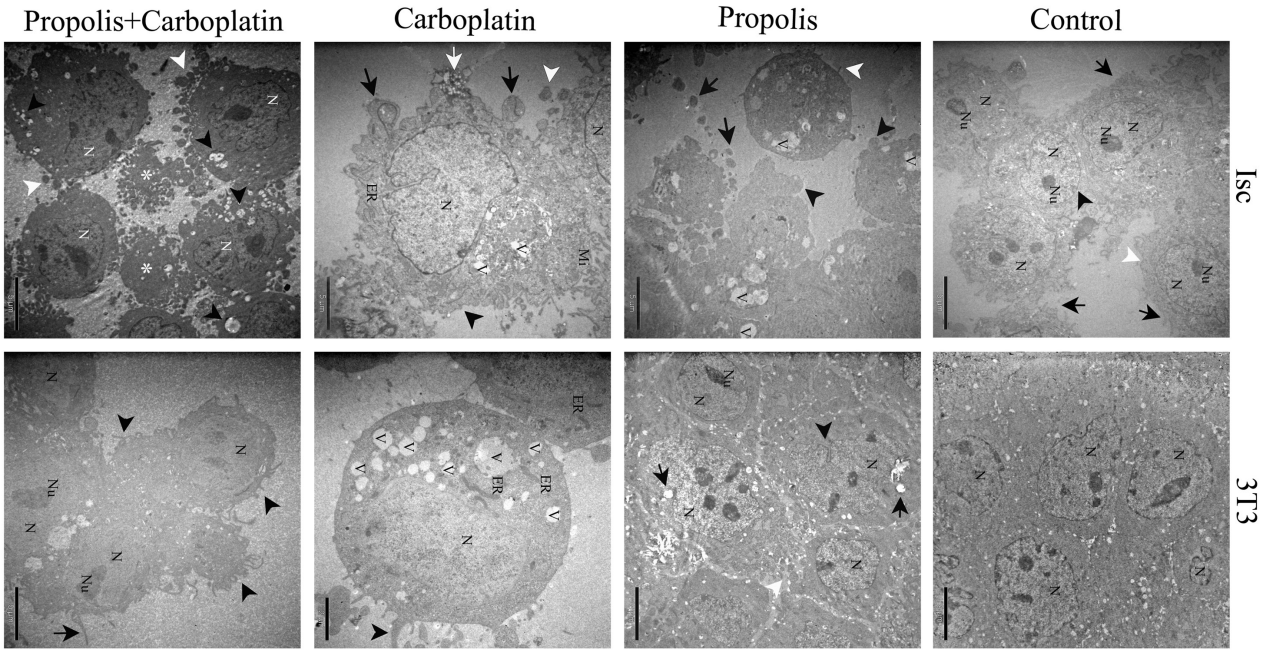

Figure 5. Electron micrographs of Ishikawa and 3T3 cells. In the left panel, electron micrographs of Ishikawa cells are shown. Control group electron micrograph: Nucleus (N) and nucleolus (Nu) are seen in normal structure, nuclear membrane (black arrowhead) and cell membrane (white arrowhead) and smooth microvilli (black arrow) are seen in intact structure. 5000x magnification. Scale bar: 5 µm. Propolis group electron micrograph: Increased number of vacuoles (V), cell budding (black arrowhead), apoptotic bodies (black arrow) and loss of microvilli (white arrowhead) are seen. 5000x magnification. Scale bar: 5 µm. Carboplatin group electron micrograph: Invaginated nucleus (N), mitochondria in normal morphology (Mi), degenerated endoplasmic reticulum (ER), vacuoles (V), cell budding (black arrow), loss of microvilli (black arrowhead), apoptotic body (white arrowhead), and migrasome-like structure (white arrow) is shown. 7500x magnification. Scale bar: 5 µm. Propolis+carboplatin group electron micrograph: Invaginated nucleus (N), vacuole (black arrowhead), apoptotic bodies (white arrowhead), and apoptotic cell remnant (asterisk) that have lost their organelles and have nuclear fragmentation are seen. 5000x magnification. Scale bar: 5 µm. In the right panel, electron micrographs of 3T3 cells are shown. Control group electron micrograph: Many cells with generally uniform morphology are seen with their nuclei (N). 5000x magnification. Scale bar: 5 µm. Propolis group electron micrograph: Although there are regular nuclei (N), nucleolus (Nu), little nuclear intussusception (black arrowhead), occasional vacuoles (black arrow), and rarely apoptotic bodies (white arrowhead), cells with smooth morphology, in general, attract attention. 5000x magnification. Scale bar: 5 µm. Carboplatin group electron micrograph: Nucleus (N), damaged endoplasmic reticulum cisterns (ER), vacuoles (V) and few cell budding (arrowhead) are seen. 10000x magnification. Scale bar: 2 µm. Propolis+carboplatin group electron micrograph: Nucleus (N), nucleolus (Nu), microvilli (arrowhead) and filopod (arrow) are seen in normal morphology. 5000x magnification. Scale bar: 5 µm.

Propolis and Carboplatin Enhanced Ishikawa Cell Apoptosis Ultrastructurally

The control group of Ishikawa cells exhibited typical cell morphology. The propolis group showed vacuoles and typical morphological features of apoptosis, including cell budding. Cell surfaces presented many apoptotic bodies and loss of microvilli. Carboplatin group displayed degeneration of endoplasmic reticulum and nucleus. The cisternae of the endoplasmic reticulum were fragmented. Migrasome-like structures were detected. Cell budding and apoptotic bodies were more prevalent. In the propolis and carboplatin combined treatment group, the nuclei were partially condensed, their size was reduced and invaginations were observed. The cells shrank, decreased in size, moved apart, and the spaces between the cells widened. Apoptotic bodies, degenerative cells, and remnants of late-phase apoptotic cells, which had already lost their organelles and had fragmented nuclei, were frequent. The apoptotic effect was severe in the propolis+carboplatin group when compared with other experimental groups (Figure 5).

The 3T3 cell line had normal morphology in the control group. In the propolis group, TEM generally showed cells with normal morphology, except for some small and few vacuoles. In the 3T3 cells carboplatin group, endoplasmic reticulum with swelling in their cisternas was found. A few cell budding and vacuoles were noted. In the propolis and carboplatin combination group, the microvilli and filopods were in regular morphology and number, and nuclei were uniform.

DISCUSSION

In our study, we investigated the effect of propolis on endometrial adenocarcinoma using cell culture techniques in combination with carboplatin, a chemotherapeutic agent commonly used in standard treatment.

Carboplatin exerts a cytotoxic effect by inhibiting cell proliferation of endometrial cancer cells (17). It increases cytochrome c release in the cytoplasm of human ovarian cancer cells and induces apoptosis in cervical carcinoma cells (18, 19). Additionally, it has an antimetastatic effect on the laryngeal carcinoma cell line (20). In our study, carboplatin increased the rate of apoptosis, reduced cell migration, and relatively elevated the rate of cytochrome c in Ishikawa cells. Since cytochrome c is associated with the intrinsic pathway of apoptosis, our study suggests that carboplatin is effective in triggering this intrinsic pathway. Although carboplatin is theoretically assumed to act on the S phase, it is not specific to the cell cycle. As an alkylating antineoplastic agent, it forms reactive platinum complexes within DNA molecule chains in the cell, leading to changes in DNA structure and inhibition of DNA synthesis. This can impact the cell cycle in every phase (21-23). Our results regarding the effect of carboplatin were consistent with the existing literature. TEM showed cell budding, increased vacuolization, the presence of apoptotic bodies, loss of microvilli, condensation of nuclei, the presence of migrasome-like structures, and organelle degeneration. These effects were minimal in the 3T3 cell line, which consists of healthy cells.

Migrasomes are classified as extracellular vesicles that mediate intercellular communication by removing unwanted molecules from cells and transferring cargo molecules to other recipient cells. Recently, migrasomes have been used to prevent resistance to cancer drugs (24-26). Our study is a first in the literature reporting that carboplatin-caused migrasome-like structure formation of Ishikawa cells is not produced in propolis treatment. The reason why migrasome structures were found only in the carboplatin experimental group of Ishikawa cells may be that tumor cells are resistant to the chemotherapeutic agent and are expelled from the cell, philopod structures are more uniform and more in number than other experimental groups, and the migration rate is high. In addition, no migrasome-like structures were found in the Ishikawa cells propolis+carboplatin treatment group, which suggested that propolis might play a role in a possible mechanism preventing the excretion of the chemotherapeutic agent carboplatin by tumor cells. However, the migrasomes observed and confirmed by three histologists with TEM were not verified by another method.

Propolis and its phenolic compounds can serve as a strong adjunct to radiotherapy and chemotherapy (27, 28). It has no known severe, moderate, or mild interactions with other drugs. Propolis decreases viability in MCF-7 and MDA-MB-231 breast cancer cell lines in a dose- and time-dependent manner but has no such effect on HUVEC cells (29). In our study, we found that propolis had a cytotoxic effect by reducing the viability of Ishikawa cells. It also had no such effect on 3T3 cells. Propolis inhibits the cell cycle in G0/G1 in human gastric cancer cells and in the G1 phase in human breast cancer cells (30, 31). As a result of our study, there was a relative increase in the p27 ratio in Ishikawa cells, which was not statistically significant. This suggested that different doses of propolis could be tested to arrest the cell cycle in the G1 phase, in line with the literature.

Propolis provides the mechanism of apoptosis both by stimulating the caspase cascade (intrinsic pathway) through the release of cytochrome-c from the mitochondria to the cytosol and by stimulating the TRAIL signalling pathway (extrinsic pathway) (32, 33). It has an apoptotic effect on the human leukemia cancer cell line U937 (34). The effect of propolis on human leukemia HL-60 cells involves the release of cytochrome-c from the mitochondria to the cytoplasm, stimulating the mitochondrial pathway, reducing cancer cell proliferation, and inducing apoptosis (35). We demonstrated that propolis induces apoptosis in the Ishikawa cell line through flow cytometry and confirmed that this occurs via the intrinsic pathway using our cytochrome-c immunocytochemical staining results. In Ishikawa cells treated with propolis; we observed increased cell budding, apoptotic bodies and vacuoles in TEM examinations, indicating the apoptotic effect of propolis. However, we did not observe apoptotic effects of propolis in 3T3 cell line experimental groups. Therefore, we concluded that propolis, which affects cancer cells, does not induce apoptosis in fibroblast cells.

Propolis inhibits cell migration in a dose-dependent manner at 48 hours on breast cancer cells. Supplements to anticancer treatments were studied in order to prevent metastasis. In this study, we investigated the metastatic activity of cancer cells using the migration test in accordance with the literature (29). Propolis slowed down cell migration of Ishikawa cells significantly when compared with the control group. Propolis was effective against metastasis.

The strengths of this study include the use of *in vitro* methods to investigate the effects of propolis and carboplatin on cancerous and healthy cells, with dosages selected based on relevant literature and preliminary studies. Another advantage is the observation of ultrastructural effects on cells without interference from *in vivo* conditions. However, a limitation is the need for further *in vivo* studies to determine the therapeutic dose for humans. Additionally, it should be noted that the composition of endemic propolis may vary geographically, which could impact its efficacy and safety in different regions. For future studies on chemotherapy resistance, a resistant cell line can be utilized, and a combination index analysis can be conducted to assess the efficacy of propolis and carboplatin in combination (36, 37).

Propolis combined with carboplatin has stronger cytotoxic and apoptotic effects on Ishikawa cells. Additionally, we observed the possibility of inhibiting treatment resistance.

This combination treatment resulted in severe apoptotic consequences for Ishikawa cells, including an increase in vacuole size and number, cell budding, apoptotic bodies, condensed relocated nuclei, a decrease in the number of microvilli, reduced cell sizes with degenerations in cytoplasmic organelles, and an increased number of advanced apoptotic degenerative cells. Our results showed that propolis and carboplatin have synergistic effects. They increased apoptosis via the intrinsic pathway and blocked the cell cycle in the G1 phase. In our examinations, we did not observe any finding suggesting any cytotoxic effect on 3T3 cells when propolis and carboplatin were administered together. In the literature, propolis did not cause cytotoxic effects in human dermal fibroblast cells; however, it increases viability, cell migration and migration rate. Hence, the increase in the migration rate of the 3T3 propolis and combination group in our study was suggested as the positive reported effect of propolis on wound healing (38). Other mechanisms of propolis on cancer cells are still under study (39).

In conclusion, propolis has demonstrated its synergistic effects with carboplatin on the endometrial cancer cell line, with no moderate or severe effects on fibroblast cells. These findings regarding the potential benefits of propolis as a dietary supplement suggest that it could be incorporated into the treatment regimens to enhance the prognosis and success of cancer chemotherapy for endometrial adenocarcinoma. Furthermore, it may warrant further investigation as a complementary approach in other chemotherapeutic studies.

Ethics Committee Approval: This research includes commercial cell lines Ishikawa and 3T3. An ethical approval is not needed because human or animal subjects or primary cell culture from human or animal subjects are not involved.

Peer-review: Externally peer-reviewed.

Authors' Contributions: Conception/Design of Study- N.I., S.S., E.K.D.; Data Acquisition: N.I., S.D., I.T., G.D., S.S., E.K.D.; Data Analysis/Interpretation: N.I., S.S., G.N.B., E.K.D., S.Y.; Drafting Manuscript: N.I., S.Y., E.K.D.; Critical Revision of Manuscript: S.D., I.T., G.D., G.N.B., S.S.; Final Approval and Accountability N.I., S.D., S.Y., I.T., G.D., G.N.B., S.S., E.K.D.

Conflict of Interest: Authors declared no conflict of interest.

Financial Disclosure: This study was funded by Scientific Research Projects Coordination Unit of Istanbul University (Project No: 37221).

REFERENCES

1. Jemal A, Bray F, Center MM, Ferlay J, Ward E, Forman D. Global cancer statistics. CA Cancer J Clin 2011; 61(2): 69-90.
2. Siegel RL, Miller KD, Jemal A. Cancer statistics, 2016. CA Cancer J Clin 2016; 66(1): 7-30.
3. Crissman JD, Azoury RS, Barnes AE, Schellhas HF. Endometrial carcinoma in women 40 years of age or younger. Obstet Gynecol 1981; 57(6): 699-704.
4. Nishida M. The Ishikawa cells from birth to the present. Hum Cell 2002; 15(3): 104-17.
5. Woodford-Thomas TA, Rhodes JD, Dixon JE. Expression of a protein tyrosine phosphatase in normal and v-src-transformed mouse 3T3 fibroblasts. J Cell Biol 1992; 117(2): 401-14.
6. Zagouri F, Bozas G, Kafantari E, Tsiatas M, Nikitas N, Dimopoulos MA, et al. Endometrial cancer: what is new in adjuvant and molecularly targeted therapy? Obstet Gynecol Int 2010; 2010: 749579.
7. Kumar A, Sirohi VK, Anum F, Singh PK, Gupta K, Gupta D, et al. Enhanced apoptosis, survivin down-regulation and assisted immunochemotherapy by curcumin-loaded amphiphilic mixed micelles for subjugating endometrial cancer. Nanomedicine 2017; 13(6): 1953-63.
8. SGO Clinical Practice Endometrial Cancer Working Group; Burke WM, Orr J, Leitao M, Salom E, Gehrig P, et al. Endometrial cancer: a review and current management strategies: part II. Gynecol Oncol 2014; 134(2): 393-402.
9. Jia N, Che X, Jiang Y, Zhu M, Yang T, Feng W. Synergistic effects of a combined treatment of PI3K/mTOR dual inhibitor LY3023414 and carboplatin on human endometrial carcinoma. Gynecol Oncol 2021; 162(3): 788-96.
10. Castaldo S, Capasso F. Propolis, an old remedy used in modern medicine. Fitoterapia 2002; 73 Suppl 1:S1-6.
11. Burdock GA. Review of the biological properties and toxicity of bee propolis (propolis). Food Chem Toxicol 1998; 36(4): 347-63.
12. Viuda Martos M, Ruiz Navajas Y, Fernández López J, Pérez Álvarez JA. Functional properties of honey, propolis, and royal jelly. J Food Sci 2008; 73(9): R117-24.
13. Turan I, Demir S, Misir S, Kilinc K, Mentese A, Aliyazicioglu Y, et al. Cytotoxic effect of Turkish propolis on liver, colon, breast, cervix and prostate cancer cell lines. Trop J Pharm Res 2015; 14(5): 777-82.
14. Demir S, Aliyazicioglu Y, Turan I, Misir S, Mentese A, Yaman SO, et al. Antiproliferative and proapoptotic activity of Turkish propolis on human lung cancer cell line. Nutr Cancer 2016; 68(1): 165-72.
15. Kubina R, Kabala-Dzik A, Dziedzic A, Bielec B, Wojtyczka RD, Buldak RJ, et al. The ethanol extract of Polish propolis exhibits anti-proliferative and/or pro-apoptotic effect on HCT 116 colon cancer and Me45 malignant melanoma cells in vitro conditions. Adv Clin Exp Med 2015; 24(2): 203-12.
16. Rantanen V, Grenman S, Kulmala J, Grenman R. Comparative evaluation of cisplatin and carboplatin sensitivity in endometrial adenocarcinoma cell lines. Br J Cancer 1994; 69(3): 482-6.
17. Kuittinen T, Rovio P, Staff S, Luukkaala T, Kallioniemi A, Grenman S, et al. Paclitaxel, carboplatin and 1,25-D3 inhibit proliferation of endometrial cancer cells in vitro. Anticancer Res 2017; 37(12): 6575-81.
18. Lee CS, Kim YJ, Jang ER, Myung SC, Kim W. Akt inhibitor enhances apoptotic effect of carboplatin on human epithelial ovarian carcinoma cell lines. Eur J Pharmacol 2010; 632(1-3): 7-13.
19. Singh S, Upadhyay AK, Ajay AK, Bhat MK. p53 regulates ERK activation in carboplatin induced apoptosis in cervical carcinoma: a novel target of p53 in apoptosis. FEBS Lett 2007; 581(2): 289-95.
20. He PJ, Ge RF, Mao WJ, Chung PS, Ahn JC, Wu HT. Oxidative stress induced by carboplatin promotes apoptosis and inhibits migration of HN-3 cells. Oncol Lett 2018; 16(6): 7131-8.
21. Coleman SC, Stewart ZA, Day TA, Netterville JL, Burkey BB, Pietenpol JA. Analysis of cell-cycle checkpoint pathways in head and neck cancer cell lines: implications for therapeutic strategies. Arch Otolaryngol Head Neck Surg 2002; 128(2): 167-76.

22. Kelland L. The resurgence of platinum-based cancer chemotherapy. Nat Rev Cancer 2007; 7(8): 573-84.
23. Sousa GFd, Wlodarczyk SR, Monteiro G. Carboplatin: molecular mechanisms of action associated with chemoresistance. Brazilian J Pharma Sci 2014; 50: 693-701.
24. Eguchi T, Taha EA, Calderwood SK, Ono K. A novel model of cancer drug resistance: oncosomal release of cytotoxic and antibody-based drugs. Biology (Basel) 2020; 9(3): 47.
25. Eguchi T, Ono K, Calderwood S, Okamoto K. Exosome release of drugs: coupling with epithelial-mesenchymal transition. Preprints 2019; 2019120386. doi:10.20944/preprints201912.0386.v1
26. Zhao X, Wu X, Qian M, Song Y, Wu D, Zhang W. Knockdown of TGF-beta1 expression in human umbilical cord mesenchymal stem cells reverts their exosome-mediated EMT promoting effect on lung cancer cells. Cancer Lett 2018; 428: 34-44.
27. Orsolic N, Knezevic AH, Sver L, Terzic S, Basic I. Immunomodulatory and antimetastatic action of propolis and related polyphenolic compounds. J Ethnopharmacol 2004; 94(2-3): 307-15.
28. Lamoral-Theys D, Pottier L, Dufrasne F, Nève J, Dubois J, Kornienko A, et al. Natural polyphenols that display anticancer properties through inhibition of kinase activity. Curr Med Chem 2010; 17(9):812- 25.
29. Xuan H, Li Z, Yan H, Sang Q, Wang K, He Q, et al. Antitumor activity of Chinese propolis in human breast cancer MCF-7 and MDA-MB-231 cells. Evid Based Complement Alternat Med 2014; 2014: 280120.
30. Desamero MJ, Kakuta S, Tang Y, Chambers JK, Uchida K, Estacio MA, et al. Tumor-suppressing potential of stingless bee propolis in in vitro and in vivo models of differentiated-type gastric adenocarcinoma. Sci Rep 2019; 9(1): 19635.
31. Misir S, Aliyazicioglu Y, Demir S, Turan I, Hepokur C. Effect of Turkish propolis on miRNA expression, cell cycle, and apoptosis in human breast cancer (MCF-7) cells. Nutr Cancer 2020; 72(1): 133-45.
32. Szliszka E, Czuba ZP, Domino M, Mazur B, Zydowicz G, Krol W. Ethanolic extract of propolis (EEP) enhances the apoptosis-inducing potential of TRAIL in cancer cells. Molecules 2009; 14(2): 738-54.
33. Sawicka D, Car H, Borawska MH, Niklinski J. The anticancer activity of propolis. Folia Histochem Cytobiol 2012; 50(1): 25-37.
34. Motomura M, Kwon KM, Suh SJ, Lee YC, Kim YK, Lee IS, et al. Propolis induces cell cycle arrest and apoptosis in human leukemic U937 cells through Bcl-2/Bax regulation. Environ Toxicol Pharmacol 2008; 26(1): 61-7.
35. Eom HS, Lee EJ, Yoon BS, Yoo BS. Propolis inhibits the proliferation of human leukaemia HL-60 cells by inducing apoptosis through the mitochondrial pathway. Nat Prod Res 2010; 24(4): 375-86.
36. Viscarra T, Buchegger K, Jofre I, Riquelme I, Zanella L, Abanto M, et al. Functional and transcriptomic characterization of carboplatin-resistant A2780 ovarian cancer cell line. Biol Res 2019; 52(1): 1-13.
37. Castañeda AM, Meléndez CM, Uribe D, Pedroza-Díaz J. Synergistic effects of natural compounds and conventional chemotherapeutic agents: Recent insights for the development of cancer treatment strategies. Heliyon 2022; 8(6): e09519.
38. Ebadi P, Fazeli M. Evaluation of the potential in vitro effects of propolis and honey on wound healing in human dermal fibroblast cells. South African J Botany 2021; 137: 414-22.
39. Altabbal S, Athamnah K, Rahma A, Wali AF, Eid AH, Iratni R, et al. Propolis: a detailed insight of its anticancer molecular mechanisms. Pharmaceuticals 2023; 16(3), 450.

Experimed 2023; 13(3): 205-212

RESEARCH ARTICLE

DOI: 10.26650/experimed.1358971

Exploring PI3K Pathway Inhibitors for Acute Myeloid Leukemia: A Drug-Repurposing Approach

Cansu Ergun[1], Buse Zeren Kiremitci[1], Gizem Arslantas[1], Busenur Bozkurt[1], Gizem Ayna Duran[1], Yagmur Kiraz[1]

[1]Department of Genetics and Bioengineering, Faculty of Engineering, Izmir University of Economics, Izmir, Turkiye

ORCID ID: C.E. 0009-0004-4968-0315; B.Z.K.0009-0005-1478-0858; G.A. 0009-0008-0693-0731; B.B. 0009-0007-9154-1847; G.A.D. 0000-0002-2168-753X; Y.K. 0000-0003-3508-5617

Cite this article as: Ergun C, Kiremitci BZ, Arslantas G, Bozkurt B, Duran GA, Kiraz Y. Exploring PI3K pathway inhibitors for acute myeloid leukemia: a drug-repurposing approach. Experimed. Experimed 2023; 13(3): 205-212.

ABSTRACT

Objective: Acute myeloid leukemia (AML) is a malignant disease characterized by the uncontrolled growth, differentiation, and proliferation of immature hematopoietic cells. Patients with AML often have poor survival rates, which are associated with specific gene mutations in *FLT3, CEBPA*, and *NPM1*. The phosphatidylinositol 3-kinase (PI3K) pathway, a lipase pathway, is activated in many malignancies, including AML. Given the low survival rates in AML, this study identified candidate drugs that could inhibit the PI3K pathway, thereby offering a potential treatment for AML, by using a drug-repurposing approach.

Materials and Methods: Online bioinformatics tools were utilized to identify pathway-related genes and FDA-approved drugs. Subsequently, molecular docking was performed to determine the binding affinity values. Important genes were identified by evaluating their impact on survival and their aberrant expression in the tumor. In this study, genes such as *VAV1, GSK3B, MTOR, PDPK1, PRR5, TSC2, AKT3,* and *CREB1* were determined and docked with their potential inhibitors. Particular attention was paid to *VAV1* because there were no known potential *VAV1* inhibitors used in AML.

Results: The docking results were ranked, and the proposed gene–drug pairs were identified as tideglusib and fostamatinib for the inhibition of *GSK3B*, pimecrolimus and fostamatinib for the inhibition of *MTOR*, and fostamatinib for the inhibition of *PDPK1*. Furthermore, nebivolol, darifenacin, dihydroergotamine, libanserin and entereg were identified as potential inhibitors of *VAV1* in AML.

Conclusion: To sum up, most effective gene–drug pairs according to binding affinities were proposed as candidate inhibitor drugs for AML.

Keywords: AML, repurposing, molecular docking, survival, PI3K pathway, *VAV1*

INTRODUCTION

As a malignant disease, acute myeloid leukemia (AML) is a disorder of the hematopoietic system. Blasts of the myeloid lineage differentiate abnormally with clonal expansion. This uncontrollable proliferation led to immature blast cell accumulation and consequently to several infections such as anemia. AML is the most prevalent type of leukemia in adults, with the average age of diagnosis being 68. The genesis of AML remain largely unknown. However, stem cell analysis has provided insights into the self-renewal capabilities of hematopoietic progenitors and their potential for oncogenic transformation. These progenitors are typically dormant and rare, contributing to chemotherapy resistance and disease recurrence. In addition, some specific mutations in *ASXL1*, *TET2*, and *DNMT3A* were detected before the genesis of leukemia in hematopoietic progenitors. These mutations were considered to be primary indicators of leukemia occurrence (1).

For the diagnosis of AML, the threshold for the amount of myeloblasts in peripheral blood or bone marrow is set at 20%. The World Health Organization's 2008 classification of AML is based on oncogenes such as *FLT3, CEBPA*, and *NPM1*. These genes are of significant importance in the

Corresponding Author: Yagmur Kiraz **E-mail:** yagmur.kiraz@ieu.edu.tr
Submitted: 19.09.2023 **Revision Requested:** 09.10.2023 **Last Revision Received:** 17.10.2023 **Accepted:** 01.11.2023

prognosis of AML. Approximately 50% of AML cases exhibit an *NPM1* mutation. Additionally, 25–45% of cases possess *FLT3* mutations, and 5–10% of patients have *CEBPA* mutations (2). Other genetic abnormalities, such as mutations in *RUNX*, *TP53*, and *IDH1*, are also detected in AML cases (3). AML is cured using conventional therapy, mutation-specific targeted therapy, immunotherapy, apoptotic pathway targeted therapy, checkpoint inhibitors, vaccines, checkpoint inhibitors, and cellular therapy (4).

The PI3K pathway contributes to several cellular mechanisms such as metabolism, survival, transcription and translation, proliferation, organization of the cytoskeleton, and growth (5, 6). The PI3K signaling pathway is a member of the heterodimeric lipid kinase family. PI3K proteins are divided into three groups of isomers 1, 2, and 3. Class 1A proteins of the PI3K family are activated by tyrosine kinases, while the activation of class 1B proteins is maintained by the G protein receptor. Upon activation by an external or internal messenger, PI3K triggers various mechanisms. In contrast, the phosphatase and tensin homolog (PTEN) acts as a tumor suppressor gene and a negative regulator of the pathway (5). This pathway is overactivated in many types of cancer. There are two specific activation mechanisms of the pathway: tyrosine kinase activation and mutations in the pathway elements. Moreover, the functional loss of the *PTEN* gene promotes the stimulation of the PI3K pathway (6).

AML patients generally exhibit an activated pattern in the PI3K pathway. This activation decreases the survival rate of the patients. PI3K plays a crucial role in hematopoietic cell functions, including survival, differentiation, and proliferation. Additionally, the *FLT3* gene, which is commonly mutated in AML cases, stimulates pathway activation (7).

Conventional chemotherapy serves as one of the treatment options for AML, with daunorubicin and cytarabine being commonly used as chemotherapy agents (8). In addition to conventional therapy, targeted therapy presents a promising alternative for patients. Given that the *FLT3* gene is frequently mutated in AML patients, midostaurin is employed as an *FLT3* inhibitor. Furthermore, enasidenib and ivosidenib are used to inhibit mutated *IDH1*, while decitabine and venetoclax are used to inhibit *DNMT3A* and *BCL2*, respectively (9). In addition to these currently used therapies, specific mutated protein targeted therapies have been developed owing to a better understanding of the genomic complexity of AML. Menin inhibitors that target *KMT2Ar* or *NPM1*, *TP53*-targeted drugs, and apoptotic inhibitors that target MCL1 and PDL-1 targeted inhibitors as immune checkpoint inhibitors were developed to effectively treat AML patients according to their genomic circumstances (10). Development, preclinical studies, and clinical trials are the steps of drug development for a specific indication. Indeed, the process of drug development is highly complex and requires significant investment and time. To overcome these challenges, drug repurposing is often employed. This involves using drugs to treat diseases that are different from their original intended use. Aspirin and sildenafil are well-known examples of repurposed drugs. Sildenafil, for instance, was originally developed for heart diseases, but it was later discovered to be effective for treating erectile dysfunction. Likewise, aspirin was originally an anti-inflammatory drug that was described as a preventative drug for several cancers, such as gastric, colorectal, and ovarian cancers (11).

Inhibition of the PI3K pathway in AML patients has a novel therapeutic significance in increasing the survival rate of patients and the success of the therapy. Our study identifies FDA-approved inhibitory drugs for pathway inhibition through a repurposing approach.

MATERIALS AND METHODS

Identification of PI3K Pathway-related Genes in AML

The KEGG and DAVID databases were utilized to identify genes related to the PI3K pathway (12, 13). Genes obtained from these databases were analyzed in terms of their relationship with AML by using CTD databases (14).

Gene Expression and Survival Plot Analysis

The genes were analyzed in order to compare their expression levels between AML patients and normal samples. This analysis was conducted using the GEPIA web tool. The most differentially expressed genes were also analyzed to identify their effect on survival rates in patients with AML (15).

Determination of Inhibitory Drugs

The inhibitors targeting the identified genes were determined using the DrugBank database, applying specific filters: those not used in any clinical trial for AML treatment and FDA approved (16). The ZINC15 database is known to comprise over millions of compounds; therefore, to achieve a comprehensive analysis to identify inhibitor drugs for repurposing, the ZINC15 database was used with the filters of "named," "FDA approved," and "for sale" (17). We have excluded drugs that are still in clinical trials or lack validation from further studies. This decision was made to focus our work exclusively on commercially available and FDA-approved drugs.

Molecular Docking

The 3D structures of candidate target proteins were obtained from the PDB and/or AlphaFold databases (18, 19). In addition, ligand structures were sourced from the PubChem and Zinc15 databases for subsequent docking analysis (17, 20).

The structures of *AKT3*, *PDPK1*, *MTOR*, *GSK3A*, *TSC2*, and *CREB1* genes were obtained from the AlphaFold database (19). The binding sites of these structures were identified based on literature and Biovia Discovery Studio (21). For *AKT3*, the binding site was determined at coordinates x = −15.687, y = 5.811, and z = 16.164 (21). The PIF region of the PDPK1 gene was designated as the active site of the structure (22). Additionally, the active region of the *MTOR* gene was identified between the coordinates x = −8.123, y = 26.991, z = 36.301. Similarly, for the *GSK3A* gene, the active region was defined as x = 24.996, y = 24.926, z = 27.613. For *CREB1* gene, x =5.5, y = 5.5, z =−10

was the coordinate of the binding region, and the *TSC2* gene binds actively to the ligand between x = 10, y = 1, and z = 0.2 coordinates (21).

The PDB database was employed to identify the structures of *NR4A1*, *GSK3B*, and *VAV1* genes. The 3D structure with PDB code "2QW4" was associated with *NR4A1*. This structure, recognized as the ligand binding domain of the gene, was utilized in its entirety for docking analysis. For the *GSK3B* gene, the structure with code "5K5N" was utilized, and the ligand binding region was specified with coordinates x = 24.996, y = 24.926, z = 27.613 (18, 23). 3D structure of the *VAV1* gene was detected as "6NFA" code from the PDB database (18). However, binding regions of the *VAV1* structure could not be found in the literature. Therefore, the structure was analyzed by using PyMol with the "center of mass" command. The mass center of the structure was between x = –0.791, y = 8.502, z = –24.333 coordinates and this region was determined as a binding region of the *VAV1* gene (24). Autodock Vina was used to perform docking analysis (25).

Toxicity Analysis

Eleven ligands (Raloxifene, Accolate, Nebivolol, Darifenacin, Flibanserin, Indinavir, Glipizide, Dihydroergotamine, Entereg (Alvimopan), Suvorexant, and Ergotamine) successfully docked with *VAV1*, exhibiting high docking scores. These ligands were subjected to analysis using ProTox-II, a tool for predicting the toxicity of chemicals, to unveil their toxicity parameters (26).

RESULTS

Identified Genes were PI3K Related, Overexpressed in AML, and Related to Poor Prognosis in AML

Using the KEGG and DAVID databases, primary genes of the PI3K pathway were detected. For further analysis, the CTD database was used, and 90 genes related to the AML and PI3K pathway were detected (12, 13, 14). The analysis of these 90 genes was conducted using the GEPIA database to assess their impact on patient survival and expression level increases in tumor samples (15). Among them, 14 genes emerged as significant, demonstrating both high gene expression levels and a hazardous status in terms of patient survival. The identified genes include *AKT3, CREB1, GAB1, GSK3A, GSK3B, HGF, MTOR, NR4A1, NRG4, PDPK1, PIK3AP1, PRR5, TSC2,* and *VAV1*, as detailed in Table 1.

Potential Inhibitor Drugs Identified for Selected Genes

In structure based virtual screening, predicted ligand classification and evaluation play crucial roles in several courses of computational drug design. Chemical library screening, characterization, and prediction of potential targets for combination of small molecules are included in this process. To implement this process, the Drug Bank and ZINC15 database were screened by focusing on nine specific candidate genes for the study to identify the targeted drugs associated with each gene (16, 17). Consequently, twenty one drugs for *AKT3*, four for *CREB1*, four for *GSKA*, ten for *NR4A1*, five for *HGF*, one for *GSK3B*, three for *TSC2*, four for *MTOR*, and thirty four for *PDPK1* were recorded. No drugs targeting the *GAB1*, *PRR5*, *NRG4A*, and *PI3AP1* genes were identified. However, one drug was found to inhibit the action of *VAV1*. Notably, the *HGF* gene was excluded from the study due to its reverse survival plot compared to hazardous genes (15).

Table 1: PI3K-related genes obtained from the KEGG, DAVID, and CTD databases and subsequently analyzed using the GEPIA tool.

GENE ID	NAME
AKT3	AKT serine/threonine kinase 3
CREB1	Camp responsive element binding protein
GAB1	GBR2 associated binding protein
GSK3A	Glycogen synthase kinase 3 alpha
GSK3B	Glycogen synthase kinase 3 beta
HGF	Hepatocyte growth factor
MTOR	Mechanistic target of rapamycin kinase
NR4A1	Nuclear receptor subfamily 4 group A member
NRG4	Neuregulin 4
PDPK1	3-phosphoinositide dependent protein kinase 1
PIK3AP1	Phosphoinositide-3-kinase adaptor protein
PRR5	Proline rich 5
TSC2	TSC complex subunit 2
VAV1	Guanine nucleotide exchange factor 1

FDA-approved Drugs Paired with Selected Genes

To identify potential new therapeutic agents, we conducted a drug screening process. We focused on drug candidates that had not been previously studied in patients with AML but were FDA approved for other indications. During the screening process, certain drugs were eliminated for each gene, resulting in the following recorded gene–drug pairs: *AKT3*: fostamatinib, anastrozole, and fulvestrant, *GSK3A*: fostamatinib, *TSC2*: cannabidiol, *PDPK1*: fostamatinib, *CREB1*: citalopram, *NR4A1*: acetylcysteine, *GSK3B*: tideglusib, *MTOR*: pimecrolimus and fostamatinib. It is important to highlight that epoetin alpha was previously proposed for the *VAV1* gene. Nevertheless, this inhibitor drug did not meet the criteria set by our filters.

Binding Affinities of Drugs Ranked as per Threshold

Docking analysis was conducted using these pairs, and the pairs were ranked based on the docking results to identify the strongest inhibitory effect on the pathway. The results were sorted according to the binding affinities of the ligands to the genes. For *AKT3*, the binding affinities of the drugs were –4.9 kcal/mol, –6.2 kcal/mol, and –6.9 kcal/mol for fostamatinib, anastrozole, and fulvestrant, respectively. Fostamatinib exhibited an affinity of –8.2 kcal/mol for *PDPK1*. *MTOR* was

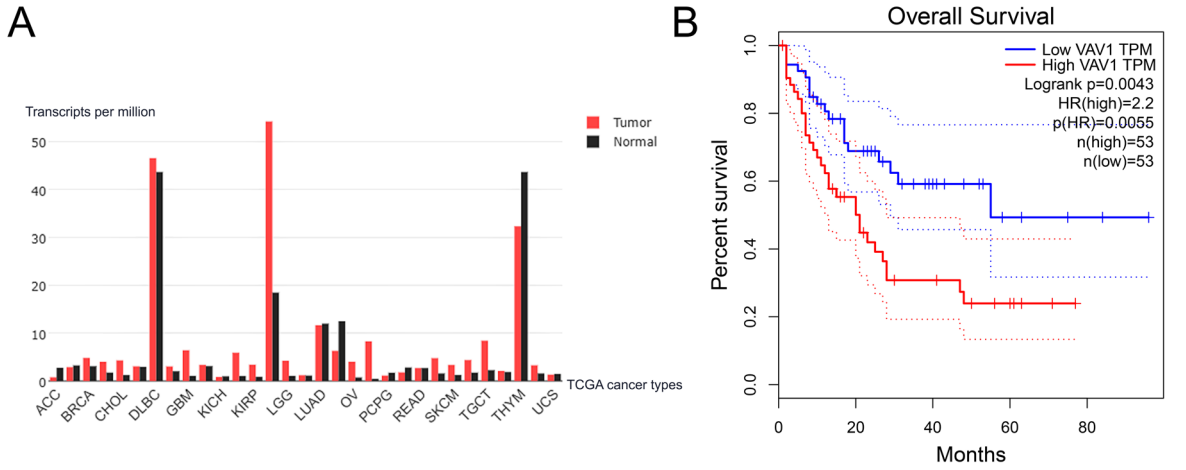

Figure 1. *VAV1* expression and survival plot in patients with acute myeloid leukemia, analyzed using GEPIA. A) The expression plot of *VAV1*; the black bar represents normal expression levels, while the red bar represents tumor expression levels. B) The survival plot of *VAV1* with a p-value of 0.0043 and a hazard ratio of 2.2; the red line indicates high expression levels, while the blue line indicates low expression levels.

paired with two inhibitors, and pimecrolimus gave a binding affinity of –19 kcal/mol to the gene. This higher affinity could not be recorded with any of the gene–drug pairs. This high binding affinity, assumed to be caused by pimecrolimus, is a well-known MTOR inhibitor. Furthermore, fostamatinib and the *MTOR* pair bind with an affinity of –8.4 kcal/mol. The docking results of acetylcysteine and *NR4A1* were –4.5 kcal/mol. This result was found to be less significant when compared with other pairs. Tideglusib gave an affinity of –8.3 kcal/mol with *GSK3B*, and the binding affinity of fostamatinib was recorded as–9 kcal/mol. The *TSC2* and cannabidiol ligand pair gave the best affinity result as –5.5 kcal/mol. Fostamatinib binds *GSK3A* with a binding affinity of –7.4 kcal/mol, and the *CREB1*–citalopram pair showed an affinity of –4.2 kcal/mol.

The binding affinity results were sorted based on whether they were below or above the threshold of –8.0 kcal/mol, considering all recorded results. Pairs with binding affinity below the specified threshold were documented as effective inhibitory pairs (Table 2).

Table 2: Binding affinity results for *PDPK1*, *MTOR*, and *GSK3B* genes and their paired drugs that fall below the threshold of –8.0 kcal/mol.

GENE	DRUG	BINDING AFFINITY (kcal/mol)
PDPK1	Fostamatinib	–8.2
MTOR	Pimecrolimus	–19.0
	Fostamatinib	–8.4
GSK3B	Tideglusib	–8.3
	Fostamatinib	–9.0

Drug Identification of *VAV1* and Docking Analysis of Candidate Drugs

Because there were not proper inhibitors for *VAV1*, although the gene is novel and hazardous for AML patients (Figure 1), drugs were screened by using the ZINC 15 database for the inhibition of *VAV1* (17). A total of 1,400 candidate drugs were retrieved from the database. Drugs with binding affinities above –9.0 kcal/mol, representing the best pairs, were subjected to docking. The analyzed drugs were further assessed for their clinical trial status in AML and their impact on specific organs. The drugs that remained in consideration, namely suvorexant, nebivolol, darifenacin, ergotamine, accolate, raloxifene, dihydroergotamine, glipizide, flibanserin, indinavir, entered with binding affinities above –9.0 kcal/mol (Figure 2).

VAV1-paired Cytotoxic Drugs were Eliminated

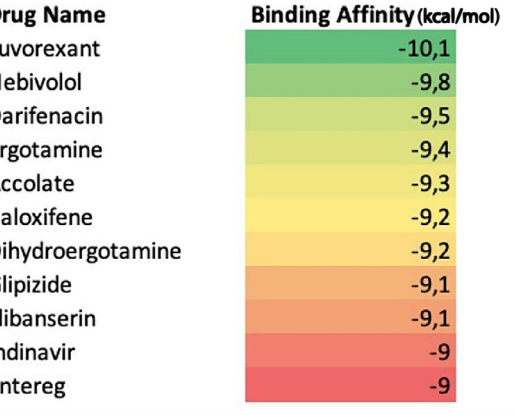

Figure 2. Binding affinities that fall below the threshold of –9.0, as determined by the molecular docking analysis results for *VAV1*.

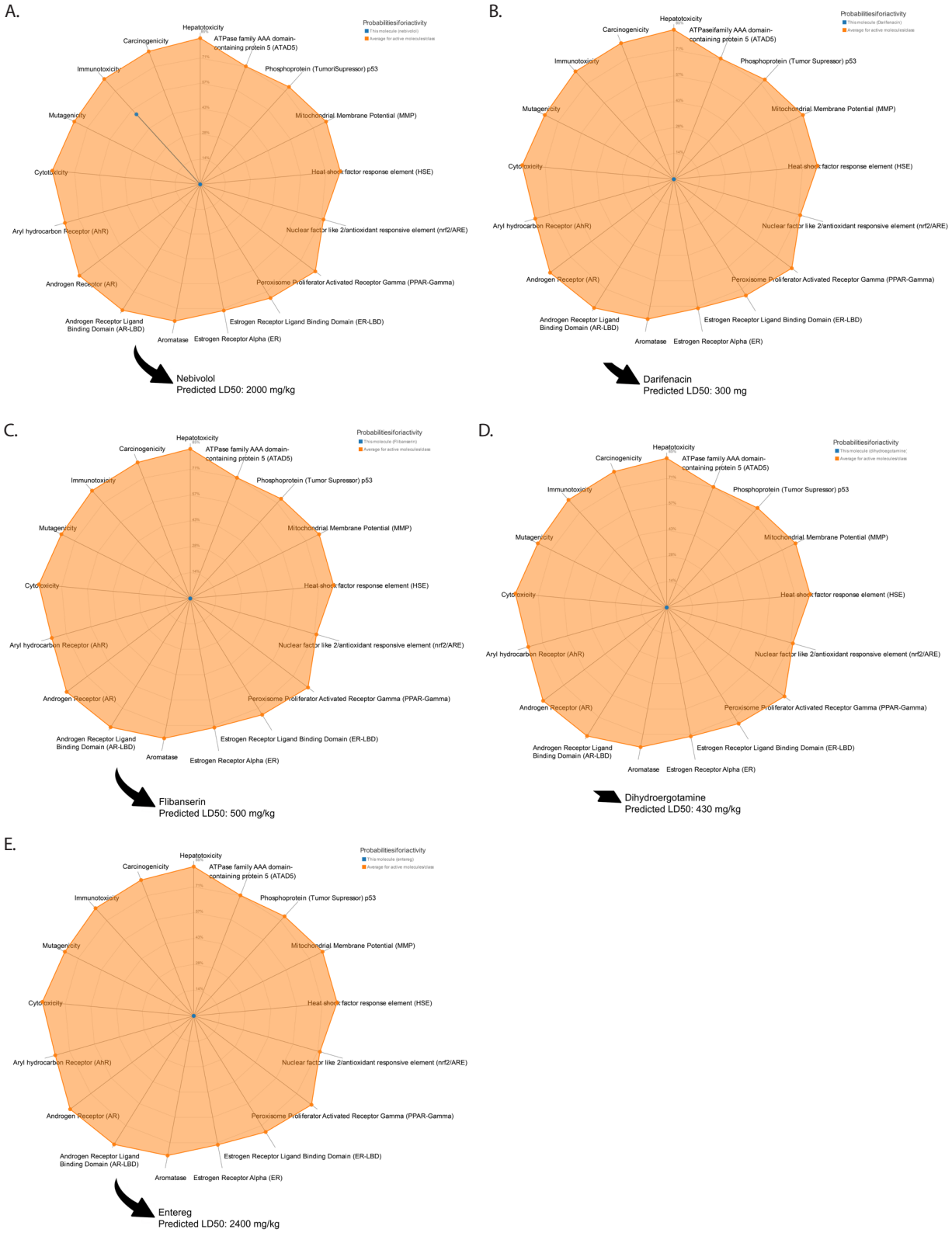

Figure 3. Toxicity analysis of drugs paired with *VAV1* and possessing high binding affinity, as analyzed using Protox-II. A) Nevivolol with an LD50 of 2000 mg/kg. B) Darifenacin with an LD50 of 300 mg/kg. C) Flibanserin with an LD50 of 500 mg/kg. D) Dihydroergotamine with an LD50 of 430 mg/kg. E) Entereg with an LD50 of 2400 mg/kg.

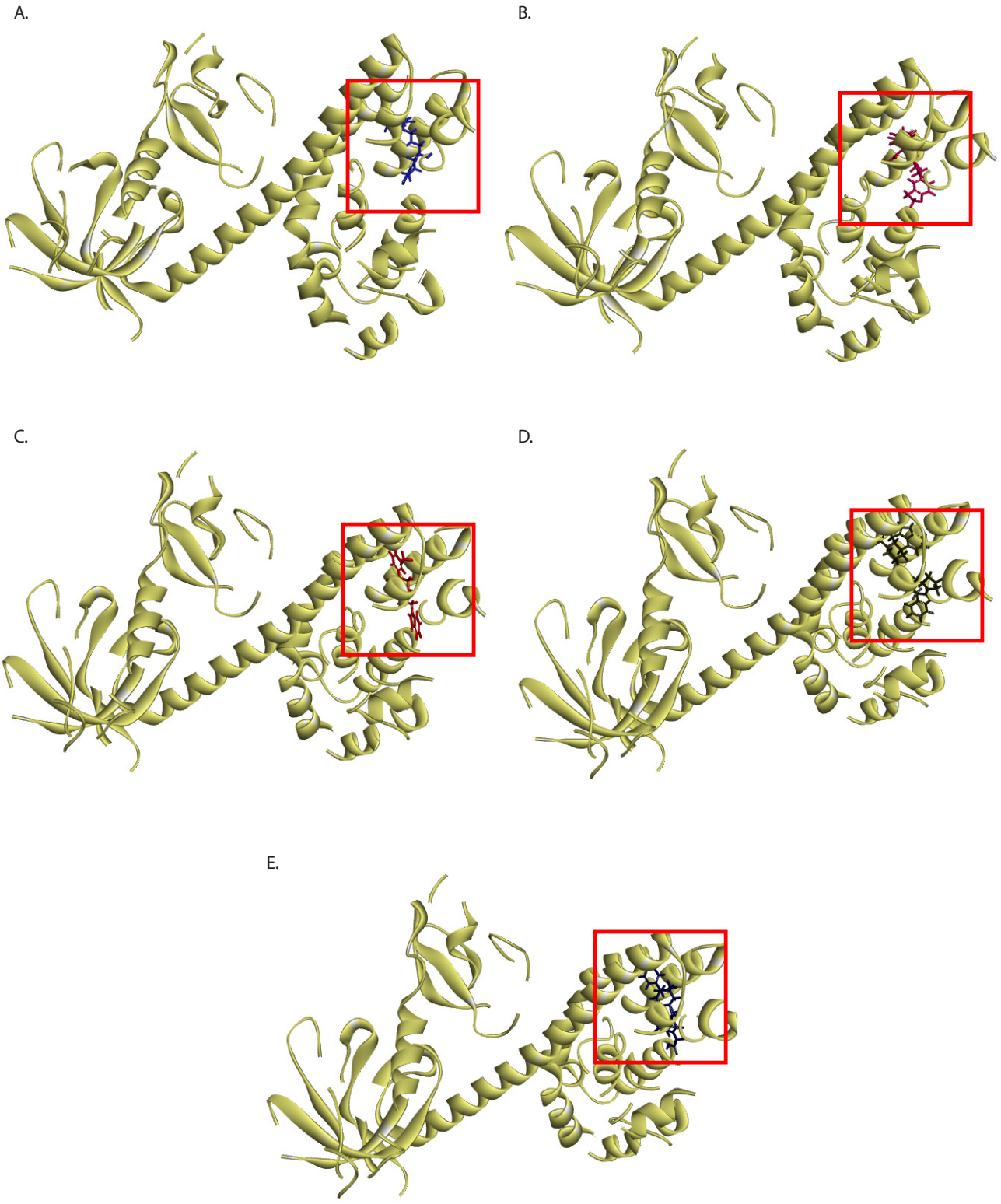

Figure 4: Molecular docking model of proposed drugs paired with *VAV1*, as visualized using Biovia Discovery Studio. The red squares indicate the ligand. A) Nebivolol, B) Darifenacin, C) Flibanserin, D) Dihydroergotamine, E) Entereg.

Due to the fact that the initially paired candidate drugs for the *VAV1* gene are not inherently inhibitors of the gene, concerns were raised regarding the toxicity status of these drugs. To address this, a toxicity analysis of the selected drugs was conducted using the Pro-tox-ii database (26). The toxicity model provided active and inactive predictions, along with LD50 values (Figure 3), where values of 2500 mg/kg and above were considered non-toxic. Subsequently, drugs were excluded based on their clinical trial status in AML and their lack of antipsychotic properties. The drugs that remained in consideration, namely nebivolol, darifenacin, dihydroergotamine, flibanserin, glipizide, and entereg, were confirmed as inhibitors of *VAV1* (Figure 4).

DISCUSSION

AML is a highly lethal cancer type with very low survival rates. The survival of patients with AML is significantly influenced by the activation of various signaling pathways. One such critical pathway is the PI3K pathway, which is known to be activated in numerous cancer types, including AML. To counteract this activation, both dual and single inhibitors are employed to inhibit PI3K activity in patients (27). In our study, the initial step involved identifying genes associated with the PI3K pathway using pathway analysis tools. Subsequently, these related genes underwent analysis to assess their expression levels and impact on patient survival. We then identified potential inhibitor drugs that were both FDA approved and novel in the context of AML treatment from online databases. The interaction between potential drugs and gene structures was further explored using molecular docking techniques to determine their binding affinities. According to the docking results, thresholds were determined for the *VAV1* gene as −9.0 and −8.0 for other genes of interest, and gene–drug pairs were ranked and potential pairs were identified. The best gene–drug pairs with the highest binding affinities *VAV1* were proposed to be the *VAV1*: nebivolol, darifenacin, dihydroergotamine, flibanserin, and entereg; *GSK3B*: tideglusib and fostamatinib; *MTOR:* pimecrolimus and fostamatinib; and *PDPK1*: fostamatinib.

We cite similar studies from the literature that propose the dual inhibition of PI3K and AKT pathways for AML treatment. Specifically, a compound C16, was suggested as an inhibitor of both pathways based on molecular docking results involving PI3K and AKT proteins, specifically PI3KCG, PI3KCD, and AKT (26-28).

Furthermore, a molecular docking approach was used to determine inhibitor drugs for AML. RNA-seq data were obtained and genes were analyzed to determine differentially expressed genes. In addition, enrichment and network analysis were performed. Following these analyses, the *CFD* and *ALDH1A1* genes were identified as prognostic target genes in AML. Molecular docking was then conducted to assess the inhibitory effects of paired drugs on these genes. The structures of the biomarkers were acquired from the PDB, and FDA-approved drugs were searched for docking analysis. Enasidenib and *ALDH1A1*, as well as gilteritinib and *CFD*, exhibited the best binding affinities and were proposed as inhibitor pairs for AML treatment (29).

Our study is guided and motivated by the findings from similar studies, which encompass analyses of FDA-approved existing drugs for repurposing candidate drugs, molecular docking analyses, and endeavors to propose novel drug–gene pairs. Most importantly, investigations to identify the most effective and novel inhibitory drugs for target prognostic genes.

Moreover, identification of *VAV1* as a potential target for AML treatment was the most significant outcome of our study because of its novelty and effect on the survival of patients with AML. In a very similar study, the *VAV* gene family was previously shown to be associated with a poor prognosis of AML. This study used several databases to identify the effect of the *VAV* gene family on the prognosis of AML. Additionally, a gene network analysis was conducted. Following computational findings, *VAV1* was identified as being over-expressed in KG-1 and MV4-11 AML cell lines. Subsequently, the GEPIA dataset was utilized to assess the impact of *VAV1* on survival. The survival plot for *VAV1* revealed a diminished profile as the gene's expression increased (30). While our study primarily comprised computational findings, the results from Mu et al. served as a guide for further analysis of *VAV1* activity in AML disease (30). The consistency in identifying the adverse prognostic effect of *VAV1* underscores the novelty and targetability of this gene

CONCLUSION

In summary, our objective was to identify inhibitor drug candidates for the treatment of AML by targeting the PI3K pathway, utilizing FDA-approved existent drugs originally developed for specific indications other than AML. Through various database and molecular docking analyses, we proposed the most effective gene–drug pairs as the most suitable candidates. These pairs include *GSK3B* with tideglusib and fostamatinib, *MTOR* with pimecrulimus and fostamatinib, and *PDPK1* with fostamatinib. Additionally, we identified *VAV1* as a novel target and therapeutic candidate for pathway inhibition, suggesting its combination with nebivolol, darifenacin, dihydroergotamine, flibanserin, glipizide, and entereg. Moreover, *VAV1* is proposed for further analysis and investigation due to its significance for AML.

Ethics Committee Approval: A publicly available dataset of AML patients from the GEPIA database was used. Ethics committee approval was excluded in this study because online bioinformatics tools are open sources and freely used in all research.

Peer-review: Externally peer-reviewed.

Author Contributions: Conception/Design of Study- Y.K., Data Acquisition- C.E., B.Z.K., G.A., B.B. Data Analysis/Interpretation- G.A.D., Y.K.; Drafting Manuscript- C.E., G.A.D., Y.K., B.Z.K., G.A., B.B.; Critical Revision of Manuscript- G.A.D., Y.K.; Final Approval and Accountability- C.E., G.A.D., Y.K., B.Z.K., G.A., B.B.

Conflict of Interest: All authors declare that they have no conflicts of interest.

Financial Disclosure: The authors declare that this study has received no financial support.

REFERENCES

1. Short NJ, Rytting ME, Cortes JE. Acute myeloid leukaemia. Lancet 2018; 392(10147): 593–606.
2. Hasserjian RP. Acute myeloid leukemia: advances in diagnosis and classification. Int J Lab Hematol 2013; 35(3): 358–66.
3. Kayser S, Levis MJ. Clinical implications of molecular markers in acute myeloid leukemia. Eur J Haematol 2019; 102(1): 20-35.
4. Short NJ, Konopleva M, Kadia TM, Borthakur G, Ravandi F, DiNardo CD, et al. Advances in the treatment of acute myeloid leukemia: new drugs and new challenges. Cancer Discov 2020; 10(4): 506–25.
5. Jiang N, Dai Q, Su X, Fu J, Feng X, Peng J. Role of PI3K/AKT pathway in cancer: the framework of malignant behavior. Mol Biol Rep 2020; 47(6): 4587–629.
6. The relation between PI3K/AKT signaling pathway and cancer. Gene 2019; 698: 120–8.
7. Nepstad I, Hatfield KJ, Grønningsæter IS, Reikvam H. The PI3K-Akt-mTOR signaling pathway in human acute myeloid leukemia (AML) Cells. Int J Mol Sci 2020; 21(8): 2907.
8. Kantarjian HM, Short NJ, Fathi AT, Marcucci G, Ravandi F, Tallman M, et al. Acute myeloid leukemia: historical perspective and progress in research and therapy over 5 decades [Internet]. Vol. 21, Clinical Lymphoma Myeloma and Leukemia. Elsevier BV; 2021. p. 580–97.
9. Fleischmann M, Schnetzke U, Hochhaus A, Scholl S. Management of acute myeloid leukemia: current treatment options and future perspectives. Cancers 2021; 13(22): 5722.
10. Totiger TM, Ghoshal A, Zabroski J, Sondhi A, Bucha S, Jahn J, et al. Targeted therapy development in acute myeloid leukemia. Biomedicines 2023; 11(2): 641.
11. Turabi KS, Deshmukh A, Paul S, Swami D, Siddiqui S, Kumar U, et al. Drug repurposing—an emerging strategy in cancer therapeutics. Naunyn Schmiedebergs Arch Pharmacol 2022; 395(10): 1139–58.
12. KEGG pathway Database [Internet]. [cited 2023 Aug 25]. Available from: https://www.genome.jp/kegg/pathway.html
13. DAVID Functional Annotation Bioinformatics Microarray Analysis [Internet]. [cited 2023 Aug 25]. Available from: https://david.ncifcrf.gov/home.jsp
14. The Comparative Toxicogenomics Database [Internet]. [cited 2023 Aug 25]. Available from: https://ctdbase.org/
15. GEPIA (Gene Expression Profiling Interactive Analysis) [Internet]. [cited 2023 Aug 25]. Available from: http://gepia.cancer-pku.cn/
16. DrugBank Online [Internet]. [cited 2023 Aug 25]. Available from: https://go.drugbank.com/
17. ZINC [Internet]. [cited 2023 Aug 25]. Available from: https://zinc15.docking.org/
18. Bank RPD. RCSB PDB: Homepage [Internet]. [cited 2023 Aug 25]. Available from: https://www.rcsb.org/
19. Database APS. AlphaFold Protein Structure Database [Internet]. [cited 2023 Aug 25]. Available from: https://alphafold.ebi.ac.uk/
20. PubChem. PubChem [Internet]. [cited 2023 Aug 25]. Available from: https://pubchem.ncbi.nlm.nih.gov/
21. BIOVIA Discovery Studio - BIOVIA - Dassault Systèmes® [Internet]. [cited 2023 Aug 25]. Available from: https://www.3ds.com/products-services/biovia/products/molecular-modeling-simulation/biovia-discovery-studio/
22. Collins BJ, Deak M, Arthur JSC, Armit LJ, Alessi DR. In vivo role of the PIF-binding docking site of PDK1 defined by knock-in mutation. EMBO J 2003; 22(16): 4202–11.
23. Ogunleye AJ, Olanrewaju AJ, Arowosegbe M, Omotuyi OI. Molecular docking based screening analysis of GSK3B. Bioinformation 2019; 15(3): 201-8.
24. PyMOL [Internet]. [cited 2023 Aug 25]. Available from: https://pymol.org/2/
25. Welcome to the PyRx Website [Internet]. [cited 2023 Aug 25]. Available from: https://pyrx.sourceforge.io/
26. ProTox-II - Prediction of TOXicity of chemicals [Internet]. [cited 2023 Aug 25]. Available from: https://tox-new.charite.de/protox_II/
27. Rodrigues ACBDC, Costa RGA, Silva SLR, Dias IRSB, Dias RB, Bezerra DP. Cell signaling pathways as molecular targets to eliminate AML stem cells. Crit Rev Oncol Hematol 2021; 160: 103277.
28. Abohassan M, Alshahrani M, Alshahrani MY, Rajagopalan P. Insilco and Invitro approaches identify novel dual PI3K/AKT pathway inhibitors to control acute myeloid leukemia cell proliferations. Med Oncol 2022; 39(12): 1–10.
29. Alom MM, Faruqe MO, Molla MKI, Rahman MM. Exploring prognostic biomarkers of acute myeloid leukemia to determine its most effective drugs from the FDA-approved list through molecular docking and dynamic simulation. Biomed Res Int 2023; 2023: 1946703.
30. Mu D, Long S, Guo L, Liu W. High Expression of VAV gene family predicts poor prognosis of acute myeloid leukemia. Technol Cancer Res Treat 2021: 20: 15330338211065877.

Experimed 2023; 13(3): 213-217

ORIGINAL ARTICLE

DOI: 10.26650/experimed.1364227

Indomethacin Affects the Inflammatory Response via Interaction with the RhoA-Actin Cytoskeleton in THP-1 Cells

Ebru Haciosmanoglu Aldogan[1], Fulya Dal Yontem[2,3], Seyma Bulut[4,5], Hande Yapislar[6], Basak Guncer[7], Muhammet Bektas[7]

[1]Department of Biophysics, Faculty of Medicine, Bezmialem Vakif University, Istanbul, Turkiye
[2]Department of Biophysics, Faculty of Medicine, Koç University, Istanbul, Turkiye
[3]Koc University Research Center for Translational Medicine (KUTTAM), Istanbul, Turkiye
[4]Department of Biotechnology, Institute of Health Sciences, Bezmialem Vakif University, Istanbul, Turkiye
[5]Department of Medical Biology, Faculty of Medicine, Bezmialem Vakif University, Istanbul, Turkiye
[6]Department of Physiology, Faculty of Medicine, Acıbadem University, Istanbul, Turkiye
[7]Department of Biophysics, Istanbul Faculty of Medicine, Istanbul University, Istanbul, Turkiye

ORCID ID: E.H.A. 0000-0001-9559-4515; F.D.Y. 0000-0003-4767-083X; S.B. 0000-0001-7540-1456; H.Y. 0000-0002-2762-357X; B.G. 0000-0002-0597-4571; M.B. 0000-0002-4438-1664

Cite this article as: Haciosmanoglu Aldogan E, Dal Yontem F, Bulut S, Yapislar H, Guncer B, Bektas M. Indomethacin affects the inflammatory response via interaction with the rhoA-actin cytoskeleton in THP-1 cells. Experimed. Experimed 2023; 13(3): 213-217.

ABSTRACT

Objective: Inflammation is a complex reaction present in numerous disorders. Indomethacin, a compound possessing an indoline core, is a Nonsteroidal Anti-Inflammatory Drug (NSAID) that is commonly prescribed for inflammation and pain. The actin network, plays a major role in cellular activities and it's regulated by by Rho GTPases has important implications for cellular dynamics and orientation. In this research, we explore the effects of indomethacin on the inflammatory response as mediated via RhoA and pyrin inflammatory complexes using an inflammatory disease model with relation actin cytoskeleton.

Materials and Methods: This study used Western blotting to examine the impact of indomethacin on the assembly processes related to the pyrin inflammasome complex and the RhoA signaling pathway in Lipopolysaccharide-stimulated THP-1 cells. Actin-indomethacin interaction was analyzed by Differential Scanning Fluorimetry (DSF).

Results: We found that while the expression levels of pyrin decreased, phosphorylated-RhoA increased but overall RhoA levels did not change. The equilibrium dissociation constant (K_D) for the G-actin-indomethacin complex was calculated to be 9.591± 1.608 ng/mL (R^2= 0.8582) using ΔT_m measurements of indomethacin by DSF.

Conclusion: Moreover, the effects of indomethacin on inflammation pathways may provide insight into the molecular mechanisms of pyrin inflammasome formation in various autoimmune diseases.

Keywords: Actin, differential scanning fluorimetry, GTPases, indomethacin, RhoA, Rho pyrin

INTRODUCTION

Autoinflammatory disorders arise from chronic inflammatory episodes caused by malfunctions in the body's innate immune defense mechanisms (1). For example, Familial Mediterranean Fever (FMF) stands out as a prevalent autoinflammatory condition and is characterized by pyrin synthesis caused due by Mediterranean Fever (*MEFV*) gene mutations (2). Pyrin plays a central role in the pyrin inflammasome, and mutations or reactions to bacterial-induced changes in RhoA GTPase can result in the activation of caspase-1, which subsequently leads to the secretion of Interleukin-1β (IL-1β)

Corresponding Author: Ebru Haciosmanoglu Aldogan **E-mail:** ehaciosmanoglu@bezmialem.edu.tr
Submitted: 25.09.2023 **Revision Requested:** 08.11.2023 **Last Revision Received:** 20.11.2023 **Accepted:** 27.11.2023

(3, 4). Interestingly, pyrin has also been found to associate with cellular skeletal components including actin and related binding proteins (4). The actin structure plays a major role in a variety of cellular activities, ranging from movement and cell division to vesicle transport and phagocytosis (5). Many Actin Binding Proteins (ABPs), which arrange actin polymerization, filament nucleation, and depolymerization, are downstream targets of Rho GTPases (6). A recent study suggested that the activation of RhoA GTPase can result in the inhibition of pyrin due to the phosphorylation activities of Protein Kinases N1 and N2 (PKN1 and PKN2) (3). Indomethacin, a widely recognized Non-steroidal Anti-Inflammatory Drug (NSAID) that is a member of the indole compound family, addresses pain-inducing inflammatory conditions by interrupting prostaglandin production (7). Recent evidence also indicates that indomethacin suppresses the inflammation process by reducing the levels of NOD-, LRR- and pyrin domain-containing protein 3 (NLRP3) (8). Thus, this study aimed to investigate the role of indomethacin in the phosphorylation of pyrin and RhoA, the mechanism responsible for this role, and the relationship between indomethacin and the actin cytoskeleton *in vitro*.

MATERIALS AND METHODS

Differential Scanning Fluorimetry (DSF)

DSF experiments were performed using a real time polymerase chain reaction (qPCR) system (BioRad CFX 96, California, USA). Reaction mixtures (25 µL) comprised 2 µM rabbit skeletal muscle actin (1 mg/mL) procured from Cytoskeleton, Inc. (AKL99, Denver, CO, USA), suspended in a buffer (pH 7.4) containing 20 mM HEPES, 150 mM NaCl, 1mM DTT, and 5% sucrose. These reaction mixtures were combined with 50X SYPRO Orange (diluted from a 5000X stock at Thermo Fisher Scientific, Waltham, MA, USA) and incubated in the presence of indomethacin ($C_{19}H_{16}ClNO_4$- Sigma Aldrich, St. Louis, MO) at concentrations ranging from 1-100 ng/mL. After incubation, these mixtures were placed in a PCR plate and subjected to gradual heating from 25°C to 90°C (using ascending increments of 0.5°C every 15 seconds) in the thermocycler (9). Three replicates per compound and six internal controls (which contained only free protein in 10% DMSO) were included in 96-well plates. The melting point (T_m) was assessed by plotting the derivative of initial fluorescence against temperature, then determining the midpoint temperature during the transition via the Boltzmann equation (10).

Cell Cultivation Process

THP-1 human monocytic cells (TIB-202, ATCC, Manassas, Virginia, USA) were grown in RPMI-1640 medium (Gibco, MD, USA) enriched with 10% FBS and 1% penicillin/streptomycin. Cells were housed in a 5% CO_2 humidified environment. Following standard trypsinization methods, cells were detached and subsequently passaged two to three times. For our experimental setup, cells were seeded into 6-well plates (at 1 x 10^5 cells/ per well) then incubated with a 20 µg/mL lipopolysaccharide (LPS) treatment for 1h followed by treatment with increasing concentrations of indomethacin for 24h.

SDS-PAGE and Western Blotting Procedure

Cells were lysed using RIPA buffer and a protease/phosphatase inhibitor cocktail (Sigma Aldrich, St. Louis, MO) using a half-hour ice incubation. Next, lysates were centrifuged at 10,000 g for 15 minutes at 4°C, after which supernatants were collected. SDS-PAGE was performed to separate proteins (40 µg), which were then transferred onto PVDF membranes (Bio-Rad, Marnes-la-Coquette, France) (11). These membranes were then incubated with primary antibodies targeting RhoA, phosphorylated-RhoA (Ser188), pyrin, and β-actin (Santa Cruz Biotechnology, Texas, USA). Subsequently, membranes were incubated with secondary peroxidase-conjugated goat anti-rabbit IgG (Cell Signaling Technology, Beverly, MA, USA) to reveal specific protein bands via chemiluminescence (Amersham Pharmacia Biotech, Piscataway, NJ). Protein quantification was then performed using densitometry analysis as implemented by NIH ImageJ software (NIH, Bethesda, MD, USA). For all blotting experiments, β-actin was used as a reference standard (12).

Statistical Analyses

Data analysis was performed with using CFX Manager and GraphPad software and protein–ligand dissociation constants (K_D) were calculated. Graphs were then presented as normalized plots and were generated using Microsoft Excel. $p<0.05$ was accepted as the significance limit.

Table 1. T_m and the difference (ΔT_m) in T_m in the absence and presence of indomethacin.

Concentration of indomethacin (ng/mL)	T_m (°C)	T_m Slope (ΔT_m, °C)
Control	57.65	5.4
1	58.42	5.7
5	59.54	6.1
10	59.96	6.3
50	60.08	6.7
100	61.22	7.1

RESULTS

Effect of Indomethacin on Actin Thermodynamic Stability

DSF measurements were taken to evaluate how indomethacin binding affects the thermodynamic stability of G-actin and to quantify the binding affinity of these proteins. The thermal unfolding characteristics of G-actin, whether alone or in the presence of indomethacin, were tracked by observing changes in the fluorescence intensity of SYPRO Orange. This dye exhibits an enhanced fluorescence signal as it binds to hydrophobic regions that become exposed during protein unfolding. For example, when a ligand binds to a protein, there is a shift in ΔT_m. These data suggest that the newly observed peak corresponds to the actin–indomethacin complex. The observed T_m was 57.65 °C for G-actin alone but 61.06 °C when G-actin was incubated with 100 ng/mL indomethacin (Figure 1, Table1). This obviously differs from the ΔT_m of untreated actin. The elevated T_m value of the actin monomers bound to indomethacin suggests that the conformational alteration induced by indomethacin on monomeric actin is associated with an enhancement in the thermodynamic stability of the actin monomers. Using ΔT_m measurements for indomethacin, the equilibrium dissociation constant (K_D) for the G-actin–indomethacin complex was determined to be 9.591± 1.608 (R^2= 0.8582) (10). These results therefore show that indomethacin binding to G-actin can affect pyrin inflammasome formation and the actin cytoskeleton.

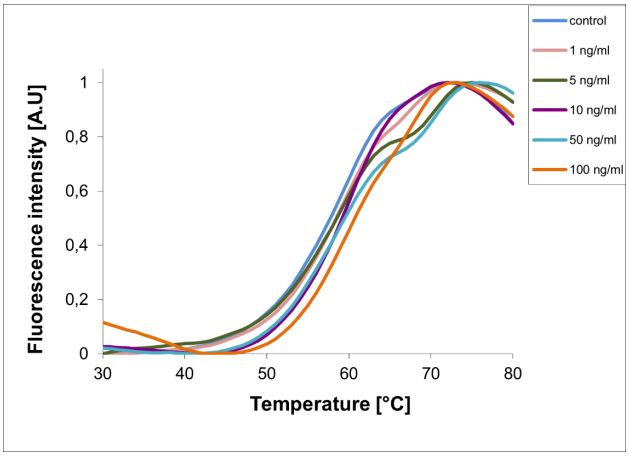

Figure 1. *In vitro* characterization of indomethacin binding to G-actin. DSF of G-actin alone and G-actin incubated with indomethacin at different concentrations. G-actin alone is shown in blue, 1 ng/mL in pink, 5 ng/mL in green, 10 ng/mL in purple, 50 ng/mL in turquoise and 100 ng/ mL in orange.

The Expression Levels of RhoA, Phosphorylated-RhoA, and Pyrin Protein Following Indomethacin Treatment

Western blotting was performed to determine the effects of indomethacin on the expression of RhoA, phosphorylated-RhoA, and pyrin in LPS-induced THP-1 cells (Figure 2A). Pyrin expression levels n significantly decreased after indomethacin

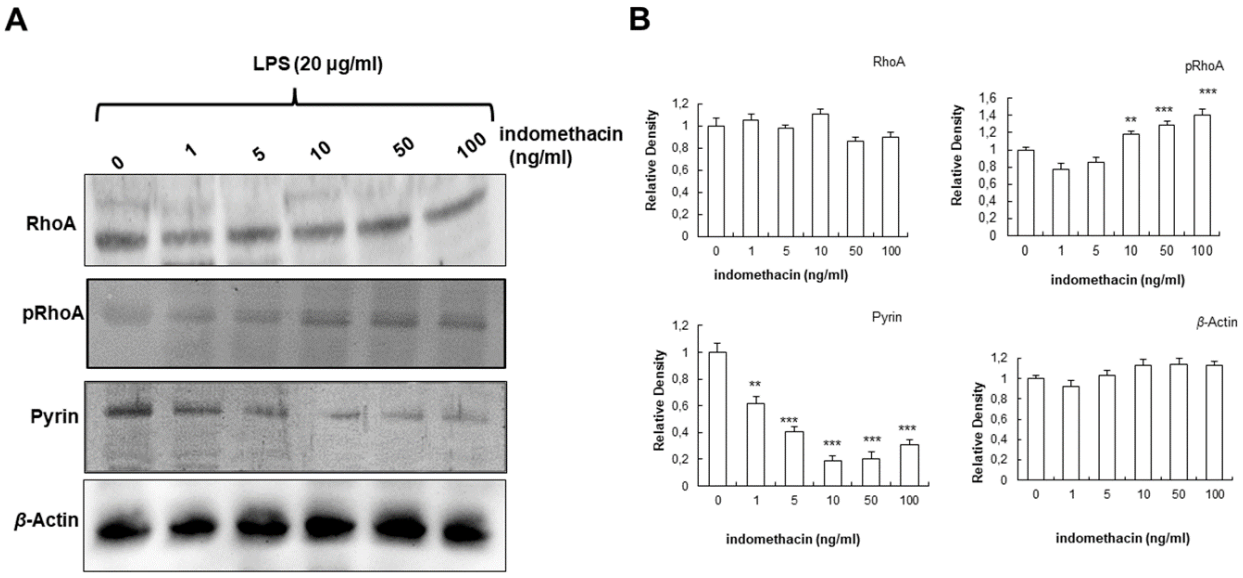

Figure 2. Effects of indomethacin on RhoA, phospho-RhoA, and pyrin expression in LPS-induced inflammation. (A) Western blots showing proteins extracted from THP-1 cells pretreated with 20 µg/mL LPS for 1 h and exposed to 1, 5, 10, 50, or 100 ng/mL indomethacin for 24 h. **(B)** Protein expression levels of RhoA, phospho-RhoA, and pyrin as determined via analysis with ImageJ. Values were expressed as mean ± SEM of three experiments. ** p < 0.01, ***p < 0.001 compared to cells treated only with LPS.

treatment relative to the control group ($p < 0.001$) (Figure 2B). Moreover, the RhoA expression level remained unchanged post-treatment, but the level of phosphorylated-RhoA increased relative to the control ($p < 0.005$) (Figure 2B). Taken together, these data suggest that indomethacin reduces inflammation by indirectly decreasing the pyrin component of the pyrin inflammasome, potentially facilitated by induced phosphorylation of the RhoA protein. Furthermore, changes to the phosphorylation of RhoA and pyrin may be result of indomethacin-G-actin.

DISCUSSION

The actin cytoskeleton, which is traditionally associated with cellular structure and motility, has also been found to be a key player in the regulation of the inflammasome. Actin dynamics in cells depend on changes between its monomeric (G-actin) and filamentous (F-actin) forms (13). Actin dynamics modulate the mobility of inflammasome components within the cell, thereby affecting their ability to form functional complexes. Studies have indicated that actin polymerization is crucial for both the formation and activation of the NLRP3 inflammasome (14). Furthermore, the RhoA-actin cytoskeletal system is known to play a major role in facilitating various cellular functions, including modulating cell morphology, mobility, and adhesion. RhoA, which belongs to the Rho GTPase family, serves as a crucial molecular switch governing the dynamics of actin. Activation of RhoA triggers actin polymerization, the development of stress fibers, and the formation of focal adhesions. These processes are indispensable for cell mobility and mechanosensory responses (15). Indomethacin, an NSAID, is primarily known for its role in inhibiting prostaglandin synthesis. However, recent studies have revealed that indomethacin can also modulate inflammasome activation. This effect is attributed to its ability to inhibit caspase 1, a key enzyme involved in inflammasome assembly, via mechanisms independent of cyclooxygenase (COX) inhibition (7).

In the present study, we demonstrated the effect of indomethacin on the pyrin inflammasome and explored how indomethacin affects the relationship between actin cytoskeleton and RhoA. DSF analysis revealed that indomethacin binds to G-actin and induces the thermal stability of monomeric actin. In addition, according to the shifting T_m values recorded here, the binding constant of indomethacin to-actin was 9.591 ± 1.608 ng/mL. Furthermore, Western blotting indicated a reduction in the expression of pyrin, one of the main components of the pyrin inflammasome, following indomethacin treatment. Together, these data suggest that the indomethacin-monomeric actin complex may be responsible for the observed decrease in the inflammatory response attributed to the pyrin inflammasome complex. For example, a previous study found that indomethacin restores actin cytoskeleton dynamics disrupted by amyloid β in differentiated human neuroblastoma cells (16). In our study, an increase in the level of phosphorylated-RhoA was observed, despite the fact that the total RhoA level remained unchanged. Phosphorylated-RhoA is known to be one of the key regulators of the actin cytoskeleton (17). Apart from binding to G-actin, indomethacin can influence Rho-kinase activity or indirectly lead to RhoA phosphorylation. In conclusion, the effect of indomethacin on the actin–pyrin inflammasome and the RhoA pathway represents an important area of research that has implications for our understanding of inflammation regulation. However, further investigation should be undertaken to understand the molecular mechanisms involved in this pathway as well as its potential significance for health and disease.

Ethics Committee Approval: Since this study is a cell culture study, no ethics committee approval is required.

Peer-review: Externally peer-reviewed.

Author Contributions: Conception/Design of Study- E.H.A., M.B., B.V.; Data Acquisition- E.H.A., F.D.Y., S.B.; Data Analysis/Interpretation- E.H.A., F.D.Y., H.Y., S.B.; Drafting Manuscript- E.H.A., F.D.Y., H.Y.; Critical Revision of Manuscript- F.D.Y., H.Y., M.B., B.V.; Final Approval and Accountability- E.H.A.

Conflicts of Interests: The authors declare that they have no competing interests.

Financial Disclosure: This study was funded by Scientific Research Projects Coordination Unit of Bezmialem Vakif University (project number: 2.2019/17).

REFERENCES

1. Ozen S. What's new in autoinflammation? Pediatr Nephrol 2019; 34(12): 2449-56.
2. Samuels J, Ozen S. Familial Mediterranean fever and the other autoinflammatory syndromes: evaluation of the patient with recurrent fever. Curr Opin Rheumatol 2006; 18(1): 108-17.
3. Park YH, Wood G, Kastner DL, Chae JJ. Pyrin inflammasome activation and RhoA signaling in the autoinflammatory diseases FMF and HIDS. Nat Immunol 2016; 17(8): 914-21.
4. Waite AL, Schaner P, Hu C, Richards N, Balci-Peynircioglu B, Hong A, et al. Pyrin and ASC co-localize to cellular sites that are rich in polymerizing actin. Exp Biol Med (Maywood) 2009; 234(1): 40-52.
5. Kustermans G, Piette J, Legrand-Poels S. Actin-targeting natural compounds as tools to study the role of actin cytoskeleton in signal transduction. Biochem Pharmacol 2008; 76(11): 1310-22.
6. Rajakyla EK, Vartiainen MK. Rho, nuclear actin, and actin-binding proteins in the regulation of transcription and gene expression. Small GTPases 2014; 5: e27539.
7. Pantovic A, Bosnjak M, Arsikin K, Kosic M, Mandic M, Ristic B, et al. In vitro antiglioma action of indomethacin is mediated via AMP-activated protein kinase/mTOR complex 1 signalling pathway. Int J Biochem Cell Biol 2017; 83: 84-96.
8. Lu G, Pan Y, Kayoumu A, Zhang L, Yin T, Tong Z, et al. Indomethacin inhabits the NLRP3 inflammasome pathway and protects severe acute pancreatitis in mice. Biochem Biophys Res Commun 2017; 493(1): 827-32.
9. Alburquerque-Gonzalez B, Bernabe-Garcia A, Bernabe-Garcia M, Ruiz-Sanz J, Lopez-Calderon FF, Gonnelli L, et al. The FDA-approved antiviral raltegravir inhibits fascin1-dependent invasion of colorectal tumor cells in vitro and in vivo. Cancers (Basel) 2021; 13(4).

10. Vivoli M, Novak HR, Littlechild JA, Harmer NJ. Determination of protein-ligand interactions using differential scanning fluorimetry. J Vis Exp 2014; 91 : 51809.
11. Laemmli UK. Cleavage of structural proteins during the assembly of the head of bacteriophage T4. Nature 1970; 227(5259): 680-5.
12. Sen S, Haciosmanoglu E. Comparing the neuroprotective effects of telmisartan, perindopril, and nebivolol against lipopolysaccharide-induced injury in neuron-like cells. Cureus. 2022; 14(7): e27429.
13. Dominguez R, Holmes KC. Actin structure and function. Annu Rev Biophys 2011; 40: 169-86.
14. Misawa T, Takahama M, Kozaki T, Lee H, Zou J, Saitoh T, et al. Microtubule-driven spatial arrangement of mitochondria promotes activation of the NLRP3 inflammasome. Nat Immunol 2013; 14(5): 454-60.
15. Smith EC, Teixeira AM, Chen RC, Wang L, Gao Y, Hahn KL, et al. Induction of megakaryocyte differentiation drives nuclear accumulation and transcriptional function of MKL1 via actin polymerization and RhoA activation. Blood 2013; 121(7): 1094-101.
16. Ferrera P, Zepeda A, Arias C. Nonsteroidal anti-inflammatory drugs attenuate amyloid-beta protein-induced actin cytoskeletal reorganization through Rho signaling modulation. Cell Mol Neurobiol 2017; 37(7): 1311-8.
17. Riento K, Ridley AJ. Rocks: multifunctional kinases in cell behaviour. Nat Rev Mol Cell Biol 2003; 4(6): 446-56.

Experimed 2023; 13(3): 218-256

ORIGINAL ARTICLE

DOI: 10.26650/experimed.1374173

Epigenetic Regulation and Therapeutic Potential of Gasdermin Genes in Colorectal Adenocarcinoma

Feyzanur Caldiran[1], Rumeysa Senol[1], Ercan Cacan[1]

[1]Department of Molecular Biology and Genetics, Faculty of Science and Art, Tokat Gaziosmanpasa University, Tokat, Turkiye

ORCID ID: F.C. 0000-0001-7778-194X; R.S. 0009-0006-3227-6484, E.C. 0000-0002-3487-9493

Cite this article as: Caldiran F, Senol R, Cacan E. Epigenetic regulation and therapeutic potential of gasdermin genes in colorectal adenocarcinoma. Experimed. Experimed 2023; 13(3): 218-256.

ABSTRACT

Objective: Colorectal adenocarcinoma (COAD) is a complex and lethal cancer characterized by genetic mutations and epigenetic alterations. Gasdermin proteins, such as gasdermin C (GSDMC) and gasdermin D (GSDMD), play crucial roles in pyroptotic cell death, presenting these proteins as potential targets for diagnosis markers and therapy across various cancers, including COAD. Our study investigated the epigenetic regulation of *GSDMC* and *GSDMD* in COAD using bioinformatics and *in vitro* experiments.

Materials and Methods: This study examined the expression and epigenetic control of pyroptosis-related proteins in COAD using bioinformatics tools and databases such as Timer2.0, UALCAN, EWAS Open Platform, Gene Set Cancer Analysis (GSCA), Receiver Operating Characteristic (ROC) plotter, and WANDERER. To investigate target gene expression, HTC-116 and SW620 cell lines were subjected to treatments with estrogen, a DNA methylation inhibitor (5-azacytidine), and a histone deacetylase inhibitor (vorinostat).

Results: The results showed that the expression of *GSDMC* and *GSDMD* varies based on the subtype of COAD. We established that these genes are regulated through DNA hypermethylation in the cg05316065 island for *GSDMC* and the cg10810860 island for *GSDMD*. Additionally, the identification of 5-fluorouracil, oxaliplatin, fluoropyrimidine monotherapy, and capecitabine as predictive biomarkers for *GSDMC* and *GSDMD* genes underscores the potential clinical utility in cancer therapy. Our results showed that a combined treatment involving 5-azacytidine, vorinostat, and estrogen increases the expression of these genes, potentially guiding cells toward pyroptosis.

Conclusions: This comprehensive analysis reveals the complex roles of *GSDMC* and *GSDMD* genes in cancer progression, showcasing their susceptibility to epigenetic regulation and impact on chemotherapy responses. These findings offer crucial insights into their significance as potential targets for diagnosis and therapy in cancer, thereby paving the way for personalized treatment strategies.

Keywords: Colorectal adenocarcinoma, gasdermin C, gasdermin D, epigenetic regulation, vorinostat, 5-azacytidine

INTRODUCTION

Colorectal adenocarcinoma (COAD) stands as the third leading cause of cancer-related morbidity and mortality globally (1). Understanding the complex molecular mechanisms steering the initiation, progression, and therapeutic resistance to therapy in COAD is crucial for enhancing diagnostic and therapeutic approaches. Recent research has increasingly focused on understanding the molecular mechanisms of COAD pathogenesis, aiming to identify novel therapeutic targets and diagnostic biomarkers.

Epigenetic mechanisms, including chromosome remodeling, DNA methylation, non-coding RNAs, and histone modifications, play crucial roles in tumor initiation, advancement, and progression by influencing gene expression. Their dysregulation is a hallmark of the disease (2,3). In COAD, DNA hypermethylation commonly occurs, particularly within the promoter regions of tumor suppressor genes among COAD patients (4). This hypermethylation effectively silences essential tumor suppressor genes, promoting cancer development and progression in many cases (2-4). Likewise, histone modifications significantly impact COAD formation.

Corresponding Author: Ercan Cacan **E-mail:** ercan.cacan@gop.edu.tr
Submitted: 10.10.2023 **Revision Requested:** 13.11.2023 **Last Revision Received:** 21.11.2023 **Accepted:** 23.11.2023

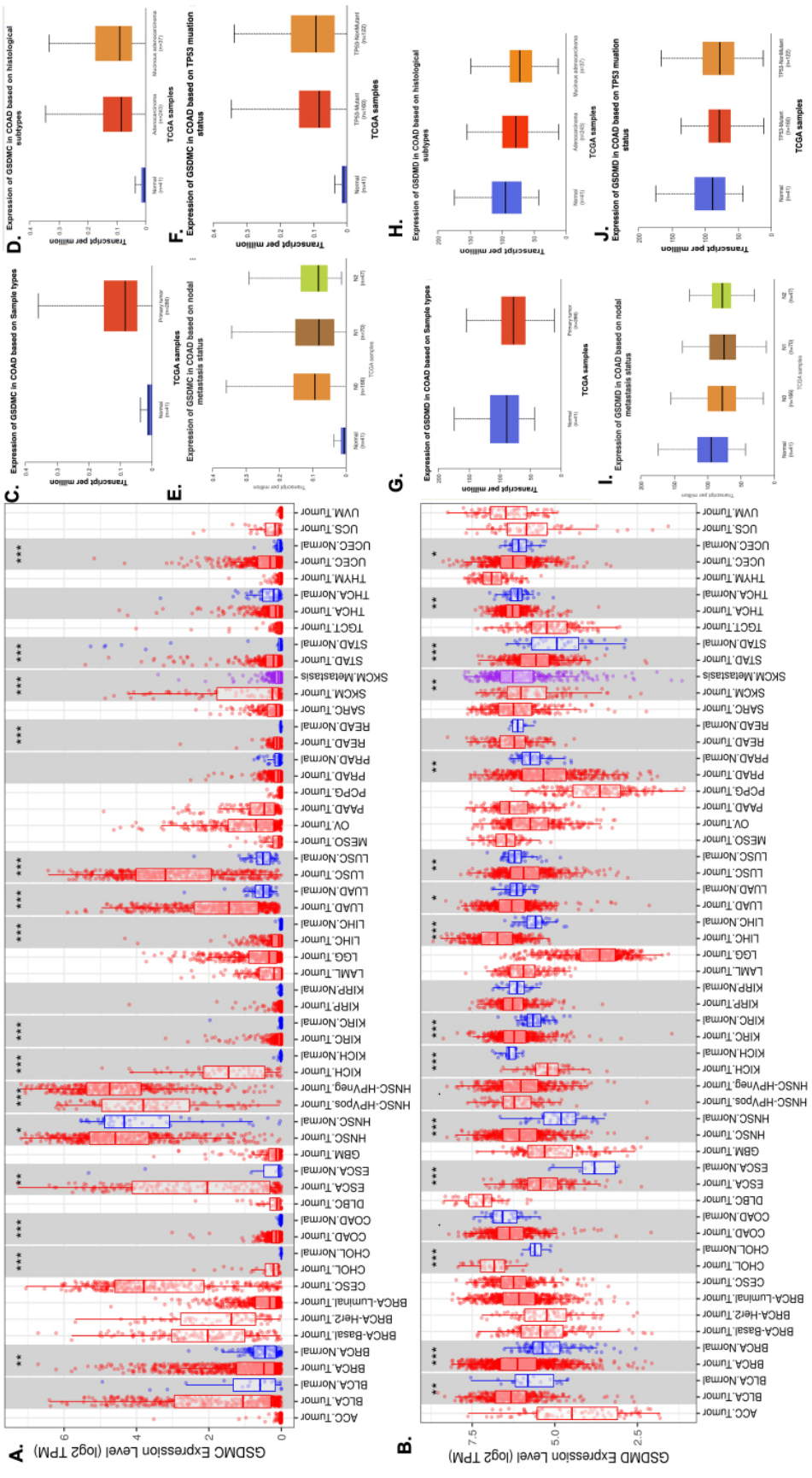

Figure 1. Pan-Cancer analysis of genes expressing gasdermin proteins C and D (*GSDMC* and *GSDMD*) in all cancer types. (A) Relative *GSDMC* expression in tumor and normal tissues. (B) Relative *GSDMD* expression in tumor and normal tissues. (C) *GSDMC* expression of colorectal adenocarcinoma (COAD) based on tumor and normal tissues. (D) *GSDMC* expression of COAD based on histological subtypes. (E) *GSDMC* expression of COAD based on nodal metastasis status. (F) *GSDMC* expression of COAD based on TP53 mutation. (G) *GSDMD* expression of COAD based on tumor and normal tissues. (H) *GSDMD* expression of COAD based on histological subtypes. (I) *GSDMD* expression of COAD based on nodal metastasis status. (J) *GSDMD* expression of COAD based on *TP53* mutation. The *GSDMC* and *GSDMD* expression in cancer (red box) and normal (blue box) tissues from TIMER. Box plots were visualized using UALCAN. *** represents a significant difference at $p < 0.01$.

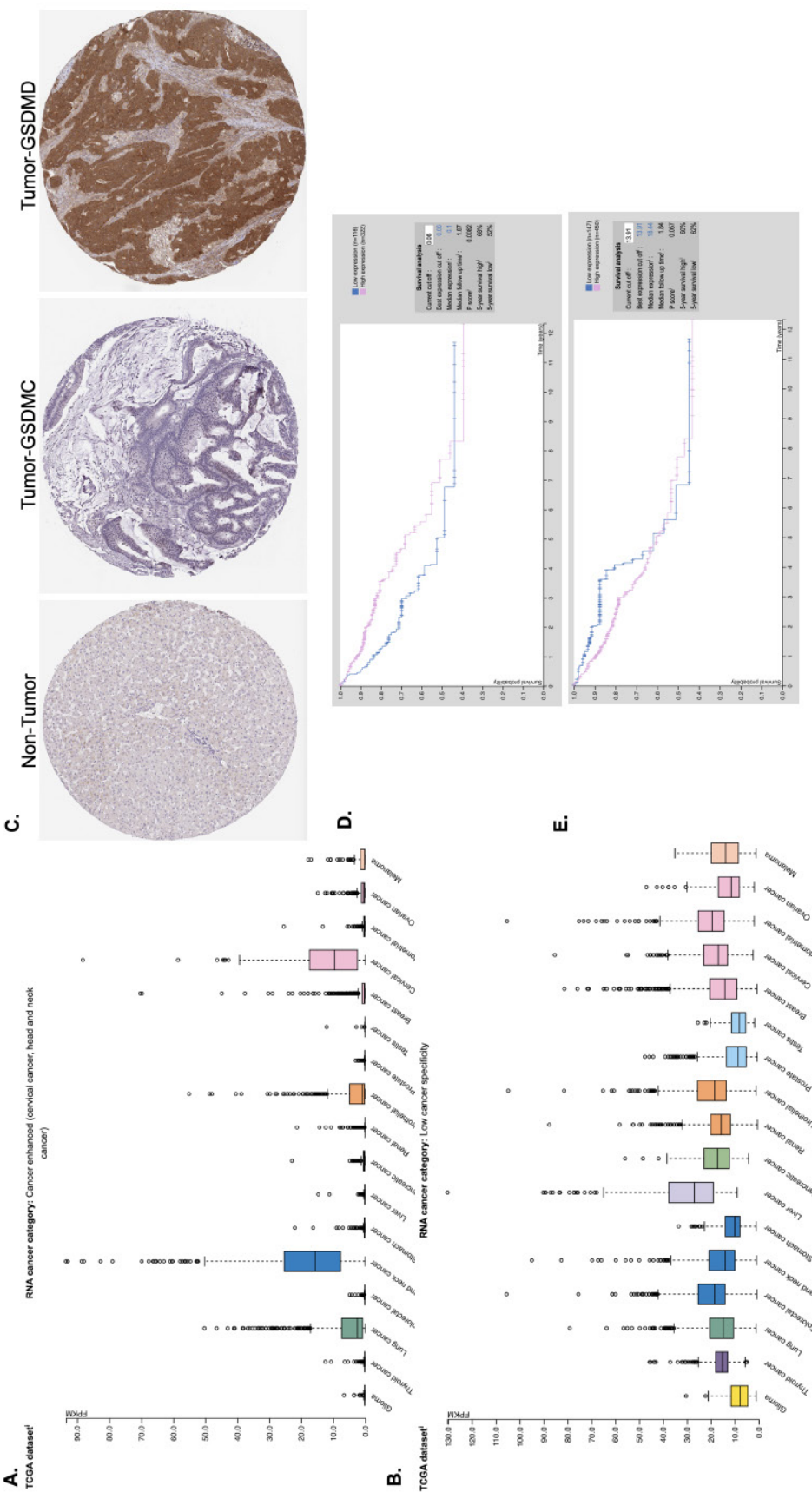

Figure 2. Proteomics analyses of *GSDMC* and *GSDMD* in COAD. (A) Comparison of *GSDMC* protein expression across various tumor types. (B) Comparison of *GSDMD* protein expression across various tumor types. (C) Representative immunohistochemistry images of GSDMC and GSDMD protein expression in high- and low-grade normal and COAD tissues. (D) Correlation between survival outcomes and *GSDMC* protein expression in COAD. (E) Correlation between survival outcomes and *GSDMD* protein expression in COAD. All analyses were conducted and visualized using the Human Protein Altas.

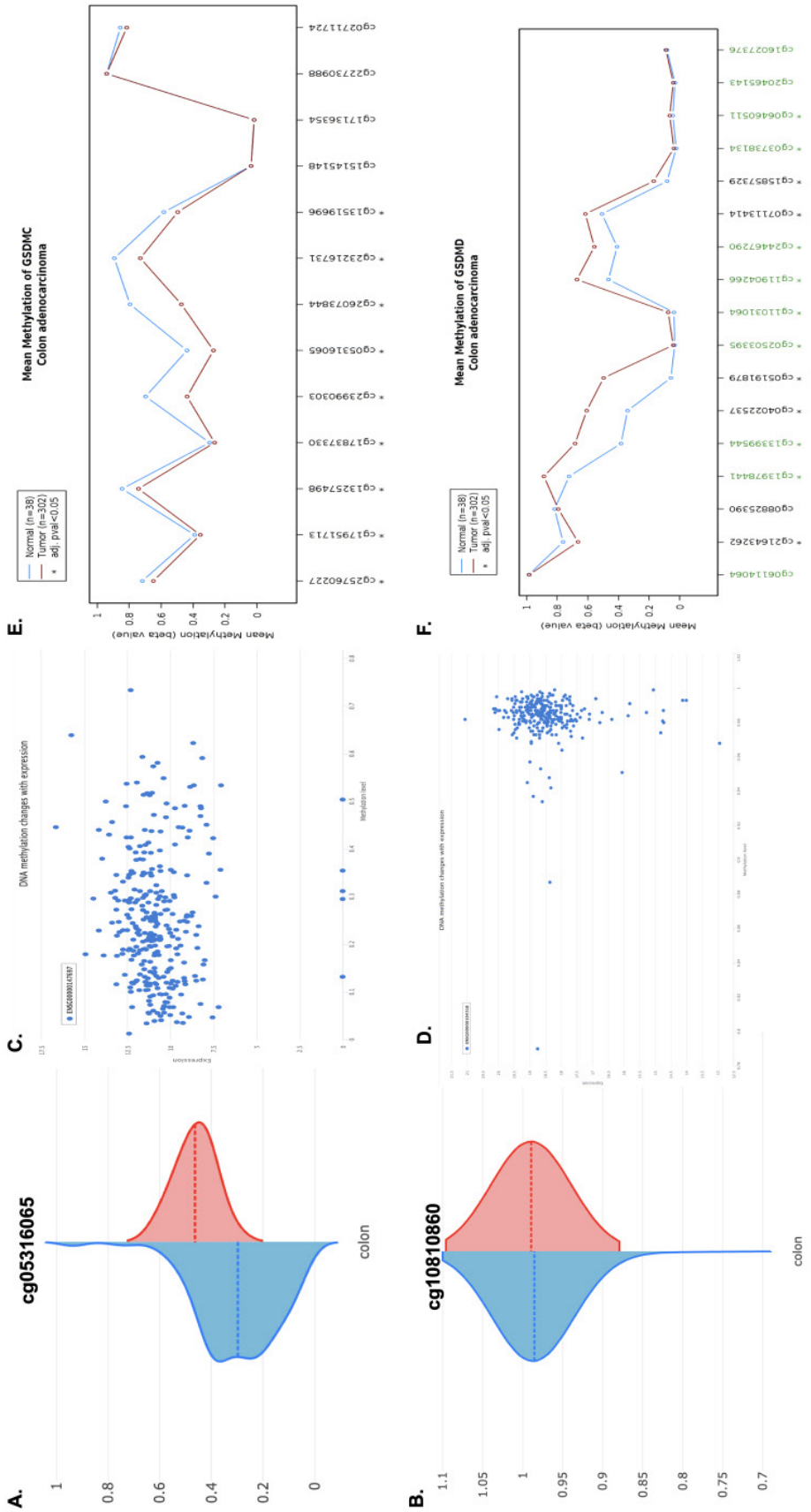

Figure 3. DNA methylation profiles of genes expressing *GSDMC* and *GSDMD* in COAD. (A) Comparison of the most methylated CpG site of *GSDMC* in COAD. (B) Comparison of the most methylated CpG site of *GSDMD* in COAD. (C) Relationship between *GSDMC* hypermethylation and gene expression. (D) Relationship between *GSDMD* hypermethylation and gene expression. (E) Comparison of methylated CpG islands of *GSDMC* in normal and tumor tissues. (F) Comparison of methylated CpG islands of *GSDMD* in normal and tumor tissues.

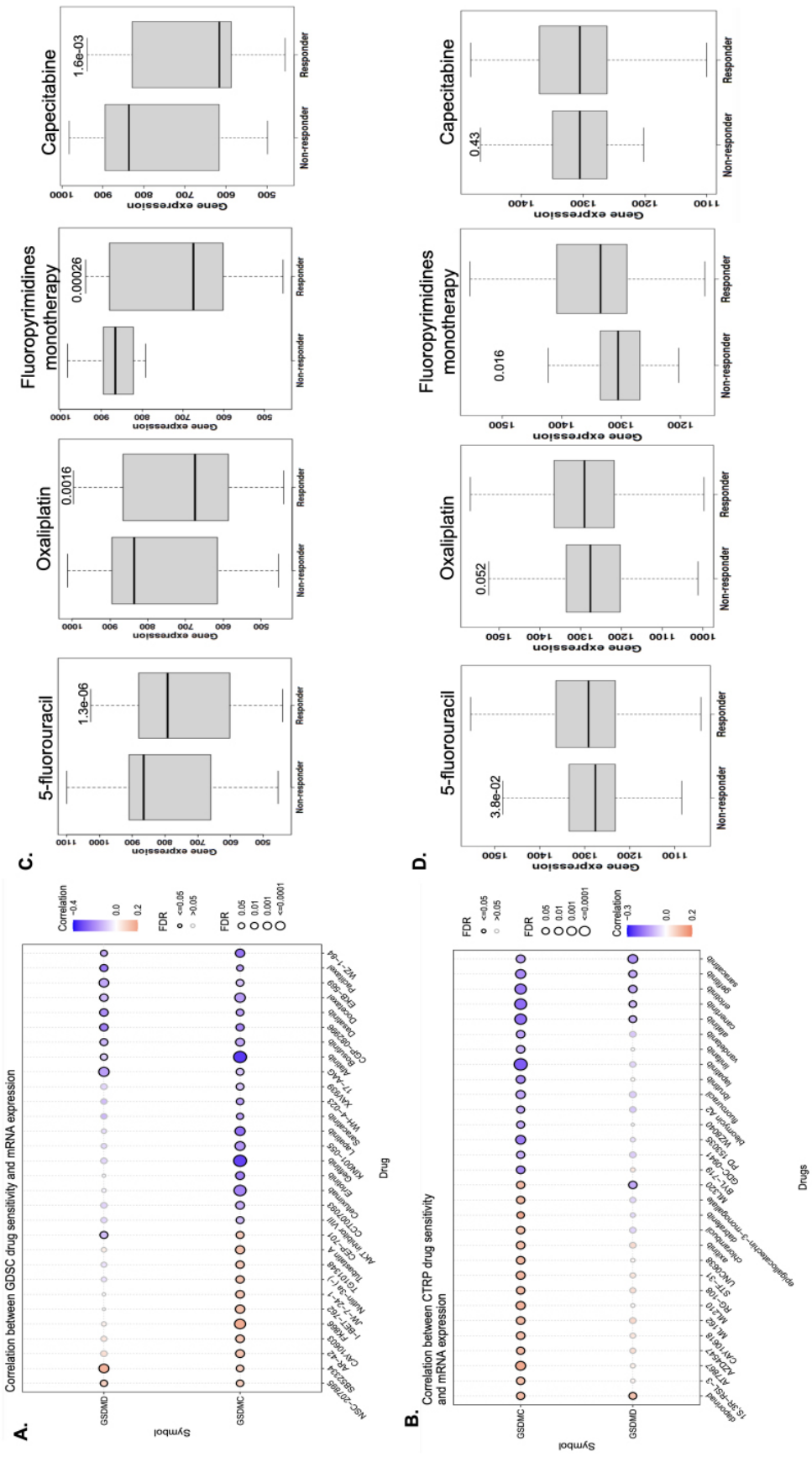

Figure 4. Analysis of drug sensitivity. (A, B) Correlation between Drug Sensitivity Genomics and Cancer Therapeutics Response Portal by Gene Set Cancer Analysis of *GSDMC* and *GSDMD* genes for drug sensitivity. (C) Differences in drug sensitivity between non-response and response groups of patients based on the *GSDMC* gene. (D) Differences in drug sensitivity between non-response and response groups of patients based on the *GSDMD* gene.

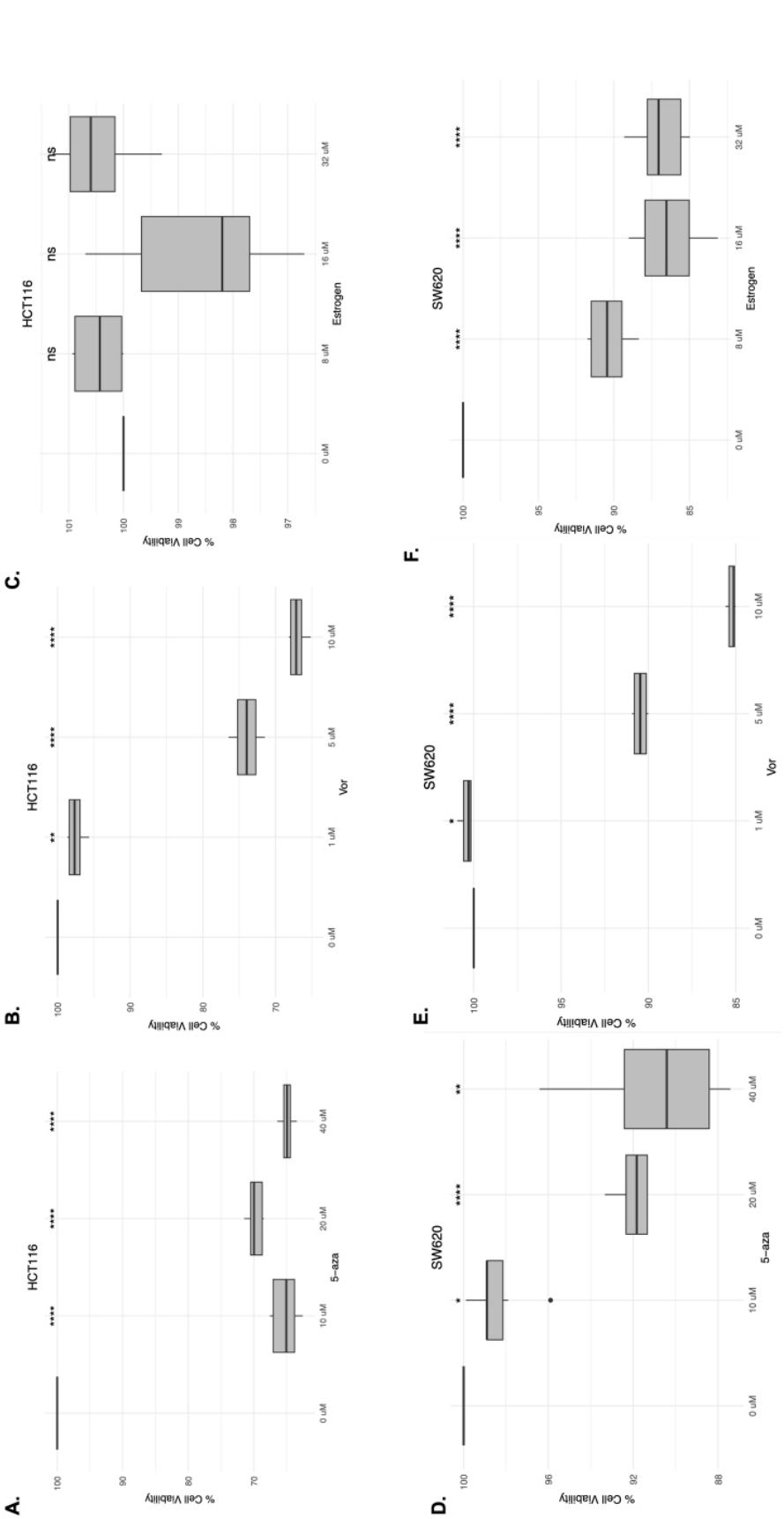

Figure 5. Cell viability assay (A) The effect of 5-azacytidine in HCT116 cells. (B) The effect of vorinostat in HCT116 cells. (C) The effect of estrogen in HCT116 cells. (D) The effect of 5-azacytidine in SW620 cells. (E) The effect of vorinostat in SW620 cells. (F) The effect of estrogen in SW620 cells. Independent experiments values symbolized the mean ± standard error of the mean; ****: $p \leq 0.0001$, **: $p \leq 0.01$, *: $p \leq 0.05$.

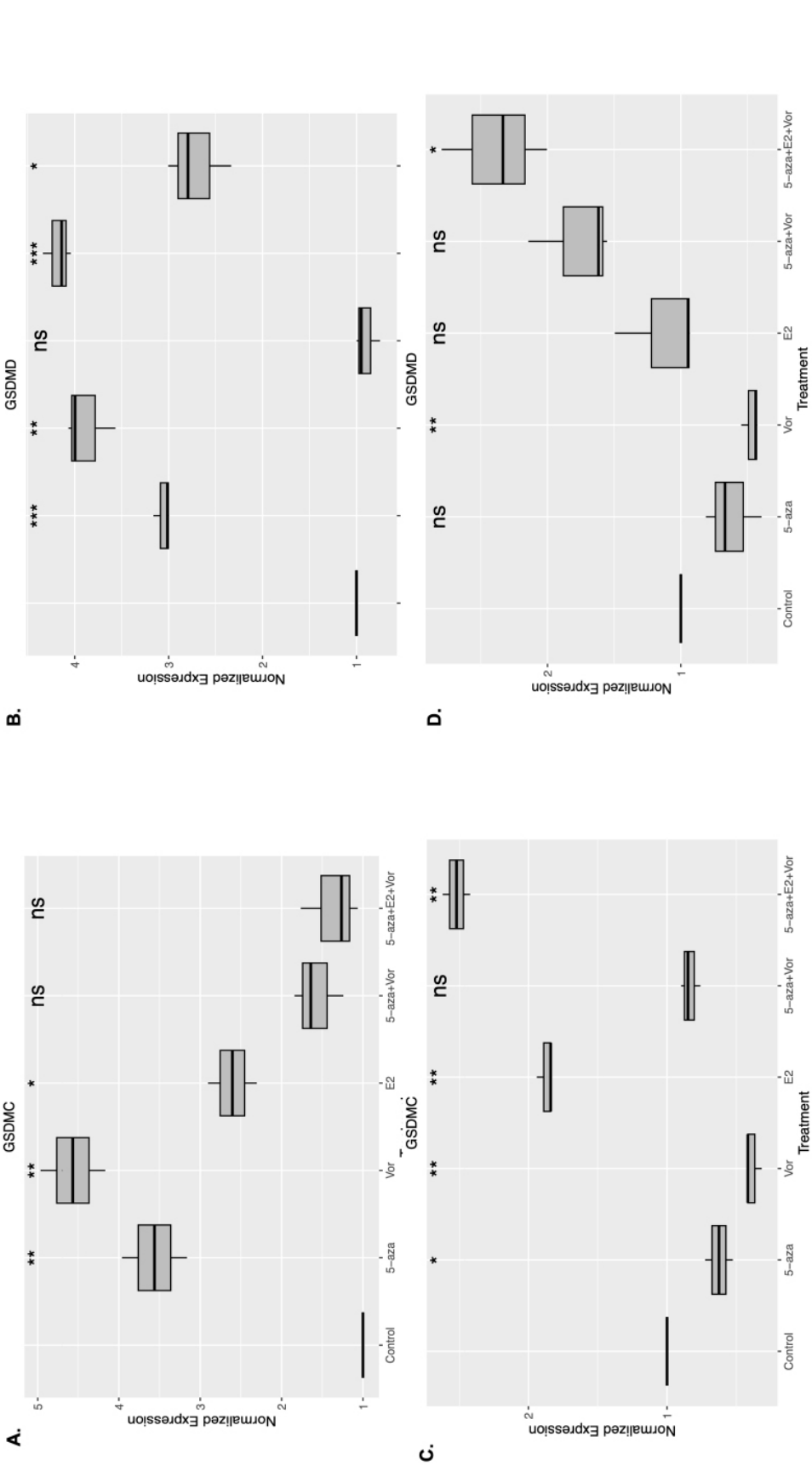

Figure 6. The effect of epigenetic drugs on genes expressing *GSDMC* and *GSDMD* in colorectal adenocarcinoma. (A) The differential expression profiles of *GSDMC* in HCT116 after treatment with 5-azacytidine, vorinostat, and estrogen alone or their combined treatment (B) The differential expression profiles of *GSDMD* in HCT116 after treatment with 5-azacytidine, vorinostat, and estrogen alone or their combined treatment (C) The differential expression profiles of *GSDMC* in SW620 after treatment with 5-azacytidine, vorinostat, and estrogen alone or their combined treatment (D) The differential expression profiles of *GSDMD* in SW620 after treatment with 5-azacytidine, vorinostat, and estrogen alone or their combined treatment. Independent experiments values symbolized the mean ± standard error of the mean; ****: $p \leq 0.0001$, **: $p \leq 0.01$, *: $p \leq 0.05$.

Abnormalities in histone modifications can alter chromatin structure and accessibility, influencing the expression of crucial genes involved in cell proliferation and tumor suppression (5). Estrogens exert influential effects on cancer initiation and progression within hormone-regulated tissues such as the ovaries, endometrium, and breast (6-8). Orzołek et al. reported that while estrogen enhances the growth and development of estrogen-dependent cancers like breast and ovarian cancer, it exhibits a protective effect in some other cancers owing to its anti-inflammatory properties (6). Studies have reported that specific estrogen-dependent epigenetic mechanisms influence tissue gene regulation (9). However, comprehensive knowledge regarding estrogen's effects on individual cancer types and its precise regulation of epigenetic mechanisms remains limited.

Gasdermin proteins are fundamental regulators involved in crucial cellular life and death processes, prominently functioning in inflammatory cell death pyroptosis which is linked to immune responses and inflammation, a highly regulated type of cell death. Dysregulation of gasdermin proteins has been related with cancer initiation, therapy resistance, and progression (10-12). Specifically, within the gasdermin protein family, gasdermin C (GSDMC) and gasdermin D (GSDMD) are recognized for their pivotal roles in pyroptosis (13). Therefore, investigating the expression, regulation, and epigenetic modifications of *GSDMC* and *GSDMD* in COAD holds considerable promise in unraveling the intricacies of colorectal tumorigenesis and may uncover potential therapeutic avenues.

In this study, our primary aim was to investigate the expression profiles of GSDMC and GSDMD proteins belonging to the gasdermin family within COAD and to understand how epigenetic modifications impact the disease's progression. To achieve this, we initially explored the mRNA transcript and protein expressions of *GSDMC* and *GSDMD* genes across various cancer types. We simultaneously analyzed their methylation status, specifically in COAD, using various bioinformatics tools and databases such as Timer2.0, UALCAN, EWAS Open Platform, GSCA, Receiver Operating Characteristic (ROC) plotter, and WANDERER. Moreover, we investigated the effects of treatments with DNA methylation inhibitor (5-azacytidine), histone deacetylase (HDAC) inhibitor vorinostat, and estrogen on the expression of *GSDMC* and *GSDMD*. Our research sheds light on the mechanisms underlying COAD pathogenesis, exploring the potential involvement of alterations in *GSDMC* and *GSDMD* genes in the disease's progression. Our objective is to develop novel therapeutic strategies and diagnostic markers for COAD.

MATERIALS AND METHODS

Data Acquisition

Differential Gene and Protein Expression Analysis

The Timer2.0 (http://timer.cistrome.org/) online tool was employed to examine the distinct expression profiles of *GSDMC* and *GSDMD* across various cancer types (14). This tool utilizes RNA sequencing data sourced from The Cancer Genome Atlas (TCGA) and GETx, allowing for comparisons of differential expressions between tumor and normal tissues. The normal tissue data undergo simultaneous log2 transformation, with statistical significance set at $p < 0.05$. For the analysis of *GSDMC* and *GSDMD* genes concerning stage, grade, and histotype, the UALCAN tool was utilized (15). The criteria specified in this study were: "Gene: *GSDMC* and *GSDMD*"; "Cancer Type: Colorectal Cancer"; "Data Type: TCGA dataset." Furthermore, to determine the expression of *GSDMC* and *GSDMD* at the Human Protein Atlas (HPA) was utilized (16).

Methylation Analysis

We investigated the association between *GSDMC* and *GSDMD* methylation and their expression status utilizing the EWAS Open Platform (17), a database encompassing DNA methylation sequence data and metadata. This platform allowed us to explore the relationship between DNA methylation at specific CpG islands and the expression data of GSDMC and GSDMD in COAD using the WANDERER database (18).

Drug Sensitivity Analysis

We used GSCA to establish the correlation between the Drug Sensitivity Genomics (GDSC) and the Cancer Therapeutics Response Portal (CTRP) of GSDMC and GSDMD proteins in COAD. This analysis aimed to explore the drug sensitivity of the 30 most effective drugs across various cancers (19). Utilizing the ROC plotter (20), we assessed the capability to correlate gene expression with the response to treatment using transcriptome-level data from patients with COAD.

Cell Viability

To assess the impact of drugs on cell viability, we performed the 3-(4,5-dimethylthiazol-2-yl)-2-5-diphenyltetrazolium bromide (MTT) assay. HCT-116 and SW620 cells were seeded into 96-well plates at a density of 7,500 cells per well and cultured overnight. Following incubation, 100 µl of MTT reagent was added to each well, and the cells were further incubated for approximately 2 h. Subsequently, 100 µl of dissolution solution (dimethyl sulfoxide) was added to each well. Absorbance was measured at 540 nm and 570 nm (Thermo Fischer Scientific, USA), and % cell viability was calculated.

mRNA Expression Analysis

The effects of 5-azacytidine (Sigma-Aldrich, USA), (20 µl/mL), vorinostat (Abcam, USA), (10 µl/mL), and estrogen (Sigma-Aldrich, USA), (32 µg/mL) drugs on GSDMC and GSDMD gene expression were assessed using the HCT-116 and SW620 COAD cell lines. Initially, RNA isolation was conducted utilizing TRIZOL (Invitrogen, California). Following the quantification of cell concentrations, 10 ng/µL of RNA sample was used in each reaction. The One-Step Reverse Transcription-Polymerase Chain Reaction (RT-PCR)

Kit (New England Biolabs, USA) and the Roche Light Cycler 480 (Roche, Switzerland) were used for the RT-PCR reaction.

Statistical Analyses

The Shapiro–Wilk test and was employed to assess the normal distribution of study groups, and Student's t-test used for determining statistical significance when comparing control and treatment groups. Visualization and statistical analysis were conducted using the R program. Two-tailed p-values are represented in the figures and tables as follows: (*: $p \leq 0.05$; **: $p \leq 0.01$, ***: $p \leq 0.001$).

RESULTS

Pan-cancer View of *GSDMC* and *GSDMD* Methylation Level

Our analysis revealed elevated transcript expression levels of *GSDMC* and *GSDMD* in tumors compared to normal tissues across various cancer cohorts from TCGA. Statistically significant differences between tumor and normal tissues were observed in both genes in several cancer types, including breast cancer (BRCA), uterine corpus endometrial carcinoma (UCEC), cholangiocarcinoma (CHOL), lung adenocarcinoma (LUAD), head and neck squamous cell carcinoma (HNSC), kidney renal clear cell carcinoma (KIRC), liver hepatocellular carcinoma (LIHC), lung squamous cell carcinoma (LUSC), kidney chromophobe carcinoma (KIHC), stomach adenocarcinoma (STAD), and esophageal cancer (ESCA) cohorts. Specifically, GSDMC exhibited high expression in COAD and skin cutaneous melanoma (SKCM) tumor cohorts, whereas GSDMD showed elevated expression in urothelial bladder cancer (BLCA), prostate adenocarcinoma (PRAD) and thyroid cancer (THCA) cohorts (all p-values < 0.05) (Figure 1A-1B). In addition, using the UALCAN database, we determined the protein expression of *GSDMC* and *GSDMD* in normal and cancer tissues of COAD, considering subtypes, metastasis status, and P53 mutations. As a result, we observed an increase in *GSDMC* protein expression in tumor tissues, particularly in mucinous adenocarcinoma, and found that metastasis status and P53 mutations were associated with elevated protein levels (Figure 1C-F). For the *GSDMD* protein, a decreasing expression trend was observed across each condition (Figure 1G-J). All expression values can be found in Supp. Table 1-2.

GSDMC and *GSDMD* Show Different Expression Profiles Based on Cancer Types

To compare the expression profiles of *GSDMC* and *GSDMD* in tumor tissues, we utilized the HPA database. Our analysis revealed that *GSDMC* exhibited the most differential expression in cervical and head–neck cancer (Figure 2A). However, unlike *GSDMC*, *GSDMD* showed varying expression profiles across different cancer types without showing any specific expression pattern in a particular cancer (Figure 2B). To validate these results, we conducted an analysis of *GSDMC* and *GSDMD* protein expression in clinical specimens from the HPA database. This indicated a strong and positive expression of *GSDMD* in COAD samples, whereas *GSDMC* exhibited weaker expression levels in COAD tissues (Figure 2C). We also examined the effect of the expression of these relevant proteins on survival, and found that their high expression was associated with lower survival rates (Figure 2D-2E).

Pan-cancer View of *GSDMC* and *GSDMD* Methylation Level

We used the EWAS and WANDERER bioinformatics tools to examine the methylation profiles of the *GSDMC* and *GSDMD* genes in COAD. Specifically, four CpG islands within *GSDMC* displayed high methylation levels in COAD, which include cg05316065, cg23990303, cg24243265, and cg26073844 (Supp. Table 3). In contrast, *GSDMD* exhibited 33 CpG islands with detailed methylation information available in Suppl. Table 4. When we compared the methylation levels between COAD and normal colon tissue, we found higher methylation levels for *GSDMC*, specifically in tumor tissues compared with normal tissues. *GSDMD* displayed methylation in both tumor and normal tissues (Figure 3A-3B). Further examination into the expression and methylation of these genes in COAD revealed distinct patterns. An inverse relationship was observed between the expression and methylation of *GSDMC*, while *GSDMD* showed a linear association (Figure 3C-3D). The mean methylation analysis highlighted distinctive patterns for *GSDMC* and *GSDMD* genes in COAD. Hypomethylation was more pronounced in specific islands such as cg05316065, cg23990303, cg24243265, cg26073844, cg23990303, cg05316065, cg26073844, cg23216731, and cg13519696 within the *GSDMC* gene in normal tissues. For the *GSDMD* gene, higher hypomethylation was evident in tumor tissues across CpG islands (cg21643262, cg13978441, cg13399544, cg04022537, cg05191879, cg11904266, cg24467290, and cg07113414) (Figure 3E-3F).

Drug Sensitivity of *GSDMC* and *GSDMD* Gene Expressions

The GSCALite database was used to analyze the association between *GSDMC* and *GSDMD* model genes and drug sensitivity (GSDC and CTRP). In addition, validation of predictive chemotherapy biomarkers was performed using transcriptomic data from COAD patients in the ROC plotter database. The results revealed that the drug sensitivity of the *GSDMC* gene exhibited a negative correlation with 19 drugs and a positive correlation with 11 drugs. In comparison, *GSDMD* drug sensitivity displayed a negative correlation with 10 drugs and a positive correlation with two drugs, as observed in the GDSC database (Figure 4A). Detailed expression values are provided in Supp. Table 5. Furthermore, analysis using the CTRP database unveiled associations where the drug sensitivity of the *GSDMC* gene showed negative and positive correlations with 15 drugs (Supp. Table 6). *GSDMD* sensitivity showed a negative correlation with six drugs and a positive correlation with daporinad (Figure 4B). According to our ROC analyses, we identified four predictive chemotherapy biomarkers,

including 5-fluorouracil, oxaliplatin, fluoropyrimidines monotherapy, and capecitabine that indicate druggable *GSDMC* genes overexpressed and *GSDMD* downregulated among nonresponding patients (Figure 4C-4D).

The Effect of Epigenetic Drugs for *GSDMC* and *GSDMD* Expression in COAD

Based on our bioinformatics analysis, we determined that methylation plays a notable role in regulating the *GSDMC* and *GSDMD* genes in COAD. To confirm this, we conducted experiments using two COAD cell lines, HCT116 and SW620, to assess the effect of epigenetic drugs, 5-azacytidine and vorinostat, on these genes. Initially, we evaluated the effects of different drugs on cell survival to determine appropriate concentrations for subsequent experiments. Lower doses of these drugs did not dramatically decrease cell viability. However, higher doses of 5-azacytidine and vorinostat treatments reduced cell viability in HCT116 and SW620 cell lines (Figure 5). Subsequently, we examined the effects of these drugs on the expression of *GSDMC* and *GSDMD* in these cell lines. Our observations indicated that treatments involving single or combined applications of 5-azacytidine and vorinostat led to increased expression of these relevant genes compared to the control, and estrogen exhibited a promoting effect on gene expression in both cell lines (Figure 6).

DISCUSSION

COAD is a highly prevalent and fatal cancer originating from the epithelial cells of the colon and rectum. The interplay between genetic mutations and epigenetic alterations significantly contributes to the initiation and progression of COAD (1-3). Recent studies have highlighted the involvement of *GSDM* proteins in COAD, emphasizing their potential as diagnostic indicators, and targets for therapeutic interventions.

The GSDM family, encompassing *GSDMA*, *GSDMB*, *GSDMC*, *GSDMD*, *GSDME*, and *GSDMF*, has been identified for its role in cell death linked to inflammation, particularly pyroptosis, and its regulation of cancer cell proliferation, invasion, and metastasis (21). Within the vast array of genes implicated in cancer biology, gasdermins, specifically *GSDMC* and *GSDMD*, have emerged as substantial attention due to their roles in cellular death pathways, inflammation, and potential as targets for diagnosis and therapy. Previous studies have highlighted the elevated expression of *GSDMC* and *GSDMD* in COAD. This increased expression may be associated with the inactivation of signaling pathways due to mutations like the adenomatous polyposis coli (*APC*) gene or inflammatory microenvironment, affecting the progression of COAD, SKCM, and ESCA cancer progression (21-23). Similarly, Cui et al., have showed that elevated *GSDMC* is linked to low survival rates (24). A recent study suggested that increased *GSDMD* expression in serious ovarian cancer might be counterbalanced by increased apoptotic caspase activity (25). In this study, our initial analysis delved into the expression trend of *GSDMC* and *GSDMD* across various cancer types. The consistently observed increased RNA expression of *GSDMC* and *GSDMD* across diverse cancer types, particularly in comparison with the COAD subtypes and is known for its unique pathological features. The higher expression of *GSDMC* in this subtype may suggest a specific role for this protein in mucinous COAD biology. In contrast, the reduced expression of *GSDMD* in COAD might indicate a potential mechanism employed by cancer cells to evade pyroptosis, thereby promoting cell survival.

COAD, a complex malignancy, is intricately driven by genetic and epigenetic alterations. Research indicates that DNA methylation, non-coding RNAs, and alterations in histone modifications play pivotal roles in regulating *GSDM* proteins within COAD. Altered histone modification patterns in the *GSDME* gene locus might contribute to its dysregulated expression, potentially affecting cancer cell survival and proliferation. Hypermethylation, resulting in the transcriptional silencing of *GSDME*, may contribute to COAD progression by impacting cell death pathways and inducing pyroptosis, a specific form of programmed cell death (26, 27). Moreover, hypermethylation in the *GSDMC* promoter region has been associated with decreased *GSDMC* expression, potentially promoting tumorigenesis by affecting cell death and proliferation pathways in HCC. Studies on gene methylation have been associated with low gene expression in most tumors, and this correlation is most pronounced in *GSDMB*, *GSDMD*, and *GSDME* (22, 28). In this study, we observed the distinct methylation patterns of *GSDMC* and *GSDMD* in COAD. The inverse relationship between *GSDMC* expression and methylation levels suggests that hypomethylation may drive *GSDMC* upregulation in tumors. Conversely, the linear association observed with *GSDMD* indicates a more complex regulatory mechanism. Within the *GSDMC* gene, four CpG islands, namely cg05316065, cg23990303, cg24243265, and cg26073844, exhibited notable high methylation levels. This suggests that increased methylation occurs in *GSDMC* within COAD tissues, potentially leading to its downregulation. In contrast, the *GSDMD* gene showed methylation alterations across 33 CpG islands. Interestingly, tumor and normal tissues exhibited increased methylation levels in the *GSDMD* gene. This observation suggests that *GSDMD* may have a more complex methylation regulation pattern in COAD.

Analyzing drug sensitivity linked to *GSDMC* and *GSDMD* offers crucial insights into potential therapeutic interventions. The correlations observed both negative and positive with specific drugs in various databases (GDSC and CTRP) suggest that the expression levels of these genes might influence the chemotherapy response. Identification of predictive biomarkers such as 5-fluorouracil, oxaliplatin, fluoropyrimidine monotherapy, and capecitabine underscores the clinical relevance of targeting *GSDMC* and *GSDMD* for personalized cancer treatment. Gasdermin proteins play a pivotal role in pyroptosis that is essential for the antitumor activity of chemotherapeutic drugs. Studies have showed that lower *GSDME* expression in retinoblastoma cells increases resistance

to chemotherapeutic drugs, while decitabine application increases sensitivity by directing cells toward pyroptosis (29). Decitabine treatment has shown to upregulate *GSDMD* in murine bladder tumors and breast cancer, activating NLRP3 inflammasome and caspase-1 proteins (10). Chidamide, a HDAC inhibitor, has been observed to enhance *GSDMD* expression in laryngeal HN8 cancer cells (30). Estrogen known for its anti-inflammatory activities, is considered a cancer-protective hormone. However, the precise mechanisms underlying its synergistic effect remain unclear. To better understand this relationship, we investigated whether the combined impact of 5-azacytidine, vorinostat, and estrogen synergistically influences COAD HCT116 and SW620 cells. Our findings revealed an increase in the expression of both *GSMDC* and *GSDMD* following the combined treatment. This experimental validation of epigenetic regulation by 5-azacytidine and vorinostat on *GSDMC* and *GSDMD* expression in COAD cell lines reinforces the potential therapeutic implications of targeting these genes. The ability to modulate gene expression through epigenetic mechanisms suggests that epigenetic therapies in controlling *GSDMC* and *GSDMD* levels in cancer cells. However, further research is required to optimize these approaches for clinical application.

CONCLUSION

In conclusion, despite several studies indicated changes in *GSDMC* and *GSDMD* expression in associated cancers, the underlying mechanisms and functional implications remain inadequately understood. This comprehensive analysis of *GSDMC* and *GSDMD* across various cancers provides valuable insights into their multifaceted roles within cancer biology. These genes exhibit complex expression patterns, associations with patient survival, epigenetic regulatory mechanisms, and potential implications for chemotherapy response.

Acknowledgments: The authors would like to thank Caglar Berkel for his assistance.

Ethics Committee Approval: All data on patients were retrieved from the public database and commercial cell lines were used in in vitro experiments. Therefore, ethics committee approval is not required.

Informed Consent: Because the study was designed retrospectively, no written informed consent form was obtained from patients.

Peer-review: Externally peer-reviewed.

Authorship Contributions: Idea/Concept- E.C.; Design- E.C., R.S. Analysis and/or Interpretation- F.C., R.S.; Writing the Article- F.C., E.C.; Critical Review- E.C.; References and Fundings- E.C., R.S.

Conflict of Interest: The authors declare that they have no conflict of interest.

Financial Disclosure: The research was supported by the TUBITAK 2209-A (1919B012209018).

REFERENCES

1. Rawla P, Sunkara T, Barsouk A. Epidemiology of colorectal cancer: incidence, mortality, survival, and risk factors. Prz Gastroenterol 2019; 14(2): 89-103.
2. Caldiran FY, Cacan E. RGS10 suppression by DNA methylation is associated with low survival rates in colorectal carcinoma. Pathol Res Pract 2022; 236: 154007.
3. Bardhan K, Liu K. Epigenetics and colorectal cancer pathogenesis. Cancers (Basel) 2013; 5(2): 676-713.
4. Ashktorab H, Brim H. DNA methylation and colorectal cancer. Curr Colorectal Cancer Rep 2014; 10(4): 425-30.
5. Park J, Lee K, Kim K, Yi SJ. The role of histone modifications: from neurodevelopment to neurodiseases. Signal Transduct Target Ther 2022; 7(1): 217.
6. Orzołek I, Sobieraj J, Domagała-Kulawik J. Estrogens, cancer and immunity. Cancers 2022; 14(9); 2265.
7. Božović A, Mandušić V, Todorović L, Krajnović M. Estrogen Receptor Beta: The promising biomarker and potential target in metastases. Int J Mol Sci 2021; 22(4): 1656.
8. Berkel C, Cacan E. Estrogen- and estrogen receptor (ER)-mediated cisplatin chemoresistance in cancer. Life Sci 2021; 286:20029.
9. Fortress AM, Frick KM. Epigenetic regulation of estrogen-dependent memory. Front Neuroendocrinol 2014; 35(4): 530-49.
10. El-Gamal R, Abdelrahim M, El-Sherbiny M, Enan ET, El-Nablaway M. Gasdermin D: A potential mediator and prognostic marker of bladder cancer. Front Mol Biosci 2022; 9: 972087.
11. Tanaka S, Orita H, Kataoka T, Miyazaki M, Saeki H, Wada R, et al. Gasdermin D represses inflammation-induced colon cancer development by regulating apoptosis. Carcinogenesis 2023; 44(4): 341-9.
12. Yang X, Tang Z. Role of gasdermin family proteins in cancers. Int J Oncol 2023; 63(3): 100.
13. Slaufova M, Karakaya T, Di Filippo M, Hennig P, Beer HD. The gasdermins: a pore-forming protein family expressed in the epidermis. Front Immunol 2023; 14: 1254150.
14. Li T, Fu J, Zeng Z, Cohen D, Li J, Chen Q, et al. TIMER2.0 for analysis of tumor-infiltrating immune cells. Nucleic Acids Res 2020; 48(W1): W509-14.
15. Chandrashekar DS, Bashel B, Balasubramanya SAH, Creighton CJ, Ponce-Rodriguez I, Chakravarthi BVSK, et al. UALCAN: A Portal for facilitating tumor subgroup gene expression and survival analyses. Neoplasia 2017; 19(8): 649-58.
16. Thul PJ, Lindskog C. The human protein atlas: a spatial map of the human proteome. Protein Sci 2018; 27(1): 233-44.
17. Xiong Z, Yang F, Li M, Ma Y, Zhao W, Wang G, et al. EWAS Open Platform: integrated data, knowledge and toolkit for epigenome-wide association study. Nucleic Acids Res 2022; 50(D1): D1004-9.
18. Díez-Villanueva A, Mallona I, Peinado MA (). Wanderer, an interactive viewer to explore DNA methylation and gene expression data in human cancer. Epigenetics Chromatin 2015; 8: 22.
19. Liu CJ, Hu FF, Xie GY, Miao YR, Li XW, Zeng Y, et al. GSCA: an integrated platform for gene set cancer analysis at genomic, pharmacogenomic and immunogenomic levels. Brief Bioinform 2023; 24(1): bbac558.
20. Fekete JT, Győrffy B. ROCplot.org: validating predictive biomarkers of chemotherapy/hormonal therapy/anti-HER2 therapy using transcriptomic data of 3,104 breast cancer patients. Int J Cancer 2019; 145(11): 3140-51.
21. Zou J, Zheng Y, Huang Y, Tang D, Kang R, Chen R. The versatile gasdermin family: their function and roles in diseases. Front Immunol 2021; 12: 751533.

22. Feng S, Fox D, Man SM. Mechanisms of gasdermin family members in inflammasome signaling and cell death. J Mol Biol 2018; 430(18 Pt B): 3068-3080.
23. Miguchi M, Hinoi T, Shimomura M, Adachi T, Saito Y, Niitsu H, et al. Gasdermin C is upregulated by inactivation of transforming growth factor β receptor type II in the presence of mutated Apc, promoting colorectal cancer proliferation. PLoS One 2016; 11(11): e0166422.
24. Wang J, Kang Y, Li Y, Sun L, Zhang J, Qian S, et al. Gasdermin D in different subcellular locations predicts diverse progression, ımmune microenvironment and prognosis in colorectal cancer. J Inflamm Res 2021; 14: 6223-35
25. Berkel C, Cacan E. Differential expression and copy number variation of gasdermin (GSDM) family members, pore-forming proteins in pyroptosis, in normal and malignant serous ovarian tissue. Inflammation 2021; 44(6): 2203-16.
26. Li F, Xia Q, Ren L, Nie Y, Ren H, Guo X, et al. GSDME Increases chemotherapeutic drug sensitivity by inducing pyroptosis in retinoblastoma cells. Oxid Med Cell Longev 2022; 2022: 2371807.
27. Kim MS, Chang X, Yamashita K, Nagpal JK, Baek JH, Wu G, et al. Aberrant promoter methylation and tumor suppressive activity of the DFNA5 gene in colorectal carcinoma. Oncogene 2008; 27(25): 3624-34.
28. Wang YY, Shi LY, Xu MH, Jing Y, Sun CC, Yang JH, et al. A pan-cancer analysis of the expression of gasdermin genes in tumors and their relationship with the immune microenvironment. Transl Cancer Res 2021; 10(9): 4125-47.
29. Niu Q, Liu Y, Zheng Y, Tang Z, Qian Y, Qi R, et al. Co-delivery of nigericin and decitabine using hexahistidine-metal nanocarriers for pyroptosis-induced immunotherapeutics. Acta Pharm Sin B 2022; 12(12): 4458-71.
30. Zhao S, Guo J, Zhao Y, Fei C, Zheng Q, Li X, et al. Chidamide, a novel histone deacetylase inhibitor, inhibits the viability of MDS and AML cells by suppressing JAK2/STAT3 signaling. Am J Transl Res 2016; 8(7): 3169-78.

Supp. Table 1. Expression profile of *GSDMC* in different states of COAD.

Comparison	Statistical significance
Normal-vs-Primary	5.34780000283064E-08
Normal-vs-Stage1	9.91039994513443E-09
Normal-vs-Stage2	2.136800E-03
Normal-vs-Stage3	2.17460049967144E-10
Normal-vs-Stage4	8.031500E-04
Stage1-vs-Stage2	8.040200E-02
Stage1-vs-Stage3	1.648000E-01
Stage1-vs-Stage4	9.752000E-01
Stage2-vs-Stage3	1.918760E-01
Stage2-vs-Stage4	9.690300E-02
Stage3-vs-Stage4	3.320600E-01
Normal-vs-Adenocarcinoma	6.44320000020571E-07
Normal-vs-Mucinous-adenocarcinoma	3.128200E-02
Adenocarcinoma-vs-Mucinous-adenocarcinoma	3.500600E-01
Normal-vs-N0	1.823400E-04
Normal-vs-N1	2.39859999640046E-08
Normal-vs-N2	1.5830399999972E-05
N0-vs-N1	1.974230E-01
N0-vs-N2	2.694000E-01
N1-vs-N2	8.279400E-01
Normal-vs-TP53-Mutant	6.6130999998304E-07
Normal-vs-TP53-NonMutant	1.538110E-03
TP53-Mutant-vs-TP53-NonMutant	4.524400E-01

Supp. Table 2. Expression profile of *GSDMD* in different states of COAD.

Comparison	Statistical significance
Normal-vs-Primary	1.128610E-01
Normal-vs-Stage1	5.232600E-01
Normal-vs-Stage2	8.552000E-02
Normal-vs-Stage3	8.592100E-02
Normal-vs-Stage4	1.197410E-01
Stage1-vs-Stage2	3.274800E-01
Stage1-vs-Stage3	3.423000E-01
Stage1-vs-Stage4	4.184400E-01
Stage2-vs-Stage3	9.860400E-01
Stage2-vs-Stage4	9.782600E-01
Stage3-vs-Stage4	9.892800E-01
Normal-vs-Adenocarcinoma	9.300100E-02
Normal-vs-Mucinous-adenocarcinoma	2.419200E-01
Adenocarcinoma-vs-Mucinous-adenocarcinoma	9.114800E-01
Normal-vs-N0	1.679450E-01
Normal-vs-N1	6.463700E-02
Normal-vs-N2	1.255550E-01
N0-vs-N1	5.538800E-01
N0-vs-N2	7.460800E-01
N1-vs-N2	8.626200E-01
Normal-vs-TP53-Mutant	9.317900E-02
Normal-vs-TP53-NonMutant	2.013800E-01
TP53-Mutant-vs-TP53-NonMutant	7.081200E-01

Supp. Table 3. Pan-cancer view of *GSDMC* methylation level.

Probe ID	Basic Information	TS (Hyper)	TS (Hypo)	Cor(age)	Sex difference score	Ancestry (Hyper)	Ancestry (Hypo)
cg06114064	Location:chr8 144643111CpG Island: ShelfRelated Gene: GSDMD	0.0374474	0.77484	'-0.0211308	0.00234468	0.00189862	0.100095
cg07422279	Location:chr8 144635610CpG Island: ShelfRelated Gene: GSDMD	0.514985	0.0250342	0.0297773	0.00506567	0.114331	0.00852036
cg09317036	Location:chr8 144635547CpG Island: ShelfRelated Gene: GSDMD	0.467426	0.0167713	'-0.0385934	0.00647206	0.463982	0.0139364
cg10810860	Location:chr8 144639591CpG Island: ShelfRelated Gene: GSDMD	0.00771833	0.702204	0.13324	0.00127997	0.00391243	0.22768
cg12686110	Location:chr8 144635478CpG Island: ShelfRelated Gene: GSDMD	0.593581	0.012455	0.0134863	0.00353016	0.101371	0.00548918
cg18198896	Location:chr8 144635361CpG Island: ShelfRelated Gene: GSDMD	0.435809	0.0162049	'-0.00513337	0.00336136	0.171192	0.00810995
cg22995724	Location:chr8 144639363CpG Island: ShelfRelated Gene: GSDMD	0.0688239	0.543099	0.215856	0.00843402	0.160886	0.21223
cg23101464	Location:chr8 144640755CpG Island: IslandRelated Gene: GSDMD	0.645494	0.059545	0.268305	'-0.0134696	0.0697682	0.0136725
cg24493971	Location:chr8 144636113CpG Island: ShoreRelated Gene: GSDMD	0.717722	0.0444969	0.256837	0.0033797	0.36247	0.0217715
cg01088723	Location:chr8 144635861CpG Island: ShelfRelated Gene: GSDMD	0.749041	0.0217855	0.15455	0.00056777	0.153523	0.00921932
cg01134012	Location:chr8 144635316CpG Island: ShelfRelated Gene: GSDMD	0.625397	0.0160124	'-0.0529944	0.00358376	0.33056	0.0211275
cg03367493	Location:chr8 144642094CpG Island: ShoreRelated Gene: GSDMD	0.114451	0.598116	0.0380313	0.0131626	0.0448131	0.169078
cg06043315	Location:chr8 144640306CpG Island: ShoreRelated Gene: GSDMD	0.710383	0.176105	0.254368	'-0.00455408	0.0671723	0.0021351
cg06553843	Location:chr8 144642649CpG Island: ShoreRelated Gene: GSDMD	0.0587956	0.609967	0.0681331	0.00795896	0.04254	0.144907
cg08688335	Location:chr8 144635260CpG Island: ShelfRelated Gene: GSDMD	0.49512	0.0153854	'-0.0931951	'-0.000569483	0.376794	0.018253
cg10074813	Location:chr8 144637872CpG Island: ShoreRelated Gene: GSDMD	0.0507524	0.573654	0.0977066	0.0058875	0.0345586	0.218893
cg10675725	Location:chr8 144640310CpG Island: ShoreRelated Gene: GSDMD	0.753294	0.0841625	0.263813	'-0.00887712	0.111956	0.00526692
cg14721632	Location:chr8 144635430CpG Island: ShelfRelated Gene: GSDMD	0.700252	0.0175525	'-0.0204295	0.00991591	0.296632	0.0157026
cg15172061	Location:chr8 144638852CpG Island: ShelfRelated Gene: GSDMD	0.133221	0.600146	0.189963	'-0.000784746	0.264629	0.237025
cg15541193	Location:chr8 144635496CpG Island: ShelfRelated Gene: GSDMD	0.794542	0.012069	'-0.0562418	0.00542389	0.184801	0.00277694
cg16563151	Location:chr8 144640403CpG Island: IslandRelated Gene: GSDMD	0.744569	0.021425	0.246606	'-0.00509359	0.186283	0.00799428
cg17812120	Location:chr8 144639478CpG Island: ShelfRelated Gene: GSDMD	0.026755	0.470268	0.160148	0.0110324	0.06736	0.471315
cg18145080	Location:chr8 144640397CpG Island: IslandRelated Gene: GSDMD	0.763803	0.0402844	0.303255	'-0.00736297	0.140413	0.00502442

cg19661369	Location:chr8 144636025CpG Island: IslandRelated Gene: GSDMD	0.878188	0.0473552	0.281871	0.000720407	0.209593	0.00551592
cg20387272	Location:chr8 144640401CpG Island: IslandRelated Gene: GSDMD	0.800644	0.0168213	0.230224	'-0.00664629	0.135887	0.00368115
cg20583945	Location:chr8 144636462CpG Island: ShoreRelated Gene: GSDMD	0.352968	0.30731	0.204754	'-0.00394652	0.408965	0.174377
cg22012530	Location:chr8 144635309CpG Island: ShelfRelated Gene: GSDMD	0.656191	0.0208012	0.000218964	0.0031179	0.488271	0.0228124
cg22312904	Location:chr8 144639260CpG Island: ShelfRelated Gene: GSDMD	0.112199	0.446264	0.156057	'-0.00169094	0.297525	0.228638
cg22687097	Location:chr8 144640556CpG Island: IslandRelated Gene: GSDMD	0.608017	0.0181856	0.213544	'-0.0072603	0.186328	0.00745327
cg23090207	Location:chr8 144635444CpG Island: ShelfRelated Gene: GSDMD	0.792752	0.0141682	0.0158456	0.00809795	0.313986	0.0074909
cg25245261	Location:chr8 144640507CpG Island: IslandRelated Gene: GSDMD	0.860492	0.0219079	0.262442	'-0.00622538	0.138365	0.00353555
cg26173173	Location:chr8 144642813CpG Island: ShelfRelated Gene: GSDMD	0.064414	0.589783	'-0.00489139	0.00311126	0.024572	0.0986943
cg26711732	Location:chr8 144640378CpG Island: ShoreRelated Gene: GSDMD	0.873112	0.0437411	0.245965	'-0.00382704	0.27076	0.00383456

Supp. Table 4. Pan-cancer view of *GSDMD* methylation level.

Probe ID	Basic Information	TS (Hyper)	TS (Hypo)	Cor(age)	Sex difference score	Ancestry (Hyper)	Ancestry (Hypo)
cg06114064	Location:chr8 144643111CpG Island: ShelfRelated Gene: GSDMD	0.0374474	0.77484	'-0.0211308	0.00234468	0.00189862	0.100095
cg07422279	Location:chr8 144635610CpG Island: ShelfRelated Gene: GSDMD	0.514985	0.0250342	0.0297773	0.00506567	0.114331	0.00852036
cg09317036	Location:chr8 144635547CpG Island: ShelfRelated Gene: GSDMD	0.467426	0.0167713	'-0.0385934	0.00647206	0.463982	0.0139364
cg10810860	Location:chr8 144639591CpG Island: ShelfRelated Gene: GSDMD	0.00771833	0.702204	0.13324	0.00127997	0.00391243	0.22768
cg12686110	Location:chr8 144635478CpG Island: ShelfRelated Gene: GSDMD	0.593581	0.012455	0.0134863	0.00353016	0.101371	0.00548918
cg18198896	Location:chr8 144635361CpG Island: ShelfRelated Gene: GSDMD	0.435809	0.0162049	'-0.00513337	0.00336136	0.171192	0.00810995
cg22995724	Location:chr8 144639363CpG Island: ShelfRelated Gene: GSDMD	0.0688239	0.543099	0.215856	0.00843402	0.160886	0.21223
cg23101464	Location:chr8 144640755CpG Island: IslandRelated Gene: GSDMD	0.645494	0.059545	0.268305	'-0.0134696	0.0697682	0.0136725
cg24493971	Location:chr8 144636113CpG Island: ShoreRelated Gene: GSDMD	0.717722	0.0444969	0.256837	0.0033797	0.36247	0.0217715

cg01088723	Location:chr8 144635861CpG Island: ShelfRelated Gene: GSDMD	0.749041	0.0217855	0.15455	0.00056777	0.153523	0.00921932
cg01134012	Location:chr8 144635316CpG Island: ShelfRelated Gene: GSDMD	0.625397	0.0160124	'-0.0529944	0.00358376	0.33056	0.0211275
cg03367493	Location:chr8 144642094CpG Island: ShoreRelated Gene: GSDMD	0.114451	0.598116	0.0380313	0.0131626	0.0448131	0.169078
cg06043315	Location:chr8 144640306CpG Island: ShoreRelated Gene: GSDMD	0.710383	0.176105	0.254368	'-0.00455408	0.0671723	0.0021351
cg06553843	Location:chr8 144642649CpG Island: ShoreRelated Gene: GSDMD	0.0587956	0.609967	0.0681331	0.00795896	0.04254	0.144907
cg08688335	Location:chr8 144635260CpG Island: ShelfRelated Gene: GSDMD	0.49512	0.0153854	'-0.0931951	'-0.000569483	0.376794	0.018253
cg10074813	Location:chr8 144637872CpG Island: ShoreRelated Gene: GSDMD	0.0507524	0.573654	0.0977066	0.0058875	0.0345586	0.218893
cg10675725	Location:chr8 144640310CpG Island: ShoreRelated Gene: GSDMD	0.753294	0.0841625	0.263813	'-0.00887712	0.111956	0.00526692
cg14721632	Location:chr8 144635430CpG Island: ShelfRelated Gene: GSDMD	0.700252	0.0175525	'-0.0204295	0.00991591	0.296632	0.0157026
cg15172061	Location:chr8 144638852CpG Island: ShelfRelated Gene: GSDMD	0.133221	0.600146	0.189963	'-0.000784746	0.264629	0.237025
cg15541193	Location:chr8 144635496CpG Island: ShelfRelated Gene: GSDMD	0.794542	0.012069	'-0.0562418	0.00542389	0.184801	0.00277694
cg16563151	Location:chr8 144640403CpG Island: IslandRelated Gene: GSDMD	0.744569	0.021425	0.246606	'-0.00509359	0.186283	0.00799428
cg17812120	Location:chr8 144639478CpG Island: ShelfRelated Gene: GSDMD	0.026755	0.470268	0.160148	0.0110324	0.06736	0.471315
cg18145080	Location:chr8 144640397CpG Island: IslandRelated Gene: GSDMD	0.763803	0.0402844	0.303255	'-0.00736297	0.140413	0.00502442
cg19661369	Location:chr8 144636025CpG Island: IslandRelated Gene: GSDMD	0.878188	0.0473552	0.281871	0.000720407	0.209593	0.00551592
cg20387272	Location:chr8 144640401CpG Island: IslandRelated Gene: GSDMD	0.800644	0.0168213	0.230224	'-0.00664629	0.135887	0.00368115
cg20583945	Location:chr8 144636462CpG Island: ShoreRelated Gene: GSDMD	0.352968	0.30731	0.204754	'-0.00394652	0.408965	0.174377
cg22012530	Location:chr8 144635309CpG Island: ShelfRelated Gene: GSDMD	0.656191	0.0208012	0.000218964	0.0031179	0.488271	0.0228124
cg22312904	Location:chr8 144639260CpG Island: ShelfRelated Gene: GSDMD	0.112199	0.446264	0.156057	'-0.00169094	0.297525	0.228638

cg22687097	Location:chr8 144640556CpG Island: IslandRelated Gene: GSDMD	0.608017	0.0181856	0.213544	'-0.0072603	0.186328	0.00745327
cg23090207	Location:chr8 144635444CpG Island: ShelfRelated Gene: GSDMD	0.792752	0.0141682	0.0158456	0.00809795	0.313986	0.0074909
cg25245261	Location:chr8 144640507CpG Island: IslandRelated Gene: GSDMD	0.860492	0.0219079	0.262442	'-0.00622538	0.138365	0.00353555
cg26173173	Location:chr8 144642813CpG Island: ShelfRelated Gene: GSDMD	0.064414	0.589783	'-0.00489139	0.00311126	0.024572	0.0986943
cg26711732	Location:chr8 144640378CpG Island: ShoreRelated Gene: GSDMD	0.873112	0.0437411	0.245965	'-0.00382704	0.27076	0.00383456

Supp. Table 5. Drug sensitivity of *GSDMC* gene expression.

symbol	drug	cor	fdr	entrez
GSDMC	(5Z)-7-Oxozeaenol	0.069177881	0.084690764	56169
GSDMC	17-AAG	-0.103282381	0.0052149	56169
GSDMC	5-Fluorouracil	0.074694505	0.04167749	56169
GSDMC	681640	-0.073758149	0.192458667	56169
GSDMC	A-443654	-0.074396887	0.633968354	56169
GSDMC	A-770041	-0.133979411	0.054258484	56169
GSDMC	AC220	0.043906205	0.363024941	56169
GSDMC	AG-014699	0.027226293	0.55607265	56169
GSDMC	AICAR	-0.088457542	0.023708092	56169
GSDMC	AKT inhibitor VIII	-0.117162884	0.004669143	56169
GSDMC	AMG-706	0.013189918	0.86448356	56169
GSDMC	AP-24534	0.055968966	0.17895025	56169
GSDMC	AR-42	0.127048926	0.000316472	56169
GSDMC	AS601245	-0.057208292	0.271940572	56169
GSDMC	AS605240	-0.0247857	0.60536041	56169
GSDMC	AT-7519	-0.041962054	0.261575287	56169
GSDMC	ATRA	0.043184051	0.38966865	56169
GSDMC	AUY922	-0.009428857	0.892581226	56169
GSDMC	AZ628	-0.007215655	0.942681217	56169
GSDMC	AZD6482	0.020574409	0.710704886	56169
GSDMC	AZD7762	0.050210853	0.226172194	56169
GSDMC	AZD8055	0.051385184	0.205160191	56169
GSDMC	Afatinib	-0.342222453	1.20655E-25	56169
GSDMC	Axitinib	0.049851833	0.338210328	56169
GSDMC	BAY 61-3606	0.078248566	0.051277447	56169
GSDMC	BEZ235	0.029337791	0.583019922	56169
GSDMC	BHG712	0.092860354	0.009884426	56169
GSDMC	BI-2536	-0.097359325	0.294265093	56169
GSDMC	BIRB 0796	-0.05612209	0.265643715	56169
GSDMC	BIX02189	0.081945406	0.024716366	56169
GSDMC	BMS-509744	-0.05008853	0.603068169	56169
GSDMC	BMS-536924	-0.012431806	0.894673152	56169
GSDMC	BMS-708163	-0.058557447	0.146223364	56169
GSDMC	BMS-754807	0.019723474	0.757641451	56169
GSDMC	BMS345541	0.039158174	0.29964016	56169
GSDMC	BX-795	0.058667789	0.19151629	56169
GSDMC	BX-912	0.105307964	0.002849731	56169
GSDMC	Belinostat	0.081594699	0.027976749	56169
GSDMC	Bexarotene	-0.014276935	0.885969368	56169
GSDMC	Bicalutamide	-0.068570844	0.110145999	56169
GSDMC	Bleomycin	-0.003108074	0.969324033	56169
GSDMC	Bleomycin (50 uM)	-0.071787523	0.049115033	56169
GSDMC	Bortezomib	-0.037782796	0.675253379	56169
GSDMC	Bosutinib	-0.151329552	0.000301515	56169
GSDMC	Bryostatin 1	-0.021538405	0.719187573	56169
GSDMC	CAL-101	0.073236952	0.051357598	56169

GSDMC	CAY10603	0.121558321	0.00057392	56169
GSDMC	CCT007093	-0.13917973	0.000458052	56169
GSDMC	CCT018159	-0.044061933	0.396090531	56169
GSDMC	CEP-701	0.112265562	0.003769352	56169
GSDMC	CGP-082996	-0.21194048	0.002169578	56169
GSDMC	CGP-60474	-0.069614726	0.408488132	56169
GSDMC	CH5424802	0.025764461	0.700896579	56169
GSDMC	CHIR-99021	0.078899128	0.035832694	56169
GSDMC	CI-1040	-0.052333791	0.237184633	56169
GSDMC	CMK	-0.038301001	0.771535593	56169
GSDMC	CP466722	0.071110773	0.049692577	56169
GSDMC	CP724714	-0.058855368	0.246676333	56169
GSDMC	CUDC-101	0.017440664	0.670964818	56169
GSDMC	CX-5461	0.094484539	0.009199597	56169
GSDMC	Camptothecin	0.044762786	0.324331966	56169
GSDMC	Cetuximab	-0.216848592	4.35192E-09	56169
GSDMC	Cisplatin	-0.00229786	0.972368543	56169
GSDMC	Crizotinib	-0.019067494	0.921664695	56169
GSDMC	Cyclopamine	-0.005118417	0.97122667	56169
GSDMC	Cytarabine	0.04942153	0.327233377	56169
GSDMC	DMOG	-0.004944803	0.93408696	56169
GSDMC	Dabrafenib	0.091439373	0.023617516	56169
GSDMC	Dasatinib	-0.167282042	0.00611565	56169
GSDMC	Docetaxel	-0.172002804	2.3512E-06	56169
GSDMC	Doxorubicin	-0.046565081	0.460251197	56169
GSDMC	EHT 1864	0.038117583	0.577117789	56169
GSDMC	EKB-569	-0.105327637	0.005624563	56169
GSDMC	EX-527	0.015633189	0.905565414	56169
GSDMC	Elesclomol	-0.008955754	0.867021159	56169
GSDMC	Embelin	-0.029785444	0.647567201	56169
GSDMC	Epothilone B	-0.095964312	0.036765258	56169
GSDMC	Erlotinib	-0.224642916	0.000372051	56169
GSDMC	Etoposide	-0.000538445	0.993984476	56169
GSDMC	FH535	-0.032149105	0.537146119	56169
GSDMC	FK866	0.178424189	3.26028E-07	56169
GSDMC	FMK	-0.000266865	0.997458122	56169
GSDMC	FR-180204	-0.030004467	0.600490204	56169
GSDMC	FTI-277	-0.045252923	0.290317849	56169
GSDMC	Foretinib	0.052351935	0.208691901	56169
GSDMC	GDC0449	-0.035450193	0.730174639	56169
GSDMC	GDC0941	-0.016362285	0.811815355	56169
GSDMC	GNF-2	-0.092410175	0.621785417	56169
GSDMC	GSK-650394	-0.029306523	0.717021372	56169
GSDMC	GSK1070916	0.072954569	0.049284583	56169
GSDMC	GSK1904529A	-0.054821494	0.227273744	56169
GSDMC	GSK2126458	0.024773856	0.544478955	56169
GSDMC	GSK269962A	0.11482028	0.005326045	56169
GSDMC	GSK429286A	0.112375392	0.003245044	56169
GSDMC	GSK690693	0.062613402	0.094955466	56169
GSDMC	GW 441756	-0.016579829	0.956700088	56169
GSDMC	GW-2580	0.006715733	0.994893052	56169
GSDMC	GW843682X	-0.082596014	0.325806834	56169
GSDMC	Gefitinib	-0.330523365	8.86219E-21	56169
GSDMC	Gemcitabine	-0.02141163	0.703519549	56169
GSDMC	Genentech Cpd 10	0.078221411	0.03351634	56169
GSDMC	HG-5-113-01	0.012904926	0.889233531	56169
GSDMC	HG-5-88-01	-0.009769323	0.965832495	56169
GSDMC	HG-6-64-1	0.028875818	0.584522186	56169
GSDMC	I-BET-762	0.136599292	0.000076122	56169
GSDMC	IOX2	-0.050498623	0.372198529	56169
GSDMC	IPA-3	0.086013043	0.0262819	56169
GSDMC	Imatinib	-0.103996773	0.33523806	56169
GSDMC	Ispinesib Mesylate	0.022393682	0.57723524	56169
GSDMC	JNJ-26854165	-0.040923037	0.433704269	56169
GSDMC	JNK Inhibitor VIII	-0.06233044	0.142269821	56169
GSDMC	JNK-9L	-0.024947385	0.697595415	56169
GSDMC	JQ1	-0.049694061	0.248312263	56169

GSDMC	JQ12	0.027570219	0.644814786	56169
GSDMC	JW-7-24-1	0.120514688	0.000620018	56169
GSDMC	JW-7-52-1	0.001241491	0.994079702	56169
GSDMC	KIN001-055	-0.185222791	0.000010173	56169
GSDMC	KIN001-102	0.034064664	0.367354285	56169
GSDMC	KIN001-135	0.015007426	0.914451871	56169
GSDMC	KIN001-236	0.058635567	0.119893648	56169
GSDMC	KIN001-244	0.07349435	0.046570732	56169
GSDMC	KIN001-260	0.112151903	0.001672363	56169
GSDMC	KIN001-266	0.003192552	0.957804257	56169
GSDMC	KIN001-270	0.068834973	0.078023782	56169
GSDMC	KU-55933	-0.021595223	0.76775706	56169
GSDMC	LAQ824	0.055191568	0.171262236	56169
GSDMC	LFM-A13	-0.00682146	0.916798324	56169
GSDMC	LY317615	-0.0221353	0.650988141	56169
GSDMC	Lapatinib	-0.252002598	8.85822E-06	56169
GSDMC	Lenalidomide	-0.046369114	0.521456826	56169
GSDMC	Linifanib	0.029169398	0.608654133	56169
GSDMC	Lisitinib	0.021830375	0.77274323	56169
GSDMC	MG-132	-0.025546858	0.817507815	56169
GSDMC	MK-2206	0.045281604	0.383544412	56169
GSDMC	MLN4924	-0.022903943	0.720335195	56169
GSDMC	MP470	0.089793869	0.03123236	56169
GSDMC	MPS-1-IN-1	0.063898308	0.093167652	56169
GSDMC	MS-275	0.038520713	0.677795981	56169
GSDMC	Masitinib	0.062428205	0.100387474	56169
GSDMC	Methotrexate	0.074454678	0.046732625	56169
GSDMC	Midostaurin	0.047631406	0.294082855	56169
GSDMC	Mitomycin C	-0.033123289	0.5469698	56169
GSDMC	NG-25	0.070975958	0.051222191	56169
GSDMC	NPK76-II-72-1	0.104308935	0.002917246	56169
GSDMC	NSC-207895	0.104134024	0.010039938	56169
GSDMC	NSC-87877	-0.005209443	0.945738907	56169
GSDMC	NU-7441	0.008140081	0.941835284	56169
GSDMC	Navitoclax	0.10491482	0.004477672	56169
GSDMC	Nilotinib	-0.00869939	0.89374551	56169
GSDMC	Nutlin-3a (-)	0.132366963	0.001367169	56169
GSDMC	OSI-027	0.112803259	0.001544507	56169
GSDMC	OSI-930	0.050688068	0.200874638	56169
GSDMC	OSU-03012	-0.016666664	0.775680655	56169
GSDMC	Obatoclax Mesylate	-0.018614544	0.735717479	56169
GSDMC	Olaparib	0.021412738	0.660034941	56169
GSDMC	PAC-1	0.049324091	0.251795151	56169
GSDMC	PD-0325901	-0.06328282	0.117179716	56169
GSDMC	PD-0332991	0.014862789	0.830972295	56169
GSDMC	PD-173074	0.058467163	0.645356471	56169
GSDMC	PF-4708671	0.003126195	0.986289464	56169
GSDMC	PF-562271	-0.056566764	0.295386987	56169
GSDMC	PFI-1	0.034444725	0.500597424	56169
GSDMC	PHA-665752	-0.022909038	0.893936411	56169
GSDMC	PHA-793887	0.060005585	0.095443364	56169
GSDMC	PI-103	0.091015776	0.011546661	56169
GSDMC	PIK-93	0.102188244	0.003703918	56169
GSDMC	PLX4720	0.046796688	0.266601049	56169
GSDMC	Paclitaxel	-0.170120354	0.033660886	56169
GSDMC	Parthenolide	0.028306941	0.817949004	56169
GSDMC	Pazopanib	0.084183881	0.084924643	56169
GSDMC	Phenformin	0.024103245	0.55094562	56169
GSDMC	Pyrimethamine	0.041082972	0.740457063	56169
GSDMC	QL-VIII-58	-0.07688153	0.27975435	56169
GSDMC	QL-X-138	0.088642892	0.015070642	56169
GSDMC	QL-XI-92	0.083941411	0.020237702	56169
GSDMC	QL-XII-47	0.027207881	0.530622169	56169
GSDMC	QL-XII-61	0.11273085	0.060262035	56169
GSDMC	QS11	0.032372435	0.627633528	56169
GSDMC	RDEA119	-0.045366926	0.238916324	56169
GSDMC	RO-3306	-0.10262823	0.011356718	56169

GSDMC	Rapamycin	-0.086204772	0.414771411	56169
GSDMC	Roscovitine	0.036043988	0.857267057	56169
GSDMC	Ruxolitinib	0.046042002	0.362425617	56169
GSDMC	S-Trityl-L-cysteine	-0.056017908	0.510130567	56169
GSDMC	SB 216763	-0.021694127	0.691408597	56169
GSDMC	SB 505124	0.062599398	0.353250708	56169
GSDMC	SB52334	0.106190913	0.008724581	56169
GSDMC	SB590885	0.033883807	0.51647526	56169
GSDMC	SGC0946	-0.015582665	0.811673233	56169
GSDMC	SL 0101-1	-0.092286705	0.204783264	56169
GSDMC	SN-38	0.015964216	0.761817825	56169
GSDMC	SNX-2112	0.076721591	0.036274458	56169
GSDMC	STF-62247	0.052306799	0.199807114	56169
GSDMC	Salubrinal	0.052479873	0.554458491	56169
GSDMC	Saracatinib	-0.167646847	0.021947041	56169
GSDMC	Shikonin	0.035423021	0.528517651	56169
GSDMC	Sorafenib	-0.051876311	0.65105927	56169
GSDMC	Sunitinib	-0.077940829	0.286309031	56169
GSDMC	T0901317	0.064166669	0.112651938	56169
GSDMC	TAE684	-0.023321419	0.872006388	56169
GSDMC	TAK-715	-0.003579623	0.933419813	56169
GSDMC	TG101348	0.114497964	0.001182882	56169
GSDMC	TGX221	0.056038975	0.404550529	56169
GSDMC	THZ-2-102-1	0.072409236	0.047450965	56169
GSDMC	THZ-2-49	0.070956678	0.055782528	56169
GSDMC	TL-1-85	0.085787688	0.017714098	56169
GSDMC	TL-2-105	0.045223151	0.241576285	56169
GSDMC	TPCA-1	0.096789704	0.006187972	56169
GSDMC	TW 37	0.092269011	0.025073002	56169
GSDMC	Talazoparib	0.02976649	0.540505079	56169
GSDMC	Tamoxifen	-0.005370816	0.973943647	56169
GSDMC	Temozolomide	-0.003528839	0.97375044	56169
GSDMC	Temsirolimus	0.034653221	0.512413682	56169
GSDMC	Thapsigargin	-0.015623845	0.853147444	56169
GSDMC	Tipifarnib	-0.013995033	0.871107355	56169
GSDMC	Tivozanib	0.025181425	0.700996864	56169
GSDMC	Trametinib	-0.080633897	0.030169636	56169
GSDMC	Tubastatin A	0.132984914	0.000148914	56169
GSDMC	UNC0638	0.097921233	0.005147354	56169
GSDMC	UNC1215	-0.021147235	0.715254584	56169
GSDMC	VNLG/124	0.038523883	0.375179458	56169
GSDMC	VX-11e	0.011420626	0.851214702	56169
GSDMC	VX-680	-0.064366945	0.492777659	56169
GSDMC	VX-702	0.013153808	0.962823102	56169
GSDMC	Veliparib	-0.004597957	0.961839737	56169
GSDMC	Vinblastine	-0.001939802	0.973855649	56169
GSDMC	Vinorelbine	-0.070540055	0.15968347	56169
GSDMC	Vorinostat	0.114893249	0.001592396	56169
GSDMC	WH-4-023	-0.169323648	0.010318182	56169
GSDMC	WZ-1-84	-0.242314662	0.000098011	56169
GSDMC	WZ3105	0.040057915	0.283185053	56169
GSDMC	XAV939	-0.104885716	0.005550174	56169
GSDMC	XL-184	0.011043481	0.848168365	56169
GSDMC	XMD11-85h	0.000512627	0.998087599	56169
GSDMC	XMD13-2	0.083488167	0.02039634	56169
GSDMC	XMD14-99	0.089594369	0.015920484	56169
GSDMC	XMD15-27	0.062226534	0.16850979	56169
GSDMC	XMD8-85	-0.067114201	0.416681568	56169
GSDMC	XMD8-92	0.038967075	0.738318542	56169
GSDMC	Y-39983	0.104126319	0.004317898	56169
GSDMC	YK 4-279	0.004940741	0.949347787	56169
GSDMC	YM155	-0.055937063	0.260193705	56169
GSDMC	YM201636	0.102557452	0.004480021	56169
GSDMC	Z-LLNle-CHO	-0.048028621	0.548072305	56169
GSDMC	ZG-10	0.068619177	0.294074471	56169
GSDMC	ZM-447439	0.044689273	0.348839076	56169
GSDMC	ZSTK474	0.04528178	0.229820447	56169

GSDMC	Zibotentan	-0.041618633	0.854928869	56169
GSDMC	piperlongumine	0.025209812	0.604075503	56169
GSDMC	rTRAIL	-0.029400762	0.715046015	56169
GSDMC	selumetinib	-0.019349259	0.643803954	56169
GSDMD	(5Z)-7-Oxozeaenol	-0.118553722	0.00165386	79792
GSDMD	17-AAG	-0.168003351	3.27999E-06	79792
GSDMD	5-Fluorouracil	-0.066149486	0.073415943	79792
GSDMD	681640	-0.065543013	0.25422892	79792
GSDMD	A-443654	-0.103125453	0.459737822	79792
GSDMD	A-770041	-0.118176266	0.097533814	79792
GSDMD	AC220	-0.038307353	0.442069575	79792
GSDMD	AG-014699	-0.002260154	0.967156762	79792
GSDMD	AICAR	-0.15640391	0.000033322	79792
GSDMD	AKT inhibitor VIII	-0.07151257	0.100989751	79792
GSDMD	AMG-706	-0.03145611	0.634394887	79792
GSDMD	AP-24534	-0.089497849	0.023698833	79792
GSDMD	AR-42	0.06958342	0.055244206	79792
GSDMD	AS601245	-0.110245906	0.014793251	79792
GSDMD	AS605240	-0.141125488	0.00022499	79792
GSDMD	AT-7519	-0.038289736	0.308303507	79792
GSDMD	ATRA	-0.062942051	0.180547407	79792
GSDMD	AUY922	-0.122833608	0.004532811	79792
GSDMD	AZ628	-0.211097	0.000613523	79792
GSDMD	AZD6482	-0.110785904	0.005334008	79792
GSDMD	AZD7762	-0.099863247	0.010409665	79792
GSDMD	AZD8055	-0.104935347	0.006447358	79792
GSDMD	Afatinib	-0.087621629	0.016347232	79792
GSDMD	Axitinib	0.001340534	0.986330717	79792
GSDMD	BAY 61-3606	-0.015479609	0.739597316	79792
GSDMD	BEZ235	-0.095289308	0.02922256	79792
GSDMD	BHG712	-0.04800719	0.2003648	79792
GSDMD	BI-2536	-0.179470155	0.034357786	79792
GSDMD	BIRB 0796	0.007316636	0.907803557	79792
GSDMD	BIX02189	-0.049823668	0.187305421	79792
GSDMD	BMS-509744	-0.116898649	0.165507524	79792
GSDMD	BMS-536924	-0.033440157	0.65190613	79792
GSDMD	BMS-708163	-0.069295684	0.081111103	79792
GSDMD	BMS-754807	0.068071224	0.182481	79792
GSDMD	BMS345541	0.019486571	0.623198321	79792
GSDMD	BX-795	-0.088529253	0.036553519	79792
GSDMD	BX-912	-0.01194123	0.763867649	79792
GSDMD	Belinostat	0.058459616	0.123227859	79792
GSDMD	Bexarotene	-0.109865487	0.032489126	79792
GSDMD	Bicalutamide	-0.018316057	0.720108202	79792
GSDMD	Bleomycin	-0.137286089	0.001956009	79792
GSDMD	Bleomycin (50 uM)	-0.087834951	0.014946819	79792
GSDMD	Bortezomib	-0.223561384	0.0003641	79792
GSDMD	Bosutinib	-0.122952047	0.004376024	79792
GSDMD	Bryostatin 1	-0.050153733	0.330502454	79792
GSDMD	CAL-101	-0.057657501	0.13275185	79792
GSDMD	CAY10603	0.054584412	0.137704742	79792
GSDMD	CCT007093	-0.074353836	0.075647372	79792
GSDMD	CCT018159	-0.12511526	0.004380581	79792
GSDMD	CEP-701	-0.111444922	0.004060733	79792
GSDMD	CGP-082996	-0.221899911	0.001332186	79792
GSDMD	CGP-60474	-0.218320459	0.000877892	79792
GSDMD	CH5424802	-0.088054503	0.068189963	79792
GSDMD	CHIR-99021	-0.017453488	0.685548723	79792
GSDMD	CI-1040	-0.147640868	0.000154565	79792
GSDMD	CMK	-0.047485782	0.703561076	79792
GSDMD	CP466722	-0.067637487	0.062781368	79792
GSDMD	CP724714	-0.003252436	0.966331686	79792
GSDMD	CUDC-101	0.006449533	0.879989101	79792
GSDMD	CX-5461	0.039689614	0.303624468	79792
GSDMD	Camptothecin	-0.077272731	0.066473623	79792
GSDMD	Cetuximab	-0.022545757	0.615697508	79792
GSDMD	Cisplatin	-0.016777865	0.775735519	79792

GSDMD	Crizotinib	-0.182022925	0.017040651	79792
GSDMD	Cyclopamine	-0.110672741	0.214415211	79792
GSDMD	Cytarabine	-0.061517462	0.205513181	79792
GSDMD	DMOG	-0.103285745	0.011468138	79792
GSDMD	Dabrafenib	-0.096794811	0.015825061	79792
GSDMD	Dasatinib	-0.197447732	0.00096111	79792
GSDMD	Docetaxel	-0.119154782	0.001265346	79792
GSDMD	Doxorubicin	-0.077782215	0.156090272	79792
GSDMD	EHT 1864	-0.002652157	0.978241691	79792
GSDMD	EKB-569	-0.15160946	0.000041203	79792
GSDMD	EX-527	0.014451865	0.913969088	79792
GSDMD	Elesclomol	-0.005590431	0.917497547	79792
GSDMD	Embelin	-0.089048191	0.070773817	79792
GSDMD	Epothilone B	-0.093674327	0.042601109	79792
GSDMD	Erlotinib	-0.013745071	0.872885888	79792
GSDMD	Etoposide	-0.066850778	0.136720489	79792
GSDMD	FH535	-0.095022507	0.026920682	79792
GSDMD	FK866	0.030922133	0.425166218	79792
GSDMD	FMK	-0.034724789	0.629470301	79792
GSDMD	FR-180204	-0.083128353	0.071365993	79792
GSDMD	FTI-277	-0.02423494	0.590941692	79792
GSDMD	Foretinib	0.015943965	0.74236615	79792
GSDMD	GDC0449	-0.035422591	0.730281614	79792
GSDMD	GDC0941	-0.065273315	0.198172591	79792
GSDMD	GNF-2	-0.167117752	0.078244149	79792
GSDMD	GSK-650394	-0.112460818	0.043491415	79792
GSDMD	GSK1070916	-0.009704804	0.817460648	79792
GSDMD	GSK1904529A	-0.011923591	0.829400457	79792
GSDMD	GSK2126458	-0.056050084	0.143175316	79792
GSDMD	GSK269962A	0.034271078	0.535536631	79792
GSDMD	GSK429286A	0.005739334	0.911266302	79792
GSDMD	GSK690693	0.013279122	0.750978334	79792
GSDMD	GW 441756	-0.05111534	0.754599717	79792
GSDMD	GW-2580	-0.031363675	0.94324124	79792
GSDMD	GW843682X	-0.172560058	0.018349173	79792
GSDMD	Gefitinib	-0.073309396	0.073400173	79792
GSDMD	Gemcitabine	-0.093313843	0.035481092	79792
GSDMD	Genentech Cpd 10	0.009386356	0.827620058	79792
GSDMD	HG-5-113-01	-0.014696334	0.870925562	79792
GSDMD	HG-5-88-01	-0.05299629	0.717963975	79792
GSDMD	HG-6-64-1	-0.124968461	0.002112996	79792
GSDMD	I-BET-762	-0.004422161	0.912708069	79792
GSDMD	IOX2	-0.003172603	0.970909262	79792
GSDMD	IPA-3	0.017297849	0.698535183	79792
GSDMD	Imatinib	-0.145931139	0.090279176	79792
GSDMD	Ispinesib Mesylate	-0.02364406	0.554683825	79792
GSDMD	JNJ-26854165	-0.12706901	0.003034678	79792
GSDMD	JNK Inhibitor VIII	-0.064346686	0.128326225	79792
GSDMD	JNK-9L	-0.096136645	0.042765621	79792
GSDMD	JQ1	-0.101728415	0.010488442	79792
GSDMD	JQ12	-0.059082514	0.256341431	79792
GSDMD	JW-7-24-1	-0.005874519	0.887900916	79792
GSDMD	JW-7-52-1	-0.195246841	0.006171132	79792
GSDMD	KIN001-055	-0.068668716	0.204368296	79792
GSDMD	KIN001-102	-0.058582121	0.10786541	79792
GSDMD	KIN001-135	0.088889408	0.344944166	79792
GSDMD	KIN001-236	-0.027406951	0.492629315	79792
GSDMD	KIN001-244	-0.036622627	0.345652017	79792
GSDMD	KIN001-260	-0.001247288	0.976357998	79792
GSDMD	KIN001-266	0.029072958	0.573499772	79792
GSDMD	KIN001-270	0.05574019	0.161617921	79792
GSDMD	KU-55933	-0.135568942	0.003469415	79792
GSDMD	LAQ824	-0.037699172	0.3668068	79792
GSDMD	LFM-A13	-0.031776698	0.56224323	79792
GSDMD	LY317615	-0.10273193	0.010529905	79792
GSDMD	Lapatinib	-0.060992296	0.349005369	79792
GSDMD	Lenalidomide	-0.067131609	0.291057938	79792

GSDMD	Linifanib	-0.094306912	0.030556214	79792
GSDMD	Lisitinib	0.101330316	0.0430144	79792
GSDMD	MG-132	-0.124641544	0.095129131	79792
GSDMD	MK-2206	-0.034064804	0.533859444	79792
GSDMD	MLN4924	-0.141591761	0.004126014	79792
GSDMD	MP470	0.061772304	0.148694635	79792
GSDMD	MPS-1-IN-1	0.03734066	0.347107304	79792
GSDMD	MS-275	-0.113499013	0.122587778	79792
GSDMD	Masitinib	-0.041830376	0.287681197	79792
GSDMD	Methotrexate	-0.088812778	0.016564234	79792
GSDMD	Midostaurin	-0.060322088	0.168597557	79792
GSDMD	Mitomycin C	-0.092295145	0.041162554	79792
GSDMD	NG-25	-0.022253907	0.571986214	79792
GSDMD	NPK76-II-72-1	0.033665821	0.366257339	79792
GSDMD	NSC-207895	0.097950176	0.0164254	79792
GSDMD	NSC-87877	0.004038212	0.958210933	79792
GSDMD	NU-7441	-0.095382213	0.09580074	79792
GSDMD	Navitoclax	0.002021942	0.963353442	79792
GSDMD	Nilotinib	-0.09789255	0.028911185	79792
GSDMD	Nutlin-3a (-)	-0.052813553	0.265092073	79792
GSDMD	OSI-027	-0.022973121	0.560227953	79792
GSDMD	OSI-930	-0.085886468	0.023597074	79792
GSDMD	OSU-03012	-0.108958327	0.011928082	79792
GSDMD	Obatoclax Mesylate	-0.107823294	0.010244926	79792
GSDMD	Olaparib	-0.026657981	0.57311808	79792
GSDMD	PAC-1	-0.058479115	0.165913395	79792
GSDMD	PD-0325901	-0.133396206	0.000446477	79792
GSDMD	PD-0332991	-0.098364545	0.036088772	79792
GSDMD	PD-173074	-0.020441721	0.91069623	79792
GSDMD	PF-4708671	-0.051281388	0.572981717	79792
GSDMD	PF-562271	-0.092523597	0.060852283	79792
GSDMD	PFI-1	-0.07598397	0.088941411	79792
GSDMD	PHA-665752	-0.068494589	0.627503031	79792
GSDMD	PHA-793887	-0.039528312	0.283650684	79792
GSDMD	PI-103	0.022071103	0.576921382	79792
GSDMD	PIK-93	-0.017900375	0.646890602	79792
GSDMD	PLX4720	-0.057030315	0.167341052	79792
GSDMD	Paclitaxel	-0.236038197	0.003209596	79792
GSDMD	Parthenolide	-0.087321881	0.36081215	79792
GSDMD	Pazopanib	0.010107823	0.883907971	79792
GSDMD	Phenformin	-0.029518104	0.458709354	79792
GSDMD	Pyrimethamine	-0.094254405	0.372745084	79792
GSDMD	QL-VIII-58	-0.117183288	0.068225422	79792
GSDMD	QL-X-138	-0.006081322	0.887411885	79792
GSDMD	QL-XI-92	-0.072348601	0.047375863	79792
GSDMD	QL-XII-47	-0.006962967	0.88575008	79792
GSDMD	QL-XII-61	-0.071411396	0.273506248	79792
GSDMD	QS11	-0.032020263	0.632061077	79792
GSDMD	RDEA119	-0.149179521	0.000019101	79792
GSDMD	RO-3306	-0.06471448	0.12284793	79792
GSDMD	Rapamycin	-0.078142837	0.477684324	79792
GSDMD	Roscovitine	-0.051928946	0.764332853	79792
GSDMD	Ruxolitinib	-0.07286777	0.113866082	79792
GSDMD	S-Trityl-L-cysteine	-0.200701138	0.003808962	79792
GSDMD	SB 216763	-0.027266294	0.610820526	79792
GSDMD	SB 505124	0.078737881	0.208906044	79792
GSDMD	SB52334	0.164165509	0.000017897	79792
GSDMD	SB590885	-0.033006081	0.530098209	79792
GSDMD	SGC0946	-0.002895419	0.968565997	79792
GSDMD	SL 0101-1	-0.040147352	0.606236928	79792
GSDMD	SN-38	-0.102935679	0.009390032	79792
GSDMD	SNX-2112	-0.035271226	0.362115743	79792
GSDMD	STF-62247	-0.036867773	0.384873444	79792
GSDMD	Salubrinal	-0.152335781	0.040429758	79792
GSDMD	Saracatinib	-0.125252984	0.105749726	79792
GSDMD	Shikonin	-0.066613161	0.178782267	79792
GSDMD	Sorafenib	-0.180772946	0.012362055	79792

GSDMD	Sunitinib	-0.276439392	2.12125E-06	79792
GSDMD	T0901317	-0.021814531	0.63241446	79792
GSDMD	TAE684	-0.117369026	0.182134523	79792
GSDMD	TAK-715	-0.0626117	0.089642286	79792
GSDMD	TG101348	-0.04888459	0.188651653	79792
GSDMD	TGX221	-0.104651317	0.097138581	79792
GSDMD	THZ-2-102-1	0.018843087	0.636627696	79792
GSDMD	THZ-2-49	-0.06734413	0.070318831	79792
GSDMD	TL-1-85	-0.04623497	0.220184199	79792
GSDMD	TL-2-105	-0.010342023	0.808099407	79792
GSDMD	TPCA-1	-0.034981888	0.35171058	79792
GSDMD	TW 37	0.047363224	0.308096615	79792
GSDMD	Talazoparib	-0.016190381	0.757463552	79792
GSDMD	Tamoxifen	-0.051954123	0.624112886	79792
GSDMD	Temozolomide	-0.07359664	0.201317876	79792
GSDMD	Temsirolimus	-0.073562695	0.106444615	79792
GSDMD	Thapsigargin	-0.016376804	0.844439001	79792
GSDMD	Tipifarnib	-0.11600153	0.018709048	79792
GSDMD	Tivozanib	-0.030236229	0.632648161	79792
GSDMD	Trametinib	-0.117078134	0.001225082	79792
GSDMD	Tubastatin A	0.038478295	0.304941674	79792
GSDMD	UNC0638	0.036216014	0.328766034	79792
GSDMD	UNC1215	-0.007411739	0.908365494	79792
GSDMD	VNLG/124	-0.090936543	0.020375083	79792
GSDMD	VX-11e	-0.05243972	0.263160411	79792
GSDMD	VX-680	-0.19373618	0.008143091	79792
GSDMD	VX-702	-0.005495592	0.986082424	79792
GSDMD	Veliparib	-0.043107506	0.532677218	79792
GSDMD	Vinblastine	-0.096913986	0.018681436	79792
GSDMD	Vinorelbine	-0.062176989	0.228681298	79792
GSDMD	Vorinostat	0.003430962	0.935130441	79792
GSDMD	WH-4-023	-0.114593949	0.104698221	79792
GSDMD	WZ-1-84	-0.146368216	0.032189159	79792
GSDMD	WZ3105	-0.018755614	0.631414403	79792
GSDMD	XAV939	-0.072639344	0.060966976	79792
GSDMD	XL-184	-0.064598038	0.148233901	79792
GSDMD	XMD11-85h	-0.061794474	0.704099421	79792
GSDMD	XMD13-2	-0.05301151	0.151887771	79792
GSDMD	XMD14-99	-0.05341119	0.1693769	79792
GSDMD	XMD15-27	-0.05819178	0.202623344	79792
GSDMD	XMD8-85	-0.224051174	0.000569018	79792
GSDMD	XMD8-92	-0.068832359	0.498108207	79792
GSDMD	Y-39983	0.002356906	0.956482821	79792
GSDMD	YK 4-279	-0.075034466	0.126555857	79792
GSDMD	YM155	-0.003752481	0.959567063	79792
GSDMD	YM201636	0.066373584	0.073922267	79792
GSDMD	Z-LLNle-CHO	-0.319795506	3.88642E-08	79792
GSDMD	ZG-10	-0.052106605	0.451475281	79792
GSDMD	ZM-447439	-0.073928156	0.093783095	79792
GSDMD	ZSTK474	-0.081090548	0.025675208	79792
GSDMD	Zibotentan	-0.051923265	0.794808243	79792
GSDMD	piperlongumine	-0.07234258	0.082156836	79792
GSDMD	rTRAIL	-0.025430581	0.757790916	79792
GSDMD	selumetinib	-0.128283572	0.000291313	79792

Supp. Table 6. Drug sensitivity of *GSDMD* gene expression.

symbol	drug	cor	fdr	entrez
GSDMC	16-beta-bromoandrosterone	0.000964955	0.987431201	56169
GSDMC	1S,3R-RSL-3	0.102129898	0.010494474	56169
GSDMC	3-Cl-AHPC	-0.002617769	0.955097481	56169
GSDMC	968	0.057832064	0.976177471	56169
GSDMC	A-804598	0.005025342	0.983073023	56169
GSDMC	AA-COCF3	0.018048091	0.699398236	56169
GSDMC	ABT-199	0.016619701	0.800313493	56169
GSDMC	ABT-737	0.087350323	0.047303637	56169

GSDMC	AC55649	-0.04870282	0.687604993	56169
GSDMC	AGK-2	-0.010458082	0.987189679	56169
GSDMC	AM-580	-0.032058202	0.578886222	56169
GSDMC	AT-406	0.039357258	0.733514528	56169
GSDMC	AT13387	-0.019289694	0.768910269	56169
GSDMC	AT7867	0.138815634	0.000451912	56169
GSDMC	AZ-3146	0.023929405	0.609182802	56169
GSDMC	AZD1480	0.043403893	0.584973997	56169
GSDMC	AZD4547	0.108819072	0.014329462	56169
GSDMC	AZD6482	-0.036839495	0.554334784	56169
GSDMC	AZD7545	0.042454206	0.352191595	56169
GSDMC	AZD7762	-0.000380032	0.993245743	56169
GSDMC	AZD8055	-0.015911284	0.723196912	56169
GSDMC	B02	0.007920363	0.866688504	56169
GSDMC	BCL-LZH-4	-0.147442901	0.422450666	56169
GSDMC	BEC	-0.012929687	0.999979174	56169
GSDMC	BI-2536	0.049766216	0.199016728	56169
GSDMC	BIBR-1532	-0.02713146	0.603130915	56169
GSDMC	BIRB-796	0.00908345	0.868125218	56169
GSDMC	BIX-01294	0.087117539	0.026675426	56169
GSDMC	BMS-195614	0.018956143	0.802784012	56169
GSDMC	BMS-270394	-0.053418517	0.25504613	56169
GSDMC	BMS-345541	-0.029954987	0.47332863	56169
GSDMC	BMS-536924	-0.082335152	0.098650491	56169
GSDMC	BMS-754807	0.003840119	0.949377245	56169
GSDMC	BRD-A02303741	0.034962469	0.547673172	56169
GSDMC	BRD-A05715709	-0.068808752	0.640079059	56169
GSDMC	BRD-A71883111	-0.030078651	0.531452364	56169
GSDMC	BRD-A86708339	0.009709138	0.890997831	56169
GSDMC	BRD-A94377914	0.056645265	0.340183503	56169
GSDMC	BRD-K01737880	0.100920969	0.642396554	56169
GSDMC	BRD-K02251932	-0.053920534	0.29972707	56169
GSDMC	BRD-K02492147	-0.030580581	0.635069174	56169
GSDMC	BRD-K04800985	-0.036169221	0.99880963	56169
GSDMC	BRD-K09344309	0.104954543	0.81896693	56169
GSDMC	BRD-K09587429	-0.017786265	0.819754352	56169
GSDMC	BRD-K11533227	0.032598532	0.488921625	56169
GSDMC	BRD-K13999467	0.009412866	0.858902596	56169
GSDMC	BRD-K14844214	-0.011070113	0.909543002	56169
GSDMC	BRD-K16147474	-0.022147432	0.961235522	56169
GSDMC	BRD-K17060750	-0.030485779	0.582587506	56169
GSDMC	BRD-K19103580	-0.010075599	0.870343863	56169
GSDMC	BRD-K24690302	0.012601261	0.804105383	56169
GSDMC	BRD-K26531177	0.089457066	0.030650521	56169
GSDMC	BRD-K27224038	0.003801734	0.991052089	56169
GSDMC	BRD-K27986637	0.00713727	0.975051924	56169
GSDMC	BRD-K28456706	0.027355682	0.555171855	56169
GSDMC	BRD-K29086754	-0.102198768	0.584549844	56169
GSDMC	BRD-K29313308	0.006123769	0.904559449	56169
GSDMC	BRD-K30019337	0.074021561	0.794208857	56169
GSDMC	BRD-K30748066	0.006624273	0.97804698	56169
GSDMC	BRD-K33199242	-0.019299933	0.978378934	56169
GSDMC	BRD-K33514849	0.068094356	0.999288401	56169
GSDMC	BRD-K34099515	-0.013894857	0.991363606	56169
GSDMC	BRD-K34222889	0.081787359	0.035216009	56169
GSDMC	BRD-K34485477	0.070390969	0.998562234	56169
GSDMC	BRD-K35604418	-0.011283884	0.799666874	56169
GSDMC	BRD-K37390332	0.056876886	0.73831986	56169
GSDMC	BRD-K41334119	0.024080461	0.977976412	56169
GSDMC	BRD-K41597374	0.0031788	0.947628966	56169
GSDMC	BRD-K42260513	0.035269794	0.994633498	56169
GSDMC	BRD-K44224150	0.046049847	0.994574195	56169
GSDMC	BRD-K45681478	-0.004455608	0.936340636	56169
GSDMC	BRD-K48334597	0.033208754	0.816742931	56169
GSDMC	BRD-K48477130	-0.103126339	0.587632551	56169
GSDMC	BRD-K49290616	-0.056158728	0.900175972	56169
GSDMC	BRD-K50799972	-0.010397284	0.917065769	56169

GSDMC	BRD-K51490254	0.018793986	0.688725336	56169
GSDMC	BRD-K51831558	-0.010560538	0.904245966	56169
GSDMC	BRD-K52037352	-0.063805599	0.314052054	56169
GSDMC	BRD-K55116708	-0.010710132	0.847626977	56169
GSDMC	BRD-K61166597	0.018771329	0.669611356	56169
GSDMC	BRD-K63431240	0.008591449	0.870147335	56169
GSDMC	BRD-K64610608	0.017014506	0.904798232	56169
GSDMC	BRD-K66453893	-0.0415573	0.30061274	56169
GSDMC	BRD-K66532283	-0.021394948	0.629923699	56169
GSDMC	BRD-K70511574	0.047616052	0.235307267	56169
GSDMC	BRD-K71781559	-0.027260305	0.993921887	56169
GSDMC	BRD-K75293299	0.037608996	0.900544548	56169
GSDMC	BRD-K78574327	-0.003660233	0.99731699	56169
GSDMC	BRD-K80183349	-0.012374335	0.783200658	56169
GSDMC	BRD-K84807411	0.061779742	0.832967982	56169
GSDMC	BRD-K85133207	0.01996566	0.68749701	56169
GSDMC	BRD-K86535717	-0.042161417	0.917253937	56169
GSDMC	BRD-K88742110	0.013378224	0.779390159	56169
GSDMC	BRD-K90370028	-0.016535618	0.976273931	56169
GSDMC	BRD-K92856060	0.041135264	0.352696963	56169
GSDMC	BRD-K96431673	-0.054155529	0.986199957	56169
GSDMC	BRD-K96970199	0.019737229	0.998763577	56169
GSDMC	BRD-K97651142	0.068760536	0.104524214	56169
GSDMC	BRD-K99006945	0.063082616	0.394981543	56169
GSDMC	BRD-M00053801	-0.007648892	0.960345185	56169
GSDMC	BRD1378	0.015963846	0.913965545	56169
GSDMC	BRD1812	0.045045514	0.286632952	56169
GSDMC	BRD1835	0.003945957	0.952345359	56169
GSDMC	BRD4132	0.013552005	0.865118847	56169
GSDMC	BRD5468	-0.008480059	0.945751846	56169
GSDMC	BRD6340	-0.088270417	0.026899069	56169
GSDMC	BRD8899	-0.004632745	0.97643626	56169
GSDMC	BRD8958	0.039499023	0.982208781	56169
GSDMC	BRD9647	0.021783936	0.718417281	56169
GSDMC	BRD9876	-0.022418404	0.752794046	56169
GSDMC	BYL-719	-0.153135923	0.006556232	56169
GSDMC	Bax channel blocker	0.056602543	0.218881892	56169
GSDMC	C6-ceramide	-0.008341812	0.959670263	56169
GSDMC	CAL-101	-0.026216318	0.710194338	56169
GSDMC	CAY10576	0.012830267	0.892238548	56169
GSDMC	CAY10594	-0.033122773	0.605727709	56169
GSDMC	CAY10618	0.105105474	0.007427217	56169
GSDMC	CBB-1007	0.016281693	0.950196953	56169
GSDMC	CCT036477	0.051041766	0.213712908	56169
GSDMC	CD-1530	-0.031738872	0.602800365	56169
GSDMC	CD-437	0.005091842	0.909826762	56169
GSDMC	CHIR-99021	0.061033587	0.158894371	56169
GSDMC	CHM-1	0.03879052	0.332285797	56169
GSDMC	CI-976	0.009363219	0.962926213	56169
GSDMC	CID-5951923	-0.026444702	0.791143316	56169
GSDMC	CIL41	0.035009777	0.657179969	56169
GSDMC	CIL55	0.018257847	0.949161253	56169
GSDMC	CIL55A	0.01466223	0.839230425	56169
GSDMC	CIL56	-0.030004933	0.654324529	56169
GSDMC	CIL70	0.076275989	0.202555132	56169
GSDMC	COL-3	0.000030168	0.999847614	56169
GSDMC	CR-1-31B	-0.061677233	0.107679192	56169
GSDMC	Ch-55	-0.036801717	0.484529631	56169
GSDMC	Compound 1541A	0.047368018	0.460850861	56169
GSDMC	Compound 23 citrate	-0.011479248	0.795144788	56169
GSDMC	Compound 7d-cis	0.009028692	0.859025248	56169
GSDMC	DBeQ	0.003059649	0.95273858	56169
GSDMC	DNMDP	0.07117784	0.291937059	56169
GSDMC	ELCPK	0.026255369	0.704588599	56169
GSDMC	ETP-46464	0.011195002	0.864761036	56169
GSDMC	EX-527	-0.0137322	0.928993691	56169
GSDMC	FGIN-1-27	-0.069994063	0.600893622	56169

GSDMC	FQI-1	0.017583542	0.781985539	56169
GSDMC	FQI-2	0.026944295	0.514012533	56169
GSDMC	FSC231	0.075102718	0.999449861	56169
GSDMC	GANT-61	0.001271017	0.987045461	56169
GSDMC	GDC-0879	0.076444097	0.131608568	56169
GSDMC	GDC-0941	-0.10380114	0.015842328	56169
GSDMC	GMX-1778	0.079618339	0.053383811	56169
GSDMC	GSK-3 inhibitor IX	0.033539014	0.467320927	56169
GSDMC	GSK-J4	0.172644281	0.282378926	56169
GSDMC	GSK1059615	-0.083961995	0.730690615	56169
GSDMC	GSK2636771	0.034509836	0.753975139	56169
GSDMC	GSK4112	-0.009284179	0.88317398	56169
GSDMC	GSK461364	0.071420079	0.067944462	56169
GSDMC	GSK525762A	0.017704155	0.67391857	56169
GSDMC	GW-405833	-0.013255071	0.758341522	56169
GSDMC	GW-843682X	-0.004771102	0.923379099	56169
GSDMC	HBX-41108	0.062818798	0.269457197	56169
GSDMC	HC-067047	-0.012195977	0.875890047	56169
GSDMC	HLI 373	0.054376804	0.209762079	56169
GSDMC	I-BET151	0.035552191	0.372508999	56169
GSDMC	IC-87114	0.022715598	0.78054124	56169
GSDMC	IPR-456	0.00588129	0.979507738	56169
GSDMC	ISOX	0.082483172	0.034650997	56169
GSDMC	IU1	-0.024009452	0.823981634	56169
GSDMC	JQ-1	0.01599083	0.706043236	56169
GSDMC	JW-480	0.036158221	0.84475124	56169
GSDMC	JW-55	0.000055783	0.999521789	56169
GSDMC	JW-74	0.032286065	0.747517826	56169
GSDMC	KH-CB19	0.035465236	0.759989504	56169
GSDMC	KHS101	0.012668761	0.795903506	56169
GSDMC	KPT185	-0.021902904	0.662816823	56169
GSDMC	KU 0060648	-0.035249024	0.419965378	56169
GSDMC	KU-0063794	-0.001706499	0.971910199	56169
GSDMC	KU-55933	-0.076047389	0.078351088	56169
GSDMC	KU-60019	-0.029594425	0.487241759	56169
GSDMC	KW-2449	0.095651722	0.013274518	56169
GSDMC	KX2-391	0.068011765	0.084075536	56169
GSDMC	Ki8751	0.084810907	0.050055308	56169
GSDMC	Ko-143	0.019141213	0.669580129	56169
GSDMC	L-685458	-0.044511255	0.476551158	56169
GSDMC	LE-135	-0.011490486	0.822396108	56169
GSDMC	LRRK2-IN-1	0.041680732	0.391031012	56169
GSDMC	LY-2157299	-0.076200099	0.748551582	56169
GSDMC	LY-2183240	0.055855587	0.152523171	56169
GSDMC	MG-132	0.037853793	0.694274207	56169
GSDMC	MGCD-265	-0.007175009	0.874920843	56169
GSDMC	MI-1	-0.074722964	0.321273549	56169
GSDMC	MI-2	0.051018933	0.476437011	56169
GSDMC	MK-0752	-0.064745972	0.354036523	56169
GSDMC	MK-1775	-0.022973465	0.593795343	56169
GSDMC	MK-2206	-0.031805508	0.500067107	56169
GSDMC	ML006	-0.006780795	0.917076386	56169
GSDMC	ML029	0.048864725	0.29102983	56169
GSDMC	ML031	0.037121324	0.420919645	56169
GSDMC	ML050	0.022752322	0.635092911	56169
GSDMC	ML083	-0.058113966	0.609007459	56169
GSDMC	ML162	0.110983554	0.006199718	56169
GSDMC	ML203	-0.089006529	0.078238337	56169
GSDMC	ML210	0.121869807	0.002377287	56169
GSDMC	ML239	0.099038414	0.017085101	56169
GSDMC	ML258	0.004004426	0.977801246	56169
GSDMC	ML311	0.02170777	0.599833134	56169
GSDMC	ML312	-0.105530606	0.957289631	56169
GSDMC	ML320	0.109001454	0.012800459	56169
GSDMC	ML334 diastereomer	0.009135178	0.927291163	56169
GSDMC	MLN2238	-0.0030956	0.948372579	56169
GSDMC	MLN2480	0.100543935	0.262233721	56169

GSDMC	MST-312	0.010703757	0.805107935	56169
GSDMC	Mdivi-1	-0.043891486	0.32102786	56169
GSDMC	Merck60	0.014606505	0.731963655	56169
GSDMC	N9-isopropylolomoucine	-0.034160409	0.43267696	56169
GSDMC	NPC-26	0.011715021	0.943527123	56169
GSDMC	NSC 74859	0.032310302	0.572584959	56169
GSDMC	NSC19630	0.053449843	0.296316995	56169
GSDMC	NSC23766	-0.045878857	0.282742768	56169
GSDMC	NSC30930	-0.069043769	0.29410318	56169
GSDMC	NSC48300	-0.012710086	0.770415067	56169
GSDMC	NSC632839	0.016409998	0.698682808	56169
GSDMC	NSC95397	0.092449303	0.025283875	56169
GSDMC	NVP-231	0.030167841	0.472300658	56169
GSDMC	NVP-ADW742	-0.024783951	0.622746533	56169
GSDMC	NVP-BEZ235	-0.054883172	0.29452149	56169
GSDMC	NVP-BSK805	0.053384358	0.198462836	56169
GSDMC	NVP-TAE684	-0.023076562	0.675563847	56169
GSDMC	O-6-benzylguanine	0.011517373	0.946056693	56169
GSDMC	OSI-027	-0.031324567	0.503468909	56169
GSDMC	OSI-930	0.003868993	0.942810142	56169
GSDMC	PAC-1	0.01427985	0.747936858	56169
GSDMC	PD 153035	-0.171954639	0.000586046	56169
GSDMC	PD318088	-0.040431913	0.430769865	56169
GSDMC	PDMP	-0.003203813	0.951207189	56169
GSDMC	PF-184	0.042482795	0.30730193	56169
GSDMC	PF-3758309	0.014225891	0.822851841	56169
GSDMC	PF-4800567 hydrochloride	-0.003583594	0.999586205	56169
GSDMC	PF-543	-0.024620579	0.63888069	56169
GSDMC	PF-573228	0.005385949	0.90955095	56169
GSDMC	PF-750	0.04822605	0.328257681	56169
GSDMC	PHA-793887	-0.041495344	0.29561828	56169
GSDMC	PI-103	0.006420115	0.896097648	56169
GSDMC	PIK-93	-0.050982355	0.238832832	56169
GSDMC	PL-DI	0.062649781	0.115153371	56169
GSDMC	PLX-4720	0.018094815	0.845854706	56169
GSDMC	PRIMA-1	0.085846613	0.031579506	56169
GSDMC	PRIMA-1-Met	0.080999003	0.248811943	56169
GSDMC	PRL-3 inhibitor I	-0.042404547	0.753822551	56169
GSDMC	PX-12	0.090885355	0.018764708	56169
GSDMC	PYR-41	0.014387892	0.819203867	56169
GSDMC	QS-11	0.131402202	0.578930402	56169
GSDMC	QW-BI-011	0.066263863	0.500272849	56169
GSDMC	R428	0.081683871	0.110767911	56169
GSDMC	RAF265	0.015214486	0.826645417	56169
GSDMC	RG-108	0.109241189	0.00977377	56169
GSDMC	RITA	0.067000878	0.114349467	56169
GSDMC	RO4929097	0.019375081	0.827902738	56169
GSDMC	Repligen 136	0.009255183	0.855032288	56169
GSDMC	SB-225002	0.027103853	0.503681206	56169
GSDMC	SB-431542	-0.057083902	0.544832407	56169
GSDMC	SB-525334	0.057147023	0.268190808	56169
GSDMC	SB-743921	0.001898671	0.964351935	56169
GSDMC	SCH-529074	0.047884321	0.328589509	56169
GSDMC	SCH-79797	0.055412828	0.171174105	56169
GSDMC	SGX-523	-0.000753278	0.995238763	56169
GSDMC	SID 26681509	0.08606059	0.055381409	56169
GSDMC	SJ-172550	0.038777533	0.74229674	56169
GSDMC	SKI-II	0.032800502	0.503781559	56169
GSDMC	SMER-3	0.002505684	0.96431587	56169
GSDMC	SN-38	0.067116669	0.141034461	56169
GSDMC	SNS-032	-0.095608666	0.020282901	56169
GSDMC	SNX-2112	-0.074633372	0.051027796	56169
GSDMC	SR-II-138A	-0.032999507	0.398785677	56169
GSDMC	SR1001	0.038643784	0.605568558	56169
GSDMC	SR8278	-0.050338403	0.900992803	56169
GSDMC	SRT-1720	0.065608481	0.148685407	56169
GSDMC	STF-31	0.114866785	0.004041803	56169

GSDMC	SU11274	0.047439211	0.263490003	56169
GSDMC	SZ4TA2	0.015501042	0.92088258	56169
GSDMC	StemRegenin 1	-0.013736206	0.763658909	56169
GSDMC	TG-100-115	0.008185781	0.899884353	56169
GSDMC	TG-101348	0.049952544	0.241045695	56169
GSDMC	TGX-221	0.012970981	0.896594873	56169
GSDMC	TPCA-1	0.000928449	0.984488833	56169
GSDMC	TW-37	-0.010062187	0.832461633	56169
GSDMC	UNC0321	-0.079977268	0.396873043	56169
GSDMC	UNC0638	0.111769785	0.006864885	56169
GSDMC	VAF-347	0.013197792	0.868918877	56169
GSDMC	VER-155008	-0.06482213	0.128488296	56169
GSDMC	VU0155056	-0.046369099	0.889302808	56169
GSDMC	WAY-362450	0.015539639	0.99852118	56169
GSDMC	WP1130	0.069683886	0.091527644	56169
GSDMC	WZ4002	-0.069498761	0.310487539	56169
GSDMC	WZ8040	-0.111178156	0.019494086	56169
GSDMC	XL765	0.016099847	0.827635302	56169
GSDMC	YK 4-279	0.023188436	0.577532883	56169
GSDMC	YM-155	0.03655459	0.479415956	56169
GSDMC	ZSTK474	-0.04774521	0.387852662	56169
GSDMC	abiraterone	0.012342139	0.945391644	56169
GSDMC	afatinib	-0.189701967	6.05593E-06	56169
GSDMC	alisertib	0.021214376	0.623721826	56169
GSDMC	alvocidib	-0.020373391	0.751730293	56169
GSDMC	apicidin	0.003253846	0.941090024	56169
GSDMC	austocystin D	-0.026872275	0.607518399	56169
GSDMC	avicin D	-0.007322517	0.955198813	56169
GSDMC	avrainvillamide	-0.008035407	0.892353752	56169
GSDMC	axitinib	0.104952157	0.006953986	56169
GSDMC	azacitidine	-0.007496755	0.898886277	56169
GSDMC	bafilomycin A1	0.040834461	0.958140607	56169
GSDMC	barasertib	0.012210932	0.787681647	56169
GSDMC	bardoxolone methyl	-0.079373242	0.061838228	56169
GSDMC	belinostat	0.099471804	0.078822518	56169
GSDMC	bendamustine	0.042304797	0.347144328	56169
GSDMC	betulinic acid	-0.049004921	0.759237135	56169
GSDMC	bexarotene	-0.04822043	0.283644387	56169
GSDMC	birinapant	-0.054565546	0.395445273	56169
GSDMC	blebbistatin	-0.070586208	0.915382068	56169
GSDMC	bleomycin A2	-0.113267902	0.021308212	56169
GSDMC	bortezomib	0.034908337	0.412596081	56169
GSDMC	bosutinib	-0.08721423	0.033349567	56169
GSDMC	brefeldin A	0.053484139	0.247463816	56169
GSDMC	brivanib	0.00718054	0.876882633	56169
GSDMC	cabozantinib	0.011301101	0.855534764	56169
GSDMC	canertinib	-0.192271254	3.07963E-06	56169
GSDMC	cediranib	0.024015832	0.87690415	56169
GSDMC	ceranib-2	0.011337199	0.79291792	56169
GSDMC	cerulenin	0.041520527	0.308886366	56169
GSDMC	chlorambucil	0.100828972	0.01025271	56169
GSDMC	ciclopirox	0.027201633	0.496961192	56169
GSDMC	ciclosporin	-0.032140887	0.591179575	56169
GSDMC	cimetidine	0.051472043	0.972470539	56169
GSDMC	clofarabine	0.047415605	0.227086991	56169
GSDMC	crizotinib	0.052648225	0.197482414	56169
GSDMC	cucurbitacin I	0.088959425	0.030316018	56169
GSDMC	curcumin	-0.02878885	0.492343006	56169
GSDMC	cyanoquinoline 11	-0.129245252	0.099085344	56169
GSDMC	cyclophosphamide	-0.046927634	0.993392039	56169
GSDMC	cytarabine hydrochloride	0.027906797	0.489365145	56169
GSDMC	cytochalasin B	0.031188594	0.58445229	56169
GSDMC	dabrafenib	0.136103574	0.048376868	56169
GSDMC	dacarbazine	0.019192026	0.65397752	56169
GSDMC	daporinad	0.10809009	0.01347939	56169
GSDMC	darinaparsin	0.103065712	0.10257611	56169
GSDMC	dasatinib	-0.074953508	0.099983504	56169

GSDMC	decitabine	-0.032246668	0.422654732	56169
GSDMC	dexamethasone	-0.039935689	0.370040229	56169
GSDMC	dinaciclib	-0.041466107	0.493658005	56169
GSDMC	docetaxel	0.010090491	0.88690999	56169
GSDMC	doxorubicin	0.028253545	0.484182698	56169
GSDMC	elocalcitol	-0.036838571	0.369272061	56169
GSDMC	entinostat	0.056290584	0.160182731	56169
GSDMC	epigallocatechin-3-monogallate	0.111165362	0.010878216	56169
GSDMC	erastin	0.084874818	0.043896068	56169
GSDMC	erismodegib	-0.028745061	0.746196523	56169
GSDMC	erlotinib	-0.173902668	0.000013954	56169
GSDMC	etomoxir	0.017049146	0.979859873	56169
GSDMC	etoposide	0.061208327	0.11920263	56169
GSDMC	fingolimod	0.007103503	0.875943563	56169
GSDMC	fluorouracil	-0.117661468	0.002231263	56169
GSDMC	fluvastatin	0.096549239	0.044966138	56169
GSDMC	foretinib	0.037777783	0.412356801	56169
GSDMC	fulvestrant	0.067824176	0.867044974	56169
GSDMC	fumonisin B1	-0.00935205	0.91018506	56169
GSDMC	gefitinib	-0.154666995	0.000329544	56169
GSDMC	gemcitabine	0.063434792	0.124218157	56169
GSDMC	gossypol	0.027137116	0.535075009	56169
GSDMC	hyperforin	-0.027925271	0.78705785	56169
GSDMC	ibrutinib	-0.153726551	0.003045159	56169
GSDMC	ifosfamide	0.032976567	0.885551236	56169
GSDMC	imatinib	0.018911937	0.695174063	56169
GSDMC	importazole	-0.051628714	0.413417231	56169
GSDMC	indisulam	0.039059569	0.356302667	56169
GSDMC	isoevodiamine	-0.000959558	0.982260005	56169
GSDMC	isoliquiritigenin	0.045997122	0.629779816	56169
GSDMC	isonicotinohydroxamic acid	0.050724754	0.972370252	56169
GSDMC	istradefylline	-0.065135771	0.685640996	56169
GSDMC	itraconazole	0.019958795	0.817696296	56169
GSDMC	lapatinib	-0.214296557	9.36035E-08	56169
GSDMC	lenvatinib	0.073607081	0.097792498	56169
GSDMC	leptomycin B	-0.044048228	0.260676058	56169
GSDMC	linifanib	-0.103357576	0.007724279	56169
GSDMC	linsitinib	-0.05234017	0.242697912	56169
GSDMC	lomeguatrib	0.015576577	0.815291398	56169
GSDMC	lovastatin	0.064053357	0.199355401	56169
GSDMC	manumycin A	0.029188877	0.474487851	56169
GSDMC	marinopyrrole A	0.069223028	0.185230418	56169
GSDMC	masitinib	-0.020109369	0.6704016	56169
GSDMC	methotrexate	-0.008713144	0.852189705	56169
GSDMC	methylstat	0.070826999	0.154534254	56169
GSDMC	mitomycin	0.058650974	0.143116165	56169
GSDMC	momelotinib	-0.034275415	0.433570279	56169
GSDMC	myricetin	0.00628211	0.96430732	56169
GSDMC	myriocin	-0.061870631	0.89981088	56169
GSDMC	nakiterpiosin	0.044489604	0.273067175	56169
GSDMC	narciclasine	0.009684691	0.820437152	56169
GSDMC	navitoclax	0.079468526	0.060077818	56169
GSDMC	necrostatin-1	-0.004920836	0.934073733	56169
GSDMC	necrostatin-7	-0.050143947	0.286511261	56169
GSDMC	necrosulfonamide	0.073905166	0.128741871	56169
GSDMC	nelarabine	-0.041789068	0.864242265	56169
GSDMC	neopeltolide	0.083158622	0.393936253	56169
GSDMC	neratinib	-0.097388308	0.020579193	56169
GSDMC	neuronal differentiation inducer III	0.02335053	0.576091071	56169
GSDMC	niclosamide	0.007974362	0.881652667	56169
GSDMC	nilotinib	-0.009452292	0.936711176	56169
GSDMC	nintedanib	0.031715794	0.599261782	56169
GSDMC	nutlin-3	0.085232957	0.036112681	56169
GSDMC	obatoclax	0.069716563	0.077521744	56169
GSDMC	olaparib	0.04047067	0.344547341	56169
GSDMC	oligomycin A	0.071473098	0.078316962	56169
GSDMC	omacetaxine mepesuccinate	-0.03644051	0.45515117	56169

GSDMC	ouabain	0.059715706	0.128344931	56169
GSDMC	paclitaxel	-0.022923582	0.590959905	56169
GSDMC	palmostatin B	0.049561515	0.665302502	56169
GSDMC	pandacostat	-0.026833249	0.594877927	56169
GSDMC	panobinostat	0.060483888	0.120713954	56169
GSDMC	parbendazole	0.041826742	0.285828823	56169
GSDMC	parthenolide	-0.012575911	0.856646534	56169
GSDMC	pazopanib	0.015791351	0.725957036	56169
GSDMC	pevonedistat	0.043778361	0.299675962	56169
GSDMC	phloretin	-0.020159466	0.643748528	56169
GSDMC	pifithrin-alpha	0.064584288	0.264175413	56169
GSDMC	pifithrin-mu	0.088078848	0.027232797	56169
GSDMC	piperlongumine	0.08014719	0.037117115	56169
GSDMC	pitstop2	0.017602245	0.942640742	56169
GSDMC	pluripotin	0.004117851	0.951929702	56169
GSDMC	procarbazine	-0.021275409	0.928745069	56169
GSDMC	prochlorperazine	0.023967549	0.651219928	56169
GSDMC	purmorphamine	0.033278641	0.507402137	56169
GSDMC	pyrazolanthrone	-0.027757139	0.624457323	56169
GSDMC	quizartinib	0.003444112	0.96601243	56169
GSDMC	regorafenib	0.034535906	0.518950585	56169
GSDMC	rigosertib	0.056652063	0.162923989	56169
GSDMC	ruxolitinib	-0.008228173	0.872677145	56169
GSDMC	salermide	-0.054220915	0.578637828	56169
GSDMC	saracatinib	-0.123392529	0.003891712	56169
GSDMC	selumetinib	-0.056988986	0.253711298	56169
GSDMC	semagacestat	-0.002967723	0.991350965	56169
GSDMC	serdemetan	0.056936632	0.17208735	56169
GSDMC	sildenafil	-0.018045245	0.907914797	56169
GSDMC	silmitasertib	-0.085860366	0.265421248	56169
GSDMC	simvastatin	0.068447858	0.225657928	56169
GSDMC	sirolimus	-0.03831501	0.362553178	56169
GSDMC	sitagliptin	-0.033822855	0.997718377	56169
GSDMC	skepinone-L	-0.012537985	0.867237552	56169
GSDMC	sorafenib	0.069355492	0.111864693	56169
GSDMC	sotrastaurin	0.052939927	0.277493171	56169
GSDMC	spautin-1	-0.01524128	0.791863887	56169
GSDMC	staurosporine	0.060616213	0.667195847	56169
GSDMC	sunitinib	0.061922212	0.134408094	56169
GSDMC	tacedinaline	0.043777628	0.375939529	56169
GSDMC	tacrolimus	0.055691796	0.208751633	56169
GSDMC	tamatinib	-0.039336856	0.644225482	56169
GSDMC	tamoxifen	-0.045267738	0.507622723	56169
GSDMC	tandutinib	0.019224459	0.702971121	56169
GSDMC	tanespimycin	-0.08973143	0.07123696	56169
GSDMC	temozolomide	0.011293828	0.89451965	56169
GSDMC	temsirolimus	-0.045631823	0.504611911	56169
GSDMC	teniposide	0.030163006	0.610502691	56169
GSDMC	thalidomide	-0.018213801	0.947050952	56169
GSDMC	tigecycline	0.011247913	0.875930203	56169
GSDMC	tipifarnib-P1	-0.00904056	0.838269612	56169
GSDMC	tipifarnib-P2	0.040864856	0.501138099	56169
GSDMC	tivantinib	0.037989374	0.542955454	56169
GSDMC	tivozanib	0.006799045	0.913166918	56169
GSDMC	topotecan	0.058044735	0.137536831	56169
GSDMC	tosedostat	-0.022882721	0.635430144	56169
GSDMC	tozasertib	0.141640853	0.415579556	56169
GSDMC	trametinib	-0.001562615	0.989117423	56169
GSDMC	tretinoin	-0.043592605	0.318896226	56169
GSDMC	triazolothiadiazine	0.054106949	0.161960305	56169
GSDMC	trifluoperazine	-0.000924667	0.99053635	56169
GSDMC	triptolide	-0.027928171	0.508568147	56169
GSDMC	tubastatin A	0.034967261	0.612370174	56169
GSDMC	valdecoxib	0.029762946	0.489151968	56169
GSDMC	vandetanib	-0.123724745	0.006598264	56169
GSDMC	veliparib	0.023296593	0.805668224	56169
GSDMC	vemurafenib	0.045996269	0.428678058	56169

GSDMC	vincristine	0.063215967	0.095295943	56169
GSDMC	vorapaxar	0.014839906	0.79264722	56169
GSDMC	vorinostat	0.084652754	0.029910743	56169
GSDMC	zebularine	0.033531109	0.430794776	56169
GSDMD	16-beta-bromoandrosterone	0.041136615	0.418416217	79792
GSDMD	1S,3R-RSL-3	0.01753711	0.703376492	79792
GSDMD	3-Cl-AHPC	-0.03532026	0.394295918	79792
GSDMD	968	0.01014109	0.998628187	79792
GSDMD	A-804598	0.042401838	0.803842864	79792
GSDMD	AA-COCF3	0.015933361	0.734192039	79792
GSDMD	ABT-199	0.019697354	0.761922231	79792
GSDMD	ABT-737	-0.021623664	0.672225513	79792
GSDMD	AC55649	0.090532539	0.414458055	79792
GSDMD	AGK-2	-0.033129463	0.932065143	79792
GSDMD	AM-580	-0.046895605	0.385881198	79792
GSDMD	AT-406	-0.029718006	0.814108366	79792
GSDMD	AT13387	0.037351893	0.557630037	79792
GSDMD	AT7867	0.027340888	0.548972181	79792
GSDMD	AZ-3146	-0.055385694	0.201237875	79792
GSDMD	AZD1480	0.087655951	0.219249147	79792
GSDMD	AZD4547	0.052040185	0.28298588	79792
GSDMD	AZD6482	-0.034711397	0.581650378	79792
GSDMD	AZD7545	-0.034348271	0.461188683	79792
GSDMD	AZD7762	-0.156716977	0.000032243	79792
GSDMD	AZD8055	0.027295273	0.530295626	79792
GSDMD	B02	0.069410156	0.091874635	79792
GSDMD	BCL-LZH-4	-0.06107223	0.765849998	79792
GSDMD	BEC	0.039164197	0.999979174	79792
GSDMD	BI-2536	0.052494126	0.174390122	79792
GSDMD	BIBR-1532	0.068149983	0.138436765	79792
GSDMD	BIRB-796	-0.013342271	0.803139988	79792
GSDMD	BIX-01294	0.017119874	0.691565207	79792
GSDMD	BMS-195614	0.0985907	0.076952159	79792
GSDMD	BMS-270394	-0.002703332	0.965308374	79792
GSDMD	BMS-345541	-0.004823892	0.914734156	79792
GSDMD	BMS-536924	-0.083023166	0.095982223	79792
GSDMD	BMS-754807	0.080854169	0.06794324	79792
GSDMD	BRD-A02303741	0.024430475	0.690245037	79792
GSDMD	BRD-A05715709	-0.036621712	0.826825784	79792
GSDMD	BRD-A71883111	-0.034323255	0.468233965	79792
GSDMD	BRD-A86708339	0.060853997	0.332932068	79792
GSDMD	BRD-A94377914	-0.01731664	0.790307714	79792
GSDMD	BRD-K01737880	-0.034879326	0.893180928	79792
GSDMD	BRD-K02251932	-0.02344121	0.688496801	79792
GSDMD	BRD-K02492147	-0.008899163	0.905515415	79792
GSDMD	BRD-K04800985	-0.077861944	0.99880963	79792
GSDMD	BRD-K09344309	0.176508463	0.587180302	79792
GSDMD	BRD-K09587429	-0.012138306	0.879528067	79792
GSDMD	BRD-K11533227	0.018114585	0.715573426	79792
GSDMD	BRD-K13999467	-0.014273352	0.780427375	79792
GSDMD	BRD-K14844214	-0.069906062	0.287820706	79792
GSDMD	BRD-K16147474	-0.003234583	0.99541999	79792
GSDMD	BRD-K17060750	0.02250042	0.698757844	79792
GSDMD	BRD-K19103580	-0.007046673	0.910763492	79792
GSDMD	BRD-K24690302	0.031147238	0.506304211	79792
GSDMD	BRD-K26531177	-0.000296281	0.995383427	79792
GSDMD	BRD-K27224038	-0.066216104	0.807806238	79792
GSDMD	BRD-K27986637	-0.133541533	0.339943153	79792
GSDMD	BRD-K28456706	0.031264329	0.49374851	79792
GSDMD	BRD-K29086754	-0.136488303	0.416789147	79792
GSDMD	BRD-K29313308	-0.049503922	0.265647697	79792
GSDMD	BRD-K30019337	0.055836986	0.858690635	79792
GSDMD	BRD-K30748066	-0.198662293	0.252241628	79792
GSDMD	BRD-K33199242	-0.043187362	0.948158325	79792
GSDMD	BRD-K33514849	-0.275178061	0.999288401	79792
GSDMD	BRD-K34099515	0.135275592	0.827209842	79792
GSDMD	BRD-K34222889	0.016710287	0.692908151	79792

GSDMD	BRD-K34485477	0.06868971	0.998562234	79792
GSDMD	BRD-K35604418	0.058927008	0.148603987	79792
GSDMD	BRD-K37390332	-0.021475545	0.948798174	79792
GSDMD	BRD-K41334119	-0.062905297	0.920196991	79792
GSDMD	BRD-K41597374	-0.006023952	0.900115922	79792
GSDMD	BRD-K42260513	0.050760502	0.994633498	79792
GSDMD	BRD-K44224150	-0.095935207	0.96369476	79792
GSDMD	BRD-K45681478	0.004611655	0.934209826	79792
GSDMD	BRD-K48334597	-0.056721834	0.656634668	79792
GSDMD	BRD-K48477130	-0.165006843	0.366778942	79792
GSDMD	BRD-K49290616	-0.006210402	0.993657479	79792
GSDMD	BRD-K50799972	-0.111245918	0.068147074	79792
GSDMD	BRD-K51490254	0.121312082	0.003433975	79792
GSDMD	BRD-K51831558	0.068420925	0.341521968	79792
GSDMD	BRD-K52037352	-0.031074897	0.659279514	79792
GSDMD	BRD-K55116708	-0.125249011	0.003293979	79792
GSDMD	BRD-K61166597	-0.038132289	0.368180616	79792
GSDMD	BRD-K63431240	-0.133265105	0.001078107	79792
GSDMD	BRD-K64610608	0.071670507	0.501247721	79792
GSDMD	BRD-K66453893	-0.019950162	0.630659342	79792
GSDMD	BRD-K66532283	-0.047149427	0.262992109	79792
GSDMD	BRD-K70511574	-0.00770296	0.860632994	79792
GSDMD	BRD-K71781559	-0.002200153	0.999729774	79792
GSDMD	BRD-K75293299	0.04632255	0.874591617	79792
GSDMD	BRD-K78574327	0.061484078	0.97005555	79792
GSDMD	BRD-K80183349	0.004436616	0.92649022	79792
GSDMD	BRD-K84807411	-0.036581638	0.915299717	79792
GSDMD	BRD-K85133207	-0.00438439	0.934827242	79792
GSDMD	BRD-K86535717	0.000240798	0.999287713	79792
GSDMD	BRD-K88742110	0.002786155	0.955789743	79792
GSDMD	BRD-K90370028	0.065664715	0.871459419	79792
GSDMD	BRD-K92856060	0.039246366	0.377070877	79792
GSDMD	BRD-K96431673	0.025384209	0.996125153	79792
GSDMD	BRD-K96970199	-0.016958036	0.998763577	79792
GSDMD	BRD-K97651142	0.060960565	0.154085816	79792
GSDMD	BRD-K99006945	-0.121006259	0.081938972	79792
GSDMD	BRD-M00053801	0.123784736	0.140207967	79792
GSDMD	BRD1378	-0.029833642	0.812790169	79792
GSDMD	BRD1812	0.04632818	0.272104296	79792
GSDMD	BRD1835	-0.017707333	0.754182267	79792
GSDMD	BRD4132	0.087786844	0.138857672	79792
GSDMD	BRD5468	-0.058105302	0.47350437	79792
GSDMD	BRD6340	-0.016367677	0.710867429	79792
GSDMD	BRD8899	-0.031492227	0.792304307	79792
GSDMD	BRD8958	0.006064245	0.993130306	79792
GSDMD	BRD9647	-0.018356851	0.768353234	79792
GSDMD	BRD9876	0.1075442	0.057905166	79792
GSDMD	BYL-719	0.039975573	0.593211307	79792
GSDMD	Bax channel blocker	-0.017241833	0.738571899	79792
GSDMD	C6-ceramide	0.02409646	0.858710768	79792
GSDMD	CAL-101	-0.08342092	0.121050489	79792
GSDMD	CAY10576	0.031255697	0.69470264	79792
GSDMD	CAY10594	0.0018781	0.980054968	79792
GSDMD	CAY10618	0.04039761	0.34288821	79792
GSDMD	CBB-1007	-0.054314395	0.758051294	79792
GSDMD	CCT036477	-0.030951963	0.464465212	79792
GSDMD	CD-1530	-0.01575606	0.814125756	79792
GSDMD	CD-437	-0.038285908	0.349279734	79792
GSDMD	CHIR-99021	-0.150299125	0.000192569	79792
GSDMD	CHM-1	0.041917435	0.293165119	79792
GSDMD	CI-976	0.074779689	0.553821916	79792
GSDMD	CID-5951923	0.106132821	0.175016728	79792
GSDMD	CIL41	0.07978222	0.253040416	79792
GSDMD	CIL55	-0.003206018	0.993303299	79792
GSDMD	CIL55A	-0.03719114	0.575938955	79792
GSDMD	CIL56	-0.121294138	0.041195705	79792
GSDMD	CIL70	0.013469541	0.84844983	79792

GSDMD	COL-3	-0.069871085	0.136586783	79792
GSDMD	CR-1-31B	-0.024576783	0.538682464	79792
GSDMD	Ch-55	0.018817777	0.748321625	79792
GSDMD	Compound 1541A	-0.000813838	0.992966587	79792
GSDMD	Compound 23 citrate	-0.084294276	0.034189904	79792
GSDMD	Compound 7d-cis	0.019849907	0.684942578	79792
GSDMD	DBeQ	0.094508256	0.027419463	79792
GSDMD	DNMDP	-0.061198091	0.375722235	79792
GSDMD	ELCPK	0.077276718	0.21471265	79792
GSDMD	ETP-46464	0.026471538	0.668256366	79792
GSDMD	EX-527	0.17769282	0.021001008	79792
GSDMD	FGIN-1-27	0.062086906	0.650283494	79792
GSDMD	FQI-1	-0.046815365	0.433422018	79792
GSDMD	FQI-2	-0.026254513	0.525369364	79792
GSDMD	FSC231	0.073442148	0.999449861	79792
GSDMD	GANT-61	-0.040694095	0.516222051	79792
GSDMD	GDC-0879	-0.059926954	0.263228948	79792
GSDMD	GDC-0941	-0.066052	0.143022867	79792
GSDMD	GMX-1778	0.067129336	0.109287969	79792
GSDMD	GSK-3 inhibitor IX	-0.094378456	0.024666001	79792
GSDMD	GSK-J4	-0.128424207	0.4456683	79792
GSDMD	GSK1059615	0.055040615	0.839306845	79792
GSDMD	GSK2636771	0.015924437	0.902088487	79792
GSDMD	GSK4112	-0.043538042	0.398195517	79792
GSDMD	GSK461364	0.007237838	0.86613978	79792
GSDMD	GSK525762A	-0.070636013	0.06869914	79792
GSDMD	GW-405833	-0.037731814	0.356940965	79792
GSDMD	GW-843682X	0.003954389	0.937365954	79792
GSDMD	HBX-41108	0.055014644	0.343822832	79792
GSDMD	HC-067047	-0.013992674	0.857654417	79792
GSDMD	HLI 373	-0.017365983	0.714881424	79792
GSDMD	I-BET151	-0.056568555	0.145504484	79792
GSDMD	IC-87114	-0.161637852	0.00140618	79792
GSDMD	IPR-456	0.011477532	0.956219846	79792
GSDMD	ISOX	0.028665118	0.490116588	79792
GSDMD	IU1	0.027973776	0.790129916	79792
GSDMD	JQ-1	-0.022127066	0.595997978	79792
GSDMD	JW-480	-0.009415554	0.966580852	79792
GSDMD	JW-55	0.175795453	0.141550713	79792
GSDMD	JW-74	0.018838123	0.866491464	79792
GSDMD	KH-CB19	0.022936493	0.855558133	79792
GSDMD	KHS101	0.024751609	0.597149812	79792
GSDMD	KPT185	0.041953931	0.386998979	79792
GSDMD	KU 0060648	-0.078887711	0.054050644	79792
GSDMD	KU-0063794	0.021166278	0.637414463	79792
GSDMD	KU-55933	-0.076755954	0.075309257	79792
GSDMD	KU-60019	-0.042679866	0.305326783	79792
GSDMD	KW-2449	-0.016718953	0.695667677	79792
GSDMD	KX2-391	0.052252869	0.190383301	79792
GSDMD	Ki8751	0.043504772	0.35446434	79792
GSDMD	Ko-143	0.003596595	0.939306715	79792
GSDMD	L-685458	-0.01064762	0.894532173	79792
GSDMD	LE-135	-0.047239913	0.299456592	79792
GSDMD	LRRK2-IN-1	0.002462897	0.963334657	79792
GSDMD	LY-2157299	-0.077064293	0.744544251	79792
GSDMD	LY-2183240	0.020023652	0.625727531	79792
GSDMD	MG-132	0.179376459	0.016275876	79792
GSDMD	MGCD-265	-0.028177038	0.505555945	79792
GSDMD	MI-1	0.014924135	0.895007684	79792
GSDMD	MI-2	0.111821388	0.088984276	79792
GSDMD	MK-0752	0.008074927	0.932078433	79792
GSDMD	MK-1775	-0.056070973	0.16775239	79792
GSDMD	MK-2206	-0.002136279	0.969451502	79792
GSDMD	ML006	0.036007069	0.524393449	79792
GSDMD	ML029	0.028653633	0.558741959	79792
GSDMD	ML031	0.097714171	0.022816363	79792
GSDMD	ML050	0.054571817	0.216337391	79792

GSDMD	ML083	0.038124032	0.763040244	79792
GSDMD	ML162	0.062607397	0.14255229	79792
GSDMD	ML203	-0.002909823	0.966236352	79792
GSDMD	ML210	0.009264288	0.84612494	79792
GSDMD	ML239	0.073008668	0.087949158	79792
GSDMD	ML258	0.018222474	0.885851264	79792
GSDMD	ML311	-0.017137287	0.682879008	79792
GSDMD	ML312	-0.084711883	0.961818313	79792
GSDMD	ML320	-0.110493894	0.011552376	79792
GSDMD	ML334 diastereomer	0.052523283	0.476552229	79792
GSDMD	MLN2238	-0.040244146	0.332446683	79792
GSDMD	MLN2480	0.03834717	0.747603199	79792
GSDMD	MST-312	0.106055291	0.006081283	79792
GSDMD	Mdivi-1	-0.057781354	0.180607836	79792
GSDMD	Merck60	-0.025547515	0.537572819	79792
GSDMD	N9-isopropylolomoucine	-0.046265519	0.277681014	79792
GSDMD	NPC-26	-0.009711878	0.956684069	79792
GSDMD	NSC 74859	0.000382203	0.996382579	79792
GSDMD	NSC19630	-0.025027835	0.644549071	79792
GSDMD	NSC23766	-0.08393003	0.039719286	79792
GSDMD	NSC30930	0.018451329	0.836935791	79792
GSDMD	NSC48300	-0.017153906	0.691409262	79792
GSDMD	NSC632839	0.002931908	0.949072149	79792
GSDMD	NSC95397	-0.028358873	0.522661574	79792
GSDMD	NVP-231	-0.051783414	0.201373371	79792
GSDMD	NVP-ADW742	0.040483007	0.396534005	79792
GSDMD	NVP-BEZ235	0.05644693	0.280033278	79792
GSDMD	NVP-BSK805	-0.097849809	0.013807371	79792
GSDMD	NVP-TAE684	0.008775279	0.883083513	79792
GSDMD	O-6-benzylguanine	-0.057208386	0.662781702	79792
GSDMD	OSI-027	0.005853992	0.911975601	79792
GSDMD	OSI-930	-0.060388057	0.186193049	79792
GSDMD	PAC-1	0.018131241	0.680756901	79792
GSDMD	PD 153035	-0.039646218	0.536932957	79792
GSDMD	PD318088	-0.085455443	0.058211949	79792
GSDMD	PDMP	-0.022015388	0.646519659	79792
GSDMD	PF-184	-0.012877223	0.770901412	79792
GSDMD	PF-3758309	0.05363774	0.364988366	79792
GSDMD	PF-4800567 hydrochloride	-0.064373023	0.999586205	79792
GSDMD	PF-543	0.0027868	0.960453866	79792
GSDMD	PF-573228	-0.02077717	0.640859071	79792
GSDMD	PF-750	0.082735007	0.075822384	79792
GSDMD	PHA-793887	-0.038570032	0.332819059	79792
GSDMD	PI-103	0.076390286	0.066697796	79792
GSDMD	PIK-93	-0.049563264	0.253470497	79792
GSDMD	PL-DI	-0.040082423	0.324418702	79792
GSDMD	PLX-4720	-0.075571726	0.237715303	79792
GSDMD	PRIMA-1	-0.015044776	0.731098524	79792
GSDMD	PRIMA-1-Met	-0.031195859	0.697673871	79792
GSDMD	PRL-3 inhibitor I	0.053607551	0.663629454	79792
GSDMD	PX-12	-0.011509017	0.785429611	79792
GSDMD	PYR-41	0.053139653	0.322916659	79792
GSDMD	QS-11	-0.003056008	0.995295912	79792
GSDMD	QW-BI-011	0.014401641	0.898841974	79792
GSDMD	R428	-0.061778836	0.241576571	79792
GSDMD	RAF265	-0.080903613	0.130216042	79792
GSDMD	RG-108	0.052251367	0.262836915	79792
GSDMD	RITA	-0.091061591	0.027844605	79792
GSDMD	RO4929097	-0.02551462	0.767684035	79792
GSDMD	Repligen 136	-0.004905265	0.924202726	79792
GSDMD	SB-225002	0.047694727	0.224963394	79792
GSDMD	SB-431542	-0.064226501	0.475881069	79792
GSDMD	SB-525334	0.134855641	0.002999403	79792
GSDMD	SB-743921	0.026123214	0.517087637	79792
GSDMD	SCH-529074	0.11857199	0.007670483	79792
GSDMD	SCH-79797	0.045391155	0.268550817	79792
GSDMD	SGX-523	0.082008339	0.131816273	79792

GSDMD	SID 26681509	-0.042390663	0.382358042	79792
GSDMD	SJ-172550	-0.068963971	0.497221034	79792
GSDMD	SKI-II	0.032416955	0.509404315	79792
GSDMD	SMER-3	0.011205101	0.834326121	79792
GSDMD	SN-38	-0.053772258	0.248592248	79792
GSDMD	SNS-032	-0.047659599	0.268883268	79792
GSDMD	SNX-2112	-0.103428693	0.006065929	79792
GSDMD	SR-II-138A	-0.018491427	0.645014927	79792
GSDMD	SR1001	0.035838578	0.638984575	79792
GSDMD	SR8278	-0.090161203	0.802895656	79792
GSDMD	SRT-1720	-0.02570952	0.609156989	79792
GSDMD	STF-31	0.042334705	0.328906171	79792
GSDMD	SU11274	0.001854188	0.969705553	79792
GSDMD	SZ4TA2	0.100492353	0.318596242	79792
GSDMD	StemRegenin 1	-0.009969899	0.82906703	79792
GSDMD	TG-100-115	-0.018069723	0.773489979	79792
GSDMD	TG-101348	-0.130558863	0.000909668	79792
GSDMD	TGX-221	-0.087961872	0.153068998	79792
GSDMD	TPCA-1	-0.095846448	0.015366257	79792
GSDMD	TW-37	0.075992913	0.063033701	79792
GSDMD	UNC0321	-0.008155315	0.959265245	79792
GSDMD	UNC0638	0.015297057	0.75894044	79792
GSDMD	VAF-347	0.02987593	0.683080106	79792
GSDMD	VER-155008	-0.051729029	0.234387463	79792
GSDMD	VU0155056	-0.014556645	0.978654209	79792
GSDMD	WAY-362450	0.002826808	0.99852118	79792
GSDMD	WP1130	0.037724728	0.384024652	79792
GSDMD	WZ4002	-0.021010597	0.810966112	79792
GSDMD	WZ8040	-0.001193695	0.986975982	79792
GSDMD	XL765	0.050729056	0.391659331	79792
GSDMD	YK 4-279	0.001505751	0.973169441	79792
GSDMD	YM-155	0.087006769	0.062099883	79792
GSDMD	ZSTK474	0.015398107	0.810910622	79792
GSDMD	abiraterone	0.108567423	0.408596593	79792
GSDMD	afatinib	-0.094788867	0.036352377	79792
GSDMD	alisertib	0.022890697	0.594349632	79792
GSDMD	alvocidib	0.072725483	0.223703027	79792
GSDMD	apicidin	-0.001033933	0.981651169	79792
GSDMD	austocystin D	0.057549966	0.23188628	79792
GSDMD	avicin D	-0.030503104	0.778101585	79792
GSDMD	avrainvillamide	-0.011007173	0.850487867	79792
GSDMD	axitinib	0.058248562	0.149804365	79792
GSDMD	azacitidine	-0.033298527	0.516023627	79792
GSDMD	bafilomycin A1	-0.267356578	0.51907984	79792
GSDMD	barasertib	0.006555359	0.888043146	79792
GSDMD	bardoxolone methyl	-0.017609682	0.708340142	79792
GSDMD	belinostat	0.113115087	0.044261367	79792
GSDMD	bendamustine	0.014229582	0.771489925	79792
GSDMD	betulinic acid	0.002834931	0.992976756	79792
GSDMD	bexarotene	0.025542469	0.592444157	79792
GSDMD	birinapant	-0.179036613	0.000271755	79792
GSDMD	blebbistatin	-0.025854726	0.979397912	79792
GSDMD	bleomycin A2	-0.073886075	0.15907731	79792
GSDMD	bortezomib	-0.008169167	0.858948796	79792
GSDMD	bosutinib	-0.164706066	0.000032448	79792
GSDMD	brefeldin A	0.043816299	0.352935744	79792
GSDMD	brivanib	-0.013171496	0.774058445	79792
GSDMD	cabozantinib	0.016457856	0.781380841	79792
GSDMD	canertinib	-0.088825815	0.046657046	79792
GSDMD	cediranib	0.025394807	0.867096431	79792
GSDMD	ceranib-2	0.079748313	0.038706416	79792
GSDMD	cerulenin	0.027742556	0.507758272	79792
GSDMD	chlorambucil	-0.056069995	0.169624064	79792
GSDMD	ciclopirox	-0.011964986	0.770921443	79792
GSDMD	ciclosporin	-0.03520834	0.548780107	79792
GSDMD	cimetidine	0.041661353	0.977681146	79792
GSDMD	clofarabine	-0.108029465	0.004161596	79792

GSDMD	crizotinib	-0.054863476	0.177830512	79792
GSDMD	cucurbitacin I	0.042128887	0.335769793	79792
GSDMD	curcumin	-0.024415818	0.565042627	79792
GSDMD	cyanoquinoline 11	-0.028276831	0.78910952	79792
GSDMD	cyclophosphamide	-0.034764886	0.993392039	79792
GSDMD	cytarabine hydrochloride	-0.044980735	0.253981986	79792
GSDMD	cytochalasin B	0.032253432	0.570207753	79792
GSDMD	dabrafenib	-0.049883471	0.540370339	79792
GSDMD	dacarbazine	-0.111536067	0.004043326	79792
GSDMD	daporinad	0.095627079	0.030807409	79792
GSDMD	darinaparsin	0.009517025	0.907834245	79792
GSDMD	dasatinib	-0.17692875	0.000012916	79792
GSDMD	decitabine	-0.097026752	0.010732465	79792
GSDMD	dexamethasone	-0.06566771	0.125063932	79792
GSDMD	dinaciclib	0.078265	0.17785314	79792
GSDMD	docetaxel	-0.014386422	0.83764393	79792
GSDMD	doxorubicin	-0.007180981	0.866008297	79792
GSDMD	elocalcitol	-0.045575439	0.260708084	79792
GSDMD	entinostat	0.056859703	0.155776577	79792
GSDMD	epigallocatechin-3-monogallate	-0.054714266	0.245209111	79792
GSDMD	erastin	0.035922056	0.441511639	79792
GSDMD	erismodegib	0.088543012	0.190441053	79792
GSDMD	erlotinib	-0.10912794	0.009778351	79792
GSDMD	etomoxir	0.014459395	0.980957667	79792
GSDMD	etoposide	-0.018824458	0.652323354	79792
GSDMD	fingolimod	-0.05917168	0.146519012	79792
GSDMD	fluorouracil	-0.066122959	0.09428308	79792
GSDMD	fluvastatin	0.028907075	0.626842568	79792
GSDMD	foretinib	0.034642607	0.456774486	79792
GSDMD	fulvestrant	0.001123068	0.998907876	79792
GSDMD	fumonisin B1	-0.145908243	0.002251116	79792
GSDMD	gefitinib	-0.109122527	0.01624926	79792
GSDMD	gemcitabine	-0.026147014	0.546293699	79792
GSDMD	gossypol	0.102124353	0.011062118	79792
GSDMD	hyperforin	0.105102801	0.150259544	79792
GSDMD	ibrutinib	0.009895679	0.889357591	79792
GSDMD	ifosfamide	0.022811258	0.925013739	79792
GSDMD	imatinib	-0.094035161	0.024608251	79792
GSDMD	importazole	-0.01657479	0.826481121	79792
GSDMD	indisulam	0.016215487	0.716941942	79792
GSDMD	isoevodiamine	0.047190922	0.234594313	79792
GSDMD	isoliquiritigenin	0.020964366	0.833643421	79792
GSDMD	isonicotinohydroxamic acid	0.058642207	0.96369176	79792
GSDMD	istradefylline	0.034259823	0.858452592	79792
GSDMD	itraconazole	-0.005432093	0.957495544	79792
GSDMD	lapatinib	-0.056016465	0.225090717	79792
GSDMD	lenvatinib	0.058633309	0.201255083	79792
GSDMD	leptomycin B	-0.050755734	0.191362718	79792
GSDMD	linifanib	0.002421046	0.957072794	79792
GSDMD	linsitinib	0.059628135	0.178281076	79792
GSDMD	lomeguatrib	-0.029976165	0.621808624	79792
GSDMD	lovastatin	-0.026266708	0.653285203	79792
GSDMD	manumycin A	-0.058860805	0.134961402	79792
GSDMD	marinopyrrole A	0.097262612	0.056489898	79792
GSDMD	masitinib	0.00940636	0.848534383	79792
GSDMD	methotrexate	-0.038396293	0.37763418	79792
GSDMD	methylstat	-0.023687587	0.661871764	79792
GSDMD	mitomycin	0.053542481	0.18427459	79792
GSDMD	momelotinib	-0.073084883	0.078100389	79792
GSDMD	myricetin	0.077955669	0.451677634	79792
GSDMD	myriocin	0.065067085	0.895026002	79792
GSDMD	nakiterpiosin	0.006503616	0.88457452	79792
GSDMD	narciclasine	-0.059909179	0.130513497	79792
GSDMD	navitoclax	-0.014147321	0.778640235	79792
GSDMD	necrostatin-1	-0.048765868	0.317787657	79792
GSDMD	necrostatin-7	0.079303092	0.075163696	79792
GSDMD	necrosulfonamide	-0.006994716	0.898287687	79792

GSDMD	nelarabine	-0.007990443	0.987176714	79792
GSDMD	neopeltolide	0.002384875	0.985179188	79792
GSDMD	neratinib	-0.088011223	0.038175564	79792
GSDMD	neuronal differentiation inducer III	0.053234052	0.182661899	79792
GSDMD	niclosamide	0.136160004	0.00089372	79792
GSDMD	nilotinib	0.029114045	0.754349049	79792
GSDMD	nintedanib	-0.008970435	0.902753699	79792
GSDMD	nutlin-3	0.04341184	0.310890781	79792
GSDMD	obatoclax	0.013286253	0.763181689	79792
GSDMD	olaparib	0.044446136	0.295433815	79792
GSDMD	oligomycin A	0.110179385	0.005441281	79792
GSDMD	omacetaxine mepesuccinate	0.046043439	0.33774494	79792
GSDMD	ouabain	0.073971531	0.056683925	79792
GSDMD	paclitaxel	-0.004831057	0.915582102	79792
GSDMD	palmostatin B	-0.102332797	0.284417843	79792
GSDMD	pandacostat	-0.030409319	0.540580181	79792
GSDMD	panobinostat	0.060940906	0.117788543	79792
GSDMD	parbendazole	0.000919699	0.982718888	79792
GSDMD	parthenolide	0.135520669	0.00741766	79792
GSDMD	pazopanib	-0.003065705	0.948143214	79792
GSDMD	pevonedistat	-0.095587963	0.016898716	79792
GSDMD	phloretin	0.027607425	0.51842567	79792
GSDMD	pifithrin-alpha	0.006029281	0.944490256	79792
GSDMD	pifithrin-mu	-0.005196639	0.910693812	79792
GSDMD	piperlongumine	-0.033757136	0.401555953	79792
GSDMD	pitstop2	-0.022734206	0.927723793	79792
GSDMD	pluripotin	-0.101527121	0.024741691	79792
GSDMD	procarbazine	0.004099497	0.988670752	79792
GSDMD	prochlorperazine	0.002742635	0.96389292	79792
GSDMD	purmorphamine	0.021388495	0.682994372	79792
GSDMD	pyrazolanthrone	-0.086476595	0.063768634	79792
GSDMD	quizartinib	0.072993705	0.195700767	79792
GSDMD	regorafenib	0.059577043	0.231074966	79792
GSDMD	rigosertib	-0.002891406	0.950118986	79792
GSDMD	ruxolitinib	-0.098538638	0.016462956	79792
GSDMD	salermide	0.068150259	0.459529709	79792
GSDMD	saracatinib	-0.142257851	0.000710899	79792
GSDMD	selumetinib	-0.083963335	0.070913162	79792
GSDMD	semagacestat	-0.024388593	0.888711736	79792
GSDMD	serdemetan	0.029261243	0.502154852	79792
GSDMD	sildenafil	-0.013170712	0.940613911	79792
GSDMD	silmitasertib	0.000032481	0.999718736	79792
GSDMD	simvastatin	-0.025070194	0.710523699	79792
GSDMD	sirolimus	-0.021042348	0.631641417	79792
GSDMD	sitagliptin	0.008679813	0.997718377	79792
GSDMD	skepinone-L	0.047040692	0.481152355	79792
GSDMD	sorafenib	0.109229228	0.009695922	79792
GSDMD	sotrastaurin	-0.076235133	0.109244631	79792
GSDMD	spautin-1	-0.00399204	0.947352833	79792
GSDMD	staurosporine	-0.132175427	0.250672046	79792
GSDMD	sunitinib	-0.048440266	0.250515813	79792
GSDMD	tacedinaline	0.062159851	0.198197959	79792
GSDMD	tacrolimus	-0.002464647	0.96370435	79792
GSDMD	tamatinib	-0.058106112	0.456432774	79792
GSDMD	tamoxifen	0.042126216	0.542651053	79792
GSDMD	tandutinib	0.059189531	0.189813654	79792
GSDMD	tanespimycin	-0.018572134	0.76043492	79792
GSDMD	temozolomide	0.034949276	0.619087485	79792
GSDMD	temsirolimus	-0.057697601	0.382562609	79792
GSDMD	teniposide	-0.095817392	0.08195261	79792
GSDMD	thalidomide	-0.019749469	0.941978627	79792
GSDMD	tigecycline	-0.095696212	0.113913662	79792
GSDMD	tipifarnib-P1	0.040895014	0.323181474	79792
GSDMD	tipifarnib-P2	-0.11827503	0.031941102	79792
GSDMD	tivantinib	0.090556892	0.120864651	79792
GSDMD	tivozanib	-0.001122722	0.98694028	79792
GSDMD	topotecan	-0.029397328	0.471274607	79792

GSDMD	tosedostat	-0.062767878	0.151521332	79792
GSDMD	tozasertib	-0.073515987	0.701908148	79792
GSDMD	trametinib	-0.095201121	0.196077153	79792
GSDMD	tretinoin	-0.041167621	0.348590455	79792
GSDMD	triazolothiadiazine	-0.003325779	0.938779373	79792
GSDMD	trifluoperazine	-0.033421452	0.557591745	79792
GSDMD	triptolide	-0.072202381	0.071398175	79792
GSDMD	tubastatin A	0.015084689	0.838163307	79792
GSDMD	valdecoxib	0.026148588	0.546630233	79792
GSDMD	vandetanib	-0.071154619	0.150262668	79792
GSDMD	veliparib	-0.057128494	0.446611379	79792
GSDMD	vemurafenib	-0.001787195	0.983421733	79792
GSDMD	vincristine	0.043165703	0.263919995	79792
GSDMD	vorapaxar	0.003208917	0.958468537	79792
GSDMD	vorinostat	0.035503335	0.384134251	79792
GSDMD	zebularine	-0.036422481	0.390060342	79792

Experimed 2023; 13(3): 257-262

RESEARCH ARTICLE

DOI: 10.26650/experimed.1374959

Quantitative Measurement of HER2/neu Oncogene Amplification and p53 Tumor Suppressor Gene Deletion by RT-PCR in Breast Cancer*

Gozde Ulfer[1]

[1]Department of Biochemistry, Faculty of Medicine, Istanbul Medipol University, Istanbul, Turkiye

ORCID ID: G.U. 0000-0003-2350-6381

Cite this article as: Ulfer G. Quantitative measurement of HER2/neu oncogene amplification and p53 tumor suppressor gene deletion by RT-PCR in breast cancer. Experimed. Experimed 2023; 13(3): 257-262.

ABSTRACT

Objective: The aim of the study was to quantitatively evaluate HER2/neu oncogene amplification and p53 tumor suppressor gene deletion in breast cancer with real-time polymerase chain reaction (RT-PCR).

Materials and Methods: Sections obtained from the tumor tissues of 50 patients were paraffinized on slides, and DNA extraction was performed. HER2/neu amplification and p53 deletion were analyzed using RT-PCR with respect to immunohistochemistry (IHC).

Results: For 25 patients with breast cancer, we compared IHC and RT-PCR results for the quantitative measurement of HER2/neu expression. We found a significant correlation between the results obtained using IHC and RT-PCR ($p < 0.05$). Taking the results of IHC as reference, the sensitivity and specificity of the RT-PCR method were 57% and 83%, respectively. HER2/neu amplification and p53 deletion did not have a significant correlation with tumor size, histological grade, lymph node invasion, and status of estrogen receptor and progesterone receptor ($p>0.05$, for all).

Conclusion: RT-PCR measured gene levels reliably and accurately with high sensitivity and specificity, making it superior to IHC, which is subjective.

Keywords: Breast cancer, p53, HER2/neu, RT-PCR

INTRODUCTION

Breast cancer is the most common malignant disease in women (1). Breast cancer has the second highest mortality rate, following lung cancer, in women, and therefore, is frequently researched (2). The HER2/neu protooncogene has key functions in regulating normal cell growth under physiological conditions, with oncogenic amplification in 25%–30% of the patients with breast cancer. Patients with this oncogene amplification have frequent relapses of cancer, a shorter life expectancy, and resistance to existing treatments, all indicating a poor prognosis. Clinicians have used anti-HER therapy to target this oncogene, modifying therapy protocols (3). p53 gene mutation has been reported in 30%–50% of breast cancer cases. p53 is a tumor suppressor gene and is called the protector of genomes. Normal functions of p53 include regulation of cell growth, gene transcription, DNA repair, and genomic stability. The presence of p53 mutations is critical to tumor growth, prognosis, and treatment response. Any alterations in the p53 gene and amplification of the HER2/neu oncogene jointly affect the pathogenesis of invasive ductal breast cancer (4). Therefore, researchers have investigated the co-existence of HER2/neu and p53 mutations in breast cancer, with controversial results (5, 6). The presence of both HER2/neu amplification and p53 tumor suppressor gene mutation is prognostically crucial for breast cancer. Researchers have detected a poor prognosis in patients with HER2/neu amplification and p53 mutations. However, the

*The current study is part of a specilization in medicine thesis entitled "Quantitative Measurement of HER2/neu Oncogene Amplification and p53 Tumor Suppressor Gene Deletion by RT-PCR in Patients with Breast Cancer and Their Comparison with Prognostic Factors" by Gözde Ülfer.

Corresponding Author: Gozde Ulfer **E-mail:** gozde.ulfer@medipol.com.tr
Submitted: 16.10.2023 **Revision Requested:** 12.11.2023 **Last Revision Received:** 28.11.2023 **Accepted:** 29.11.2023

results concerning histopathological prognostic factors, such as lymph node status and tumor size, remain unclear. In this study, we aimed to compare immunohistochemistry (IHC) and real-time polymerase chain reaction (RT-PCR) RT-PCR results for the quantitative measurement of HER2/neu amplification in patients with breast cancer. Moreover, we aimed to examine the presence of a relationship between patients with p53 deletion and patients with HER2/neu amplification by quantitatively measuring the gene copy number with RT-PCR. We also examined the correlation between RT-PCR analysis of HER2/neu amplification, as well as p53 gene deletion, and histopathological prognostic factors in these patients.

MATERIALS AND METHODS

Patient Samples

This retrospective study was conducted with 50 patients, of which 46 had invasive breast cancer and 4 had benign breast disease. The histological type, grade, and size of the tumor; presence of lymph node invasion; and status of estrogen receptor (ER) and progesterone receptor (PR) were known for all patients, as assessed by IHC. Results for HER2/neu quantification by IHC were available for 25 patients. IHC is based on the principle of revealing specific proteins in tissues and cells using monoclonal and polyclonal antibodies. The cellular localization of the target protein is examined under light microscopy. Tumor tissues sections (10-µm thick and 50–100 mg in weight) were obtained, paraffinized on slides, and stored in a refrigerator at +4°C until DNA isolation was performed using High Pure PCR Template Preparation Kit (Roche Diagnostics Systems).

RT-PCR Analysis

RT-PCR provides quantitative results in a short time by measuring the fluorescence signal, which increases simultaneously with nucleic acid amplification. Mutations in the target nucleic acid can be detected using fluorescence probes (7). HER2/neu was quantified using DNA isolated from tumor tissues using a LightCycler (LC) RT-PCR device from Roche Diagnostics Systems. The LC HER2/neu DNA Quantification Kit was used for the quantitative measurement of HER2/neu. The results of the samples run in the LC PCR program were exported to the quantification software. The ratio of HER2/neu copy number targeted for each sample to the reference gene copy number was calculated. HER2/neu amplification was considered negative or positive if this ratio was <2 or ≥2, respectively. DNA samples from the same patients were quantified with RT-PCR on the LC device to detect p53 deletion. Using the appropriate PCR program, a standard calibration curve was generated using DNA obtained from the blood of a healthy individual. Then, p53 was detected in the DNA sample of each patient. The PCR program provided the gene copy number and the insulin like growth factor 1 (IGF1) gene copy number, which served as the reference gene. These values were entered into the loss of heterozygosity (LOH) formula, as follows:

$$LOH = 2X \frac{n_T^{p53} / n_T^{IGF\text{-}1} - 1}{nNp53 / nNIGF - 1}$$

n_T^{p53} = p53 gene copy number in tumor tissue

$n_T^{IGF\text{-}1}$ = IGF-1 gene copy number in tumor tissue

nNp53 = p53 gene copy number in control blood

nNIGF -1 = IGF-1 gene copy number in control blood

The LOH values were interpreted as follows:

LOH = 1 → No difference between the tumor tissue and healthy control in terms of allelic status

0 < LOH < 1 → Deletion in one p53 allele or IGF1 amplification

LOH > 1 → Amplification of one p53 allele or presence of one IGF-1 deletion

Statistical Analyses

Statistical analyses were performed using SPSS 13.0 software. The correlation between the results yielded by IHC and RT-PCR for the quantification of HER2/neu in 25 patients with breast cancer was evaluated by the chi-square test. The sensitivity and specificity of RT-PCR were calculated with reference to IHC. The correlation between HER2/neu positivity and p53 gene deletion was investigated by the chi-square test. Tumor grade and size, presence of lymph node invasion, and ER and PR results assessed by IHC were known for 46 patients with invasive ductal breast cancer. The Mann–Whitney U test was

Table 1. Comparison of the RT-PCR and IHC methods.

		RT-PCR HER2/neu oncogene						p
		Positive		Negative		Total		
		n	%	n	%	n	%	
IHC HER2/neu oncogene	Positive	4	57.1	3	16.7	7	28.0	0.043*
	Negative	3	42.9	15	83.3	18	72.0	
	Total	7	100.0	18	100.0	25	100.0	

RT-PCR: Real-time polymerase chain reaction, IHC: Immunohistochemistry; *p < 0.05

used to compare quantitative data for HER2/neu amplification and p53 deletion, according to prognostic factors. The chi-square test and Fisher's exact chi-square test were used for the comparison of qualitative data. The results were assessed at 95% confidence interval and $p < 0.05$ significance level.

RESULTS

The ratio of HER2/neu measured quantitatively by RT-PCR to the reference gene ranged between 0.31 and 24.3 (average = 2.76 ± 4.29). According to RT-PCR analysis, 24% of the

Table 2. Correlation between HER2/neu oncogene amplification and p53 gene deletion.

		HER2/neu oncogene						p
		Positive		Negative		Total		
		n	%	n	%	n	%	
p53	Positive	6	50.0	14	40.0	20	42.6	0.545
	Negative	6	50.0	21	60.0	27	57.4	
	Total	12	100.0	35	100.0	47	100.0	

Table 3. Correlation between HER2/neu oncogene amplification and prognostic factors.

Prognostic factors		HER2/neu oncogene						p
		Positive		Negative		Total		
		n	%	n	%	n	%	
Grade	2	8	66.7	24	70.6	32	69.6	0.800
	3	4	33.3	10	29.4	14	30.4	
Lymph node	Positive	10	83.3	29	85.3	39	84.8	0.871
	Negative	2	16.7	5	14.7	7	15.2	
ER	–	3	25.0	7	20.6	10	21.7	0.804
	+	-	-	2	5.9	2	4.3	
	++	4	33.3	9	26.5	13	28.3	
	+++	5	41.7	16	47.1	21	45.7	
ER	Positive	9	75.0	27	79.4	36	78.3	0.750
	Negative	3	25.0	7	20.6	10	21.7	
PR	–	2	16.7	6	17.6	8	17.4	0.804
	+	4	33.3	5	14.7	9	19.6	
	++	1	8.3	11	32.4	12	26.1	
	+++	5	41.7	12	35.3	17	37.0	
PR	Positive	10	83.3	28	82.4	38	82.6	0.939
	Negative	2	16.7	6	17.6	8	17.4	
Tumor size	≥2 cm	5	41.7	19	55.9	24	52.2	0.939
	<2 cm	7	58.3	15	44.1	22	47.8	
Tumor size (Mean ± SD)		1.93 ± 0.73		2.72 ± 2.04		2.52 ± 1.82		0.373

ER, estrogen receptor; PR, progesterone receptor

Table 4. Correlation between the presence of p53 gene deletion and prognostic factors.

Prognostic factors		p53						p
		Positive		Normal		Total		
		n	%	n	%	n	%	
Grade	**2**	11	55.0	18	78.3	29	67.4	0.104
	3	9	45.0	5	21.7	14	32.6	
Lymph node	**Positive**	18	90.0	18	78.3	36	83.7	0.420
	Negative	2	10.0	5	21.7	7	16.3	
ER	**–**	4	20.0	6	26.1	10	23.3	0.232
	+	1	5.0	1	4.3	2	4.7	
	++	8	40.0	3	13.0	11	25.6	
	+++	7	35.0	13	56.5	20	46.5	
ER	**Positive**	16	80.0	17	73.9	33	76.7	0.637
	Negative	4	20.0	6	26.1	10	23.3	
PR	**–**	3	15.0	5	21.7	8	18.6	0.613
	+	5	25.0	4	17.4	9	20.9	
	++	6	30.0	4	17.4	10	23.3	
	+++	6	30.0	10	43.5	16	37.2	
PR	**Positive**	17	85.0	18	78.3	35	81.4	0.704
	Negative	3	15.0	5	21.7	8	18.6	
Tumor size, cm	**≥2 cm**	13	65.0	10	43.5	23	53.5	0.158
	<2 cm	7	35.0	13	56.5	20	46.5	
Tumor size, cm (Mean ± SD)		2.21 ± 0.70		2.85 ± 2.46		2.52 ± 1.82		0.616

ER, estrogen receptor; PR, progesterone receptor

cases were positive and 76% were negative for HER2/neu amplification. The LOH values calculated for the detection of p53 gene deletion by RT-PCR varied between 0.01 and 9.0, (average = 2.07 ± 2.60). For the p53 deletion, 43% of the cases were positive and 57% were negative. A statistically significant correlation was found between the HER2/neu results obtained using RT-PCR and IHC ($p < 0.05$). In addition, 4/7 HER2-positive cases detected by RT-PCR tested positive with IHC, whereas 15/18 HER2-negative cases tested by RT-PCR tested negative with IHC. When evaluated with respect to IHC, RT-PCR had a sensitivity of 57.1% and specificity of 83.3% (Table 1).

Chi-square test analysis showed no significant correlation between the HER2/neu results for 46 patients with invasive ductal breast cancer and 4 patients with benign breast disease by RT-PCR and the results for p53 quantified using RT-PCR ($p = 0.545$; Table 2).

No statistically significant correlation was found between HER2/neu amplification and tumor grade, lymph node invasion, status of ER and PR, or tumor size ($p > 0.05$ for all; Table 3).

No statistically significant correlation was found between the presence of p53 deletion and tumor grade, lymph node invasion, status of ER and PR, or tumor size ($p > 0.05$ for all; Table 4).

DISCUSSION

In breast cancer, neoplastic transformation and tumor growth occur through multistep, complex genetic alterations. Oncogenic activation and inactivation of tumor suppressor genes result in cancer development. HER2/neu amplification and p53 mutations play an important role in the development of invasive ductal breast cancer (8). Alterations in these two genes are not only crucial for tumorigenesis, but also have prognostic significance. RT-PCR is a quantitative method that

provides rapid results by measuring fluorescence signals that increase with nucleic acid amplification (9). Gene level measurements provide insights into cancer development, progression, and response or resistance to treatment or tumor behavior (10).

Königshoff et al. (4) quantitatively measured HER2/neu in DNA samples from breast tumor tissues with RT-PCR and compared the results obtained with IHC. The authors detected a good correlation between the results obtained with these two methods ($p = 0.029$). Murad et al. (11) reported that the concordance rate between IHC and RT-PCR was 79.3%. In our study, DNA isolation was performed on paraffinized tumor tissues of patients with breast cancer, and the quantitative measurement of HER2/neu amplification was performed using RT-PCR, which is the most commonly used method for measurement. We found a statistically significant correlation between the results obtained by RT-PCR and IHC ($p = 0.043$). Studies have reported that HER2/neu is present in 25%–30% of the patients with breast cancer, who experienced frequent relapse and had a shorter life expectancy (12, 13). In our study, HER2/neu was detected in 24% of the patients with breast cancer by RT-PCR. In a study investigating the correlation between HER2/neu and other prognostic factors, Borg et al. (14) reported a negative correlation between HER2/neu positivity and steroid receptors. The authors noted that HER2/neu amplification was accompanied by a high histological grade; however, the correlation of HER2/neu amplification with lymph node status and tumor size was unclear. In our study, we did not observe any significant correlation between HER2/neu amplification with tumor size, histological grade, lymph node invasion, ER status, or PR status ($p > 0.05$). Consistent with our findings, tumor size and lymph node status are not associated with HER2/neu amplification (15). Although HER2/neu amplification is expected to be associated with high histological grade, the retrospective study yielded no statistically significant result, probably because most of the randomly selected cases were grade 2. Although a negative correlation was reported between HER2/neu amplification and steroid receptors (15), we detected no such correlation in our study, because many of our patients were positive for ER and PR.

Gentile et al. (16) detected LOH in p53 deletion in 43% of the patients with breast cancer. In our study, LOH in p53 gene deletion was calculated using RT-PCR, and p53 gene deletion was detected in 43% of the patients with breast cancer. Dimitrakakis et al. (6) reported a correlation between p53 gene expression and the presence of the HER2/neu oncogene ($p = 0.005$). Fedorava et al. (17) reported an indirect association of p53 gene deletion and HER2/neu expression. Tsutsui et al. (5) determined that the p53 protein and the HER2/neu oncogene were independent prognostic factors. In this study, there was no significant correlation between HER2/neu amplification quantified using RT-PCR and p53 gene deletion ($p = 0.545$).

High-grade tumors, ER negativity, and PR negativity are common in the presence of changes in p53 gene (18, 19). Our study lacked a significant relationship probably because most of our randomly selected patients had grade 2 tumors and many had ER and PR positivity.

Sadia et al. (20) determined an abnormal gene expression of p53 in all grades of breast tumors, but no significant difference in the down-regulation or up-regulation of p53 across different grades of breast tumor ($p > 0.05$). Similarly, we detected no significant correlation between p53 gene deletion and histological grade ($p > 0.05$).

In conclusion, RT-PCR can be successfully used for quantifying gene expression due to its high sensitivity and specificity. In this study, we quantified HER2/neu amplification and p53 deletion using RT-PCR. With respect to IHC, RT-PCR had a sensitivity of 57% and specificity of 83%. Therefore, it can be confidently used to replace IHC, which is a subjective method. Although HER2/neu amplification and p53 deletion play a joint role in the pathogenesis of breast cancer, the results of our study suggest that they are two independent prognostic factors.

This study was presented as a poster at the 19th National Biochemistry Congress held in Antalya, Turkey, in 2005, and as an oral presentation at the 2nd International Cancer and Ion Channels Congress held in Izmir, Turkey, on September 22–24, 2019.

Acknowledgements: I would like to thank my deceased thesis advisor, Professor Yavuz Taga.

Ethics Committee Approval: Approval was received for this study from Marmara University Ethics Committee (MAR-YÇ -2005-0011).

Informed Consent: Informed consent from patients was obtained.

Peer-review: Externally peer-reviewed.

Financial Disclosure: The author declare that this study has received no financial support.

REFERENCES

1. Ferlay J, Colombet M, Soerjomataram I, Parkin DM, Piñeros M, Znaor A, et al. Cancer statistics for the year 2020: an overview. Int J Cancer 2021; 149: 778–9.
2. Yedjou CG, Sims JN, Miele L, Noubissi F, Lowe L, Fonseca DD, et al. Health and racial disparity in breast cancer. Adv Exp Med Biol 2019; 1152: 31–49.
3. Tanani ME, Al Khatib AO, Al-Najjar BO , Shakya AK, El-Tanani Y , Lee YF et al. Cellular and molecular basis of therapeutic approaches to breast cancer. Cellular Signalling 2023; 101: 1-12.
4. Königshoff M, Wilhelm J, Bohle RM, Pingoud A, Hahn M. Her-2/neu Gene copy number quantified by real-time PCR: comparison of gene amplification, heterozigoty, and immunohistochemical status in breast cancer tissue. Clin Chem 2003; 49: 219-9.
5. Tsutsui S, Ohno S, Murakami S, Kataoka A, Kinoshita J, Hachitanda Y. Prognostic significance of the coexpression of p53 protein and c-erbB2 in breast cancer. Am J Surg 2003; 185: 165-7.
6. Dimitrakakis C, Konstadoulakis M, Messaris E, Kymionis G, Karayannis M, Panoussopoulos D, et al. Molecular markers in breast cancer: Can we use c-erbB-2, p53, bcl-2 and bax gene expression as prognostic factors? Breast 2002; 11: 279-5.

7. KKaltenboeck B, Wang C. Advances in real-time PCR: application to clinical laboratory diagnostics. Adv Clin Chem 2005; 40: 219–59.
8. Behl T, Kumar A, Vishakha, Sehgal A , Singh S , Sharma N , et al. Understanding the mechanistic pathways and clinical aspects associated with protein and gene based biomarkers in breast cancer. Int J Biol Macromol 2023; 253(Pt 1): 126595.
9. Mocellin S, Rossi CR, Pilati P, Nitti D, Marincola FM. Quantitative real-time PCR: a powerful ally in cancer research. Trends Mol Med 2003; 9: 189-5.
10. Viani GA, Afonso SL, Stefano EJ, De Fendi LI, Soares FV. Adjuvant trastuzumab in the treatment of her-2-positive early breast cancer: a metaanalysis of published randomized trials. BMC Cancer 2007; 7: 153.
11. Murad NA, Razak ZA, Hussain RM, Hussain SA, Huat CK, Ali SA, et al. Quantification of Her-2/Neu gene in breast cancer patients using real time-polymerase chain reaction (Q-PCR) and correlation with immunohistochemistry findings. Asian Pacific J Cancer Prev 2013; 14: 1655-59.
12. Slamon DJ, Clark GM, Wong SG, Levin WJ, Ulrich A, McGuire WL. Human breast cancer: correlation of relapse and survival with amplification of the HER-2/neu onkogene. Science 1987; 235: 177-2.
13. Slamon DJ, Godolphin W, Jones LA, Holt JA, Wong SG, Keith DE, et al. Studies of the HER-2/neu proto-onkogene in human breast and overian cancer. Science 1989; 244: 707-2.
14. Borg A, Baldetotp B, Fernö M, Killander D, Olsson H, Ryden S, et al. ERBB2 amplification is associated with tamoxifen resistance in steroid –receptor positive breast cancer. Cancer Lett 1994; 81: 137-4.
15. Battifora H, Gaffey M, Estaban J, Mehta P, Biley A, Faucett C, et al. Immunohistochemical assay of neu/ cerb2 onkogene product in parafin-embedded tissues in early breast cancer: retrospective follow-up study of 245 stage I and II cases. Modern Pathol 1991; 4: 466-4.
16. Gentile M, Jungestrom MB, Olsen KE, Soderkvist P. p53 and survival in early onset breast cancer: analysis of gene mutations, loss of heterozygosity and protein Accumulation. Eur J Cancer 1999; 35: 1202-07.
17. Fedorova O, Daks A , Shuvalov O, Kizenko A , Petukhov A, Gnennaya Y, et al.Attenuation of p53 mutant as an approach for treatment Her2-positive cancer. Cell Death Discovery 2020; 6: 100-8.
18. Sangrajrang S, Arpornwirat W, Cheirsilpa A, Thisuphakorn P, Kalalak A, Sornprom A, et al. Serum p53 antibodies in correlation to other biological parameters of breast cancer. Cancer Detec Prev 2003; 27: 182–6.
19. Keohavonga P, Gaoa W, Mady HH, Kanbour-Shakirb A, Melhemb MF. Analysis of p53 mutations in cells taken from paraffin-embedded tissue sections of ductal carcinoma in situ and atypical ductal hyperplasia of the breast. Cancer Lett 2004; 212: 121–30.
20. Sadia H, Bhinder MA, Irshad A, Zahid B, Ahmed R, Ashiq S, et al. Determination of expression profile of p53 gene in different grades of breast cancer tissues by real time PCR. Afr Health Sci 2020; 20: 1273-82.

Experimed 2023; 13(3): 263-275

ORIGINAL ARTICLE

DOI: 10.26650/experimed.1380210

Copy Number Variations in a Turkish Cohort of Children with Intellectual Disability*

Deniz Sunnetci-Akkoyunlu[1], Bulent Kara[2], Naci Cine[1], Seda Eren-Keskin[1], Buket Dogruoglu[1], Zeynep Ilkay[1], Tolgahan Ozer[1], Hakan Savli[1]

[1]Department of Medical Genetics, Faculty of Medicine, Kocaeli University, Kocaeli, Turkiye
[2]Department of Child Health and Diseases, Pediatric Neurology, Faculty of Medicine, Kocaeli University, Kocaeli, Turkiye

ORCID ID: D.S.A. 0000-0001-9297-8222; B.K. 0000-0003-3780-6596; N.C. 0000-0001-9063-1073; S.E.K. 0000-0002-8315-646X; B.D. 0000-0002-1138-7680; Z.I. 0000-0001-7256-6992; T.O. 0000-0001-5427-3811; H. S. 0000-0003-2836-9881

Cite this article as: Sunnetci-Akkoyunlu D, Kara B, Cine N, Eren-Keskin S, Dogruoglu B, Ilkay Z, Ozer T, Savli H. Copy number variations in a Turkish cohort of children with intellectual disability. Experimed. Experimed 2023; 13(3): 263-275.

ABSTRACT

Objective: Intellectual disability (ID) is a complex, variable, and clinically heterogeneous neurodevelopmental disorder that affects 1% – 3% of the global population. Copy number variations (CNVs) contribute to approximately 15%–20% of ID cases. Array comparative genomic hybridization (aCGH) is the first-line test for diagnosing patients with ID with/without multiple congenital anomalies (MCAs). This study aimed to present CNVs identified in a retrospective aCGH cohort of Turkish patients with ID with/without other medical conditions.

Materials and Methods: The study population consisted of 210 patients (139 male, 71 female) aged 2–18 years. aCGH analysis was performed using oligo and bacterial artificial chromosome (BAC)-based microarray platforms. CNVs were interpreted using public databases and literature mining and categorized according to international guidelines.

Results: Forty-five CNVs were detected in 38 (18%) patients. Among these CNVs, 21 (46.6%) were pathogenic, 4 (8.8%) were likely pathogenic, and 8 (17.7%) were variants of uncertain clinical significance (VUS). Nineteen CNVs corresponded to rare microdeletion/microduplication syndromes.

Conclusions: This study reports rare CNVs or syndromes among Turkish patients with ID with/without other medical conditions. Data revealed an overall diagnostic rate of 11.43%, which confirms aCGH as the first-line technology allowing geneticists to diagnose complex phenotypes, identify candidate genes involved in ID, and explore novel CNV effects.

Keywords: Intellectual disability, copy number variation, Turkish cohort, array CGH, deletion, duplication

INTRODUCTION

The Diagnostic and Statistical Manual of Mental Disorders, fifth edition (DSM-5), describes intellectual disability (ID) as a neurodevelopmental disorder that is complex, variable, and clinically heterogeneous (1). Approximately 1%–3% of the global population has ID (2) with or without multiple congenital anomalies (MCAs) (3). Environmental factors and genetics play a role in ID etiology (4). Genetic causes include copy number variations (CNVs), chromosomal aberrations, and single gene mutations (5).

Current analyses have indicated that submicroscopic CNVs contribute to approximately 15%–20% of ID cases (3). Conventional karyotyping has a resolution of 5–10 Mb and detects chromosomal aberrations in 5% of individuals with ID (except clinically recognizable chromosomal syndromes such as Down syndrome). Array comparative genomic hybridization (aCGH) enables identifying CNVs responsible for ID, with a commonly reported average diagnosis rate of 15%–20% (6). aCGH is still accepted as a first-line test for diagnosing patients with ID, global developmental delay,

*The current study is part of a master's thesis entitled "Detection of deletions and duplications that cause mental retardation by whole genome microarray method" by Deniz Sunnetci- Akkoyunlu.

Corresponding Author: Deniz Sunnetci-Akkoyunlu **E-mail:** deniz.sunnetci@kocaeli.edu.tr
Submitted: 24.10.2023 **Revision Requested:** 09.11.2023 **Last Revision Received:** 13.11.2023 **Accepted:** 27.11.2023

Table 1. Summary of clinical and molecular features of patients with CNVs.

Case	Sex	Age (year)	Clinical Features	Karyotyping	FISH	aCGH result	Size (Mb)	Number of affected coding genes	OMIM morbid genes/associated syndromes	Classification
1	F	14	Specific learning disability, ID, nasal speech, tubular nose, thin and long fingers, and cardiac anomaly			arr[GRCh37] 21q22.3(47,316,377_ 48,075,565)x1	0.759	13	*PCNT, COL6A2, COL6A1, LSS, FTCD*	Pathogenic
2	F	11	ID, epilepsy, and dysmorphic face			arr[GRCh37] Xq26.2(130,675,805 _130,963,121)x3	0.287	2	*IGSF1*	VUS
3	M	8	ID, epilepsy, and dysmorphic face			arr[GRCh37] Xp22.33 (113,071_ 2,709,818)x2	2.596	16	*CSF2RA, SHOX*	VUS
						arr[GRCh37] Xq28 (154,560,225_ 155,223,860)x2	0.663	8	*TMLHE, CLIC2*	VUS
4	M	11	ID, microcephaly, and dysmorphic face			arr[GRCh37] Xp22.31 (6,554,861_ 7,932,908)x2	1.328	4	*STS*	VUS
5	F	13	ID, behavioral problems, Simian crease on the left hand, partial Simian crease on the right hand, operated strabismus, epicanthus, long face, talipes equinovarus, and heart valve defects			arr[GRCh37] Xp22.33p22.2 (466,805_ 11,623,233)x3	11.1	41	*ARSL, STS, HCCS, SHOX, GPR143, MID1, CLCN4, NLGN4X*	Pathogenic
						arr[GRCh37] 6q27 (168,145,844_ 170,926,453)x1	2.780	16	*THBS2, TBP, SMOC2, ERMARD, DLL1, PSMB1* 6q27 Terminal Deletion Syndrome	Pathogenic
6	M	7	ID, anteverted ears, blue eyes, tubular nose, narrow nares, thin upper lip, systolic heart murmurs, and prognathia			arr[GRCh37] 10q26.2q26.3 (128,993,707_ 133,811,505)x3	4.8	14	*EBF3* Distal trisomy 10q syndrome	Likely pathogenic

Table 1 (continuous). Summary of clinical and molecular features of patients with CNVs.

Case	Sex	Age (year)	Clinical features	Karyotyping	FISH	aCGH result	Size (Mb)	Number of affected coding genes	OMIM Morbid genes/ associated syndromes	Classification
7	M	15	ID, autism, big hands and feet, downslanted palpebral fissures, retrognathia, hypoplasia of the maxilla, prominent forehead, hypertelorism, rotting teeth, and genu valgus			arr[GRCh37] 15q11.2q13.1 (23,639,473_ 28,356,321)x3	4.839	14	*UBE3A, OCA2, HERC2, GABRB3, MKRN3, GABRA5* 15q11q13 microduplication syndrome	Pathogenic
8	F	11	ID, epilepsy, and dysmorphic face			a arr[GRCh37] 15q11.2q13.2 (22,777,056_ 30,370,684)x3	7.593	27	*UBE3A, OCA2, HERC2, GABRB3, MKRN3, GABRA5, NSMCE3, MAGEL2* 15q11q13 microduplication syndrome	Pathogenic
9	M	10	ID, deep-set eyes, downslanted palpebral fissures, prognathia, bulbous nose, dysplastic ears, and large forehead			arr[GRCh37] 16p11.2 (32,066,962_ 33,933,923)x1	1.866	13		Benign
10	M	7	ID, tubular nose, behavioral problems			arr[GRCh37] 16p11.2 (32,066,962_33,862,112) x1	1.795	13		Benign
11	M	4	ID, behavioral problems, pes planus, narrow forehead, deep-set eyes, tubular nose, long philtrum, thin upper and lower lip, epicanthus, hyperextansibility, and upslanted palpebral fissures			arr[GRCh37] 1q23.2q23.3 (159,785,281 _164,270,792)x3	4.5	76	*MPZ, ATP1A2, SDHC, APOA2, FCGR2A, KCNJ10, FCGR2B, DDR2, CFAP45, PIGM, CASQ1, DCAF8, PEX19, COPA, NCSTN, VANGL2, CD244, USF1, NECTIN4, UFC1, PPOX, NDUFS2, FCGR3A, ATF6, NOS1AP, RGS5*	Pathogenic

Table 1 (continuous). Summary of clinical and molecular features of patients with CNVs.

Case	Sex	Age (year)	Clinical Features	Karyotyping	FISH	aCGH result	Size (Mb)	Number of affected coding genes	OMIM morbid genes/ associated syndromes	Classification
12	F	3	ID, epilepsy, deafness			arr[GRCh37] 2p11.2p11.1 (89,323,730_91,413,804)x1	2.09			Benign
13	F	4	ID, delayed walking, speech delay, corpus callosum hypoplasia, delayed myelination, deep-set eyes, high palate, short hand fingers, down-slated palpebral fissures, micrognathia, and microcephaly			arr[GRCh37] 2q22.3 (145,149,256_145,269,121) x3	0.12	1	*ZEB2* Mowat–Wilson syndrome	Likely pathogenic
14	M	7	Mild ID, depressed nasal bridge, hypertelorism, irregular teeth, and Fragile X syndrome phenotype			arr[GRCh37] 16p11.2 (32,066,962_33,862,112)x1	1.795	13		Benign
						arr[GRCh37] Xq27.3 (146,410,692_147,029,643) x2	0.618	1	*FMR1* Fragile X syndrome	Likely pathogenic
15	F	5	ID, retrognathia, and temporal bossing			arr[GRCh37] 17p11.2 (17,393,323_19,977,668)x1	2.584	41	*RAI1, SREBF1, TOP3A, B9D1, ATPAF2, MYO15A, MIEF2, GRAP, ALDH3A2* Smith–Magenis syndrome	Pathogenic
16	M	7	ID, autism, dolichocephaly, slanted eyes, long philtrum, clinodactyly, and prognathia	Patient: 46,XY,del(4) (q12q13)[20] Mother:46,XX[20] Father:46,XY[20]		arr[GRCh37] 4q12q13.3 (58,520,002_71,755,523)x1	13.235	46	*UGT2B17, MUC7, GNRHR, ENAM, TCRL, AMTN, AMBN*	Pathogenic

Table 1 (continuous). Summary of clinical and molecular features of patients with CNVs.

Case	Sex	Age (year)	Clinical features	Karyotyping	FISH	aCGH result	Size (Mb)	Number of affected coding genes	OMIM morbid genes/associated syndromes	Classification
17	F	8	ID, agenesis of corpus callosum, upslanted palpebral fissures, tubular nose, and thin lips			arr[GRCh37] 16p11.2 (32,070,356_34,197,186)x1	2.076	13		Benign
18	M	17	ID, pulmonary valve stenosis, cubitus valgus, micropenis, cafe au lait spots, Simian crease, hypospadias, pes cavus, and short metacarpals	46,XY[20]		arr[GRCh37] 8p23.1 (9,165,634_10,952,305)x1	1.8	9	*RP1L1* 8p23.1 microdeletion syndrome	Pathogenic
19	M	4	ID			arr[GRCh37] 8p23.1 (7,011,414_7,689,941)x1	0.678	32		Benign
20	F	15	ID, behavioral problems, epilepsy, prognathia, long face, tubular nose, cubitus valgus, high palate, deep-set eyes, prominent glabella, short philtrum, and hirsutism			arr[GRCh37] 8p23.1 (6,919,229_7,689,941)x1	0.77	32		Benign
21	M	10	Moderate ID, nasal speech, seizures, scoliosis, strabismus, high palate, anteverted nares, dysplastic ears, and thoracal mass			arr[GRCh37] 6q26q27 (163,503,546_170,921,603) x1	7.3	32	*PDE10A, TBXT, RNASET2, CEP43, SMOC2, ERMARD, DLL1, THBS2, TBP, MPC1* 6q terminal deletion syndrome	Pathogenic
22	M	6	ID, downslanted palpebral fissures, thin upper lip, high palate, and dysplastic ears			arr[GRCh37] 13q21.33q22.2 (71,772,677_75,318,330)x1	3.546	7	*PIBF1*	Pathogenic

Table 1 (continuous). Summary of clinical and molecular features of patients with CNVs.

Case	Sex	Age (year)	Clinical features	Karyotyping	FISH	aCGH result	Size (Mb)	Number of affected coding genes	OMIM Morbid genes/ associated syndromes	Classification
23	F	5	ID, epilepsy, behavioral problems			arr[GRCh37] 14q22.3q23.1 (57,622,904_58,397,426)x1	0.774	5		VUS
24	M	3	ID, Angelman syndrome phenotype			arr[GRCh37] 15q11.2q13.1 (23,813,089_28,525,601)x1	4.835	13	*UBE3A, GABRB3, HERC2, OCA2, GABRA5, MAGEL2, MKRN3* Angelman syndrome	Pathogenic
25	M	6	Mild ID, autism, hyperextensibility			arr[GRCh37] 16p13.11 (15,078,280_15,366,031)x1	0.28	3	16p13.11 Microdeletion Syndrome	Pathogenic
						arr[GRCh37] 16p11.2(32,066,962_33,961,234) x1	1.89	13		Benign
26	F	5	ID, speech delay, Smith–Magenis syndrome phenotype		Nuc ish(SMCRx1) [100]	arr[GRCh37] 17p11.2(16,723,001_20,291,167) x1	3.56	47	*MYO15A, TNFRSF13B, ATPAF2, RAI1, ALDH3A2, FLCN, SREBF1, TOP3A, B9D1, MIEF2, GRAP* Smith–Magenis syndrome	Pathogenic
27	M	8	Mild ID, depressed nasal bridge, upslanted palpebral fissures, short philtrum, thin upper lip, hyperextensibility, and light-colored eyes and hair		Nuc ish(N25x1) [100]	arr[GRCh37] 22q11.21(18,641,420_21,457,610) x1	2.766	51	*GP1BB, SNAP29, RTN4R, COMT, TBX1, PRODH, PI4KA, LZTR1, SLC25A1, USP18, CDC45, TXNRD2, TANGO2, SCARF2, SERPIND1* 22q11.2 deletion syndrome	Pathogenic

Table 1 (continuous). Summary of clinical and molecular features of patients with CNVs.

Case	Sex	Age (year)	Clinical features	Karyotyping	FISH	aCGH result	Size (Mb)	Number of affected coding genes	OMIM morbid genes/associated syndromes	Classification
28	M	14	ID, hyperactivity, upslanted palpebral fissures, long philtrum, retrognathia, tubular nose, high palate, hypotelorism, anteverted alae nasi, irregular teeth, and thick lower and upper lips			arr[GRCh37] 5p14.3 (20,693,806_21,723,899) x1	1.03			Likely benign
						arr[GRCh37] 7q11.23 (75,985,508_76,810,806) x1	0.825	10	*YWHAG, ZP3* Distal chromosome 7q11.23 deletion syndrome	Likely pathogenic
29	M	17	Moderate ID, triangular face, prominent nasal bridge, thick ala nasi, broad nasal tip, deep-set eyes, low-set posteriorly located ears, downslanted palpebral fissures, chin dimple, prognathism, short distal phalanx of the hands and broad thumb, hyperextensibility, and large testis	Patient: 46,XY[20]	Nuc ish(8q11.1–q11.23x1)[100]	arr[GRCh37] 8q11.1q11.23 (47,355,673_54,495,215) x1	7.183	16	PRKDC, RB1CC1, *MCM4, SPIDR* Silver–Russel-like syndrome	Pathogenic
30	M	9	Severe ID, autistic behaviors, epilepsy, speech delay, attention deficit, strabismus, cryptorchidism, tubular nose, short stature, microcephaly, prognathia, flat forehead, long palpebral fissures, long philtrum, dysplastic ears, bilateral epicanthus, and thin upper lip			arr[GRCh37] 8p23.1 (6,925,491_7,689,941)x1	0.764	32		Benign
						arr[GRCh37] 16p13.3 (446,285_1,421,168)x1	0.97	42	*CACNA1H, STUB1, PIGQ, LMF1, CAPN15, CCDC78, GNPTG* ATR-16 syndrome	Pathogenic
31	F	11	ID, epilepsy, high palate, narrow forehead, low-set frontal hairline, cubitus valgus, thin upper lip, retrognathia, low-set dysplastic ears, short philtrum, malocclusion, and hypotonia	47,XX+mar[20]		arr[GRCh37] 15q11.2q13.3 (20,406,312_32,757,361) x3	12.351	64	*NIPA1, UBE3A, GABRB3, OCA2, HERC2, MAGEL2, TRPM1, FAN1, NSMCE3, GABRA5, MKRN3* 15q11q13 microduplication syndrome	Pathogenic

Table 1 (continuous). Summary of clinical and molecular features of patients with CNVs.

Case	Sex	Age (year)	Clinical features	Karyotyping	FISH	aCGH result	Size (Mb)	Number of affected coding genes	OMIM Morbid genes/associated syndromes	Classification
32	F	8	ID, epilepsy, narrow forehead, high palate, bulbous nose, tapering fingers, deep-set eyes, upslanted palpebral fissures, obesity, supernumerary nipple, and cardiac murmur		Nuc ish(1p34.3–p34.2x3) [100]	arr[GRCh37] 1p34.3p34.2 (34,785,012_41,468,186)x3	6.68	86	*GJB3, COL8A2, CSF3R, ZMPSTE24, COL9A2, GJB4, NCDN, AGO1, ADPRS, SNIP1, DNALI1, RSPO1, EPHA10, YRDC, MACF1, TRIT1, MFSD2A, PPT1, KCNQ4, CTPS1*	Pathogenic
33	M	15	ID, high palate, narrow forehead, prognathia, anteverted ears, thick lower lip, and pes cavus			arr[GRCh37] 10q26.3 (135,110,555_135,405,799)x3	0.295	13	*SYC1, ECHS1, TUBGCP2*	VUS
34	M	13	ID, epilepsy, micropenis, scoliosis, narrow forehead, tubular nose, cubitus valgus, downslanted palpebral fissures, short philtrum, thick upper and lower lips, hypoplasia of the maxilla, and high palate			arr[GRCh37] 10q26.3 (135,095,033_135,405,799)x3	0.31	13	*SYC1, ECHS1, TUBGCP2*	VUS
						arr[GRCh37] 15q11.2 (22,763,424_23,221,732)x1	0.45	4	*NIPA1* 15q11.2 BP1–BP2 microdeletion syndrome	Pathogenic
35	M	7	Moderate ID, epilepsy, behavioral problems, speech impairment, hypotonia, high palate, and low-set frontal hairline	46,XY[20]	Nuc ish(3p12.1–p11.1x1) [100]	arr[GRCh37] 3p12.1p11.1 (85,301,035_88,258,694)x1	2.95	8	*CHMP2B, POU1F1* 3p11.2–p12.1 deletion syndrome	Pathogenic
36	M	3	ID, hyperactivity, narrow forehead, downslanted palpebral fissures, epicanthus, tubular nose, facial hemiparesis, short philtrum, micrognathia, and hirsutism on the back			arr[GRCh37] Xp22.2 (11,291,711_11,913,836)x2	0.62	4	*AMELX, MSL3, FRMPD4*	VUS

Table 1 (continuous). Summary of clinical and molecular features of patients with CNVs.

Case	Sex	Age (year)	Clinical features	Karyotyping	FISH	aCGH result	Size (Mb)	Number of affected coding genes	OMIM norbid genes/associated syndromes	Classification
37	M	11	ID, epilepsy, narrow forehead, tubular nose			arr[GRCh37] Xp22.33 (2,167,170_2,270,373)x2	0.1	1		Benign
38	M	11	ID, epilepsy, short philtrum, high palate, synophrys, and thick lower lip	46,XY[20]		arr[GRCh37] Xp22.33 (1,804,303_2,131,027)x2	0.327			Benign

v* according to the International System for Human Cytogenetic Nomenclature (ISCN) 2020
F, female; M, male; ID, intellectual disability; VUS, variant of uncertain clinical significance.
Patients in gray were detected using BAC array platform.

MCAs, and autism spectrum disorders (ASDs) (2).

Thus, this study aimed to present CNVs identified in a retrospective cohort of 210 patients having ID with/without other medical conditions (such as ASDs, psychomotor retardation, epilepsy, attention deficit disorder, dysmorphic facial features, and/or MCAs) referred to our laboratory between 2009 and 2012. The CNVs identified in 38 patients with ID were summarized.

MATERIALS AND METHODS

Patients

This single-center retrospective cross-sectional study included 210 patients (139 male, 71 female, male/female ratio of 1.96) with unexplained ID with/without other medical conditions (such as ASD, psychomotor retardation, epilepsy, attention deficit disorder, dysmorphic facial features, and/or MCAs) and referred to our genetic laboratory from Pediatric Neurology, Pediatric Psychiatry, Pediatric Cardiology and Pediatric Endocrinology Departments of Kocaeli University, between 2009 and 2012. The median age was 8 (range, 2–18) years. The medical history (anamnesis, personal and family histories, and physical and dysmorphological examination) of the patients was provided by medical geneticists. Patients who refused to provide informed consent and whose genetic alterations explaining their clinical features were detected by one of the other techniques (e.g., karyotyping, fluorescent in situ hybridization (FISH), multiplex ligation-dependent probe amplification, and sequencing) before the aCGH were excluded from the study.

All procedures were conducted following the ethical standards outlined in the 1964 Declaration of Helsinki and its subsequent revisions. Owing to the patient's age, guardians or parents signed the informed consent forms approved by the Human Subjects Research Ethical Committee of Kocaeli University, under Project number 2009/102.

aCGH

In this study, 3 mL of peripheral blood was collected from each patient, and genomic DNA was extracted using DNeasy Blood & Tissue kit (Qiagen, Germany), following the manufacturer's instructions. aCGH analysis was performed using the oligo-based CytoSure Syndrome Plus ISCA Design (v2) Microarray 4 × 44K (Oxford Gene Technology, Oxford, UK) in 142 patients and bacterial artificial chromosome (BAC) CytoChip Focus Constitutional (v1.1) arrays (BlueGnome Ltd., Cambridge, UK) in 68 patients according to the manufacturer's recommendations. Data analysis was performed using CytoSure visualization software (Oxford Gene Technology) for oligo arrays and BlueFuse Software v2.2 (BlueGnome Ltd.) for BAC arrays. Karyotyping was performed in only six patients according to standardized procedures (7) and was used for segregation analysis in one patient (case 16). Chromosome observations were performed using an Olympus microscope and CytoVision analysis software. FISH was performed for validation using BlueFish tile BAC probes (BlueGnome Ltd.) RP11-101E19 (Chr:8, Start:47728696, and Stop:47901824), RP11-327P22 (Chr:1, Start:34876928, and Stop:35068982), RP11-14B7 (Chr:3, Start:85446954, and Stop:85621157), and Cytocell FISH probes LPU 007-S (Smith–Magenis (FLII)/Miller–Dieker Probe Combination) and LPU 010 (VCFS N25) according to the manufacturer's instructions.

CNV interpretation

To determine the pathogenicities of CNVs, they were evaluated using public databases and literature mining. The UCSC Genome Browser was used to display gene distributions. Coordinates of aberrations were based on the UCSC NCBI36/hg18. For the translation of the coordinates to hg19, UCSC LiftOver was used (https://genome.ucsc.edu/cgi-bin/hgLiftOver). Benign CNVs were identified using the Database of Genomic Variants, which contains CNVs of the normal population. CNVs were compared with the Database of Chromosomal Imbalance and Phenotype in Humans Using Ensembl Resources (DECIPHER), dbVar, ClinVar, and ClinGen that provide CNVs with clinical features. The ClinGen Dosage Sensitivity Map was used to determine the dosage sensitivity of the genes in the aberrant region. The NCBI Gene Database, GeneCards, PubMed, Genetic Home Reference, and OMIM provided information on the functions of genes located in genomic aberrations. Genes related to neurodevelopmental disorders were searched using Gene2Phenotype.

According to ACMG/ClinGen guidelines, CNVs were classified as pathogenic, likely pathogenic, VUS, likely benign, and benign (8, 9). In addition, Franklin by genoox (https://franklin.genoox.com/clinical-db/home) and XCNV (http://119.3.41.228/XCNV/index.php) were used in CNV interpretation.

RESULTS

In this study, 45 CNVs were found in 38 (18%) patients. Among the CNVs, 18 (40%) were duplications, and 27 (60%) were deletions. Thirteen CNVs (28.8%) were large genomic aberrations encompassing a region of ≥3 Mb. Forty-five CNVs were classified into five categories: 21 (46.7%) were pathogenic, 4 (8.9%) were likely pathogenic, 8 (17.8%) were VUS, 1 (2.2%) was likely benign, and 11 (24.4%) were benign.

Multiple CNVs were found in 7 (18.4%) patients. Segregation analysis could be performed in only one patient (case 16) using karyotyping, which resulted in a *de novo* deletion. Detected CNVs were validated by FISH in five patients (cases 26, 27, 29, 32, and 35) and karyotyping in one patient (case 16). The clinical features of patients with CNVs are shown in Table 1.

Among 45 CNVs, 19 corresponded to rare microdeletion/microduplication syndromes. Microdeletions associated with syndromes were Smith–Magenis syndrome (n = 2), 8p23.1 microdeletion syndrome, 6q terminal deletion syndrome, Angelman syndrome, distal chromosome 7q11.23 deletion

syndrome, Silver–Russel-like syndrome,15q11.2 BP1-BP2 microdeletion syndrome, 3p11.2–p12.1 deletion syndrome, 16p13.11 microdeletion syndrome, ATR-16 syndrome, and 22q11.2 deletion syndrome. Microduplications associated with syndromes were 15q11.q13 microduplication syndrome (n = 3), Mowat–Wilson syndrome, distal trisomy 10q syndrome, and fragile X syndrome.

In this study, pathogenic CNVs, including deletions of 21q22.3 and 4q12q13.3 and duplications of Xp22.33p22.2, 1q23.2q23.3, and 1p34.3-p34.2, were not found to be associated with a syndrome.

Breakpoints of the marker chromosome detected by karyotyping were identified using aCGH in one patient. Case 31 showed a gain for the region 15q11.2q13.3 with a size of approximately 12 Mb. In 172 patients (82%), no aberrations were observed.

The pathogenic/likely pathogenic chromosomal changes that could explain the phenotype or be related to the patient's findings were detected in 24 of 210 (11.43%) patients. The diagnostic rate in this study was 11.43%.

DISCUSSION

In the present study, 45 CNVs were found in 38 (18%) patients. Among the CNVs, 18 (40%) were duplications, and 27 (60%) were deletions. A study reported that random duplications may occur less frequently than random deletions in the genome (6).

Among the CNVs, 21 (46.7%) were pathogenic, and 4 (8.9%) were likely pathogenic. Pathogenic CNVs were more prevalent in our study by detecting large CNVs, and the detected CNVs were predominantly deletions.

In this study, deletions were found to be associated with Smith–Magenis syndrome (n = 2), 8p23.1 microdeletion syndrome, 6q terminal deletion syndrome, Angelman syndrome, distal chromosome 7q11.23 deletion syndrome, Silver–Russel-like syndrome,15q11.2 BP1-BP2 microdeletion syndrome, 3p11.2–p12.1 deletion syndrome, 16p13.11 microdeletion syndrome, ATR-16 syndrome, and 22q11.2 deletion syndrome. Duplications were associated with 15q11.q13 microduplication syndrome (n = 3), Mowat–Wilson syndrome, distal trisomy 10q syndrome, and fragile X syndrome. Microduplication syndromes are frequently unnoticed because of their mild phenotype, although microdeletion syndromes have been more frequent owing to their recognizable features (10).

In this study, pathogenic CNVs, which could not be found to be associated with a syndrome, have been also detected. A pathogenic deletion of 21q22.3 encompassing *PCNT, COL6A2, COL6A1, LSS,* and *FTCD* was detected in case 1 with a specific learning disability, ID, nasal speech, tubular nose, thin and long fingers, and a cardiac anomaly. *S100B, DIP2A, PCNT,* and *PRMT2,* which are located in the breakpoints of our CNV, are candidate genes for dyslexia. A study suggested that *COL18A1, COL6A1*, and *COL6A2* are causal for cardiac abnormalities such as ascending aorta dilatation (11).

A complex CNV (pathogenic 6q27 deletion and pathogenic Xp22.33p22.2 duplication) was found in case 5 with ID, behavioral problems, Simian crease on the left hand, partial Simian crease on the right hand, operated strabismus, epicanthus, long face, talipes equinovarus, and heart valve defects. Interpreting the phenotypic consequences of patients with complex CNVs is challenging. Strabismus, ID, epicanthus, and behavioral problems have been reported in 6q27 terminal deletion syndrome (12). A large pathogenic Xp22.33p22.2 duplication including *ARSL, STS, HCCS, SHOX, GPR143, MID1, CLCN4,* and *NLGN4X* was detected in the same patient. Among these genes, *CLCN4* is a morbid OMIM gene associated with Raynaud–Claes syndrome. In Genereviews (https://www.ncbi.nlm.nih.gov/books/NBK575836/), *CLCN4*-related neurodevelopmental disorder (*CLCN4*-NDD) has been reported with phenotypic features such as developmental delay or ID, behavioral problems (e.g., ASD, hyperactivity, anxiety, and bipolar disorder), epilepsy, and gastrointestinal dysfunction. In Genereviews, chromosomal microarray analysis (CMA) has been suggested as the first genetic test for diagnosis in children with developmental delay or older patients with ID. We think that the patient findings were caused by the combined effects of the detected deletion and duplication. Complex CNVs should be verified whether they arise from a parental balanced rearrangement.

Marker chromosomes cannot be identified by conventional cytogenetic methods (13). In this study, the CNV size, chromosomal breakpoints, and gene content of the marker chromosome detected in case 31 were identified using aCGH. A large pathogenic duplication was found in case 11. Pure and partial trisomy 1q very rarely occur (14). The reported duplications are predominantly distal trisomy 1q and are caused by unbalanced translocations with partial deletions at other chromosomes. The size, location, and genes implicated in the duplication determine the severity of its symptoms. Individuals with chromosome 1q duplications may have various features including developmental delay, learning disabilities, slow growth, short stature, birth defects (e.g., cleft palate and heart defect), and facial dysmorphic features (e.g., retrognathia). To our knowledge, no 1q23.2q23.3 duplication was reported in the literature. In addition, in DECIPHER, no duplications overlap exactly with our region, and there are either smaller (95–953 kb) or larger (7–103 Mb) ones. Patient 342100 with ID and autism, reported in DECIPHER, has a duplication with a size of 953.57 Kb. This duplication contains *MPZ, SDHC, APOA2, CD244, NECTIN4, UFC1, PPOX, USF1,* and *NDUFS2* overlapping with our region. In Franklin genoox, *SDHC, UFC1, PPOX,* and *NDUFS2* were found to be associated with ID and behavioral problems phenotypes. These genes may be responsible for the ID and behavioral problems in our patient.

A large 4q12q13.3 deletion was detected in case 16 with ID, autism, dolichocephaly, slanted eyes, long philtrum, clinodactyly, and prognathia. Proximal 4q aberrations (deletions/duplications) have been reported in different sizes and regions so far. ID and autism findings in our patient were associated with *UBA6* located in the deleted region (15). Thus, this gene may be responsible for the cognitive and behavioral features.

A pathogenic 13q21.33q22.2 deletion was found in a male patient (case 22) with ID, downslanted palpebral fissures, thin upper lip, high palate, and dysplastic ears. Partial 13q deletions are uncommon. No pure 13q21.33q22.2 deletion was reported in the literature. The reported 13q deletions are larger CNVs including our breakpoints. Kirchhoff et al. have evaluated molecular and clinical data, belonging to 14 European patients who had *de novo* 13q deletions, for the genotype–phenotype mapping of 13q. Their data and earlier study have indicated that 13q21.1–q21.33 and 13q31 are associated with mild ID or even normal mental development (16). In addition, our CNV region contains one of the ID-related gene, i.e., *PIBF1*, which has been associated with Joubert syndrome 33.

A rare 1p34.3–p34.2 duplication of 6.68 Mb in size was detected in a female patient (case 32) with ID, epilepsy, narrow forehead, high palate, bulbous nose, tapering fingers, deep-set eyes, upslanted palpebral fissures, obesity, supernumerary nipple, and cardiac murmur. Few interstitial 1p duplications were described. Reported duplications have been larger than our duplicated region and have been associated with phenotypic features such as severe intrauterine growth retardation, ambiguous genitalia, Kabuki syndrome-like symptoms, sex reversal, and MCAs including a heart defect. A girl presenting with heart defects, developmental delay, midface hypoplasia, speech delay, broad nasal bridge, frontal bossing, fifth finger clinodactyly, low-set posteriorly rotated ears, tapering fingers, microdontia, pes planus, and varus positioning of feet was reported previously. She had interstitial 1p34.1–p34.3 duplication detected by FISH. In that report, *COL8A2,* which is located in our duplicated region, was suggested to be responsible for congenital heart defects (17). Jacher et al. described a female patient who had *de novo* 1p34.3p34.2 deletion with a size of 2.3 Mb and presented delayed development, mild ID, bone age delay, vocal cord paralysis, bilateral metatarsus adductus, bilateral vesicoureteral reflux, aberrant right subclavian artery, kyphoscoliosis, and genu valgum. They suggested that the haploinsufficiencies of *AGO1, SLC2A1, AGO3*, *RIMS3,* and *GRIK3* may cause neurocognitive impairments and other symptoms presented in their patient, and *SNIP1* may have an important role in central nervous system disorders, particularly delayed development, cognitive impairment, epilepsy, structural brain deformities, and ID (18). To understand the triplosensitivity effect of *SNIP* and other genes in the 1p34.3–p34.2 region, more cases of patients with similar duplications must be reported.

This study presents CNV data from a cohort of 210 Turkish patients with ID. Pathogenic/likely pathogenic CNVs were found in 24 of 210 (11.43%) patients. The diagnostic rate of aCGH is variable and is determined by various factors such as the phenotype complexity of the patients being tested and the array design being used (19). Our diagnostic rate (11.43%) was lower than the average diagnostic rate of 15%–20% reported recently (6) but in concordance with the 10%–20% reported in previous aCGH studies (20, 21).

In this study, any CNV could not be observed in 172 (82%) patients. One of the next-generation sequencing methods such as whole-exome sequencing is recommended for patients in whom no CNVs were detected or whom VUS/likely benign/benign CNV is detected that does not clarify their phenotypes. In addition, VUS CNVs should be followed because their pathogenicity may change over time.

This study has some limitations. First, parental inheritance could not be identified. Parental inheritance information would have been useful to interpret CNV data, particularly VUS. Second, high-resolution aCGH could not be used. If a high-resolution aCGH could be used, a higher diagnostic yield could be achieved. Third, the study analyzed a small sample. Fourth, few patients (n = 6) with CNVs detected by aCGH underwent FISH or karyotyping to validate the results of aCGH.

In summary, this study presents rare CNVs or syndromes among Turkish patients having ID with/without other medical conditions. In addition, our results identified VUS CNVs that may be reclassified after further functional studies. CGH remains the first-tier technology allowing geneticists to diagnose complex phenotypes, identify candidate genes involved in ID, and explore novel CNV effects.

Ethics Committee Approval: All procedures were conducted following the ethical standards outlined in the 1964 Declaration of Helsinki and its subsequent revisions. Approved by the Human Subjects Research Ethical Committee of Kocaeli University, under Project number 2009/102.

Informed Consent: Owing to the patient's age, guardians or parents signed the informed consent forms.

Peer-review: Externally peer-reviewed.

Author Contributions: Conception/Design of Study- D.S.A., N.C. H.S.; Data Acquisition- D.S.A., B.K.; Data Analysis/Interpretation- D.S.A.; Drafting Manuscript- D.S.A., N.C., T.O.; Critical Revision of Manuscript- D.S.A., N.C.; Final Approval and Accountability- D.S.A., N.C.

Conflict of Interest: All authors declare that they have no conflicts of interest.

Financial Disclosure: The authors declare that this study has received no financial support.

REFERENCES

1. Pereira RR, Pinto IP, Minasi LB, de Melo AV, da Cruz e Cunha DM, Cruz AS, et al. Screening for intellectual disability using high-resolution CMA technology in a retrospective cohort from Central Brazil. PLoS One 2014; 9: e103117.
2. Quintela I, Eirís J, Gómez-Lado C, Pérez-Gay L, Dacruz D, Cruz R, et al. Copy number variation analysis of patients with intellectual disability from North-West Spain. Gene 2017; 626: 189-99.
3. Vianna GS, Medeiros PF, Alves AF, Silva TO, Jehee FS. Array-CGH analysis in patients with intellectual disability and/or congenital malformations in Brazil. Genet Mol Res 2016; 15.
4. Wolfe K, Strydom A, Morrogh D, Carter J, Cutajar P, Eyeoyibo M, et al. Chromosomal microarray testing in adults with intellectual disability presenting with comorbid psychiatric disorders. Eur J Hum Genet 2016; 25: 66-72.
5. Di Gregorio E, Riberi E, Belligni EF, Biamino E, Spielmann M, Ala U, et al. Copy number variants analysis in a cohort of isolated and syndromic developmental delay/intellectual disability reveals novel genomic disorders, position effects and candidate disease genes. Clin Genet 2017; 92: 415-22.
6. Lee CL, Lee CH, Chuang CK, Chiu HC, Chen YJ, Chou CL, et al. Array-CGH increased the diagnostic rate of developmental delay or intellectual disability in Taiwan. Pediatr Neonatol 2019; 60: 453-60.
7. Moorhead PS, Nowell PC, Mellman WJ, Battıps DM, Hungerford DA. Chromosome preparations of leukocytes cultured from human peripheral blood. Exp Cell Res 1960; 20: 613-6.
8. Kearney HM, Thorland EC, Brown KK, Quintero-Rivera F, South ST, Working Group of the American College of Medical Genetics Laboratory Quality Assurance Committee. American College of Medical Genetics standards and guidelines for interpretation and reporting of postnatal constitutional copy number variants. Genet Med 2011; 13: 680-5.
9. Riggs ER, Andersen EF, Cherry AM, Kantarci S, Kearney H, Patel A, et al. Technical standards for the interpretation and reporting of constitutional copy-number variants: a joint consensus recommendation of the American College of Medical Genetics and Genomics (ACMG) and the Clinical Genome Resource (ClinGen). Genet Med 2020; 22: 245-57.
10. Türkyılmaz A, Geckinli BB, Tekin E, Ates EA, Yarali O, Cebi AH, et al. Array-based comparative genomic hybridization analysis in children with developmental delay/intellectual disability. Balkan J Med Genet 2022; 24: 15-24.
11. Chen CP, Wang LK, Chern SR, Wu PS, Chen SW, Wu FT, et al. Prenatal diagnosis and molecular cytogenetic characterization of mosaic ring chromosome 21 associated with low PAPP-A and low PlGF in the first-trimester maternal serum screening. Taiwan J Obstet Gynecol 2022; 61: 359-63.
12. Conti V, Carabalona A, Pallesi-Pocachard E, Parrini E, Leventer RJ, Buhler E, et al. Periventricular heterotopia in 6q terminal deletion syndrome: role of the C6orf70 gene. Brain 2013; 136: 3378-94.
13. Jang W, Chae H, Kim J, Son JO, Kim SC, Koo BK, et al. Identification of small marker chromosomes using microarray comparative genomic hybridization and multicolor fluorescent in situ hybridization. Mol Cytogenet 2016; 9: 61.
14. Sifakis S, Eleftheriades M, Kappou D, Murru R, Konstantinidou A, Orru S, et al. Prenatal diagnosis of proximal partial trisomy 1q confirmed by comparative genomic hybridization array: molecular cytogenetic analysis, fetal pathology and review of the literature. Birth Defects Res A Clin Mol Teratol 2014; 100: 284-93.
15. Quintela I, Barros F, Fernandez-Prieto M, Martinez-Regueiro R, Castro-Gago M, Carracedo A, et al. Interstitial microdeletions including the chromosome band 4q13.2 and the UBA6 gene as possible causes of intellectual disability and behavior disorder. Am J Med Genet A 2015; 167A: 3113-20.
16. Kirchhoff M, Bisgaard AM, Stoeva R, Dimitrov B, Gillessen-Kaesbach G, Fryns JP, et al. Phenotype and 244k array-CGH characterization of chromosome 13q deletions: an update of the phenotypic map of 13q21.1-qter. Am J Med Genet A 2009; 149A: 894-905.
17. Lennon PA, Boerkoel CF, Plunkett K, Soukam S, Cheung SW, Patel A. A novel 8.5 MB dup(1)(p34.1p34.3) characterized by FISH in a child presenting with congenital heart defect and dysmorphic features. Am J Med Genet A 2006; 140A: 1864-70.
18. Jacher JE, Innis JW. Interstitial microdeletion of the 1p34.3p34.2 region. Mol Genet Genomic Med 2018; 6: 673-7.
19. Rosenfeld JA, Patel A. Chromosomal microarrays: understanding genetics of neurodevelopmental disorders and congenital anomalies. J Pediatr Genet. 2017; 6: 42-50.
20. Miller DT, Adam MP, Aradhya S, Biesecker LG, Brothman AR, Carter NP, et al. Consensus statement: chromosomal microarray is a first-tier clinical diagnostic test for individuals with developmental disabilities or congenital anomalies. Am J Hum Genet 2010; 86: 749-64.
21. Hochstenbach R, van Binsbergen E, Engelen J, Nieuwint A, Polstra A, Poddighe P, et al. Array analysis and karyotyping: workflow consequences based on a retrospective study of 36,325 patients with idiopathic developmental delay in the Netherlands. Eur J Med Genet 2009; 52: 161-9.

Experimed 2023; 13(3): 276-280

ORIGINAL ARTICLE

DOI: 10.26650/experimed.1381077

Effect of MCP-1 and CCR2 Serum Levels on COVID-19 Severity

Selen Zeliha Mart Komurcu[1], Seydanur Dogan[2,3], Ebru Kaya[4], Sevim Yavas[5], Serkan Dogan[6], Utku Murat Kalafat[6], Hayriye Senturk Ciftci[3], Selcuk Dasdemir[3]

[1]Department of Microbiology, Kanuni Sultan Suleyman Training and Research Hospital, Istanbul, Turkiye
[2]Medical Laboratory Techniques Program, School of Health Services, Nisantası University, Istanbul, Turkiye
[3]Department of Medical Biology, Istanbul Faculty of Medicine, Istanbul University, Istanbul, Turkiye
[4]Department of Anesthesia and Reanimation, Kanuni Sultan Suleyman Training and Research Hospital, Istanbul, Turkiye
[5]Department of Infectious Diseases, Kanuni Sultan Suleyman Training and Research Hospital, Istanbul, Turkiye
[6]Department of Emergency Medicine, Kanuni Sultan Suleyman Training and Research Hospital, Istanbul, Turkiye

ORCID ID: S.Z.M.K. 0000-0001-7500-0783; S.D. 0000-0001-5245-5275; E.K. 0000-0002-9506-0756; S.Y. 0000-0001-8010-7454; S.D. 0000-0001-8923-2489; U.M.K. 0000-0003-1749-8098; H.S.C. 0000-0003-3507-482X; S.D. 0000-0002-7816-8909

Cite this article as: Mart Komurcu SZ, Dogan S, Kaya E, Yavas S, Dogan S, Kalafat UM, Senturk Ciftci H, Dasdemir S. Effect of MCP-1 and CCR2 serum levels on COVID-19 severity. Experimed. Experimed 2023; 13(3): 276-280.

ABSTRACT

Objective: Approximately 80% of people with coronavirus disease 2019 (COVID-19) are asymptomatic, and only a small proportion of cases show serious consequences leading to hospitalization. The interplay between chemokines and their receptors can affect the severity of several infectious diseases, such as severe acute respiratory syndrome and Middle East Respiratory Syndrome. The interplay of monocyte chemoattractant protein-1 (MCP-1) with its receptor C-C motif chemokine receptor 2 (CCR2) may affect the pathogenesis of COVID-19 by functioning in the dispatch of lymphocytes and monocytes/macrophages to the infection site.

Materials and Methods: The serum MCP-1 and CCR2 concentrations were measured using the enzyme-linked immunosorbent assay (ELISA) in 49 asymptomatic, 50 severe, and 57 critical COVID-19 cases.

Results: Serum MCP-1 levels were considerably higher in critical cases than in cases in the other two groups, suggesting an increased risk for disease severity ($p = 0.008$; $p = 0.01$, respectively). Serum CCR2 levels were significantly higher in asymptomatic cases than in critical cases suggesting a protective role against disease severity ($p = 0.001$).

Conclusion: MCP-1 and CCR2 may be candidate biomarkers for the prediction of disease severity. Therefore, by measuring serum levels of MCP-1 and CCR2 early, the disease course can be predicted , and necessary precautions can be taken before the disease becomes severe.

Keywords: MCP-1, CCR2, COVID-19 severity, risk factors, candidate biomarkers

INTRODUCTION

The coronavirus disease 2019 (COVID-19) is a multifaceted respiratory ailment, with initial symptoms ranging from fever and dry cough to fatigue (1, 2). In confirmed cases, less common yet noteworthy symptoms include headaches, dizziness, abdominal discomfort, and gastrointestinal distress (3). In addition, approximately 80% of individuals with infection remain asymptomatic, whereas only a fraction of cases progress to a severe state necessitating hospitalization (4). Older people, men, smokers, and people with chronic diseases have more severe COVID-19 (5, 6). COVID-19 may cause pneumonia, liver injury, cardiac injury, sepsis, and death (7).

The course of COVID-19 not only depends on viral infection, but the host immune response also determines the disease outcome. The above normal inflammatory responses in cases that have advanced to the pneumonia stage increased the release of proinflammatory cytokines and chemokines, known as the "cytokine storm," which is more lethal than the viral infection itself and causes widespread

Corresponding Author: Selcuk Dasdemir **E-mail:** selcuk.dasdemir@istanbul.edu.tr
Submitted: 25.10.2023 **Revision Requested:** 19.11.2023 **Last Revision Received:** 29.11.2023 **Accepted:** 29.11.2023

alveolar destruction, fibrosis, worsening respiratory failure, and multiorgan dysfunction (8). Central to this cytokine storm is the heightened release of Interleukin (IL)-6, and high levels of IL-10 and IL-1 receptor antagonists also correlated with disease severity (9, 10).

Levels of chemokines, such as C-X-C motif chemokine ligand 10 (CXCL10) and monocyte chemoattractant protein-1 (MCP1), are markedly high in severe cases, contributing to the exacerbated inflammatory response (11). Notably, specific chemokine levels correlate positively with viral load exclusively in severe cases (12). Given their role in attracting leukocytes to infection sites, regulating their function holds significant promise in mitigating inflammation above normal levels in patients with COVID-19 (13).

By binding to its receptor C-C motif chemokine receptor 2 (CCR2), MCP-1 orchestrates the recruitment of monocytes and basophils, influencing processes such as inflammation, angiogenesis, and coagulation (14). This interaction may play a pivotal role in the pathogenesis of viral infections by facilitating the dispatch of lymphocytes and monocytes/macrophages to the infection site (15). Although MCP-1 has been proposed as a disease biomarker (16), unraveling the precise role of the MCP-1/CCR2 pathway in COVID-19 remains imperative. This study endeavors to elucidate the association between MCP-1 and CCR2 serum levels in COVID-19 to pinpoint potential biomarkers for disease severity and prognosis.

Table 1. Demographic features and the clinical characteristics of patients with COVID-19.

	Grup A (Asymptomatic) (n=49)	Grup B (Severe) (n=50)	Grup C (Critical) (n=57)	p Values		
Variables				**Grup A vs B**	**Grup A vs C**	**Grup B vs C**
Age (Mean ± SD, years)	45.6 ± 13.9	52.7 ± 13.5	59.3 ± 15.5	0.001	0.001	0.396
Gender						
Female, n (%)	29 (59.2%)	21 (42.0%)	20 (35.1%)	0.087	0.013	0.483
Male, n (%)	20 (40.8%)	29 (58.0%)	37 (64.9%)			
Comorbidity						
Yes, n (%)	32 (65.3%)	37 (74.0%)	39 (68.4%)	0.470	0.894	0.673
No, n (%)	17 (34.7%)	13 (26.0%)	18 (31.6%)			
Diabetes						
Yes, n (%)	8 (16.3%)	14 (28.0%)	13 (22.8%)	0.248	0.555	0.693
No, n (%)	41 (83.7%)	36 (72.0%)	44 (77.2%)			
Hypertension						
Yes, n (%)	6 (12.2%)	12 (24.0%)	16 (28.1%)	0.209	0.077	0.796
No, n (%)	43 (87.8%)	38 (76.0%)	41 (71.9%)			
Blood Test Results, median (IQR)						
D-dimer (µg/mL)	0.4 (0.6)	0.5 (1.2)	3.3 (6.7)	0.983	0.001	0.001
Hemoglobin (g/dL)	13.2 (13.1)	12.9 (12.9)	13.3 (12.2)	0.189	0.947	0.344
Lymphocytes ($x10^9$/L)	1.4 (1.5)	1 (1.2)	0.7 (3.6)	0.874	0.453	0.713
WBC ($x10^9$/L)	5.8 (6.4)	6.6 (9.3)	10.9 (11.2)	0.437	0.0001	0.001
Platelets ($x10^9$/L)	205.5 (218.7)	222.5 (229.5)	250 (238.5)	0.798	0.999	0.761
CRP (mg/L)	24.3 (34)	45.5 (70.1)	100.3 (134.2)	0.075	0.001	0.0001
Ferritin (mg/mL)	148.4 (186.4)	492.6 (664.3)	887.4 (1719.7)	0.001	0.0001	0.001

MATERIALS AND METHODS

Patients

In this study, the case group comprised 49 patients with asymptomatic COVID-19 who required only home quarantine, 50 patients who were hospitalized, and 57 patients with critical conditions who had severe COVID-19 and needed intensive care. Real-time reverse transcription polymerase chain reaction (RT-PCR) of viral nucleic acid was accepted as the reference standard in the diagnosis of COVID-19. Chest computed tomography was used to detect patients with COVID-19 pneumonia. These patients originated from Turkiye and were enrolled in the study to measure the serum MCP-1 and CCR2 levels. Participants were selected from cases coming to Kanuni Sultan Suleyman Training and Research Hospital between June 2022 and September 2022 and volunteered to participate in the study randomly.

Measurements of Serum MCP-1 and CCR2 Levels

Blood samples were taken from patients with asymptomatic COVID-19 when they first applied to the outpatient clinic, patients with severe disease while they were hospitalized in the service, and patients with critical disease while they were in the intensive care unit. The enzyme-linked immunosorbent assay (ELISA) was conducted to determine MCP-1 and CCR2 serum levels, which are taken from patients' whole blood. The analytical measurement ranges were 62.5–4000 pg/mL for MCP-1 and 0.16–10 ng/mL for CCR2.

Statistical Analyses

The obtained data were statistically analyzed using the IBM SPSS Statistics version 21.0. For the correlation of countable values with each other, r and p values were given by looking at the correlation. A normality test was performed for the values. The Kolmogorov–Smirnov test was used. Spearman's rho correlation was applied because MCP-1 and CCR2 values of the variables showed no normal distribution. The Kruskal–Wallis test and then the post-hoc test were used for crosschecking the MCP-1 and CCR2 values among the three groups. A multivariate logistic test was applied for the effect of independent variables (age, sex, biochemical parameters, diabetes, hypertension, and comorbidity) on MCP-1 and CCR2 between groups. A sample size was calculated with a two-sided confidence interval. Considering a 0.80 power and a 0.05 error, 43 patients were needed for a standard deviation of 0.2. Considering a possible loss of 15% during data collection, at least 150 patients were included. p significance limit was accepted as less than 0.05.

RESULTS

In the study group, participants in the critical COVID-19 group (age range: 28–91; mean age: 59.3 ± 15.5 years; female/male: 20/37) were statistically significantly older than those in the asymptomatic group (age range: 21–75; mean age: 45.6 ± 13.9 years; female/male: 29/20) and severe group (age range: 18–79; mean age: 52.7 ± 13.5 years; female/male: 21/29), and the number of male patients was greater as noted in previous studies. No statistically significant relationship was found between diabetes, hypertension, comorbidities, and disease severity in the study group. In addition, D-dimer, C-reactive protein (CRP), and ferritin levels in the study group were statistically significantly higher than those in the asymptomatic to the critical group. Table 1 demonstrates all parameters related to the aim of this study.

Table 2 shows the distribution of the serum MCP-1 and CCR2 levels in the three groups. Serum MCP-1 levels were considerably higher in the critical group than those in the other two groups, suggesting an increased risk for severe disease ($p = 0.008$; $p = 0.01$, respectively). Serum CCR2 levels were significantly higher in the asymptomatic group than in the critical group, suggesting a protective role against severe disease ($p = 0.001$).

In addition, the relevance between clinical parameters and serum MCP-1 and CCR2 levels was examined in the study group. An inverse relationship (negative correlation) was found between serum MCP-1 levels and platelet count in the asymptomatic and critical groups ($r = -0.356$, $p = 0.015$; $r = -0.361$, $p = 0.013$, respectively). An inverse relationship was found between serum CCR2 and CRP levels in the asymptomatic group ($r = -0.295$, $p = 0.044$). A linear relationship (positive correlation) was found between MCP-1 serum, ferritin, D-dimer, and white blood cell count as expected considering the literature on critical COVID-19 ($r = 0.279$, $p = 0.037$; $r = 0.349$, $p = 0.009$; and $r = 0.295$, $p = 0.029$, respectively). A linear

Table 2. MCP-1 and CCR2 levels in asymptomatic, severe and critical COVID-19 patients.

	Grup A (Asypmtomatic) (n=49)	Grup B (Severe) (n=50)	Grup C (Critical) (n=57)	p Values		
Variables				**Grup A vs B**	**Grup A vs C**	**Grup B vs C**
MCP-1 (pg/mL), median (IQR)	315.2 (149.9)	267.7 (262.9)	549.6 (954.8)	0.999	0.008	0.01
CCR2 (ng/mL), median (IQR)	8.8 (3.5)	6.6 (6.3)	5.6 (4.2)	0.082	0.001	0.431

relationship was noted between serum CCR2 levels and age in the critical group ($r = 0.307$, $p = 0.02$). Moreover, an inverse relationship was found between serum CCR2 and lymphocyte levels in the critical group ($r = -0.337$, $p = 0.013$). Serum MCP-1 and CCR2 levels were not related to any of the clinical parameters in the severe group (data not shown).

Practical Implications of the Study's Findings

Clinicians can more closely monitor patients who they consider at risk based on serum MCP-1 and CCR2 levels and can take precautions in advance in patients who they predict will have increased inflammatory response. They can develop treatments to reduce inflammatory responses in these patients. Researchers can investigate different treatment possibilities and discover new drugs that affect the MCP-1 and CCR2 pathways.

DISCUSSION

The interplay between chemokines and their corresponding receptors holds implications for susceptibility to various diseases, including atherosclerosis, multiple sclerosis, and colitis (17, 18, 19). These molecules have also been implicated in infectious diseases such as severe acute respiratory syndrome (SARS) and Middle East Respiratory Syndrome (MERS) (20). Notably, deficiencies in chemokine receptors such as CCR1, CCR2, and CCR5 have been linked to severe illness and fatality because of diminished recruitment of infection-fighting cells into the lungs (21).

MCP-1 and CXCL10 suppress the proliferation of cells that cause lymphopenia in SARS and MERS, and their plasma levels positively correlated with mortality in MERS-CoV infection (22, 23). Thus, chemokines may also affect ones susceptibility to COVID-19, and the severity of COVID-19 can be stratified by measuring serum chemokine levels.

In this study, serum MCP-1 levels were significantly higher in the critical group than in the asymptomatic and severe groups. This observation is consistent with prior findings indicating a proportional increase in MCP-1 levels with the COVID-19 severity (24). Anderberg et al. similarly established that high serum MCP-1 levels were related to respiratory failure and mortality in critical COVID-19 (25). Genetic studies further supported our findings, with polymorphisms associated with high MCP-1 levels aligning with disease severity (26). In addition, a linear relationship between serum MCP-1 levels and D-dimer levels was noted in the critical group, suggesting interplay between inflammation and coagulation in the progression of COVID-19 (27).

Interestingly, CCR2 levels were considerably higher in the asymptomatic group than in the critical group. This implies that high serum CCR2 levels may confer protection against the severe effects of COVID-19. Previous studies have indicated the upregulation of CCR2, alongside CXCR3, in pulmonary responses to MERS infection (28). Mouse models infected with SARS-CoV have also demonstrated deficiencies in CCR2 and CCR5, which increases the mortality risk (29). Genetic analyses have further identified CCR2, CCR3, and CXCR6 as potential causal genes for COVID-19 severity, emphasizing the critical role of chemokine receptors in disease progression (30).

Potential limitations of this study included the relatively small sample size, recruitment of patients from a single center, and short sampling window (up to 10 days from intubation) during a prolonged course of an acute illness.

This study confirmed that MCP-1 could be used to predict COVID-19 severity and showed that CCR2 may be a candidate biomarker for the prediction of disease severity. Considering that COVID-19 severity is affected by similar factors in studies conducted in other countries, our findings may be valid in other populations. Therefore, by measuring serum MCP-1 and CCR2 levels early, the disease course can be predicted, and necessary precautions can be taken before the disease becomes severe. In addition, by reducing the response to MCP-1 by using certain antagonists for CCR2 receptor blockade, increased inflammation and disease exacerbation can be prevented.

Ethics Committee Approval: Ethics committee approval was obtained for this study from the Kanuni Sultan Suleyman Training and Research Hospital (Date: 22.06.2022, No: 150).

Informed Consent: Signed consent was obtained from the participants.

Peer-review: Externally peer-reviewed.

Author Contributions: Conception/Design of Study- Selcuk D.; Data Acquisition- S.Z.M.K., E.K., S.Y., Seydanur D., Serkan D.; Data Analysis/Interpretation- Selcuk D., H.S.C.; Drafting Manuscript- Selcuk D.; Critical Revision of Manuscript- Selcuk D., Seydanur D., S.Z.M.K.; Final Approval and Accountability- Selcuk D., E.K., S.Y., Serkan D., H.S.C.; Technical or Material Support- H.S.C., U.M.K., Seydanur D., S.Z.M.K; Supervision- Selcuk D.

Conflict of Interest: All authors declare that they have no conflicts of interest.

Financial Disclosure: The authors declare that this study has received no financial support.

REFERENCES

1. Wang EY, Mao T, Klein J, Dai Y, Huck JD, Jaycox JR, et al. Diverse functional autoantibodies in patients with COVID-19. Nature 2021; 595(7866): 283-8.
2. Huang C, Wang Y, Li X, Ren L, Zhao J, Hu Y, et al. Clinical features of patients infected with 2019 novel coronavirus in Wuhan, China. Lancet 2020; 395(10223): 497-506.
3. Wang D, Hu B, Hu C, Zhu F, Liu X, Zhang J, et al. Clinical characteristics of 138 hospitalized patients with 2019 novel coronavirus-infected pneumonia in Wuhan, China. JAMA 2020; 323(11): 1061-69.
4. Frater JL, Zini G, d'Onofrio G, Rogers HJ. COVID-19 and the clinical hematology laboratory. Int J Lab Hematol 2020; 42(Suppl 1): 11-8.

5. Zhou F, Yu T, Du R, Fan G, Liu Y, Liu Z, et al. Clinical course and risk factors for mortality of adult inpatients with COVID-19 in Wuhan, China: a retrospective cohort study. Lancet 2020; 395(10229): 1054-62.
6. Nakeshbandi M, Maini R, Daniel P, Rosengarten S, Parmar P, Wilson C, et al. The impact of obesity on COVID-19 complications: a retrospective cohort study. Int J Obes (Lond) 2020; 44(9): 1832-7.
7. Wiersinga WJ, Rhodes A, Cheng AC, Peacock SJ, Prescott HC. Pathophysiology, transmission, diagnosis, and treatment of Coronavirus Disease 2019 (COVID-19): a review. JAMA 2020; 324(8): 782-93.
8. Teijaro JR, Walsh KB, Rice S, Rosen H, Oldstone MB. Mapping the innate signaling cascade essential for cytokine storm during influenza virus infection. Proc Natl Acad Sci U S A 2014; 111(10): 3799-804.
9. Macciò A, Oppi S, Madeddu C. COVID-19 and cytokine storm syndrome: can what we know about interleukin-6 in ovarian cancer be applied? J Ovarian Res 2021; 14(1): 28.
10. Zhao Y, Qin L, Zhang P, Li K, Liang L, Sun J, et al. Longitudinal COVID-19 profiling associates IL-1RA and IL-10 with disease severity and RANTES with mild disease. JCI Insight 2020; 5(13): e139834.
11. Chen Y, Wang J, Liu C, Su L, Zhang D, Fan J, et al. IP-10 and MCP-1 as biomarkers associated with disease severity of COVID-19. Mol Med 2020; 26(1): 97.
12. Blanco-Melo D, Nilsson-Payant BE, Liu WC, Uhl S, Hoagland D, Møller R, et al. Imbalanced host response to SARS-CoV-2 drives development of COVID-19. Cell 2020; 181(5): 1036-45.e9.
13. Rotondi M, Chiovato L, Romagnani S, Serio M, Romagnani P. Role of chemokines in endocrine autoimmune diseases. Endocr Rev 2007; 28(5): 492-520.
14. Deshmane SL, Kremlev S, Amini S, Sawaya BE. Monocyte chemoattractant protein-1 (MCP-1): an overview. J Interferon Cytokine Res 2009; 29(6): 313-26.
15. Fantuzzi L, Tagliamonte M, Gauzzi MC, Lopalco L. Dual CCR5/CCR2 targeting: opportunities for the cure of complex disorders. Cell Mol Life Sci 2019; 76(24): 4869-86.
16. Cabaro S, D'Esposito V, Di Matola T, Sale S, Cennamo M, Terracciano D, et al. Cytokine signature and COVID-19 prediction models in the two waves of pandemics. Sci Rep 2021; 11(1): 20793.
17. Ogawa H, Iimura M, Eckmann L, Kagnoff MF. Regulated production of the chemokine CCL28 in human colon epithelium. Am J Physiol Gastrointest Liver Physiol 2004; 287(5): G1062-9.
18. Sørensen TL, Tani M, Jensen J, Pierce V, Lucchinetti C, Folcik VA, et al. Expression of specific chemokines and chemokine receptors in the central nervous system of multiple sclerosis patients. J Clin Invest 1999; 103(6): 807-15.
19. Nelken NA, Coughlin SR, Gordon D, Wilcox JN. Monocyte chemoattractant protein-1 in human atheromatous plaques. J Clin Invest 1991; 88(4): 1121-7.
20. Li G, Fan Y, Lai Y, Han T, Li Z, Zhou P, et al. Coronavirus infections and immune responses. J Med Virol 2020; 92(4): 424-32.
21. Kawabata K, Hagio T, Matsuoka S. The role of neutrophil elastase in acute lung injury. Eur J Pharmacol 2002; 451(1): 1-10.
22. Peiris JS, Guan Y, Yuen KY. Severe acute respiratory syndrome. Nat Med 2004; 10(12 Suppl): 88-97.
23. Zhou J, Chu H, Li C, Wong BH, Cheng ZS, Poon VK, et al. Active replication of Middle East respiratory syndrome coronavirus and aberrant induction of inflammatory cytokines and chemokines in human macrophages: implications for pathogenesis. J Infect Dis 2014; 209(9): 1331-42.
24. Lin L, Lu L, Cao W, Li T. Hypothesis for potential pathogenesis of SARS-CoV-2 infection-a review of immune changes in patients with viral pneumonia. Emerg Microbes Infect 2020; 9(1): 727-32.
25. Bülow Anderberg S, Luther T, Berglund M, Larsson R, Rubertsson S, Lipcsey M, et al. Increased levels of plasma cytokines and correlations to organ failure and 30-day mortality in critically ill Covid-19 patients. Cytokine 2021; 138: 155389.
26. Dogan S, Mart Komurcu SZ, Korkmaz MD, Kaya E, Yavas S, Dogan S, et al. Effect of chemokine gene variants on Covid-19 disease severity. Immunol Invest 2022; 51(7): 1965-74.
27. Wu C, Chen X, Cai Y, Xia J, Zhou X, Xu S, et al. Risk factors associated with acute respiratory distress syndrome and death in patients with coronavirus disease 2019 pneumonia in Wuhan, China. JAMA Intern Med 2020; 180(7): 934-43.
28. Jafarzadeh A, Chauhan P, Saha B, Jafarzadeh S, Nemati M. Contribution of monocytes and macrophages to the local tissue inflammation and cytokine storm in COVID-19: lessons from SARS and MERS, and potential therapeutic interventions. Life Sci 2020; 257: 118102.
29. Sheahan T, Morrison TE, Funkhouser W, Uematsu S, Akira S, Baric RS, et al. MyD88 is required for protection from lethal infection with a mouse-adapted SARS-CoV. PLoS Pathog 2008; 4(12): e1000240.
30. Pairo-Castineira E, Clohisey S, Klaric L, Bretherick AD, Rawlik K, Pasko D, et al. Genetic mechanisms of critical illness in COVID-19. Nature 2021; 591(7848): 92-8.

Experimed 2023; 13(3): 281-289

ORIGINAL ARTICLE

DOI: 10.26650/experimed.1382282

Peroxisome Proliferator-activated Receptor-alpha (*PPARA*) and – Gamma (*PPARG*) Polymorphisms as Risk Factors for Dyslipidemia and MetS in Turkish Adults

Filiz Guclu-Geyik[1], Evrim Komurcu-Bayrak[1,2], Gunay Can[3], Nihan Erginel-Unaltuna[1]

[1]Department of Genetics, Aziz Sancar Institute of Experimental Medicine, Istanbul University, Istanbul, Turkiye
[2]Departments of Medical Genetics, Istanbul Faculty of Medicine, Istanbul University Istanbul, Turkiye
[3]Department of Public Health, Cerrahpasa Medical Faculty, Istanbul University-Cerrahpasa, Istanbul, Turkiye

ORCID ID: F.G.G. 0000-0003-4257-9930; E.K.B. 0000-0003-1271-1208; G.C. 0000-0001-5815-6700; N.E.U. 0000-0003-0562-0455

Cite this article as: Guclu-Geyik F, Komurcu-Bayrak E, Can G, Erginel-Unaltuna N. Peroxisome proliferator-activated receptor-alpha (*PPARA*) and – gamma (*PPARG*) Polymorphisms as risk factors for Dyslipidemia and MetS in Turkish adults. Experimed. Experimed 2023; 13(3): 281-289.

ABSTRACT

Objective: Dyslipidemia and metabolic syndrome (MetS) are complex diseases affected by environmental factors such as lifestyle and genetic predisposition. The genes encoding peroxisome proliferator-activated receptor-gamma (*PPARG*) and alpha (*PPARA*) are crucial in the development of dyslipidemia and MetS. We aimed to investigate the relation of these genes with dyslipidemia and MetS in the Turkish adult population.

Materials and Methods: The Turkish Adult Risk Factor (TARF-TEKHARF) cohort was randomly selected, and a cross-sectional analysis was performed. The *PPARA* rs1800206 C>G genotypes were determined in a sample of 339 unrelated Turkish adults by a polymerase chain reaction-restriction fragment length polymorphism (PCR-RFLP) and 12% polyacrylamide gel electrophoresis (PAGE) methods. The PPARG rs1801282 C>G genotypes were determined in a sample of 436 unrelated Turkish adults by a PCR-RFLP method.

Results: Both single nucleotide polymorphisms (SNPs) minor alleles were related to a risk of dyslipidemia. Logistic regression analysis showed a significantly increased risk for dyslipidemia in G allele carriers of rs1800206 C>G (Odds Ratio (OR)= 3.26; 95% CI= 1.16-9.12), and in G risk allele carriers of rs1801282 (OR= 1.85; 95% CI= 1.07-3.19), after adjustment for age, gender, lipid-lowering medication usage, physical activity and smoking status. Regarding MetS risk in the TARF study group, the G-allele of rs1800206 PPARA gene exhibited a significant OR of 3.75, after adjustment for gender, age, smoking status, and physical activity.

Conclusion: The G alleles of the studied SNPs in the *PPARA* and *PPARG* genes are related to increased dyslipidemia risk. Furthermore, The G allele of the *PPARA* gene is related to increased MetS risk.

Keywords: Dyslipidemia, metabolic syndrome, *PPARA*, *PPARG* and Turkish adults

INTRODUCTION

Cardiometabolic disorders are common public health issues, including metabolic syndrome (MetS), dyslipidemia, diabetes mellitus (DM), obesity, and hypertension (HT). The prevalence of MetS and dyslipidemia increases worldwide, with age and with changes in people's lifestyle (such as lack of physical activity and nutritional changes) in different ethnic groups and genders (1-4). MetS is a complicated disease characterized by the cluster co-existence of many cardiovascular risk factors. It is described by the co-instantaneous presence of abdominal obesity, disrupted glucose tolerance, atherogenic dyslipidemia, hypertension, and insulin resistance (5-7). This combination also leads to the development of DM and/or cardiovascular diseases (8). The dyslipidemia refers to a condition characterized by

Corresponding Author: Filiz Geyik **E-mail:** gfiliz@istanbul.edu.tr
Submitted: 27.10.2023 **Revision Requested:** 07.11.2023 **Last Revision Received:** 08.11.2023 **Accepted:** 01.12.2023

elevated levels of triglycerides (TG), total cholesterol (Total-C), low-density lipoprotein cholesterol (LDL-C), as well as low high-density lipoprotein cholesterol (HDL-C) levels. Environmental and genetic variables combine to determine the complicated etiology of dyslipidemia and MetS.

Members of the nuclear hormone receptor superfamily 1, peroxisome proliferator-activated receptors (PPARs) are transcription factors that are activated by ligands and play a crucial role in the regulation and continuation of energy balance (9,10). In humans, PPAR has three isotypes: PPAR-alpha (PPARα), PPAR-gamma (PPARγ) and PPAR-delta (PPARδ). These isotypes have various target genes, biological functions, and roles, and they each bind to different ligands. Each isotope is encoded by different genes. PPARα is encoded by the PPAR-alpha *(PPARA*) gene, which is located on human chromosome 22q12.2-13.1 (11). It affects carbohydrate and lipid metabolism through regulation of the expression of genes related to the transportation, β oxidation, and catabolism of triglycerides (12-14).

The PPAR-gamma (PPARG) gene, located on chromosome 3p25.2, modulates the transcription of several genes related to adipocyte separation and insulin-mediated glucose absorption in a variety of tissues (15). PPARγ controls glucose metabolism by lowering free fatty acids and increasing the activity of insulin (16).

Recently, a growing number of studies have shown that *PPARA* and *PPARG* gene polymorphisms may be genetic markers for complex diseases such as MetS, DM, obesity, and hyperlipidemia, which develop as a result of disorders of glucose and lipid metabolism. The Human *PPARA* and *PPARG* genes contain thousands of polymorphic loci, among them two exonic polymorphisms (rs1801282 and rs1800206) in *PPARG* and *PPARA* genes, respectively, were reported to be significantly associated with MetS, dyslipidemia, DM and obesity in different populations worldwide. The rs1801282 (also named rs1805192) polymorphism in *PPARG* gene is a C to G transversion at position 34 in exon 2 (NM_001354668.2, c.34C>G), leading to a substitution of alanine from proline at codon 12 (p.Pro12Ala), which has been shown to regulate the transcriptional activity of the *PPARG* (17) and is linked to distorted insulin sensitivity (18).

The rs1800206 missense polymorphism is located at position 484 in exon 5 (NM_005036.6, c.484C>G) of the *PPARA* gene and causes an amino acid change from leucine to valine at codon 162 (p.Leu162Val), which has functional effects on PPARα activity (19-22).

The associations between the rs1801282 and rs1800206 polymorphisms and their implications in MetS, dyslipidemia, obesity, DM, and HDL-C and LDL-C metabolism have been documented in Caucasian, Asian, and American populations, in several case-control, GWAS, and meta-analysis studies. However, the findings are still controversial (23-34). The influence of *PPARG* (rs1801282) and *PPARA* (rs1800206) polymorphisms, if any, on dyslipidemia and MetS is unknown for the Turkish adult population. As a result, we focused on examining the association between the rs1800206 C>G polymorphism at the *PPARA* and rs1801282 C>G polymorphism at the *PPARG* locus with dyslipidemia and MetS in the TARF study (TEKHARF), which is composed of Turkish adults.

MATERIALS AND METHODS

Study Subjects

The Turkish Adult Risk Factor Study (TARF-TEKHARF) design and methodology have previously been detailed (35). In summary, participants were chosen at random from residents of seven distinct locations in Turkiye and they participated in five surveys that were conducted between 2005 and 2009. A survey was used to collect information on the patient's prior history, as well as an assessment of the cardiovascular system and blood sampling.

The study encompassed unrelated individuals who provided a written agreement to take part in the investigation after being made aware of its purpose. *PPARG* and *PPARA* genotypes were examined in unselected individuals 436 and 339, respectively. The inclusion of different numbers of individuals in the study for two single nucleotide polymorphisms (SNPs) is due to the fact that 97 individuals could not be genotyped for *PPARA*. The Istanbul University Ethics Committee agreed to the study protocol (Date of last version: February 18, 2009/No:2005/446 and date of first version: May 04, 2005/No:2005/446).

Risk Variable Measurement

Obesity parameters (weight, height, waist circumference, and body mass index (BMI) calculation) and other variables (blood pressure, cigarette and alcohol use, physical activity) have previously been detailed (36).

Definitions

A body mass index of 30 kg/m^2 or more was considered obese. The combined presence of high triglyceride (>150 mg/dL) and low HDL-C (<40/<50 mg/dL; male/female) levels were referred to as dyslipidemia (37). A blood pressure reading of at least 140 mmHg over 90 mmHg, as well as the usage of antihypertensive medication, were considered hypertension.

According to the American Diabetes Association's guidelines (38), a person was diagnosed with diabetes if their plasma fasting glucose level was 126 mg/dL or their 2-hour postprandial glucose level was 200 mg/dL, and if they reported using diabetes medication now (39).

When three of the five National Cholesterol Education Program Adult Treatment Panel III (NCEP ATP III) criteria were identified, a person was diagnosed with MetS (37).

Genetic Analyses

SNPs Genotyping

The genomic DNA extraction method has been previously detailed (36). The *PPARA* rs1800206 C>G (Leu162Val) genotype was determined by polymerase chain reaction-restriction fragment length polymorphism (PCR-RFLP) and 12% polyacrylamide gel electrophoresis (PAGE) methods. The mismatch PCR technique was used to genotype the rs1800206 C>G polymorphism. The mutant allele primer was designed to have a HinfI restriction site that was removed in the presence of C at position 484. The sequences of the primers used were as follows: *PPARA* forward primer: 5′- ACT CAA GCT GGT GTA TGA CA -3′, *PPARA* reverse primer: 5′- TGTGTGACATCCCGACAGAAT -3′. When digesting the PCR product with HinfI, the mutant allele yields two fragments of 93 bp and 20 bp, while the normal allele yields a fragment of 113 bp in PAGE. PCR-RFLP was used for the *PPARG* rs1801282 C>G (Pro12Ala) genotype determination as previously reported (40).

Statistical Analyses

SPSS version 21 was used to perform all statistical analyses. Pearson's Chi-square test was used to compare genotype and allele distributions. To the expected genotype distribution, the Hardy Weinberg equilibrium (HWE) was calculated. A dominant model (specified as CC vs. CG+GG) was used to assess genotype-phenotype associations for both polymorphisms due to the small number of people with the GG genotype.

For categorical variables, the Chi-square test was applied, while two-tailed t-tests and analysis of variance tests were employed for continuous variables. Covariance analysis utilized logistic regression models. p-values <0.05 were considered significant.

RESULTS

PPARG rs1801282 and *PPARA* rs1800206 Genotypes and Allele Distribution

Table 1 describes the details of the genotyped SNPs, including genomic, cDNA and amino acid positions. *PPARA* and *PPARG* genes are located at chromosome positions 22q13 and 3p25, respectively. A genotype distribution of rs1801282 was found in 436 individuals of the TARF study cohort (Table 1). The minor allele frequency (MAF) of the rs1801282 G allele in the Turkish adults was 0.08 and the frequencies of genotypes were in HWE ($p > 0.05$).

The genotype distribution of the rs1800206 *PPARA* polymorphism was 95.6% (n=323), 4.7% (n=16) and 0% (n=0) for the CC, CG and GG genotypes respectively in the Turkish adults (n=339), the G allele frequency was 0.02 (Table 1). The genotype frequencies of the rs1800206 polymorphism were in HWE ($p > 0.05$).

Effects of the *PPARG* rs1801282 and *PPARA* rs1800206 Polymorphisms on Dyslipidemia and MetS

The distribution of the genotype frequencies of *PPARG* rs1801282 C>G between the groups of dyslipidemia and non-dyslipidemia were significantly different in the study group, with the genotypes CC+CG being more frequent in dyslipidemia compare with non-dyslipidemia individuals *(*p=0.043*)* (Table 2). Table 3 shows that, in logistic regression analysis, after adjusting for gender, age, lipid lowering medication usage, smoking status, and physical activity, the rs1801282 G allele has a strong association with dyslipidemia in the adult Turkish population. (OR=1.85, p=0.028).

The genotype frequencies of *PPARA rs1800206 C>G* polymorphism were obviously significantly different in individuals with both dyslipidemia and MetS in the TARF study population (p=0.023 and p=0.024, respectively), the

Table 1. Description, genotypic, and allelic frequencies of the two polymorphisms in PPARs genes studied in this study

Gene	Description of SNPs			Genotype frequency			Allele frequency		
	Genomic position	cDNA and amino acid position	rsID	CC % (n)	CG % (n)	GG % (n)	C %	G %	*p**
PPARG	chr3:12351626 (GRCh38.p14)	c. 34C>G (p.Pro12Ala)	rs1801282	83.4 (366)	15.9 (70)	0.7 (3)	0.9134	0.0866	0.8614
PPARA	chr22:46218377 (GRCh38.p14)	c.484C>G (p.Leu162Val)	rs1800206	95.3 (323)	4.7 (16)	0 (0)	0.9764	0.0236	0.6563

*Frequencies are computed using the Chi-square test

Table 2. Association analysis of the *PPARG* rs1801282 and *PPARA* rs1800206 genotypes with metabolic and clinical status, including risk factors for cardiovascular diseases.

Characteristics	***PPARG* rs1801282 (n=436)**			***PPARA* rs1800206 (n=339)**		
	Genotypes			**Genotypes**		
	CC	**CG +GG**	**p**	**CC**	**CG +GG**	**p**
Age (years)	51.32 ± 13.0 (366)	50.71 ± 12.4 (70)	0.722	51.27 ± 13.1 (323)	50.56 ± 12.2 (16)	0.835
Waist circumference (cm)	92.9 ± 12.3 (344)	94.5 ± 13.1 (69)	0.371	92.9 ± 12.5 (304)	97.0 ± 8.5 (16)	0.066
Body mass index (kg/m^2)	28.38 ± 4.7 (3339	29.38 ± 5.8 (66)	0.198	28.59 ± 4.8 (292)	29.11 ± 3.5 (169)	0.587
Systolic BP (mmHg)	129.83 ± 23.4 (345)	130.25 ± 20.2 (69)	0.880	129.41 ± 21.7 (305)	125.75 ± 15.5 (16)	0.382
Diastolic BP (mmHg)	82.32 ± 13.3 (345)	83.87 ± 13.0 (69)	0.378	82.53 ± 12.8 (305)	82.56 ± 13.7 (16)	0.993
Apolipoprotein A-I (mg/dL)	131.97 ± 28.8 (226)	126.27 ± 26.03 (48)	0.181	131.71 ± 28.18 (2129)	118.57 ± 38.9 (13)	0.253
Apolipoprotein B (mg/dL)	108.05 ± 34.2 (207)	112.57 ± 32.2 (44)	0.406	109.2 ± 33.8 (196)	115.5 ± 29.5 (12)	0.539
Total Cholesterol (mg/dL)	188.38 ± 41.7 (346)	187.58 ± 44.6 (69)	0.886	186.59 ± 40.6 (306)	200.2 ± 50.9 (16)	0.309
HDL-Cholesterol (mg/dL)	42.81 ± 12.6 (346)	40.38 ± 10.9 (69)	0.106	42.52 ± 12.6 (306)	39.17 ± 8.4 (16)	0.149
LDL-Cholesterol (mg/dL)	114.66 ± 35.3 (342)	114.95 ± 37.6 (69)	0.954	113.41 ± 33.9 (304)	126.46 ± 48.9 (16)	0.308
Triglycerides † (mg/dL)	128.8 ± 1.76 (346)	141.2 ± 1.69 (69)	0.232	128.8 ± 1.74 (306)	120.2 ± 1.72 (16)	0.263
C-reactive protein,† mg/L	2.23 ± 2.9 (221)	2.23 ± 4.4 (40)	0.971	2.23 ± 3.1 (209)	2.23 ± 1.6 (8)	0.598
Glucose (mg/dL)	100.53 ± 30.6 (336)	97.89 ± 27.9 (67)	0.349	101.5 ± 32.5 (305)	88.89 ± 10.5 (16)	**0.000**
Insulin (IU/L)	0.90 ± 0.292 (206)	1.00 ± 0.306 (46)	**0.044**	0.92 ± 0.296 (215)	0.87 ± 0.298 (10)	0.566
HOMA Index †	1.90 ± 1.61 (193)	2.34 ± 2.1 (45)	0.084	2.04 ± 2.1 (202)	1.54 ± 1.9 (10)	0.232
Clinical status **Prevalence, % (n)**						
Sex						
Male	49.7 (192)	44.3 (31)	0.404	94.4 (153)	5.5 (9)	0.488
Female	50.3 (184)	55.7 (39)		96.0 (170)	4.0 (7)	
Obesity						
No	83.8 (217)	16.2 (42)	0.812	95.0 (188)	5.0 (10)	0.878
Yes	82.8 (116)	17.1 (24)		94.5 (104)	5.5 (6)	
Type 2 Diabetes						
No	83.4 (322)	16.6 (64)	0.406	94.6 (284)	5.3 (16)	0.140

Yes	88 (44)	12 (6)		100.0 (39)	0.0 (0)	
Metabolic syndrome						
No	86.5 (192)	13.5 (30)	0.141	**97.8 (174)**	**2.2 (4)**	**0.024**
Yes	81.3 (174)	18.7 (40)		**92.5 (149)**	**7.5 (12)**	
Dyslipidemia						
No	**85.8 (248)**	**14.2 (41)**	**0.043**	**96.9 (216)**	**3.10 (7)**	**0.023**
Yes	**77.7 (98)**	**22.2 (28)**		**90.9 (90)**	**9.10 (9)**	
Hypertension						
No	84.3 (220)	15.7 (41)	0.810	96.1 (199)	3.9 (8)	0.353
Yes	83.4 (146)	16.6 (29)		93.9 (124)	6.1 (8)	
Diabetes medication usage	91.4 (32)	8.6 (3)	0.209	100 (25)	0.0 (0)	0.248
Lipid lowering medication usage	100 (17)	0.0 (0)	0.066	92.9 (15)	7.1 (1)	0.662
Alcohol consumption	5.8 (20)	11.6 (8)	0.081	5.6 (17)	6.3 (1)	0.909
Low Physical activity	31.3 (108)	21.7 (15)	0.112	27.2 (83)	43.8 (7)	0.151
Smoking status	44.0 (152)	42.0 (29)	0.765	42.9 (131)	43.75 (7)	0.651

Strong relationships are bolded and deemed significant at $p < 0.05$.

Dichotomous variables are shown as percentages, and continuous variables are shown as mean ± SD. Means were compared using a two-tailed t test, and percentages were compared using a chi-square test.

BP; blood pressure

† Log-transformed variables expressed in geometric values.

Table 3. Adjusted association by logistic regression of *PPARG* rs1801282 and *PPARA* rs1800206 genotypes with dyslipidemia and MetS.

Genotypes	Risk of Dyslipidemia		Risk of MetS	
	OR (95%CI)	p*	OR (95%CI)	p**
***PPARG*, rs1801282**				
CC (n=345)	1		1	
CG + GG (n=69)	**1.85 (1.070 - 3.197)**	**0.028**	1.46 (0.852 - 2.522)	0.168
***PPARA*, rs1800206**				
CC (n=305)	1		1	
CG + GG (n=16)	**3.26 (1.165 - 9.128)**	**0.024**	**3.75 (1.156 - 12.167)**	**0.028**

Odds ratios were calculated regarding the presence of the minor allele. CI: Confidence interval, OR: odds ratio, n: Number of individuals, p* age, gender, physical activity, currently smoking, lipid lowering medication usage, p** age, gender, physical activity, smoking status.

Table 4. Association analysis of the of *PPARG* rs1801282 and *PPARA* rs1800206 interaction with dyslipidemia and MetS.

	Dyslipidemia		MetS	
	p	**OR (95% CI)**	**p**	**OR (95% CI)**
Age	0.506	1.00 (0.98 - 1.02)	**0.003**	1.03 (1.01 - 1.05)
Gender	0.520	0.80 (0.42 - 1.54)	0.424	1.27 (0.70 - 2.32)
Smoking status	0.134	1.65 (0.85 - 3.18)	0.386	1.31 (0.76 - 2.45)
Physical activity	0.508	0.81 (0.44 - 1.49)	0.593	1.16 (0.66 - 2.06)
Rs1801282				
G allele	**0.020**	**2.09 (1.12 - 3.88)**	0.054	1.84 (0.99 - 3.46)
Rs1800206				
G allele	**0.025**	**3.29 (1.16 - 9.29)**	**0.028**	**3.76 (1.15 - 12.26)**

Odds ratios were calculated regarding the presence of the minor allele. CI: Confidence interval, OR: odds ratio, n: Number of individuals; strong relationships are bolded and deemed significant at $p < 0.05$

genotypes CG+GG being more common in dyslipidemia than in non-dyslipidemia individuals and in MetS than in non-MetS individuals (Table 2). The logistic regression analysis demonstrates a significant association between the rs1800206 G allele and dyslipidemia after adjusting for gender, age, smoking status, physical activity, and use of lipid-lowering medications (OR=3.26, p=0.024) (Table 3). In logistic regression analysis, the G-allele had a significant OR of 3.75 for MetS risk in the TARF population after adjustment for age, gender, physical activity and smoking status (p=0.028).

We further investigated a genotype interaction between *PPARG* rs1801282 C>G and *PPARA* rs1800206 C>G polymorphisms for the risk of dyslipidemia and MetS. The *PPARA* rs1800206 G allele showed a significant OR of 3.76 (p= 0.028) for the risk of MetS, and an OR of 3.29 (p=0.025) for the risk of dyslipidemia after adjustment for gender, age, physical activity, smoking status and *PPARG* rs1801282 G (Table 4). The *PPARG* rs1801282 G allele showed borderline significance for the risk of MetS (OR=1.84, p=0.054) and a significant risk for dyslipidemia (OR=2.09, p=0.020) after adjustment for gender, age, physical activity, smoking status and *PPARA* rs1800206 G (Table 4).

Effects of the *PPARG* rs1801282 and *PPARA* rs1800206 Polymorphisms on Metabolic Variables

We investigated the relation between *PPARGG rs1801282* C>G polymorphism and baseline characteristics (anthropometric and biochemical variables) of the TARF population (Table 2). In a crude analysis, there were no differences between HDL-C, LDL-C, total-C, triglycerides, C-reactive protein, glucose, HOMA index, apoB and apoA-1 concentrations and PPARG rs1801282 C>G genotypes, whereas there were substantial associations with insulin (p=0.044) (t-test). In analysis of covariance (ANCOVA) analysis, those with the CG+GG genotype did not exhibit significantly higher insulin levels (mean ± SD, 1.00 ± 0.306) compared with the CC carriers (mean ± SD, 0.90 ± 0.292) when adjusted for gender, age, smoking status, DM medication usage and physical activity (p>0.05).

We examined the relationship between the *PPARA* gene's rs1800206 C>G polymorphism and anthropometric and biochemical factors in the TARF population. A crude analysis revealed no differences with other variables, although there were statistically significant relationships with fasting glucose levels (p<0.001). When gender, age, physical activity, smoking status, and use of diabetes medication were taken into account, the significance of this association with regard to glucose concentrations was lost (p>0.05).

DISCUSSION

The relationships between the *PPARA rs1800206* C>G and *PPARG* rs1801282 C>G polymorphisms with MetS and dyslipidemia were examined in this population-based cross-sectional study using data from the Turkish adult representative TARF study. In Turkish adults, while carriage of the G allele of *PPARA* rs1800206 C>G polymorphism had exhibited significantly elevated risk for dyslipidemia (OR=3.26) and MetS (OR=3.75), carriage of the G allele of *PPARG* rs1801282 C>G polymorphism indicated significantly elevated risk only for dyslipidemia (OR=1.85).

The study's findings on the MAF of the *PRARA* gene rs1800206 C>G and PPARG rs1801282 C>G polymorphisms (2% and 8%, respectively) are comparable to those found in the 1000 Genomes Phase 3 combined population (https://www.internationalgenome.org /1000-genomes-browsers/index.html (last accessed July 2023). The minor G allele of the rs1800206 polymorphism shows a similar distribution among several populations (1-6% in African, South Asian, American, and European populations), but it has not been observed in East Asians. The distribution of the minor G allele of the rs1801282 polymorphism is similar in American, European and South Asian populations (12%), but is lower in African (1%) and East Asian (3%) populations. The MAF obtained for the two polymorphisms in this study was lower than in European populations.

Previous research has found conflicting associations between dyslipidemia or phenotypes associated with dyslipidemia and the rs1800206 C>G polymorphism of the *PPARA* gene. Bage et.al. found no significant association between rs1800206 C>G polymorphism of the *PPARA* gene and diabetic dyslipidemia among the South Indian population (30).

Gu et al. found that the G allele of rs1800206 was linked to an increased risk of dyslipidemia in 192 dyslipidemic patients compared to 628 controls in the Chinese Han population (28). In a similar study, Mazzotti et al. also found an association between the *PPARA* rs1800206 polymorphism and dyslipidemia in the 570 adult/elderly cohort from Cuiaba City (Brazilian populations) (24). Additionally, an association between rs1800206 C>G polymorphism and hypertriglyceridemia have been reported by Gu et al. in the 346 hypertriglyceridemia and 474 non-hypertriglyceridemia subjects from the prevention of MetS and multi-metabolic disorders in Jiangsu Province of China Study (26). In a Lithuanian study, it has been found that the CG genotype of the rs1800206 C>G polymorphism is associated with higher TG levels only in men with dyslipidemia (34). In diabetic patients, *PPARA* rs1800206 G allele carriers had higher HDL, apoA1, total cholesterol, and cholesterol (21). Our findings are in accordance with these positive results. The G allele of the *PPARA* rs1800206 C>G polymorphism increases the risk of dyslipidemia by 3.26-fold, regardless of age, gender, smoking status, physical activity and lipid-lowering medication usage in the adult Turkish population. PPARα activates proteins that control the binding and transport of fatty acids, and it controls genes involved in fatty acid oxidation (41) Consequently, it has been hypothesized that the rs1800206 polymorphism located in the *PPARA* gene's DNA binding domain might influence lipid metabolism, specifically TG levels (42).

The *PPARA* rs1800206 C>G polymorphism is strongly linked to the risk of MetS in addition to contributing to the development of dyslipidemia. MetS is characterized by abdominal obesity, glucose intolerance and dyslipidemia (5-7).

According to Robitaille et al., there may be a higher chance of developing certain components of the metabolic syndrome in carriers of the *PPARA* rs1800206 G allele. This suggests that the rs1800206 C>G polymorphism could regulate the relationship between dietary fat intake and abdominal obesity (29). Utjurraltta et al., identified an association between high TG and low HDL, both of which are components of the metabolic syndrome (43), and Smalinskiene et al., also found a relationship with TG as well (34). The majority of the r studies discussed above focus on the relationship between MetS components and the *PPARA* rs1800206 C>G polymorphism. Research exploring the link of this polymorphism with MetS revealed no association in the Malaysian population (31). Our study firstly examined the influence of *PPARA* rs1800206 C>G polymorphism on MetS in Turkish adults. Here, we find an independent relationship between the rs1800206 C>G polymorphism and MetS in adult Turkish individuals with an OR of 3.75.

Several studies evaluated genetic contributions of the *PPARG* rs1801282 C>G polymorphism to dyslipidemia and MetS. Results for dyslipidemia and MetS have been inconsistently associated with the *PPARG* rs1801282 C>G polymorphism. Gu et al. reported that the CG and GG genotypes of rs1801282 were associated with dyslipidemia (OR=1.77 and OR=2.96, respectively) in a Chinese Han population (28). In accordance with this positive finding, our results showed association between GG genotype of this polymorphism and dyslipidemia in Turkish adults (OR=1.85). In contrast, the absence of association of the rs1801282 genotypes with diabetic dyslipidemia among South Indian patients was reported by Bage et al. (30). Barbieri et al., discovered an inverse relationship between blood TG concentrations and the G allele of rs1801282 in Caucasian participants (44). Additionally, it has been demonstrated that the G allele is linked to decreased serum total HDL levels in a Japanese population (45). Gu et al., reported the association of the GG carrier genotype of *PPARG* rs1801282 and hypertriglyceridemia in MetS (27).

Studies investigating the association between *PPARG* rs1801282 C>G polymorphism and the risk of MetS in several populations have been inconsistent. According to Tellechea et al., those with the rs1801282 G allele, particularly non-smokers, are more likely to develop MetS and insulin resistance (46). Furthermore, compared to CC homozygotes, G carriers had greater BMI, waist circumference, and fat mass in The Québec Family Study, indicating that this polymorphism may be able to modify the relationship between dietary fat intake and elements of the MetS (47). Meirhaeghe et al., showed no link between the *PPARG* rs1801282 C>G polymorphism and MetS in a large French population (48). *PPARG* rs1801282 C>G polymorphism was not directly linked to MetS, according to Yang et al.'s study that included 423 individuals with MetS and families without the condition (49). Consistent with these results, middle-aged Swedish individuals who carried the G allele in the *PPARG* gene did not exhibit statistically significant differences in fasting glucose, TG, HDL-cholesterol, waist circumference, or blood pressure when compared to GG homozygotes (50). This suggests that the rs1801282 polymorphism in the *PPARG* gene does not play a significant role in determining the prevalence of MetS. Even after stratifying by ethnicity and MetS component, a meta-analysis of ten case-control studies revealed no statistically significant association between the rs1801282 polymorphism and MetS (51). In our study, no significant difference was observed in the distribution of *PPARG* rs1801282 genotypes in MetS, but the rs1801282 G allele confers a borderline risk for MetS independent from the *PPARA* rs1800206 G allele. We suggest that differences in association studies may be caused by the effects of other genes and variations in gender, physical activity, BMI, ethnicity, sample size, and study methodology.

The study contains limitations and strengths. One limitation of this study is the absence of information in our investigation regarding potential interactions between other genetic variations and *PPARA* and *PPARG* genotypes. Another limitation is that we are unable to analyze the two sexes independently due to the small sample size. The primary strength of this research is its population-based design, which enables assessment of the genetic and environmental influences on the relevant phenotypic.

To conclude, this study demonstrated that the *PPARA* rs1800206 and *PPARG* rs1801282 C>G polymorphisms were associated in Turkish adults with increased dyslipidemia risk, independent

of age, gender, physical activity, lipid-lowering medication usage and smoking status. The G allele of rs1800206 *PPARA,* which is a significant risk factor for MetS, is the stronger risk factor for dyslipidemia than the G allele of rs1801282 *PPARG*. Furthermore, *PPARA* rs1800206 polymorphism increases the risk of MetS. This association requires additional studies in large, well-characterized study populations.

Ethics Committee Approval: The Istanbul University Ethics Committee agreed to the study protocol (Date of last version: February 18, 2009/No:2005/446 and date of first version: May 04, 2005/No:2005/446).

Informed Consent: Signed consent was obtained from the participants.

Peer-review: Externally peer-reviewed.

Author Contributions: Conception/Design of Study- F.G.; Data Acquisition- F.G.; Data Analysis/Interpretation- G.C., Drafting Manuscript- F.G.; Critical Revision of Manuscript- E.K.B., N.E.U.; Final Approval and Accountability- F.G., E.K.B., G.C., N.E.U.

Conflicts of Interests: The authors declare that they have no competing interest.

Financial Disclosure: This study was supported by the Scientific and Technological Research Council of Turkiye (TUBITAK Project number: SBAG-3091). Turkish Society of Cardiology and the pharmaceutical companies AstraZeneca, Pfizer, and Sanofi-Aventis (Istanbul) have financially supported the Turkish Adult Risk Factor study.

REFERENCES

1. Hildrum B, Mykletun A, Hole T, Midthjell K, Dahl AA. Age-specific prevalence of the metabolic syndrome defined by the International Diabetes Federation and the National Cholesterol Education Program: the Norwegian HUNT 2 study. BMC Public Health 2007; 7: 220.
2. Ge H, Yang Z, Li X, Liu D, Li Y, Pan Y, et al. The prevalence and associated factors of metabolic syndrome in Chinese aging population. Sci Rep 2020; 10(1): 20034.
3. Milionis HJ, Elisaf MS, Mikhailidis DP. Lipid abnormalities and cardiovascular risk in the elderly. Curr Med Res Opin 2008; 24(3): 653-7.
4. Ford ES, Giles WH, Dietz WH. Prevalence of the metabolic syndrome among US adults: findings from the third National Health and Nutrition Examination Survey. JAMA 2002; 287(3): 356-9.
5. Despres JP, Lemieux I. Abdominal obesity and metabolic syndrome. Nature 2006; 444(7121): 881-7.
6. Bosy-Westphal A, Onur S, Geisler C, Wolf A, Korth O, Pfeuffer M, et al. Common familial influences on clustering of metabolic syndrome traits with central obesity and insulin resistance: the Kiel obesity prevention study. Int J Obes (Lond) 2007; 31(5): 784-90.
7. Grundy SM, Hansen B, Smith SC Jr, Cleeman JI, Kahn RA, American Heart A, et al. Clinical management of metabolic syndrome: report of the American Heart Association/National Heart, Lung, and Blood Institute/American Diabetes Association conference on scientific issues related to management. Arterioscler Thromb Vasc Biol 2004; 24(2): e19-24.
8. Onat A, Hergenc G, Turkmen S, Yazici M, Sari I, Can G. Discordance between insulin resistance and metabolic syndrome: features and associated cardiovascular risk in adults with normal glucose regulation. Metabolism 2006; 55(4): 445-52.
9. Braissant O, Foufelle F, Scotto C, Dauca M, Wahli W. Differential expression of peroxisome proliferator-activated receptors (PPARs): tissue distribution of PPAR-alpha, -beta, and -gamma in the adult rat. Endocrinology 1996; 137(1): 354-66.
10. Tugwood JD, Issemann I, Anderson RG, Bundell KR, Mcpheat WL, Green S. The mouse peroxisome proliferator activated receptor recognizes a response element in the 5' flanking sequence of the rat acyl coa oxidase gene. Embo Journal 1992; 11(2): 433-9.
11. Sher T, Yi HF, McBride OW, Gonzalez FJ. cDNA cloning, chromosomal mapping, and functional characterization of the human peroxisome proliferator activated receptor. Biochemistry 1993; 32(21): 5598-604.
12. Xu J, Xiao G, Trujillo C, Chang V, Blanco L, Joseph SB, et al. Peroxisome proliferator-activated receptor alpha (PPARalpha) influences substrate utilization for hepatic glucose production. J Biol Chem 2002; 277(52): 50237-44.
13. Leone TC, Weinheimer CJ, Kelly DP. A critical role for the peroxisome proliferator-activated receptor alpha (PPARalpha) in the cellular fasting response: the PPARalpha-null mouse as a model of fatty acid oxidation disorders. Proc Natl Acad Sci USA 1999; 96(13): 7473-8.
14. Lefebvre P, Chinetti G, Fruchart JC, Staels B. Sorting out the roles of PPAR alpha in energy metabolism and vascular homeostasis. J Clin Invest 2006; 116(3): 571-80.
15. Carmona MC, Louche K, Lefebvre B, Pilon A, Hennuyer N, Audinot-Bouchez V, et al. S 26948: a new specific peroxisome proliferator activated receptor gamma modulator with potent antidiabetes and antiatherogenic effects. Diabetes 2007; 56(11): 2797-808.
16. Burns KA, Vanden Heuvel JP. Modulation of PPAR activity via phosphorylation. Biochim Biophys Acta 2007; 1771(8): 952-60.
17. Deeb SS, Fajas L, Nemoto M, Pihlajamaki J, Mykkanen L, Kuusisto J, et al. A Pro12Ala substitution in PPARgamma2 associated with decreased receptor activity, lower body mass index and improved insulin sensitivity. Nat Genet 1998; 20(3): 284-7.
18. Ek J, Andersen G, Urhammer SA, Hansen L, Carstensen B, Borch-Johnsen K, et al. Studies of the Pro12Ala polymorphism of the peroxisome proliferator-activated receptor-gamma2 (PPAR-gamma2) gene in relation to insulin sensitivity among glucose tolerant caucasians. Diabetologia 2001; 44(9): 1170-6.
19. Sapone A, Peters JM, Sakai S, Tomita S, Papiha SS, Dai R, et al. The human peroxisome proliferator-activated receptor alpha gene: identification and functional characterization of two natural allelic variants. Pharmacogenetics 2000; 10(4): 321-33.
20. Vohl MC, Lepage P, Gaudet D, Brewer CG, Betard C, Perron P, et al. Molecular scanning of the human PPAR alpha gene: association of the L162V mutation with hyperapobetalipoproteinemia. J Lipid Res 2000; 41(6): 945-52.
21. Flavell DM, Torra IP, Jamshidi Y, Evans D, Diamond JR, Elkeles RS, et al. Variation in the PPAR alpha gene is associated with altered function in vitro and plasma lipid concentrations in Type II diabetic subjects. Diabetologia 2000; 43(5): 673-80.
22. Flavell DM, Jamshidi Y, Hawe E, Pineda Torra I, Taskinen MR, Frick MH, et al. Peroxisome proliferator-activated receptor alpha gene variants influence progression of coronary atherosclerosis and risk of coronary artery disease. Circulation 2002; 105(12): 1440-5.
23. Sarhangi N, Sharifi F, Hashemian L, Hassani Doabsari M, Heshmatzad K, Rahbaran M, et al. PPARG (Pro12Ala) genetic variant and risk of T2DM: a systematic review and meta-analysis. Sci Rep 2020; 10(1): 12764.

24. Mazzotti DR, Singulane CC, Ota VK, Rodrigues TP, Furuya TK, de Souza FJ, et al. PPARalpha polymorphisms as risk factors for dyslipidemia in a Brazilian population. Mol Genet Metab 2011; 102(2): 189-93.
25. Li S, He C, Nie H, Pang Q, Wang R, Zeng Z, et al. G Allele of the rs1801282 polymorphism in PPARgamma gene confers an increased risk of obesity and hypercholesterolemia, while T allele of the rs3856806 polymorphism displays a protective role against dyslipidemia: a systematic review and meta-analysis. Front Endocrinol (Lausanne) 2022; 13: 919087.
26. Gu SJ, Liu MM, Guo ZR, Wu M, Chen Q, Zhou ZY, et al. Gene-gene interactions among PPARalpha/delta/gamma polymorphisms for hypertriglyceridemia in Chinese Han population. Gene 2013; 515(2): 272-6.
27. Gu SJ, Guo ZR, Zhou ZY, Hu XS, Wu M, Zhang N. Peroxisome proliferator-activated receptor gamma polymorphisms as risk factors for dyslipidemia. Mol Med Rep 2014; 10(5): 2759-63.
28. Gu SJ, Guo ZR, Zhou ZY, Hu XS, Wu M. PPAR alpha and PPAR gamma polymorphisms as risk factors for dyslipidemia in a Chinese Han population. Lipids Health Dis. 2014; 13: 23.
29. Robitaille J, Brouillette C, Houde A, Lemieux S, Perusse L, Tchernof A, et al. Association between the PPARalpha-L162V polymorphism and components of the metabolic syndrome. J Hum Genet 2004; 49(9): 482-9.
30. Bage IJ, Kamalanathan S, Selvarajan S, Sahoo J, Mathaiyan J, Naik D. Peroxisome proliferator-activated receptor alpha and gamma gene polymorphisms among South Indian patients with diabetic dyslipidaemia. Indian J Endocrinol Metab 2023; 27(2): 118-26.
31. Chia PP, Fan SH, Say YH. Screening of peroxisome proliferator-activated receptors (PPARs) alpha, gamma and alpha gene polymorphisms for obesity and metabolic syndrome association in the multi-ethnic Malaysian population. Ethn Dis 2015; 25(4): 383-90.
32. Mousavinasab F, Tahtinen T, Jokelainen J, Koskela P, Vanhala M, Oikarinen J, et al. The Pro12Ala polymorphism of the PPAR gamma 2 gene influences sex hormone-binding globulin level and its relationship to the development of the metabolic syndrome in young Finnish men. Endocrine 2006; 30(2): 185-90.
33. Rhee EJ, Oh KW, Lee WY, Kim SY, Oh ES, Baek KH, et al. Effects of two common polymorphisms of peroxisome proliferator-activated receptor-gamma gene on metabolic syndrome. Arch Med Res 2006; 37(1): 86-94.
34. Smalinskiene A, Petkeviciene J, Luksiene D, Jureniene K, Klumbiene J, Lesauskaite V. Association between APOE, SCARB1, PPARalpha polymorphisms and serum lipids in a population of Lithuanian adults. Lipids Health Dis 2013; 12: 120.
35. Onat A. Risk factors and cardiovascular disease in Turkey. Atherosclerosis 2001; 156(1): 1-10.
36. Guclu-Geyik F, Coban N, Can G, Erginel-Unaltuna N. The rs2175898 polymorphism in the ESR1 Gene has a significant sex-specific effect on obesity. Biochem Genet 2020; 58(6): 935-952.
37. Expert Panel on Detection, Evaluation, and Treatment of High Blood Cholesterol in Adults. Executive summary of the third report of The National Cholesterol Education Program (NCEP) expert panel on detection, evaluation, and treatment of high blood cholesterol in adults (Adult Treatment Panel III). JAMA 2001; 285(19): 2486-97.
38. American Diabetes Association. 2. Classification and diagnosis of diabetes: standards of medical care in diabetes-2020. Diabetes Care 2020; 43(Suppl 1): S14-31.
39. Expert Committee on the Diagnosis and Classification of Diabetes Mellitus. Report of the expert committee on the diagnosis and classification of diabetes mellitus. Diabetes Care 2003; 26 Suppl 1: S5-20.
40. Yen CJ, Beamer BA, Negri C, Silver K, Brown KA, Yarnall DP, et al. Molecular scanning of the human peroxisome proliferator activated receptor gamma (hPPAR gamma) gene in diabetic Caucasians: identification of a Pro12Ala PPAR gamma 2 missense mutation. Biochem Biophys Res Commun 1997; 241(2): 270-4.
41. Schoonjans K, Staels B, Auwerx J. Role of the peroxisome proliferator-activated receptor (PPAR) in mediating the effects of fibrates and fatty acids on gene expression. J Lipid Res 1996; 37(5): 907-25.
42. Sparso T, Hussain MS, Andersen G, Hainerova I, Borch-Johnsen K, Jorgensen T, et al. Relationships between the functional PPARalpha Leu162Val polymorphism and obesity, type 2 diabetes, dyslipidaemia, and related quantitative traits in studies of 5799 middle-aged white people. Mol Genet Metab 2007; 90(2): 205-9.
43. Uthurralt J, Gordish-Dressman H, Bradbury M, Tesi-Rocha C, Devaney J, Harmon B, et al. PPARalpha L162V underlies variation in serum triglycerides and subcutaneous fat volume in young males. BMC Med Genet 2007; 8:55.
44. Barbieri M, Rizzo MR, Papa M, Acampora R, De Angelis L, Olivieri F, et al. Role of interaction between variants in the PPARG and interleukin-6 genes on obesity related metabolic risk factors. Exp Gerontol 2005; 40(7): 599-604.
45. Iwata E, Matsuda H, Fukuda T, Fukuen S, Motomura T, Igarashi T, et al. Mutations of the peroxisome proliferator-activated receptor gamma (PPAR gamma) gene in a Japanese population: the Pro12Ala mutation in PPAR gamma 2 is associated with lower concentrations of serum total and non-HDL cholesterol. Diabetologia 2001; 44(10): 1354-5.
46. Tellechea ML, Aranguren F, Perez MS, Cerrone GE, Frechtel GD, Taverna MJ. Pro12Ala polymorphism of the peroxisome proliferatoractivated receptor-gamma gene is associated with metabolic syndrome and surrogate measures of insulin resistance in healthy men: interaction with smoking status. Circ J 2009; 73(11): 2118-24.
47. Robitaille J, Despres JP, Perusse L, Vohl MC. The PPAR-gamma P12A polymorphism modulates the relationship between dietary fat intake and components of the metabolic syndrome: results from the Quebec Family Study. Clin Genet 2003; 63(2): 109-16.
48. Meirhaeghe A, Amouyel P. Impact of genetic variation of PPARgamma in humans. Mol Genet Metab 2004; 83(1-2): 93-102.
49. Yang LL, Hua Q, Liu RK, Yang Z. Association between two common polymorphisms of PPARgamma gene and metabolic syndrome families in a Chinese population. Arch Med Res 2009; 40(2): 89-96.
50. Montagnana M, Fava C, Nilsson PM, Engstrom G, Hedblad B, Lippi G, et al. The Pro12Ala polymorphism of the PPARG gene is not associated with the metabolic syndrome in an urban population of middle-aged Swedish individuals. Diabet Med 2008; 25(8): 902-8.
51. Zhang R, Wang J, Yang R, Sun J, Chen R, Luo H, et al. Effects of Pro12Ala polymorphism in peroxisome proliferator-activated receptor-gamma2 gene on metabolic syndrome risk: a meta-analysis. Gene 2014; 535(1): 79-87.

Experimed 2023; 13(3): 290-297

ORIGINAL ARTICLE

DOI: 10.26650/experimed.1383105

Stem Cell Mobilization Efficiency and Engraftment Kinetics in Patients with Hematologic Malignancies Undergoing Autologous Stem Cell Transplantation: A Retrospective Cohort Study*

Nuri Baris Hasbal[1], Mutlu Arat[2]

[1]Department of Internal Medicine, Division of Nephrology, School of Medicine, Koc University, Istanbul, Turkiye
[2]Hematopoietic SCT Unit, Istanbul Florence Nightingale Hospital, Demiroglu Bilim University, Istanbul, Turkiye

ORCID ID: N.B.H. 0000-0002-2229-5140; M.A. 0000-0003-2039-8557

Cite this article as: Hasbal NB, Arat M. Stem cell mobilization efficiency and engraftment kinetics in patients with hematologic malignancies undergoing autologous stem cell transplantation: a retrospective cohort study. Experimed. Experimed 2023; 13(3): 290-297.

ABSTRACT

Objective: This study aimed to conduct a retrospective evaluation of clinical findings on patients undergoing autologous hematopoietic stem cell transplantation.

Materials and Methods: A total of 167 consecutive patients who were diagnosed with multiple myeloma (MM) and lymphoma and then underwent autologous hematopoietic stem cell transplantation (AHSCT) between August 2010 and May 2013 were included in our study. Demographic, disease, mobilization, apheresis, and transplantation data were reviewed from patient files.

Results: In 121 patients (72%), mobilization was achieved solely with granulocyte colony stimulating factor (G-CSF). There was no relationship between peripheral $CD34^+$ cell count and age, disease type, or previous treatment features. The total $CD34^+$ cell count post-apheresis was $3.3 \pm 3.1 \times 10^6$/kg. Only nine patients could not achieve successful mobilization with any regimen. The median day of neutrophil and platelet engraftment among the entire patient group was 11 days. As the number of $CD34^+$ cells infused into patients increased, neutrophil and platelet engraftment time decreased.

Conclusion: Mobilization was achieved in most MM cases and at least two-thirds of lymphomas using G-CSF alone. Age and body weight did not affect mobilization success. Clinicians should increase successful mobilizations on the first day of the apheresis and prescribe AHSCT at appropriate times to avoid excessive cycles of chemotherapy.

Keywords: Mobilization, apheresis, autologous stem cell transplantation, high-dose chemotherapy

INTRODUCTION

Multiple myeloma (MM) is the malignant proliferation of plasma cells originating from a single clone. It may manifest as a range of organ dysfunctions, bone pain, fractures, kidney failure, susceptibility to infections, anemia, hypercalcemia, coagulation abnormalities, neurological symptoms, and signs of hyperviscosity (1). In these cancers, immune cells differentiate at various stages, leading to a broad spectrum in morphological, immunological, and clinical presentations that range from indolent to aggressive. Cancers of the lymphatic system often present as leukemia, which primarily involves bone marrow and peripheral blood, whereas others are lymphoma, solid tumors of the immune system (2). In MM, autologous hematopoietic stem cell transplantation (AHSCT) supported by high-dose chemotherapy remains

*This article is extracted from Nuri Baris Hasbal's thesis of specialization in Internal Medicine supervised by Prof. Dr. Mutlu Arat with the Council of Higher Education Thesis Center number 341811.

Corresponding Author: Nuri Baris Hasbal **E-mail:** nhasbal@ku.edu.tr
Submitted: 30.10.2023 **Revision Requested:** 15.11.2023 **Last Revision Received:** 22.11.2023 **Accepted:** 01.12.2023

the standard treatment for patients under 65 years old and those from 65–75 years old who respond well to induction therapy (3). Previous studies have suggested that AHSCT followed by high-dose chemotherapy or immunotherapy is an appropriate treatment option for relapsed cases of chemotherapy-sensitive patients with diffuse large B-cell lymphomas as well as refractory/relapsed Hodgkin patients (4, 5).

Hematopoietic stem cells (HSCs) are a unique subset of cells within the hematopoietic system that can differentiate into any blood cell type while maintaining their capacity for self-renewal. Studies revealed increased numbers of HSCs in peripheral blood during post-chemotherapy recovery, suggesting their role in hematopoietic regeneration. It was found in the 1980s that peripheral HSCs contribute significantly to full hematopoietic recovery following myeloablative therapy, informing future stem cell studies.

There are three different types of hematopoietic stem cell transplantations (HSCTs): Allogeneic HSCT uses healthy blood stem cells from a donor or cord blood stem cell source. Syngeneic HSCT relies on blood stem cells from an identical twin, where both the donor and recipient are monozygotic. Autologous HSCT, on the other hand, collects HSCs from a patient that are subsequently re-transplanted into the same individual.

Administration of granulocyte colony-stimulating factor (G-CSF) or granulocyte–macrophage colony stimulating factor (GM-CSF) alone increases the number of HSCs in peripheral blood, a process called stem cell mobilization; chemomobilization relies on chemotherapy/chemotherapy followed by cytokine administration (G-CSF) or G-CSF in combination with plerixafor, a selective C-X-C chemokine receptor type 4 (CXCR4) antagonist. These agents synergistically elevate the number of circulating HSCs, which can be collected through apheresis (6), a critical step in stem cell transplantation in which blood components are separated and desired cells are collected. Equipment and methods such as filtration and centrifugation have been developed to optimize these steps and obtain purer stem cell products. For example, filtration utilizes differences in cell density to isolate and separate blood components (7). Ultimately, the success of AHSCT-supported high-dose chemotherapy depends on the quantity and viability of cells collected through apheresis. Generally, at least 2×10^6 $CD34^+$ cells/kg must be collected for complete and rapid hematopoietic recovery. Moreover, a product with $>5 \times 10^6$ $CD34^+$ cells/kg accelerates neutrophil and platelet engraftment while reducing hospitalization and costs (8).

Retrospective studies can show how patients respond to treatment and how disease progresses over time. The current study aims to fulfill several objectives in the Hematology Unit's apheresis facility: conduct a retrospective evaluation of patients undergoing treatment for Hodgkin's lymphoma (HL), non-Hodgkin's lymphoma (NHL), and MM; assess the accurate and effective applicability of international treatment protocols; optimize patient outcomes; and recommend ways to improve standard treatments .

MATERIALS AND METHODS

Study Group

This study was conducted at the Hematopoietic Stem Cell Transplantation Unit of Demiroglu Bilim University, Sisli Florence Nightingale Hospital. The study included patients diagnosed with HL, NHL, or MM between August 2010 and May 2013. This study was approved by the Demiroglu Bilim University Clinical Research Ethics Committee on April 11, 2013 (44140529/2013-036). These patients were either referred to our center for AHSCT or were already undergoing treatment for the same diagnoses at our hospital. Patients over the age of 18 who had an indication for AHSCT were consecutively included in the study. Patients who were diagnosed with a cancer other than lymphomas or MM, underwent HSCT collection at an external center and received AHSCT at our hospital, or were under 18 years old were not included in the study. Patients whose cells were to be cryopreserved after apheresis were included in apheresis kinetic studies but not in engraftment kinetic analyses. Demographics, disease characteristics (stage, chemotherapy, radiotherapy), mobilization (mobilization regimens: G-CSF alone, G-CSF and chemotherapy, G-CSF and plerixafor; total G-CSF dose used, number of days G-CSF was used), apheresis data (catheter) type, device type, peripheral CD34 positive ($pCD34^+$) cell count, apheresis date, total blood volume processed, processed blood volume, anti-coagulation, procedure duration, pre-apheresis leukocyte count, pre-apheresis mononuclear cells count, post-apheresis $CD34^+$ cell count, post-apheresis mononuclear cell count, product volume, total dimethyl sulfoxide (DMSO) content, and transplant data (conditioning regimen, number of infusion days, infused $CD34^+$ cell count, bag count, infused volume, neutrophil and platelet engraftment date) were recorded for each patient. Bedside apheresis procedures were conducted using two different continuous-flow apheresis devices: the Spectra Optia Apheresis System (Caridian BCT Inc., Lakewood CO, USA) and the Fresenius COM.TEC (Fresenius Kabi, Freidberg, Germany). The Spectra Optia Collection Set and the Fresenius P1Y-P1YA sets were utilized through apheresis. Patients were classified based on their body mass index (BMI) as underweight (below 20 kg/m^2), normal weight (20–25.9 kg/m^2), overweight (26–29.9 kg/m^2), or obese (above 30 kg/m^2). Supplementary Table 1 shows the formulas used to calculate BMI and other indices (Ideal Body Weight, IBW; Actual Body Weight, ABW; and Adjusted Ideal Body Weight, AdjIBW).

Quantification and Characterization of $pCD34^+$ Cells

A complete blood count was performed on peripheral blood samples from patients using the Sysmex XT-2000i Automatic Hematology Analyzer, and leukocyte counts were verified using a Thoma cell counting chamber.

To analyze pCD34$^+$ cells, whole blood staining was performed using anti-human phycoerythrin (PE) (BD Biosciences, USA) and anti-human CD45 fluorescein isothiocyanate (FITC) (BD Biosciences, USA) monoclonal antibodies (100 µL of whole blood and 10 µL of each monoclonal antibody). The prepared mixture was incubated in the dark at room temperature for 20 minutes, followed by the addition of 2 mL of FACS™ lysing solution (BD Biosciences, USA) 10x concentrate for another 15-minute incubation in the dark at room temperature. After washing, the cell suspension was analyzed using a flow cytometry device (Beckman Coulter, Epics XL-, System 3) as prescribed by the International Society of Hematotherapy and Graft Engineering protocol for cells not marked with 7-Amino-Actinomycin D (7AAD) (BD Biosciences, USA), indicating they were alive (negative = alive) (9). The flow cytometry gating and analysis strategy was as follows:

- All cells with weak and strong staining for CD45 (positive) (CD45 / SS) were gated (Gate A). Thus, all erythrocytes, platelets, and debris were excluded, and leukocyte gating was defined.
- Gate A for CD34 was introduced in the SS graph of CD34 (CD34 / SS). Cells with low SS and CD34 expression (positive) were gated (Gate B).
- Subsequently, cells from Gates A and B were introduced into the SS graph for CD45. In this graph, cells with low SS and weak to moderate fluorescence for CD45 were gated (Gate C).
- Cells were analyzed based on their size and granularity in the forward scatter (FS)/SS graph. Cells in Gates A+B+C showed low SS and a homogeneous distribution in FS (forward scatter); they were gated (Gate F).
- In the A graph, all leukocytes were gated; lymphocytes stained strongly for CD45 (Gate D). Gate D was introduced into the E graph, and homogeneously distributed lymphocytes in the graph were gated.
- Without gating, cells were evaluated for pCD34$^+$ with weak CD45 fluorescence (CD45/CD34).
- Cells positive for 7AAD (dead) were excluded from the pool of 7AAD-negative (live) cells.

Characterization of Collected CD34$^+$ Cell Quantity

Apheresis was performed at the patient's bedside using two different continuous flow apheresis devices: the Caridian BCT Inc. Spectra Optia Collection Set Apheresis System and the Fresenius P1Y-P1YA Comtec. The product obtained from each patient through apheresis was drawn into a syringe within a sterile cabinet and its volume recorded. The total CD34$^+$ cell count was obtained by multiplying the CD34$^+$ cell count detected per microliter by the product volume. The number of CD34$^+$ cells per kilogram for each patient was determined as follows:

$$\text{CD34+ cells} = \frac{\text{(CD34+ count per microliter) x (product volume in microliters)}}{\text{patient's body weight in kilograms}} \text{ x } 100$$

Storage and Use of CD34$^+$ Cells

Products containing 0.5 × 10^6/kg CD34$^+$ cells were primarily cryopreserved in our center using 6% hydroxyethyl starch (HES) and 7.5% DMSO as a cryoprotective. These products were stored in liquid nitrogen tanks inside CryoStore CS750NS containers in Oni-Gen bags in our facility. Frozen cells were thawed in a water bath at the Apheresis Unit and counted again.

High-Dose Chemotherapy

All patients diagnosed with MM received high-dose melphalan as the conditioning regimen. Day 0 was defined as the infusion day, and on day 2, 200 mg/m^2/day of melphalan (with dose adjustments made based on patient characteristics) were administered intravenously over two hours. Nearly all patients diagnosed with lymphoma underwent carmustine plus etoposide plus cytarabine plus melphalan (BEAM) conditioning, where day 0 was defined as the infusion day. On days 7, 6, 5, 4, and 3, carmustin 300 mg/m^2 (over two hours), etoposide 200 mg/m^2 (over two hours), and cytarabine (over two hours) were administered, and on day 2, melphalan 140 mg/m^2 (over one hour) was administered intravenously. One patient diagnosed with NHL received ifosfamide plus carboplatin plus etoposide (ICE) therapy as the conditioning regimen, where day 0 was the infusion day. Ifosfamide 2.5 g/m^2 (over 24 hours), mesna 2.5 g/m^2 (over 24 hours), and etoposide 300 mg/m^2 (x2, over two hours) on days 6, 5, 4, and 3 as well as carboplatin 500 mg/m^2 (over two hours) on days 6, 5, and 4 were administered intravenously.

Hematopoietic Stem Cell Transplantation

After thawing according to the conditioning regimen protocol on day 0, medications were administered through the central venous catheter in compliance with infusion guidelines. The period of pancytopenia that developed in patients following transplantation was addressed with support therapies, antibiotics based on culture results, and, when necessary, blood product replacements.

Statistical Analyses

Statistical analyses were performed using the Statistical Package for Social Sciences (SPSS) 21.0 program. Graphs were created using SPSS 21.0 and GraphPad Prism 5. Variance analysis between patient groups was conducted using ANOVA, and Mann–Whitney U test was applied for inter-group comparisons of parameters that were not normally distributed. Spearman correlation analysis was performed to determine the relationship between variables. Nonparametric categorical data were compared with the chi-square test or Fisher's exact

test as necessary. Patient demographic data were presented as the mean with standard deviation; medians were presented in figures. p-values <0.05 were considered significant.

RESULTS

Demographic and Clinical Characteristics

We examined the files of 167 patients who were diagnosed as follows: 31 with HL, 55 with NHL, and 81 with MM. The gender distribution among the patients was 57 (34.2%) female and 110 (65.8%) male. Patients ranged from 18 to 72 years old, with a mean age of 52 ± 13 years. Detailed demographics of the cohort are shown at Table 1. The average IBWs were 67.6 ± 6.9 and 50.6 ± 5.6 kg, in males and females, respectively. Average ABWs were 73.4 ± 8.5 kg and 79.9 ± 7.9 kg, respectively. Lastly, the average AdjIBWs were 69 ± 6.9 kg for males and 52.4 ± 5.4 kg for females.

Prior to the decision for high-dose therapy, four (12.9%) HL cases and nine (16.4%) NHL cases were chemorefractory, whereas 27 (87.1%) HL cases and 46 (83.6%) NHL cases were chemosensitive. Among the MM cases, 17 (20.9%) were in partial remission, 22 (27.2%) were in very good partial remission, 40 (49.5%) were in complete remission, and two (2.4%) had progressive disease when high-dose chemotherapy and AHSCT were decided upon.

Mobilization

Mobilization was achieved solely with G-CSF in 121 (72%) patients. Post-chemotherapy mobilization was performed in six (3.6%) patients. In five (6%) patients, post-chemotherapy mobilization failed initially, but successful mobilization was subsequently achieved with G-CSF. In three patients, including two MM and one NHL patient, bone marrow was collected because current regimens could not achieve mobilization. G-CSF and cyclophosphamide were used as the first-line mobilization regimen, but apheresis was not performed due to insufficient pCD34⁺ cell yield in one patient.

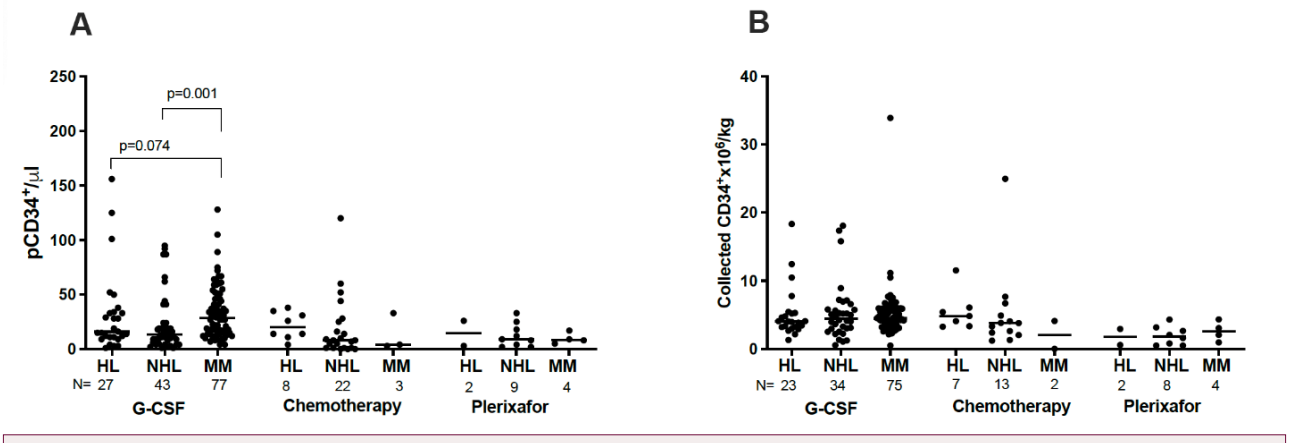

Figure 1. A. pCD34⁺ cell counts for each mobilization regimens and disease; B. Collected CD34⁺ cell counts for each mobilization regimen and diseases. HL: Hodgkin's lymphoma; NHL: Non-Hodgkin's lymphoma; MM: Multiple myeloma.

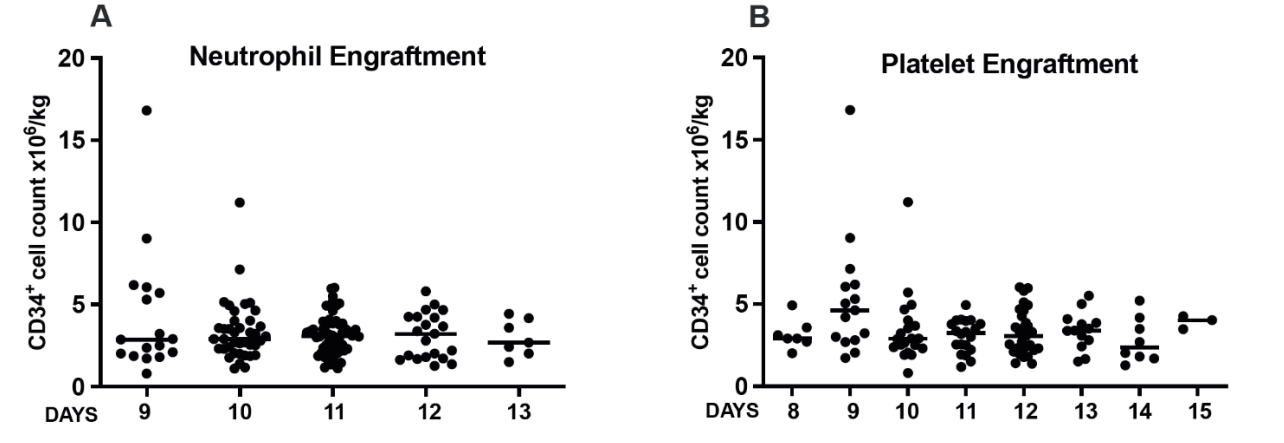

Figure 2. A. The effect of CD34⁺ cell counts on neutrophil engraftment, B. The effect of CD34⁺ cell counts on platelet engraftment.

Table 1. Demographic and clinical characteristics of the cohort.

	HL (n=31)	NHL (n=55)	MM (n=81)
Women (%)	35.5	34.5	33.3
Age, years, mean±SD	37 ± 12.7	47.4 ± 13.9	56.6 ± 7.9
Underweight (%)	6.5	9.1	2.5
Normal weight (%)	48.4	34.5	27.2
Overweight (%)	19.4	29.1	33.3
Obese (%)	25.8	27.3	37
Ideal Body Weight (IBW) kg, mean±SD	62.85 ± 10.7	62.97 ± 11.0	60.58 ± 9.7
Actual Body Weight (ABW) kg, mean±SD	68.23 ± 12.7	68.71 ± 11.6	67.65 ± 10.1
Adjusted Ideal Body Weight (AdjIBW) kg, mean±SD	64.19 ± 10.9	64.40 ± 10.8	62.35 ± 9.5
Radiotherapy (%)	32.3	32.7	43.2

HL: Hodgkin's lymphoma; NHL: Non-Hodgkin's lymphoma; MM: Multiple myeloma; SD: Standard Deviation

Radiotherapy did not significantly affect the yield of $pCD34^+$ cells (35.25 ± 40 mL vs. 29.25 ± 25.7 mL, p = 0.31). The number of collected $CD34^+$ cells after G-CSF administration decreased with an increasing number of chemotherapy cycles received, but this did not reach statistical significance. In patients who received one, two, and three series of chemotherapy, the mean $pCD34^+$ cell count was 25, 23, and 14 /µL, respectively.

The median $pCD34^+$ cell count before apheresis was 18.0/µL (0–158/µL). After mobilization with only G-CSF in MM cases, the $pCD34^+$ cell count was significantly higher than in HL and NHL cases. The $pCD34^+$ cell count in MM cases was significantly higher than in NHL cases (p = 0.001) and was almost significantly different from that in HL cases (p = 0.074) (Figure 1**)**. No difference was found in $pCD34^+$ cell counts after mobilization with either cyclophosphamide or plerixafor.

After groups were classified by age into different decades, no statistically significant difference was found in $pCD34^+$ cell count. However, comparisons based on BMI revealed significantly higher $pCD34^+$ cell counts in overweight individuals compared to those of normal body weight (28 vs. 17, p = 0.014) and those who were underweight (28 vs. 14, p = 0.034) (data not shown).

Apheresis

Apheresis was not performed on four patients due to the insufficient $pCD34^+$ cell count. Among the remaining 163 patients, 245 apheresis procedures were conducted regardless of mobilization regimens. The total blood volume collected during the procedure was 4,848 ± 1,166 mL. The processed blood volume was 11,166 ± 2,145 mL. The leukocyte counts before apheresis were 30.46 × 10^9/L. The total $CD34^+$ cell count obtained post-apheresis was 3.3 × 10^9/kg, and the post-apheresis mononuclear cell (MNC) count was 49 × 10^8/kg. No correlation was found between age and collected $CD34^+$ cell count (Supplementary Figure 1). Groups were then cumulatively evaluated regardless of mobilization regimen. There was a weak negative correlation between the pre-apheresis leukocyte count (32.84 ± 13.18 x 10^9/L) and the collected $CD34^+$ cell count (2.4 ± 1.2 × 10^9/kg) (p = 0.054, r = –0.467) in the group with a $pCD34^+$ cell count of 20–50/µL on the second day of apheresis.

Transplantation and Engraftments

In 14 patients, collected cells were not utilized because they were intended solely for storage, or the patients no longer indicated for AHSCT. Successful AHSCT was performed on the remaining 144 patients (86.2%). Cell collection was unsuccessful in nine patients (5.3%); products from the other 14 patients who did not undergo transplantation were frozen and stored. Depending on disease type and status during AHSCT, patients received one of three conditioning regimens: high-dose melphalan (140–200 mg/m^2) (n = 76), BEAM (n = 67), or high-dose ICE (n = 1).

Four product bags were infused per patient on average. Infusion was performed in a single day for 122 patients with relatively lower product volumes but required two days for the remaining 22 patients with larger volumes. On average, 69.21% of the $CD34^+$ cells counted before freezing (with a maximum loss of 60% and a minimum loss of 0.5%) were available for infusion after thawing.

Neutrophil engraftment and platelet engraftment occurred on days 8–15 and days 7–16, respectively. Across regimens, for neutrophil and platelet engraftment occurred on days 11.1, and 11.2, 10.4 and 10.9, and 12 and 15 for those receiving melphalan, BEAM conditioning, and ICE, respectively.

The number of $CD34^+$ cells infused into patients negatively correlated with the dates of neutrophil and platelet engraftment (respectively, $p = 0.074$, $r = -0.150$; $p = 0.055$, $r = -0.178$). Similarly, the percentage loss of collected and infused $CD34^+$ cells positively correlated with the days of neutrophil and platelet engraftment (respectively, $p = 0.057$, $r = 0.16$; $p = 0.15$, $r = -0.132$). The insignificant effect of $CD34^+$ cell counts on neutrophil and platelet engraftments is shown in Figure 2.

DISCUSSION

ASCT remains an integral therapeutic strategy for various hematologic malignancies; its success depends on the effective mobilization of hematopoietic stem cells from the bone marrow to the peripheral blood. Over the years, several mobilization agents and strategies have been developed, primarily G-CSF, chemotherapy, and plerixafor. There is no consensus on which mobilization regimen should be used. Thus, many studies use G-CSF alone or in combination regimens. By comparing the effects of G-CSF and chemotherapy plus G-CSF on mobilization in 223 patients with MM, Sarici et al. found that G-CSF alone is affordable and sufficient (10). Dhakal et al. showed that combination therapies like G-CSF and chemotherapy with G-CSF and plerixafor achieve better mobilization but without enhancing transplant outcomes (11). In our study of a homogeneous cohort of 167 patients, mobilization was achieved using G-CSF alone in most MM cases and in at least two-thirds of lymphomas. For cases that could not be mobilized with G-CSF alone, successful mobilization was achieved in at least half of the cases using chemotherapy and G-CSF or plerixafor as alternatives.

Some patients present insufficient mobilization and are categorized as "poor mobilizers." Several factors have been identified that contribute to this clinical challenge (12) such as the type of hematologic malignancy; multiple myeloma increases the risk of poor mobilization. Prior exposure to intensive therapies can also affect mobilization outcomes. For instance, individuals who have undergone high-dose chemotherapy or radiation might experience bone marrow damage, which increases the risk of insufficient HSC mobilization. Additionally, bone marrow reserves generally decrease with age, which may hinder mobilization in older individuals. The specific mobilization protocols and agents used can also influence the outcome. Variability in response to agents like G-CSF or plerixafor has been well-documented. For example, the rate of mobilization failure was 24.1% in patients with lymphoma (13); individuals with elevated platelet counts prior to apheresis and those undergoing chemotherapy-based mobilization had a higher success rate during the initial apheresis. However, sex, age, weight, chemotherapy regimen, radiotherapy, or type of lymphoma did not significantly affect mobilization outcomes (13). Elucidating these risk factors is a pre-requisite for developing patient-specific strategies that optimize mobilization, and ultimately improve the success rates of transplantation. In our study, mobilization success decreased as the number of chemotherapy cycles increased, but this was not observed for radiotherapy. This may be because most cases received radiotherapy outside of the pelvis. Disease-specific features suggest that effective mobilization in MM cases can be attributed not due to their relapsed/refractory disease status like the lymphoma cases, but rather due to them being less affected after primary treatment. No relationship was found between patients' body weights and indices with mobilization and HSC collection. It was unclear which BMI index should be used, as HSCs can be successfully collected in obese patients. Age was not considered a negative factor in our study group.

The success of AHSCT relies on effective engraftment. Notably, the dose of infused $CD34^+$ cells has consistently been linked to faster neutrophil and platelet recovery. A higher dose of $CD34^+$ cells generally accelerates engraftment, diminishing the period of post-transplant neutropenia and thus reducing the risk of infection (14). The mobilization strategy initiated prior to AHSCT also affects treatment outcomes. Agents such as G-CSF, chemotherapy, and plerixafor can impact mobilization success and therefore the engraftment process. For instance, chemomobilization, despite its potential toxicities, often increases yields of $CD34^+$ cells compared to growth factor mobilization alone (13). Patients in whom abundant mobilization of $CD34^+$ cells is achieved are called "super-mobilizers" and demonstrate improved engraftment and survival (15). Furthermore, the patient's underlying disease and treatment history can influence engraftment outcomes. Those with a history of extensive chemotherapy or who have received multiple lines of treatment may experience delayed engraftment. Similarly, factors such as patient age, performance status, and disease stage at the time of transplant can affect engraftment speed and success (16). Lastly, conditioning regimen intensity, whether myeloablative or reduced intensity, can influence engraftment kinetics. Myeloablative regimens, while more aggressive, may accelerate and enhance engraftment compared to their reduced-intensity counterparts (17). While ASCT benefits patients with multiple myeloma and lymphoma, the engraftment process is influenced by both treatment-related and patient-specific factors. Considering all these factors can improve post-transplant outcomes and patient prognosis. In our study, the loss of $CD34^+$ cells extended the engraftment time. The initial apheresis procedure greatly determines efficacy. Thus, the timing and effective $CD34^+$ cell yield per unit volume are critical. Our study showed that efficacy wanes in subsequent procedures. Although leukocyte count increases in sequential procedures, the number of $pCD34^+$ cells does not, reducing efficacy and the amount of $CD34^+$ cells.

Our study has several limitations. First, the retrospective design inherently restricted our ability to link cause and effect. The limited patient cohort size precludes any meaningful subgroup analysis among different disease types. Furthermore, the low number of patients who underwent mobilization with plerixafor as well as those categorized as poor mobilizers or those who experienced mobilization failure rendered any statistical evaluation infeasible.

CONCLUSION

In conclusion, clinicians should strive to achieve successful mobilization on the first day of the apheresis and to direct patients to AHSCT at an appropriate time point that avoids excessive chemotherapy cycles. Successful cell collection and AHSCT can be achieved in obese and elderly patients. Future studies should be performed in larger prospective cohorts to explore engraftment kinetics.

Acknowledgements: The authors thank to Fehmi Hindilerden, Serkan Guvenc, Songul Serefhanoglu, Emine Tulay Ozcelik, Reyhan Diz Kucukkaya, and all staff of Hematopoietic Stem Cell Transplantation Center for helping this study.

Ethics Committee Approval: This study was approved by the Demiroglu Bilim University Clinical Research Ethics Committee on April 11, 2013, with number 44140529/2013-036.

Informed Consent: Signed consent was obtained from the participants.

Peer-review: Externally peer-reviewed.

Authors' Contributions: Conception/Design of Study – N.B.H., M.A.; Data Acquisition, Performing experiments, Data Analysis/Interpretation and Statistical Analyses – N.B.H.; Drafting Manuscript – N.B.H, M.A.; Critical Revision of Manuscript – M.A.

Conflicts of Interests: The authors declare that they have no competing interests.

Financial Disclosure: The authors declare that this study has received no financial support.

Clinical Trial Registration: The authors report that this study is not a clinical trial.

REFERENCES

1. Rajkumar SV. Multiple myeloma: 2022 update on diagnosis, risk stratification, and management. Am J Hematol 2022; 97(8): 1086-107.
2. Swerdlow SH, Campo E, Pileri SA, Harris NL, Stein H, Siebert R, et al. The 2016 revision of the World Health Organization classification of lymphoid neoplasms. Blood 2016; 127(20): 2375-90.
3. Palumbo A, Cavallo F, Gay F, Di Raimondo F, Ben Yehuda D, Petrucci MT, et al. Autologous transplantation and maintenance therapy in multiple myeloma. N Engl J Med 2014; 371(10): 895-905.
4. Dunleavy K, Fanale MA, Abramson JS, Noy A, Caimi PF, Pittaluga S, et al. Dose-adjusted EPOCH-R (etoposide, prednisone, vincristine, cyclophosphamide, doxorubicin, and rituximab) in untreated aggressive diffuse large B-cell lymphoma with MYC rearrangement: a prospective, multicentre, single-arm phase 2 study. Lancet Haematol 2018; 5(12): e609-e17.
5. Herrera AF, Chen L, Nieto Y, Holmberg L, Johnston P, Mei M, et al. Brentuximab vedotin plus nivolumab after autologous haematopoietic stem-cell transplantation for adult patients with high-risk classic Hodgkin lymphoma: a multicentre, phase 2 trial. Lancet Haematol 2023; 10(1): e14-e23.
6. Lanza F, Marchetti M, Zannetti BA. Overview on novel strategies and current guidelines for hematopoietic stem cell mobilisation and collection. Transfus Apher Sci 2023: 103830.
7. Maitta RW. Current state of apheresis technology and its applications. Transfus Apher Sci 2018; 57(5): 606-13.
8. Hopman RK, DiPersio JF. Advances in stem cell mobilization. Blood Rev 2014; 28(1): 31-40.
9. Whitby A, Whitby L, Fletcher M, Reilly JT, Sutherland DR, Keeney M, et al. ISHAGE protocol: are we doing it correctly? Cytometry B Clin Cytom 2012; 82(1): 9-17.
10. Sarıcı A, Erkurt MA, Bahçecioğlu Ö F, Gök S, Kuku İ, Biçim S, et al. Filgrastim alone versus cyclophosphamide and filgrastim for mobilization in multiple myeloma patients. Transfus Apher Sci 2021; 60(4): 103159.
11. Dhakal B, Zhang MJ, Burns LJ, Tang X, Meyer C, Mau LW, et al. Efficacy, safety, and cost of mobilization strategies in multiple myeloma: a prospective, observational study. Haematologica 2023; 108(8): 2249-54.
12. Wei X, Wei Y. Stem cell mobilization in multiple myeloma: challenges, strategies, and current developments. Ann Hematol 2023; 102(5): 995-1009.
13. Demiroğlu H, Çiftçiler R, Büyükaşık Y, Göker H. Prediction of stem cell mobilization failure in patients with Hodgkin and Non-Hodgkin Lymphoma. Turk J Haematol 2021; 38(3): 204-10.
14. Dolai TK, De R, Sen A, Baul SN, Mitra S, Bhattacharya S, et al. Pattern of autologous stem cell transplants at a tertiary care government hospital, with emphasis on transplant outcomes with pre-harvest CD34+ level. Blood Cell Ther 2022; 5(1): 16-26.
15. Moreb JS, Lantos L, Chen F, Elliott K, Dugan J, Skarbnik AP, et al. The effect of mobilizing large numbers of CD34 + cells (super-mobilizers) on the engraftment and survival in patients undergoing autologous stem cell transplantation. Transfus Apher Sci 2023: 103787.
16. Sahin U, Demirer T. Current strategies for the management of autologous peripheral blood stem cell mobilization failures in patients with multiple myeloma. J Clin Apher 2018; 33(3): 357-70.
17. Holmberg LA, Linenberger M, Connelly-Smith L. successful mobilization of autologous hematopoietic peripheral blood stem cells after salvage chemotherapy in patients with low CD34 blood cell counts. Transplant Cell Ther 2022; 28(11): 754-9.

Supplemantary Table 1. Formulas used in the study.	
Metric (Unit)	**Formula**
BMI	Weight / [height in meters]^2 (kg/m^2)
IBW	Female; 50 + [0.91 x (height in cm- 152)] (kg)
	Male; 45 + [0.91 x (height in cm- 152)] (kg)
ABW	IBW + 0.4 x (body weight- IBW) (kg)
AdjIBW	IBW + [0.25 x (ABW- IBW)] (kg)

BMI, body mass index; IBW, Ideal Body Weight, ABW, Actual Body Weight , and AdjIBW, Adjusted Ideal Body Weight. Patients were classified based on their body mass index (BMI) as underweight (below 20 kg/m^2), normal weight (20-25.9 kg/m^2), overweight (26-29.9 kg/m^2), and obese (above 30 kg/m^2).

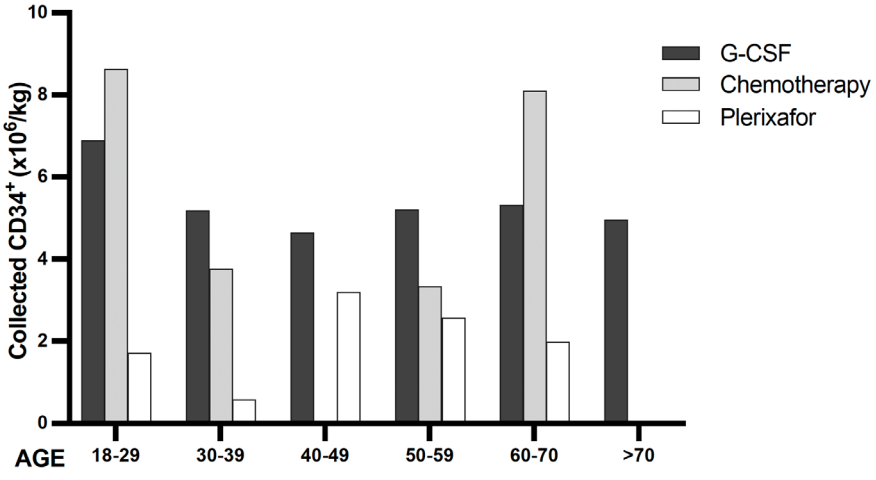

Supplementary Figure 1. Distribution of collected CD34$^+$ cell counts

EXPERIMED

AIMS AND SCOPE

Experimed is an international, scientific, open access periodical published in accordance with independent, unbiased, and double-blinded peer-review principles. The journal is the official online-only publication of Istanbul University Aziz Sancar Institute of Experimental Medicine and it is published triannually on April, August, and December. As of 2022 the publication language of the journal is only English. The manuscripts submitted for publication in the journal must be scientific work in English.

Experimed aims to contribute to the literature by publishing manuscripts at the highest scientific level on all fields of basic and clinical medical sciences. The journal publishes original articles, case reports, reviews, and letters to the editor that are prepared in accordance with ethical guidelines.

The scope of the journal includes but not limited to; experimental studies in all fields of medical sciences.

The target audience of the journal includes specialists and professionals working and interested in all disciplines of basic and clinical medical sciences.

The editorial and publication processes of the journal are shaped in accordance with the guidelines of the International Committee of Medical Journal Editors (ICMJE), World Association of Medical Editors (WAME), Council of Science Editors (CSE), Committee on Publication Ethics (COPE), European Association of Science Editors (EASE), and National Information Standards Organization (NISO). The journal is in conformity with the Principles of Transparency and Best Practice in Scholarly Publishing (doaj.org/bestpractice).

Processing and publication are free of charge with the journal. No fees are requested from the authors at any point throughout the evaluation and publication process. All manuscripts must be submitted via the online submission system, which is available at http://experimed.istanbul.edu.tr/en/_.The journal guidelines, technical information, and the required forms are available on the journal's web page.

All expenses of the journal are covered by the Istanbul University.

Statements or opinions expressed in the manuscripts published in the journal reflect the views of the author(s) and not the opinions of the Istanbul University Aziz Sancar Institute of Experimental Medicine, editors, editorial board, and/or publisher; the editors, editorial board, and publisher disclaim any responsibility or liability for such materials.

Editor in Chief: Prof. Bedia Cakmakoglu
Address: Istanbul University, Aziz Sancar Institute of Experimental Medicine, Vakıf Gureba Avenue, 34093, Capa, Fatih, Istanbul, Turkiye
Phone: +90 212 414 2000-33305
Fax: +90 212 532 4171
E-mail: bedia@istanbul.edu.tr

Publisher: Istanbul University Press
Address: Istanbul University Central Campus, 34452 Beyazit, Fatih / Istanbul - Turkiye
Phone: +90 212 440 0000

EXPERIMED

INSTRUCTIONS TO AUTHORS

Context
Experimed is an international, scientific, open access periodical published in accordance with independent, unbiased, and double-blinded peer-review principles. The journal is the official online-only publication of Istanbul University Aziz Sancar Institute of Experimental Medicine and it is published triannually on April, August, and December. The publication language of the journal is English.

Experimed aims to contribute to the literature by publishing manuscripts at the highest scientific level on all fields of basic and clinical medical sciences. The journal publishes original articles, case reports, reviews, and letters to the editor that are prepared in accordance with ethical guidelines.

Editorial Policy
The editorial and publication processes of the journal are shaped in accordance with the guidelines of the International Council of Medical Journal Editors (ICMJE), the World Association of Medical Editors (WAME), the Council of Science Editors (CSE), the Committee on Publication Ethics (COPE), the European Association of Science Editors (EASE), and National Information Standards Organization (NISO). The journal conforms to the Principles of Transparency and Best Practice in Scholarly Publishing (doaj.org/bestpractice).

Originality, high scientific quality, and citation potential are the most important criteria for a manuscript to be accepted for publication. Manuscripts submitted for evaluation should not have been previously presented or already published in an electronic or printed medium. The journal should be informed of manuscripts that have been submitted to another journal for evaluation and rejected for publication. The submission of previous reviewer reports will expedite the evaluation process. Manuscripts that have been presented in a meeting should be submitted with detailed information on the organization, including the name, date, and location of the organization.

Peer-Review Policy
Only those manuscripts approved by its every individual author and that were not published before in or sent to another journal, are accepted for evaluation. Submitted manuscripts that pass preliminary control are scanned for plagiarism using iThenticate software. After plagiarism check, the eligible ones are evaluated by editor-in-chief for their originality, methodology, the importance of the subject covered and compliance with the journal scope. The selected manuscripts are sent to at least two national/international external referees for evaluation and publication decision is given by editor-in-chief upon modification by the authors in accordance with the referees' claims. Editor-in-chief evaluates manuscripts for their scientific content without regard to ethnic origin, gender, sexual orientation, citizenship, religious belief or political philosophy of the authors and ensures a fair double-blind peer review of the selected manuscripts.
Editor in chief does not allow any conflicts of interest between the authors, editors and reviewers and is responsible for final decision for publication of the manuscripts in the Journal.

Reviewers' judgments must be objective. Reviewers' comments on the following aspects are expected while conducting the review.
- Does the manuscript contain new and significant information?
- Does the abstract clearly and accurately describe the content of the manuscript?
- Is the problem significant and concisely stated?
- Are the methods described comprehensively?
- Are the interpretations and consclusions justified by the results?
- Is adequate references made to other Works in the field?
- Is the language acceptable?

Reviewers must ensure that all the information related to submitted manuscripts is kept as confidential and must report to the editor if they are aware of copyright infringement and plagiarism on the author's side.
A reviewer who feels unqualified to review the topic of a manuscript or knows that its prompt review will be impossible should notify the editor and excuse himself from the review process.
The editor informs the reviewers that the manuscripts are confidential information and that this is a privileged interaction. The reviewers and editorial board cannot discuss the manuscripts with other persons. The anonymity of the referees is important.

Ethical Principles
The Journal takes as principle to comply with the ethical standards of World Medical Association (WMA) Declaration of Helsinki – Ethical Principles for Medical Research Involving Human Subjects and WMA Statement on Animal Use in Biomedical Research.

An approval of research protocols by the Ethics Committee in accordance with international standards mentioned above is required for experimental, clinical, and drug studies and for some case reports. If required, ethics committee reports or an equivalent official document will be requested from the authors. For manuscripts concerning experimental research on humans, a statement should be included that shows that written informed consent of patients and volunteers was obtained following a detailed explanation of the procedures that they may undergo. For studies carried out on animals, the measures taken to prevent pain and suffering of the animals should be stated clearly. Information on patient consent, the name of the ethics committee, and the ethics committee approval number should also be stated in the Materials and Methods section of the manuscript. It is the authors' responsibility to carefully protect the patients' anonymity. For photographs that may reveal the identity of the patients, signed releases of the patient or of their legal representative should be enclosed.

For studies involving animals, it is required to obtain approval of research protocols from an ethics committee. The committee reviews protocols to ensure compliance with applicable regulations and guidelines, including the Guide for the Care and Use of Laboratory Animals (8th Edition, 2011) and the International Guiding Principles for Biomedical Research Involving Animals (2012). These guidelines offer comprehensive instructions on how to carry out animal research ethically and humanely and are widely acknowledged as the benchmark for such research.

EXPERIMED

Authors should provide detailed explanation of the ethical treatment of animals in their manuscripts, including measures taken to avoid pain and distress. This is crucial to ensure the humane conduct of the study and enable verification that it conforms to the relevant ethical criteria. The ARRIVE checklist is a useful tool authors can use to present this information clearly and thoroughly.

Plagiarism
Experimed is extremely sensitive about plagiarism. All submissions are screened by a similarity detection software (iThenticate by CrossCheck) at any point during the peer-review or production process.Even if you are the author of the phrases or sentences, the text should not have unacceptable similarity with the previously published data.

When you are discussing others' (or your own) previous work, please make sure that you cite the material correctly in every instance.

In the event of alleged or suspected research misconduct, e.g., plagiarism, citation manipulation, and data falsification/fabrication, the Editorial Board will follow and act in accordance with COPE guidelines.

Authorship
Each individual listed as an author should fulfill the authorship criteria recommended by the International Committee of Medical Journal Editors

(ICMJE - www.icmje.org). The ICMJE recommends that authorship be based on the following 4 criteria:

1. Substantial contributions to the conception or design of the work; or the acquisition, analysis, or interpretation of data for the work; AND
2. Drafting the work or revising it critically for important intellectual content; AND
3. Final approval of the version to be published; AND
4. Agreement to be accountable for all aspects of the work in ensuring that questions related to the accuracy or integrity of any part of the work are appropriately investigated and resolved.

In addition to being accountable for the parts of the work he/she has done, an author should be able to identify which co-authors are responsible for specific other parts of the work. In addition, authors should have confidence in the integrity of the contributions of their co-authors.
All those designated as authors should meet all four criterias for authorship, and all who meet the four criteria should be identified as authors. Those who do not meet all four criterias should be acknowledged in the title page of the manuscript.
Experimed requires corresponding authors to submit a signed and scanned version of the authorship contribution form (available for download through http://experimed.istanbul.edu.tr/en/_) during the initial submission process in order to act appropriately on authorship rights and to prevent ghost or honorary authorship. If the editorial board suspects a case of "gift authorship," the submission will be rejected without further review. As part of the submission of the manuscript, the corresponding author should also send a short statement declaring that he/she accepts to undertake all the responsibility for authorship during the submission and review stages of the manuscript.

Conflict of Interest
The journal requires the authors and all individuals taking part in the evaluation process to disclose any existing or potential conflict of interest (such as financial ties, academic commitments, personal relationships, institutional affiliations) that could unduly influence one's responsibilities. To disclose potential conflicts of interest, the ICMJE Potential Conflict of Interest Disclosure Form should be filled in and submitted by authors as explained in the Author Form of the journal. Cases of a potential conflict of interest are resolved within the scope of COPE Conflict of Interest Flowcharts and ICMJE Conflict of Interest guidelines.

Besides conflict of interest, all financial support received to carry out research must be declared while submitting the paper.

The Editorial Board of the journal handles all appeal and complaint cases within the scope of COPE guidelines. In such cases, authors should get in direct contact with the editorial office regarding their appeals and complaints. When needed, an ombudsperson may be assigned to resolve cases that cannot be resolved internally. The Editor in Chief is the final authority in the decision-making process for all appeals and complaints.

Copyright and Licensing

Open Access Statement

Disclaimer
Statements or opinions expressed in the manuscripts published in Experimed reflect the views of the author(s) and not the opinions of the editors, the editorial board, or the publisher; the editors, the editorial board, and the publisher disclaim any responsibility or liability for such materials. The final responsibility in regard to the published content rests with the authors.

EXPERIMED

MANUSCRIPT PREPARATION

The manuscripts should be prepared in accordance with ICMJE-Recommendations for the Conduct, Reporting, Editing, and Publication of Scholarly Work in Medical Journals (updated in December 2015 - http://www.icmje.org/icmje-recommendations.pdf). Authors are required to prepare manuscripts in accordance with the CONSORT guidelines for randomized research studies, STROBE guidelines for observational original research studies, STARD guidelines for studies on diagnostic accuracy, PRISMA guidelines for systematic reviews and meta-analysis, ARRIVE guidelines for experimental animal studies, and TREND guidelines for non-randomized public behavior.

Manuscripts can only be submitted through the journal's online manuscript submission and evaluation system, available at http://experimed.istanbul.edu.tr/en/_. Manuscripts submitted via any other medium will not be evaluated.

Manuscripts submitted to the journal will first go through a technical evaluation process where the editorial office staff will ensure that the manuscript has been prepared and submitted in accordance with the journal's guidelines. Submissions that do not conform to the journal's guidelines will be returned to the submitting author with technical correction requests.

Authors are required to submit the following:

- Copyright Agreement Form,
- ICMJE Potential Conflict of Interest Disclosure Form (should be filled in by all contributing authors)

during the initial submission. These forms are available for download at http://experimed.istanbul.edu.tr/en/_.

Preparation of the Manuscript

Title page: A separate title page should be submitted with all submissions and this page should include:

- The full title of the manuscript as well as a short title (running head) of no more than 50 characters,
- Name(s), affiliations, ORCID IDs and highest academic degree(s) of the author(s),
- Grant information and detailed information on the other sources of support,
- Name, address, telephone (including the mobile phone number) and fax numbers, and email address of the corresponding author,
- Acknowledgment of the individuals who contributed to the preparation of the manuscript but who do not fulfill the authorship criteria.

Abstract: A English abstract should be submitted with all submissions except for Letters to the Editor. The abstract of Original Articles should be structured with subheadings (Objective, Material and Method, Results, and Conclusion). Please check Table 1 below for word count specifications.

Keywords: Each submission must be accompanied by a minimum of three to a maximum of six keywords for subject indexing at the end of the abstract. The keywords should be listed in full without abbreviations. The keywords should be selected from the National Library of Medicine, Medical Subject Headings database (https://www.nlm.nih.gov/mesh/MBrowser.html).

Manuscript Types

Original Articles: This is the most important type of article since it provides new information based on original research. The main text of original articles should be structured with Introduction, Material and Method, Results, and Discussion subheadings. Please check Table 1 for the limitations for Original Articles.

Statistical analysis to support conclusions is usually necessary. Statistical analyses must be conducted in accordance with international statistical reporting standards (Altman DG, Gore SM, Gardner MJ, Pocock SJ. Statistical guidelines for contributors to medical journals. Br Med J 1983: 7; 1489-93). Information on statistical analyses should be provided with a separate subheading under the Materials and Methods section and the statistical software that was used during the process must be specified.

Units should be prepared in accordance with the International System of Units (SI).

Editorial Comments: Editorial comments aim to provide a brief critical commentary by reviewers with expertise or with high reputation in the topic of the research article published in the journal. Authors are selected and invited by the journal to provide such comments. Abstract, Keywords, and Tables, Figures, Images, and other media are not included.

Review Articles: Reviews prepared by authors who have extensive knowledge on a particular field and whose scientific background has been translated into a high volume of publications with a high citation potential are welcomed. These authors may even be invited by the journal. Reviews should describe, discuss, and evaluate the current level of knowledge of a topic in clinical practice and should guide future studies. The main text should contain Introduction, Clinical and Research Consequences, and Conclusion sections. Please check Table 1 for the limitations for Review Articles.

Case Reports: There is limited space for case reports in the journal and reports on rare cases or conditions that constitute challenges in diagnosis and treatment, those offering new therapies or revealing knowledge not included in the literature, and interesting and educative case reports are accepted for publication. The text should include Introduction, Case Presentation, Discussion, and Conclusion subheadings. Please check Table 1 for the limitations for Case Reports.

Letters to the Editor: This type of manuscript discusses important parts, overlooked aspects, or lacking parts of a previously published article. Articles on subjects within the scope of the journal that might attract the readers' attention, particularly educative cases, may also be submitted in the form of a "Letter to the Editor." Readers can also present their comments on the published manuscripts in the form of a "Letter to the Editor." Abstract, Keywords, and Tables, Figures, Images, and other media should not be included. The text should be unstructured. The manuscript that is being commented on must be properly cited within this manuscript.

Table 1. Limitations for each manuscript type

Type of manuscript	Word limit	Abstract word limit	Reference limit	Table limit	Figure limit
Original Article	3500	200 (Structured)	30	6	7 or total of 15 images
Review Article	5000	200	50	6	10 or total of 20 images
Case Report	1000	200	15	No tables	10 or total of 20 images
Letter to the Editor	500	No abstract	5	No tables	No media

Tables

Tables should be included in the main document, presented after the reference list, and they should be numbered consecutively in the order they are referred to within the main text. A descriptive title must be placed above the tables. Abbreviations used in the tables should be defined below the tables by footnotes (even if they are defined within the main text). Tables should be created using the "insert table" command of the word processing software and they should be arranged clearly to provide easy reading. Data presented in the tables should not be a repetition of the data presented within the main text but should be supporting the main text.

Figures and Figure Legends

Figures, graphics, and photographs should be submitted as separate files (in TIFF or JPEG format) through the submission system. The files should not be embedded in a Word document or the main document. When there are figure subunits, the subunits should not be merged to form a single image. Each subunit should be submitted separately through the submission system. Images should not be labeled (a, b, c, etc.) to indicate figure subunits. Thick and thin arrows, arrowheads, stars, asterisks, and similar marks can be used on the images to support figure legends. Like the rest of the submission, the figures too should be blind. Any information within the images that may indicate an individual or institution should be blinded. The minimum resolution of each submitted figure should be 300 DPI. To prevent delays in the evaluation process, all submitted figures should be clear in resolution and large in size (minimum dimensions: 100 × 100 mm). Figure legends should be listed at the end of the main document.

All acronyms and abbreviations used in the manuscript should be defined at first use, both in the abstract and in the main text. The abbreviation should be provided in parentheses following the definition.

When a drug, product, hardware, or software program is mentioned within the main text, product information, including the name of the product, the producer of the product, and city and the country of the company (including the state if in USA), should be provided in parentheses in the following format: "Discovery St PET/CT scanner (General Electric, Milwaukee, WI, USA)"

All references, tables, and figures should be referred to within the main text, and they should be numbered consecutively in the order they are referred to within the main text.

Limitations, drawbacks, and the shortcomings of original articles should be mentioned in the Discussion section before the conclusion paragraph.

References

While citing publications, preference should be given to the latest, most up-to-date publications. Authors are responsible for the accuracy of references. References should be prepared according to Vancouver reference style. If an ahead-of-print publication is cited, the DOI number should be provided. Journal titles should be abbreviated in accordance with the journal abbreviations in Index Medicus/ MEDLINE/PubMed. When there are six or fewer authors, all authors should be listed. If there are seven or more authors, the first six authors should be listed followed by "et al." In the main text of the manuscript, references should be cited using Arabic numbers in parentheses. The reference styles for different types of publications are presented in the following examples.

Journal Article: Rankovic A, Rancic N, Jovanovic M, Ivanović M, Gajović O, Lazić Z, et al. Impact of imaging diagnostics on the budget – Are we spending too much? Vojnosanit Pregl 2013; 70: 709-11.

Book Section: Suh KN, Keystone JS. Malaria and babesiosis. Gorbach SL, Barlett JG, Blacklow NR, editors. Infectious Diseases. Philadelphia: Lippincott Williams; 2004.p.2290-308.

Books with a Single Author: Sweetman SC. Martindale the Complete Drug Reference. 34th ed. London: Pharmaceutical Press; 2005.

Editor(s) as Author: Huizing EH, de Groot JAM, editors. Functional reconstructive nasal surgery. Stuttgart-New York: Thieme; 2003.

Conference Proceedings: Bengisson S. Sothemin BG. Enforcement of data protection, privacy and security in medical informatics. In: Lun KC, Degoulet P, Piemme TE, Rienhoff O, editors. MEDINFO 92. Proceedings of the 7th World Congress on Medical Informatics; 1992 Sept 6-10; Geneva, Switzerland. Amsterdam: North-Holland; 1992. pp.1561-5.

Scientific or Technical Report: Cusick M, Chew EY, Hoogwerf B, Agrón E, Wu L, Lindley A, et al. Early Treatment Diabetic Retinopathy Study Research Group. Risk factors for renal replacement therapy in the Early Treatment Diabetic Retinopathy Study (ETDRS), Early Treatment Diabetic Retinopathy Study Kidney Int: 2004. Report No: 26.

EXPERIMED

Thesis: Yılmaz B. Ankara Üniversitesindeki Öğrencilerin Beslenme Durumları, Fiziksel Aktiviteleri ve Beden Kitle İndeksleri Kan Lipidleri Arasındaki Ilişkiler. H.Ü. Sağlık Bilimleri Enstitüsü, Doktora Tezi. 2007.

Manuscripts Accepted for Publication, Not Published Yet: Slots J. The microflora of black stain on human primary teeth. Scand J Dent Res. 1974.

Epub Ahead of Print Articles: Cai L, Yeh BM, Westphalen AC, Roberts JP, Wang ZJ. Adult living donor liver imaging. Diagn Interv Radiol. 2016 Feb 24. doi: 10.5152/dir.2016.15323. [Epub ahead of print].

Manuscripts Published in Electronic Format: Morse SS. Factors in the emergence of infectious diseases. Emerg Infect Dis (serial online) 1995 Jan-Mar (cited 1996 June 5): 1(1): (24 screens). Available from: URL: http:/ www.cdc.gov/ncidodlEID/cid.htm.

REVISIONS

When submitting a revised version of a paper, the author must submit a detailed "Response to the reviewers" that states point by point how each issue raised by the reviewers has been covered and where it can be found (each reviewer's comment, followed by the author's reply and line numbers where the changes have been made) as well as an annotated copy of the main document. Revised manuscripts must be submitted within 30 days from the date of the decision letter. If the revised version of the manuscript is not submitted within the allocated time, the revision option may be canceled. If the submitting author(s) believe that additional time is required, they should request this extension before the initial 30-day period is over.

Accepted manuscripts are copy-edited for grammar, punctuation, and format. Once the publication process of a manuscript is completed, it is published online on the journal's webpage as an ahead-of-print publication before it is included in its scheduled issue. A PDF proof of the accepted manuscript is sent to the corresponding author and their publication approval is requested within 2 days of their receipt of the proof.

Editor in Chief: Prof. Bedia Cakmakoglu
Address: Istanbul University, Aziz Sancar Institute of Experimental Medicine, Vakıf Gureba Avenue, 34093, Capa, Fatih, Istanbul, Turkiye
Phone: +90 212 414 2000-33305
Fax: +90 212 532 4171
E-mail: bedia@istanbul.edu.tr

Publisher: Istanbul University Press
Address: Istanbul University Central Campus, 34452 Beyazit, Fatih / Istanbul - Turkiye
Phone: +90 212 440 0000